DESIGN AND APPLICATION OF COMPLEXITY-GENERATING STRATEGIES AND TRANSFORMATIONS IN NATURAL PRODUCT SYNTHESIS

Thesis by

Andrea Anna Therese Stegner

In Partial Fulfillment of the Requirements

for the Degree of

Doctor of Philosophy

CALIFORNIA INSTITUTE OF TECHNOLOGY

Pasadena, California

2025

(Defended May 19, 2025)

Andrea Anna Therese Stegner

ORCID: 0000-0001-9408-3967

To my family and friends

ACKNOWLEDGEMENTS

Completing this dissertation while moving across the Atlantic ocean and surviving a global pandemic has been one of the most challenging life, and I'm deeply grateful to have done it in a place such as Caltech. I would like to express my sincere gratitude to my advisor, Professor Sarah Reisman, for her mentorship and commitment to scientific excellence. Her guidance has been instrumental to my growth as a researcher, and I am thankful for the opportunity to train in her group. I am also deeply grateful to my thesis committee — Professors Brian Stoltz, Max Robb, and Linda Hsieh-Wilson — for their valuable insights, thoughtful feedback, and encouragement throughout my graduate studies. Their support and perspective have shaped this work in important ways and contributed greatly to my scientific development. I would like to especially thank Professor Brian Stoltz for his generous support, insightful guidance, and genuine mentorship. In the short time I had the pleasure of working with him, our conversations profoundly shaped my thinking and growth as a scientist. Your encouragement and thoughtful perspective have left a lasting impact for which I'm deeply grateful.

I'm deeply grateful to Jeff, my first project partner and mentor, whose creativity, passion for chemistry, and endless curiosity made a lasting impression on me. His unique sense of humor, kindness, and shared love for the outdoors made every moment working with him a joy. I learned so much from his adventurous spirit both in and out of the lab.

I'm grateful to Dave, who worked with me on the total synthesis project he never planned to take on, yet approached it with thoughtfulness, patience, and quiet determination. His methodical mindset, calm under pressure, and deep grasp of chemistry

not only anchored the project but also taught me a great deal about focus, precision, and perseverance. His sense of humor and sarcasm always brought a smile to my face.

Thank you to Olivia, my mentee and collaborator, whose strength, resilience, and meticulous approach made working together genuinely enjoyable. She brings clarity and care to everything she does, and her ability to push through challenges with unwavering focus continues to inspire me.

I'm incredibly grateful to all my labmates who made this journey memorable, challenging, and full of laughter. To my baymates—Alex, who survived the pandemic by my side; Jordan, for his sharp scientific insight, steady support, and unforgettable late-night deep talks; Emily, for her humor and willingness to embrace chaos with me; and Golsa, for simply being the best and brightening my days with her kindness and smile.

To the Samarium boys—Chung, Will, and Nathan—thank you for keeping me entertained through so many late nights. Chung, for always being up for a good laugh (especially with Golsa); Will, for being the ideal desk mate and everyday sounding board; and Nathan, for sharing your passion for chemistry and your thoughtful reflections.

Thank you to Stanna, my biggest cheerleader, whose unwavering support and our conversations meant more to me than I can say. And to Kala, thank you for your steadfast support and advocacy both in and beyond the lab—it never went unnoticed and was always appreciated.

I'm especially grateful to the people who have been my scientific inspirations throughout this journey. Giulio and Dirk first sparked my love for synthesis—their passion, creativity, and mentorship helped shape the way I approach chemistry. A heartfelt thank you to Oliver, whose boundless creativity, deep passion for science, and steadfast support

have left a lasting mark on me. The opportunities he gave me, and his constant encouragement, pushed me to grow in ways I hadn't imagined. His leadership and imagination continue to inspire me.

And to Abby, whose brilliance, integrity, and kindness continue to inspire me in every way—thank you for believing in me and for always being there. I'm grateful to each of you not only for what you taught me, but for your unwavering belief in my potential.

Outside the lab, I owe endless gratitude to my mum, who always gave me the freedom to find my own path and did everything she could to make me feel confident. Her love in me has been the foundation of everything. I'll be forever grateful to her for advocating for Krümel, Nelly, and the guinea pigs.

To Julia—my true soulmate and dearest friend—there are no words that can fully capture how much you mean to me. Your kindness, humor, self-awareness, and our endless voice messages filled with deep reflection and laughter have been an anchor through it all. I truly couldn't have done this without your love and support.

To Ana, my longest friend, thank you for sharing our awkward skater days, teenage chaos, and so many life moments filled with laughter. You know me like no one else, and I'm so grateful to walk through life with you by my side.

To the crew – Michi, Sebus, Nikki, Panos, and Nico – thank you for all the Krautgarten chillerein, the joy, the chaos, and sticking together through good times and bad. Marcel, thank you for sharing a part of your journey with me – I truly adore and miss you. And to everyone else—my uni crew and the high school crowd—you've helped shape the person I am. I'm deeply grateful for your continued support, cheerleading, and the joy you bring into my life.

To Taylan – thank you for being the person I truly could not have survived grad school without. Some of my best days here were spent with you. Your unwavering support, friendship, and ability to challenge me in all the right ways made all the difference. I'm so grateful for your presence and for being the perfect teammate through it all.

To Lisa, Lars, and Isa – thank you for giving me the opportunity to ride and work with your incredible horses. What you offered me means so much more to me than just a hobby; it became a lifeline, a source of purpose and strength, and one of the main reasons I'm here today. I'm deeply grateful for the trust you placed in me, the chance to get to know your horses and the chance to grow not only as a rider but as a person.

To Annamina, thank you for your guidance and for generously sharing your remarkable skills in riding. Your trust and willingness to let me work with your horses meant the world to me.

To Katie Ginzeton, thank you for trusting me with your amazing horses – especially Kia. Your support gave me the space to continue growing as a rider even when life got overwhelming, and it truly helped me stay grounded and balanced during busy, demanding times.

To Krümel, thank you for sharing your best days with me. You were the most reliable and loving companion I could have wished for in a first horse. And to Gunther, Cassy, Sibelius, and Kia—thank you for teaching me, challenging me, and allowing me to build a partnership with you. Working with you has shaped me in so many ways.

And to Nelly, my childhood dog and best friend—thank you for being by my side with unwavering love. You were a constant source of comfort, joy, and companionship, and I'll always carry your memory with me.

To Lance – thank you for challenging me and always making me laugh. You're the silliest pup and the fluffiest pillow anyone could ever dream of. Your joy and softness made even the hardest days better.

To Smokey and Foggy—I never imagined I'd become a cat person, but with you, I had no choice. You are the cuddliest, softest, and most adorable little creatures I could ever imagine. Thank you for brightening even the worst days with your meowed demands for cuddles and your wild zoomies that never failed to make me smile.

ABSTRACT

Rapid and efficient chemical synthesis of complex molecules is critical for enabling studies of their biological function and therapeutic potential. Complexity generation can be achieved by: (1) the development of selective transformations that rapidly construct complex scaffolds from simple precursors, and (2) the application of strategic retrosynthetic disconnections that maximize the efficiency of a synthesis *i.e.*, via convergent fragment coupling strategies. We disclose efforts to address these aims by combining reaction design with the identification of strategic disconnections.

Toward the first aim, a diastereoselective dearomative pyridine cyclization that forges the tetracyclic core of the matrine-type lupin alkaloids in a single step from commodity feedstocks was developed. This reaction, paired with a C15-selective oxidation cascade and late-stage isomerization, enabled the first total synthesis of (–)-sophoridine and the shortest syntheses to date of (+)-matrine, (+)-isomatrine, (+)-allomatrine, and (+)-isosophoridine.

To address the second aim, a convergent strategy for the synthesis of 6,7-seco-*ent*-kauranoids via strategic, transition metal-catalyzed C-C bond formation was developed. Both a Ni-catalyzed sp^2–sp^3 and a dual Ni/Pd-catalyzed sp^2–sp^2 coupling were developed and enabled efficient union of complex fragments, the latter yielding 1,3 dienes that underwent divergent annulation reactions to form various complex ring systems. These transformations provided the complete skeleton of isorosthin A and advanced intermediates *en route* to isodocarpin and secoexertifolin A.

PUBLISHED CONTENT AND CONTRIBUTIONS

Portions of the work described herein were disclosed in the following publications:

1. Kerkovius, J. K.; Stegner, A.; Turlik, A.; Lam, P. H.; Houk, K. N.; Reisman, S. E. A Pyridine Dearomatization Approach to the Matrine-Type Lupin Alkaloids. *J. Am. Chem. Soc.* **2022**, *144*, 35, 15938–15943. https://doi.org/10.1021/jacs.2c06584.

A. A. S. contributed to conception of the synthetic strategy, conducted experiments, and participated in preparation of the supporting data and writing of the manuscript.

TABLE OF CONTENTS

LIST OF ABBREVIATIONS

[list the abbreviations used in your thesis, in alphabetical order, examples below]

$[\alpha]_D$	angle of optical rotation of plane-polarized light
Å	angstrom(s)
Ac	acetyl
acac	acetylacetonate
aq.	aqueous
atm	atmosphere(s)
bpy	2,2'-bipyridine
Bn	benzyl
BOM	benzyloxymethyl
bp	boiling point
br	broad
Bu	butyl
*i*Bu	*iso*-butyl
*n*Bu	*norm*-butyl
*t*Bu	*tert*-butyl
c	concentration of sample for measurement of optical rotation
^{13}C	carbon-13 isotope
°C	degrees Celsius
calcd	calculated

CAN	ceric ammonium nitrate
Cbz	benzyloxycarbonyl
cf.	consult or compare to (Latin: confer)
cis	on the same side
cm^{-1}	wavenumber(s)
CM	cross-metathesis
CO	carbon monoxide
COD	1,5-cyclooctadiene
conv.	conversion
COSY	homonuclear correlation spectroscopy
CSA	camphor sulfonic acid
D	heat or difference
d	chemical shift in ppm / doublet / deuterium
dba	dibenzylideneacetone
DBU	1,8-diazabicyclo[5.4.0]undec-7-ene
DCC	N,N'-dicyclohexylcarbodiimide
DCE	1,2-dichloroethane
DCM	dichloromethane
DDQ	2,3-dichloro-5,6-dicyano-1,4-benzoquinone
de novo	starting from the beginning; anew
DIBAL	diisobutylaluminum hydride
diglyme	bis(2-methoxyethyl) ether
DMA	N,N-dimethylacetamide

DMAP	4-(dimethylamino)pyridine
DME	1,2-dimethoxyethane
DMF	N,N-dimethylformamide
DMPU	1,3-dimethyl-3,4,5,6-tetrahydro-2(1H)-pyrimidinone
DMSO	dimethylsulfoxide
dppf	1,1'-bis(diphenylphosphino)ferrocene
dr	diastereomeric ratio
dtbbpy	4,4′-di-tert-butyl-2,2′-dipyridyl
ee	enantiomeric excess
E	trans (entgegen) olefin geometry
EDC	N-(3-dimethylaminopropyl)-N'-ethylcarbodiimide hydrochloride
e.g.	for example (Latin: exempli gratia)
EI	electron impact
ent	enantiomer of
epi	epimeric
equiv	equivalent(s)
ESI	electrospray ionization
Et	ethyl
et al.	and others (Latin: et alii)
FAB	fast atom bombardment
FD	field desorption
FI	field ionization
FTIR	fourier transform infrared spectroscopy

g	gram(s)
glyme	dimethoxyethane
h	hour(s)
1H	proton
[H]	reduction
HFIP	hexafluoroisopropanol
HMBC	heteronuclear multiple-bond correlation spectroscopy
HMDS	hexamethyldisilazide
HMPA	hexamethylphosphoramide
hv	irradiation with light
HPLC	high performance liquid chromatography
HRMS	high resolution mass spectrometry
HSQC	heteronuclear single quantum coherence spectroscopy
Hz	hertz
i.e.	that is (Latin: id est)
in situ	in the reaction mixture
iso	isomeric
J	coupling constant in Hz
k	rate constant
kcal	kilocalorie(s)
L	liter
l	levorotatory
LCMS	liquid chromatography–mass spectrometry

LDA	lithium diisopropylamide
m	multiplet or meter(s)
M	molar or molecular ion
m	*meta*
μ	micro
Me	methyl
MeOH	methanol
MeCN	acetonitrile
mg	milligram(s)
MHz	megahertz
min	minute(s)
mL	milliliter(s)
mol	mole(s)
MOM	methoxymethyl
Ms	methanesulfonyl (mesyl)
m/z	mass-to-charge ratio
NBS	*N*-bromosuccinimide
nm	nanometer(s)
nM	nanomolar
NMO	N-methylmorpholine N-oxide
NMR	nuclear magnetic resonance
nOe	nuclear Overhauser effect
NOESY	nuclear Overhauser enhancement spectroscopy

o	ortho
[O]	oxidation
OMe	methoxy
p	*para*
PCC	pyridinium chlorochromate
Ph	phenyl
pH	hydrogen ion concentration in aqueous solution
PhH	benzene
PhMe	toluene
pin	pinacol
pKa	acid dissociation constant
pm	picometer(s)
PMB	*para*-methoxybenzyl
ppm	parts per million
PPTS	pyridinium para-toluenesulfonate
Pr	propyl
*i*Pr	*iso*-propyl
*n*Pr	propyl or *norm*-propyl
psi	pounds per square inch
pyr	pyridine
q	quartet
quant.	quantitative
R	generic group

R	rectus
RCM	ring-closing metathesis
ref	reference
R_f	retention factor
rgt.	reagent
rr	regioisomeric ratio
rt	room temperature
sat.	saturated
s	singlet or seconds
S	sinister
SAR	structure-activity relationship
SFC	supercritical fluid chromatography
t	triplet
TBACl	tetra-N-butylammonium chloride
TBAF	tetra-N-butylammonium fluoride
TBAI	tetra-N-butylammonium iodide
TBS	*tert*-butyldimethylsilyl
Tf	trifluoromethanesulfonyl
TFA	trifluoroacetic acid
THF	tetrahydrofuran
TLC	thin layer chromatography
TMS	trimethylsilyl
TOF	time-of-flight

Tol	tolyl
trans	on the opposite side
Ts	*para*-toluenesulfonyl (tosyl)
UV	ultraviolet
vide infra	see below
vide supra	see above
w/v	weight per volume
X	anionic ligand or halide
xs	excess
Z	cis (zusammen) olefin geometry

Chapter 1

A Pyridine Dearomatization Approach to the Matrine-type Lupin Alkaloids[†]

1.1 INTRODUCTION: LUPIN ALKALOIDS

Lupin alkaloids are a structurally versatile class of natural products which have gathered significant interest due to their rich bioactivity that includes cytotoxic, antiviral, antimicrobial and insecticidal properties and their applications in synthetic organic chemistry.[2–5] Frequently found in Fabaceae (or legumeous plants) family, the alkaloids are especially present in many plants of the Lupinus genus, from which their name is derived and almost 400 naturally occurring lupin alkaloids have been isolated to this date.[2,6]

Structurally, these compounds are classified as quinolizidine alkaloids which are characterized by the presence of a 1-azabicyclo[4.4.0]decane moiety (see Figure 1.2). A common classification, based on the number of rings, divides lupine alkaloids into bicyclic (lupinine (**1**)), tricyclic alkaloids (angustifoline (**2**)), and tetracyclic compounds (sparteine (**3**) and matrine (**4**)), the matrine/sparteine-type subclass (Figure 1.1).[3] The latter contains the well-known compound sparteine (**2**) which has been shown to have interesting

---

[†]Portions of this chapter have been reproduced from a published manuscript.[1] [†] National Institutes of Health (NIH) (F32 to A. T.). S.E.R. acknowledges financial support from the NIH (R35GM118191), and K. N. H.acknowledges the National Science Foundation (CHE-1764328).

bioactivity (*e.g.* as antiarrythmic agent) and it is frequently employed as a useful auxiliary in asymmetric reactions, *i.e.* to facilitate asymmetric deprotonations in combination with alkyl lithium bases.[5,7,8] Another member of this class, Matrine (**4**) and its *N*-oxide oxymatrine, exhibit rich pharmacological activity, including potency against notoriously difficult-to-treat diseases such as cancer and neurological conditions.[9–11]

Figure 1.1: *Selected lupine alkaloids.*

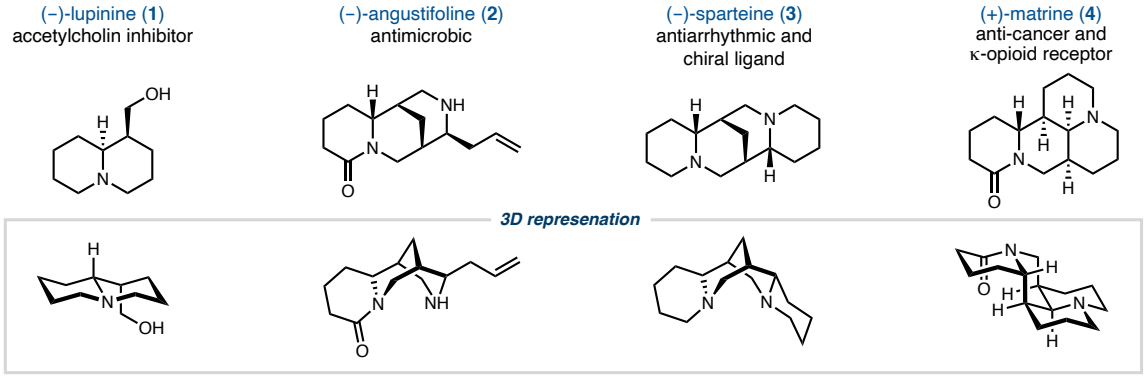

Matrine (**4**) is a lupine alkaloid isolated from *Sophora flavescens* and the main compound found in the traditional Chinese medicine Kushen which has been put into clinical application in the treatment of lung, breast and various other types of cancer.[10,12,13] It's rich bioactivity has also elevated it to a desirable target for total synthesis[14–19], and previous approaches have relied mostly on the sequential build-up of the tetracycle; In contrast, we anticipated that a bio-inspired strategy which mimics the biosynthetic condensation of Δ^1-piperidine units, could enable rapid formation of the tetracyclic core from a simple precursor such as pyridine. A dearomative cyclization strategy was envisioned to enable a rapid complexity-gaining annulation and facilitate the formation of the tetracyclic core in just one step from simple stockfeed chemicals. To undergird our

efforts to explore this approach in the total synthesis of matrine and related compounds, the following sections will discuss the key structural and biological considerations of matrine and its derivatives.

1.1.1 Structural Variety and Biosynthesis

Figure 1.2: *Subclasses of lupine alkaloids.*

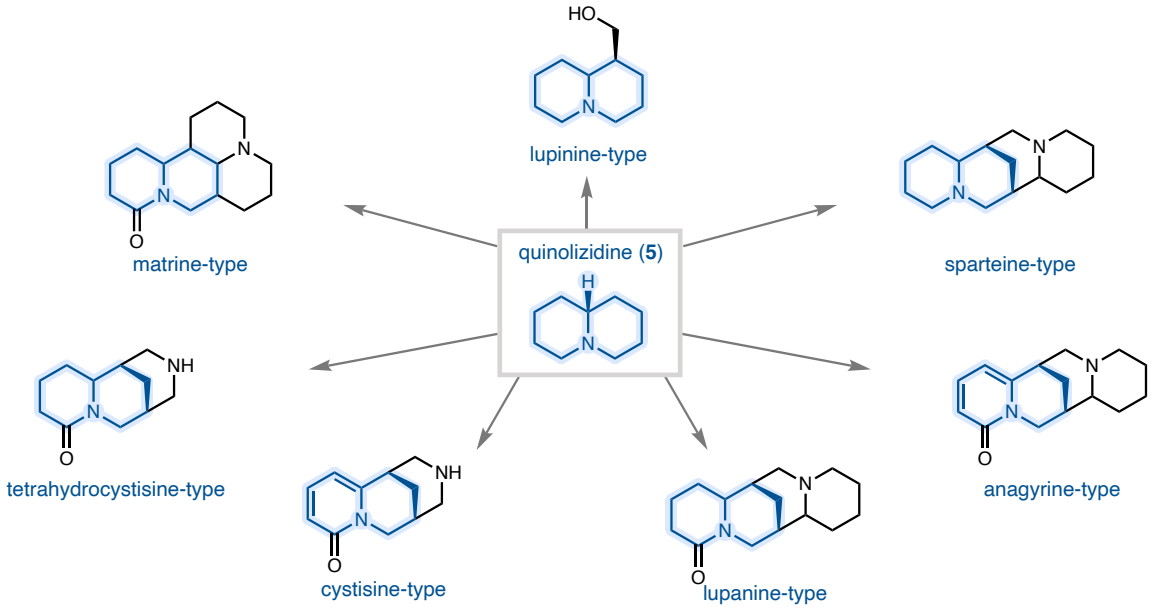

Structurally, lupine natural products are classified as quinolizidine alkaloids which are characterized by the presence of one or more 1-azabicyclo[4.4.0]decane bicycles (see Figure 1.2, quinolizidine (**5**)). Seven major categories are known; Bicyclic lupinine-type and bridged tricyclic (tetrahydro-)cysteine-type alkaloids possess one quinolizidine unit, while the tetracyclic types contain two such subunits. Further classification of the tetracyclic types into bridged (i.e. lupanine-type and sparteine-type) and fused, places

matrine into the latter category. Matrine-type alkaloids are the most frequently isolated – especially from the *Sophora* genus which constitutes about 96% of reports – and over 50 compounds have been isolated accounting for about 13.6% of reported quinolizidine alkaloids.[2,20]

Figure 1.3: *Matrine-type lupin alkaloids.*

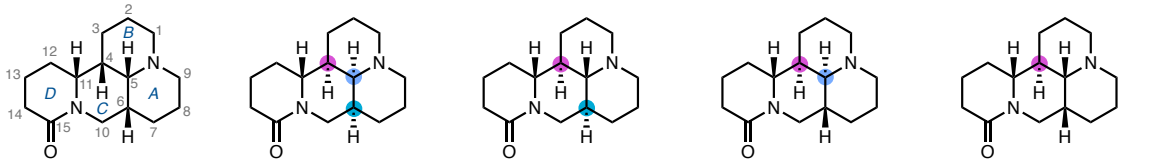

Structurally, they consist of two condensed quinolizidine motifs and their 6/6/6/6 diazatetracyclic core forms a non-linear, fused bisquinolizidine which possesses four continuous stereogenic centers.[2] Isomers, which result from differences in the relative configuration of these chiral centers, can also be isolated from natural sources; Isomatrine (**6**), allomatrine (**7**), sophoridine (**8**) and isosophoridine (**9**) only differ in the configuration of one or two stereocenters and share matrines intriguing bioactivity as evidenced *i.e.* by sophoridines application as approved chemotherapeutic in China.[21] Besides isomers, unsaturated derivatives specifically with double bonds in the D-ring and various substitution patterns have been reported for matrine-type alkaloids. *N*-oxidation, as found in oxymatrine is also a relatively common structural modification.[2]

Although the detailed enzymatic pathway has not been fully annotated, the biosynthesis of matrine is proposed to initiate with the enzymatic conversion of (–)-lysine (**10**) to Δ^1-piperidine (**17**). After oxidative decarboxylation mediated by lysine

decarboxylase, cadaverine (**11**) is obtained, which can be oxidized and eventually yield Δ^1-piperidine iminium ion **13** upon Schiff base formation.[22–24] Addition of a Δ^2-piperidine unit (**14**), is followed by a sequence of hydrolysis, oxidative amination and re-cyclization to give quinolizidine aldehyde **16**, a common precursor for several lupine-type alkaloids.

***Figure 1.4**: Biosynthesis of the lupine alkaloids.*

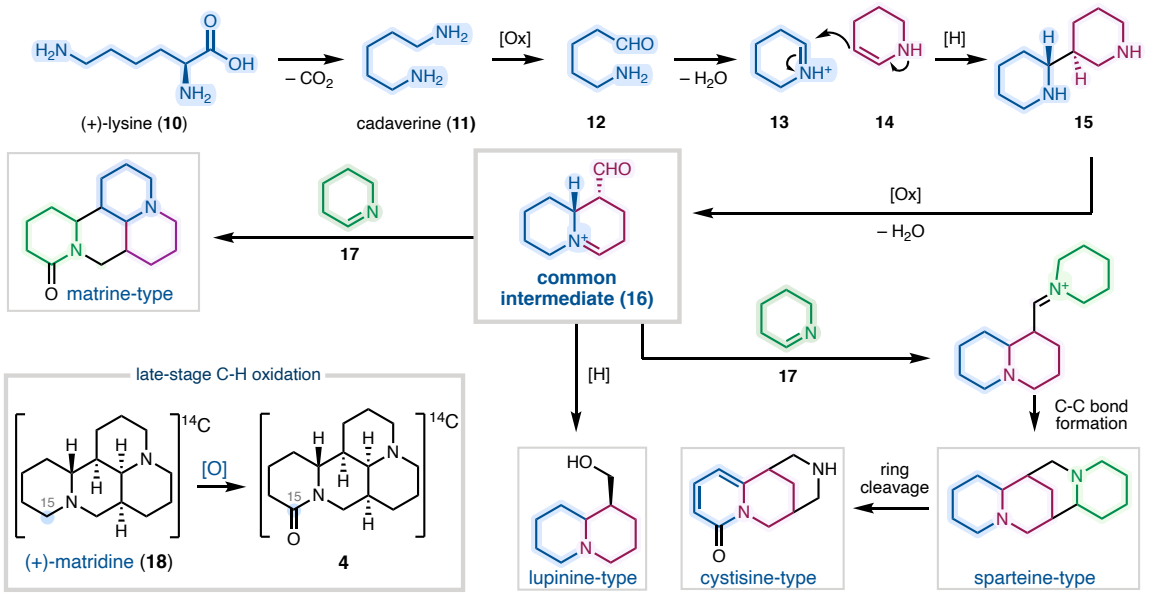

Lupinine-type alkaloids can be directly derived from this precursor, and addition of another Δ^1-piperidine equivalent leads to the formation of the tetracyclic core for the sparteine- and matrine-types.[25,26] The tricyclic lupine alkaloids are derived from the tetracyclic precursors by subsequent ring cleavage. Late-stage functionalization of the undecorated skeletons has been shown operative to further diverge the core structures into the broad array of compounds belonging to the lupine alkaloids. Seminal studies by Abdusalamov for example demonstrated that feeding ^{14}C-labeled (+)-**18** to *Goebelia Pachycarpa* resulted in the isolation of radio-labelled (+)-**4**, suggesting that the final step

in the biosynthesis of **4** is a site-selective C–H oxidation.[26,27]

1.1.2 Bioactivity and Medicinal Properties

Quinolizidine alkaloids exhibit a range of biological activities which enable their broad use as therapeutics in various applications and are covered multiple reviews.[2,9,10,28] A recent chemoinformatic analysis of their physicochemical profile — specifically, properties that determine absorption, distribution, and bioavailability, collectively referred to as "drug-likeness", revealed that 62.7% exhibit favorable profiles for the use as pharmaceuticals. The highest-scoring clusters included the matrine-, and the monoamides of sparteine (lupanine-type), many of which contain a (3-hydroxy)piperidin-2-one substructure — a feature associated with drug-like behavior. Most compounds also showed hydrophilicity and solubility values (*c*LogP and *c*LogS) within ranges typical of approved drugs, supported by the presence of several hydrogen bond acceptors per molecule. While some subclasses — like dimeric quinolizidine alkaloids and alkenyl-substituted lupinines—exhibited poor drug-likeness scores, they were in the minority. These findings support the notion that quinolizidine alkaloids are not only biologically active but also chemically well-positioned for drug development. Their favorable profiles, combined with rich structural diversity and bioactivity, make them valuable scaffolds for further exploration through synthetic modification and medicinal chemistry efforts. Matrine-type alkaloids are primarily known for their cytotoxic and anticancer properties, while lupanine- and sparteine-types have shown insecticidal and antimicrobial activity.[29–32] Cytisine- and tetrahydrocytisine-type lupine alkaloids possess both cytotoxic and antiviral effects, and

lupinine- and macrocyclic-type compounds have demonstrated antiviral and anticancer potential.[33–35]

Figure 1.4: *Summary of signal pathways and diseases related to the actions of matrine* ***4****. Adapted from Guo et. al.*[10]

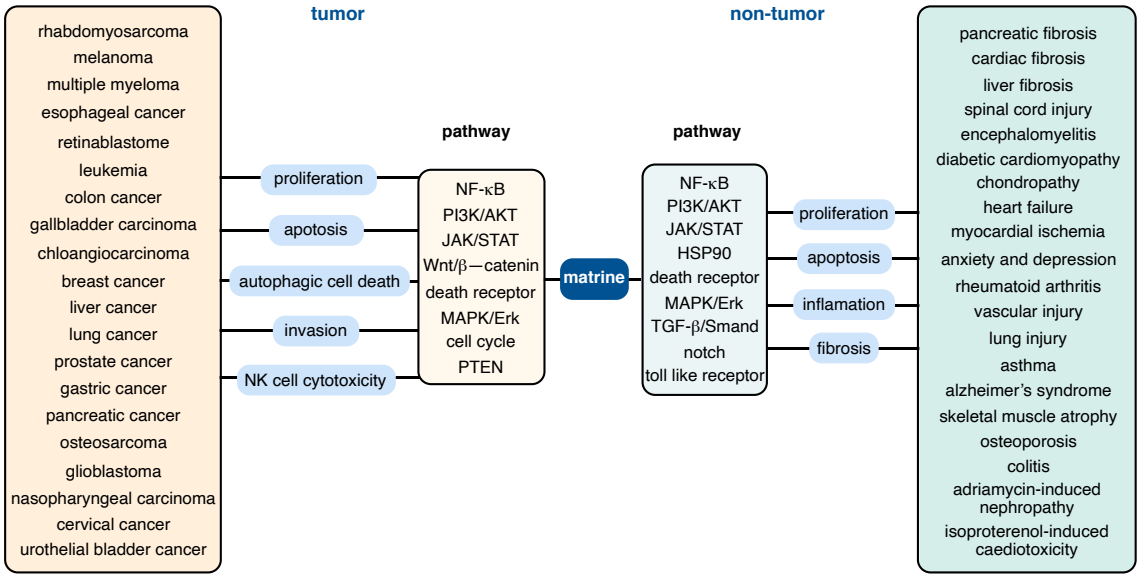

Among these, matrine-type alkaloids are considered the most biologically active, displaying various pharmacological effects, including antitumor, antiviral, and anti-inflammatory effects (Figure 1.4).[36] Their anticancer activity is particularly well established. Matrine induces apoptosis and inhibits proliferation in multiple cancer cell types, including lung, liver, cervical, and melanoma, often through modulation of the PI3K/AKT, MAPK, and NF-κB pathways.[10,37,38] For example, matrine suppressed melanoma cell growth by increasing levels of PTEN, a tumor suppressor that helps regulate cell survival, and by blocking PI3K signaling, a pathway commonly overactive in cancer that promotes uncontrolled growth.[39] Similar growth-inhibitory and cell death–inducing

effects have been observed in esophageal cancer cells through the generation of reactive oxygen species (ROS), which cause cellular damage, and through disruption of mitochondrial function.[40] In cervical cancer cells, matrine exerts its effects by inhibiting the p38 and AKT pathways, both of which help cancer cells resist stress and avoid programmed cell death.[41]

In the nervous system, matrine shows promise for treating Alzheimer's disease by preventing the buildup of amyloid-beta plaques — protein aggregates that disrupt brain function — and by modulating the RAGE signaling pathway, which is involved in inflammation and neurodegeneration. In APP/PS1 transgenic mice, which are genetically modified to develop Alzheimer-like symptoms, matrine improved cognitive performance and reduced inflammation in the brain.[11] It also enhanced learning and memory in rats injected with amyloid-beta ($A_{\beta 1}$-42) by restoring the balance between Th17 and Treg cytokines—two immune signaling pathways that influence neuroinflammation. [42]

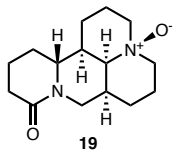

19

Figure 1.5: *Oxymatrine.*

Matrine can also protect the cardiorespiratory system. It reduces airway inflammation in both airway cells and asthmatic mice by blocking NF-κB signaling and lowering levels of the inflammation-related protein cytokine signaling 3 (SOCS3). In asthma models, it also helps improve breathing by reducing airway hyperresponsiveness, limiting mucus-producing cell growth, and decreasing the number of inflammatory cells in the lungs.[10,43] In rats with heart injury caused by restricted and restored blood flow, it activated the JAK2/STAT3 pathway, increased levels of the protective protein HSP70, and reduced cell death in small blood vessels of the heart.[44] In autoimmune conditions like

rheumatoid arthritis, matrine reduced the growth of synoviocytes—cells that contribute to joint inflammation—and triggered their death by suppressing the JAK/STAT pathway.[45] It also helped restore immune balance by inhibiting NF-κB, decreasing proinflammatory cytokines like TNF-α and IFN-γ, and increasing anti-inflammatory cytokines such as IL-4 and IL-10.[46]

Matrines *N*-oxide, oxymatrine (**19**) helps improve memory in Alzheimer's disease models by reducing brain inflammation and blocking harmful proteins like amyloid-beta (Figure 1.5).[9,47,48] Oxymatrine can also extends lifespan of mice suffering from ALS and reduces seizures and brain damage in epilepsy by balancing brain chemicals and lowering inflammation.[9,49]

The C6 epimer of matrine, (–)-sophoridine (**8**) is an approved chemotherapeutic in China, which has also demonstrated antibiotic activity.[4] In lung cancer, it boosts tumor-suppressing proteins like p53 and makes chemotherapy more effective.[50] It slows pancreatic tumor growth by triggering cancer cell death and blocking inflammation.[51] In gastric and colon cancers, it helps the immune system fight tumors and reduces their ability to grow and spread.[52,53] Little is known about the pharmacological properties of other isomers such as (+)-isomatrine (**6**) and (+)-isosophoridine (**9**), which likely reflects their limited accessibility from commercial vendors.[5]

1.1.3 Previous Synthetic Studies

Figure 1.6: *Mandell's synthesis of matrine (1965).*

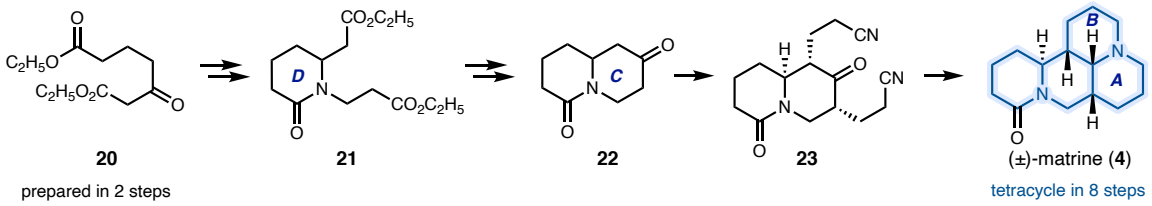

Lupine alkaloids have also been targets for total synthesis and to date four total syntheses of matrine (**4**) have been reported. The first synthesis was completed by Mandell and coworkers in 1965 (Figure 1.6).[15] Diester **20** could be prepared in two steps and was elaborated to bicycle **22** via alanine condensation, hydrogenation, formation of the C ring by Dieckman cyclization and subsequent decarboxylation in four steps. Biscyanoethylation with acrylonitrile gave dinitrile **23** which underwent spontaneous cyclization to forge the remaining A and B ring yielding matrine upon hydrogenation. The synthesis of the tetracyclic framework and the natural product matrine was completed in eight steps total.

Figure 1.7*: Tsuda's synthesis of (+)-matrine (1966).*

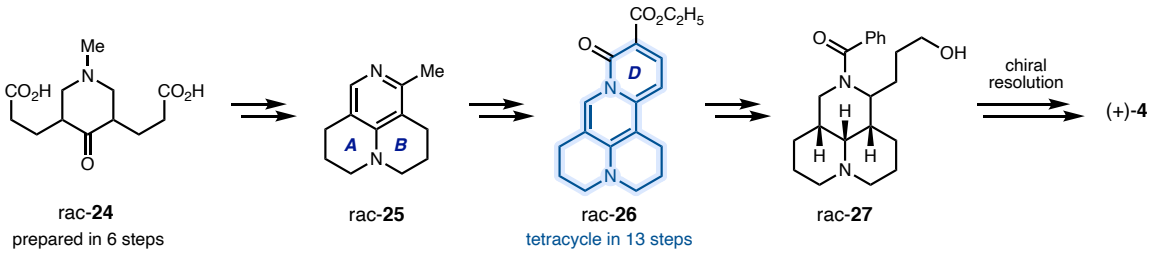

In 1966 Tsuda and coworkers completed the first and only synthesis of (+)-matrine ((+)-**4**) by employing a classic resolution to access a chiral intermediate (Figure 1.7).[16,17,54] Diacid rac-**24** was accessed in six steps and advanced to tetracycle **26** in a total of 13 steps

utilizing subsequential annulative condensations. Reductive opening of the D ring gave rac-**27** and was followed by a classic resolution to access enantioenriched alcohol **27**. Subsequent chromium trioxide oxidation followed by cyclization in acetic acid then gave (+)-matrine in a total of 21 steps.

***Figure 1.8**: Chen's synthesis of matrine (1986).*

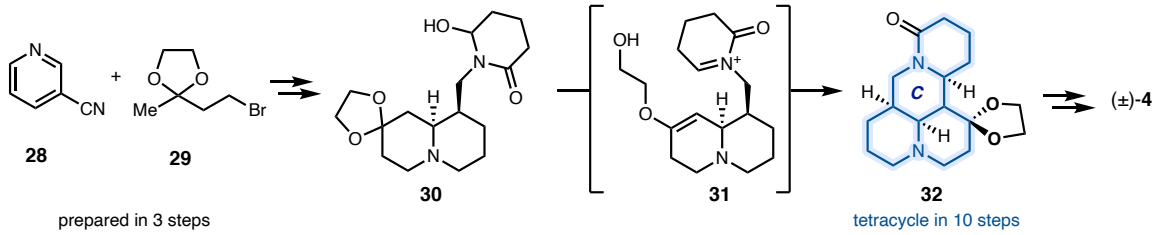

A biomimetic synthesis was reported by Chen and coworkers in 1986 which featured a Mannich-cyclization to form the C ring (Figure 1.8).[18] Quinolizidine **30** was accessed from nicotinonitrile **28** in 7 steps. Subsequent deacetylation under acidic conditions gave an enol iminium ion intermediate **31** which could undergo cyclization to forge the C ring and give tetracycle **32** in 10 steps. Four steps were required to remove the ketal and yield (±)-matrine (**4**) in a total of 14 steps.

***Figure 1.9:** Zard's synthesis of matrine (1998).*

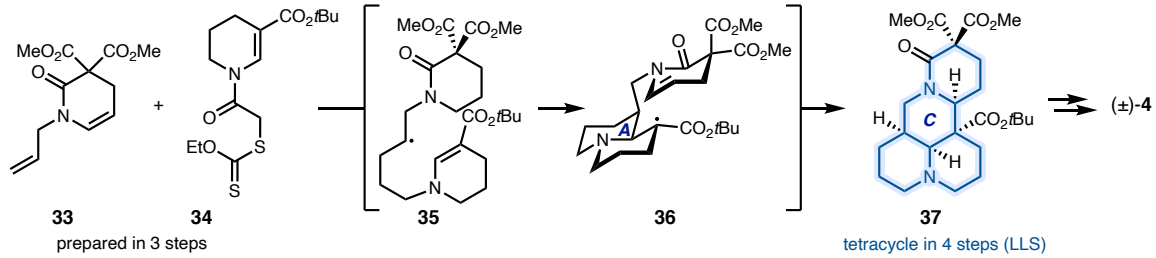

Zard and coworkers in 1998 employed a radical cascade to simultaneously construct the A and C ring (Figure 1.9).[14] Xanthate ester **34** and allylamine **33** were prepared in three steps each and could undergo radical cyclization to yield tetracycle **37**.

The tetracyclic matrine framework was obtained in a total of four steps, benchmarking the most efficient route to the tetracycle prior to our report. Removal of the ester groups, which were required to enable the radical cyclization strategy, was achieved in five steps yielding (±)-matrine (**4**) in nine steps total.

Concurrent with the publication of our synthetic approach, Sherburn and coworkers have published a divergent strategy towards matrine (**4**), isomatrine (**6**) and allomatrine (**7**) featuring two hetero intramolecular Diels-Alder reactions (hetero-IMDA) to forge the tetracycle.[19] After the synthesis of acyclic dendralene **38**, treatment with TFA initiated a hetero-IMDA forming the D and C-ring and yielding bicycle **39**. Treatment with TFA, followed by the addition of formaldehyde triggered another hetero-IMDA which completed the tetracycle and gave alkene **41**. In analogy to our approach, late-stage hydrogenation led to isomerization as previously reported by Okuda,[55] to yield matrine (**4**), isomatrine (**6**) and allomatrine (**7**).

***Figure 1.10**: Sherburn's synthesis of matrine (**4**), isomatrine (**6**) and allomatrine (**7**) (2022).*

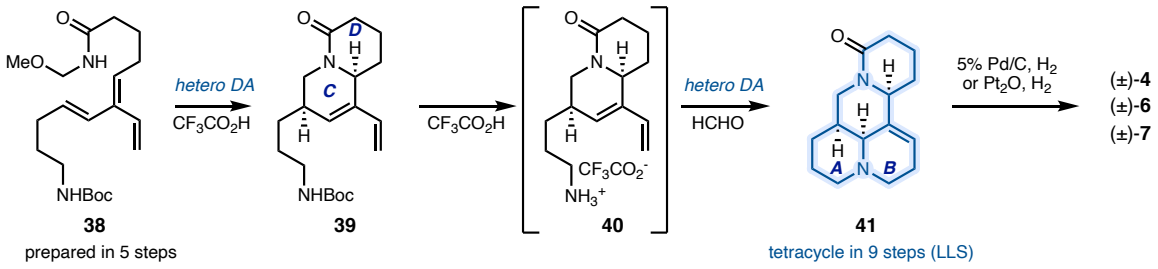

Synthetically, most of the work prior to 2022 had focused on matrine (**2**), and synthetic access to the minor congeners is far more limited: until Sherburn's concurrent report a single total synthesis each of allomatrine (**3**) and isosophoridine (**5**), and no total

syntheses of isomatrine or sophoridine (**4**) were reported.[17,18]

1.2 CONCEPTUAL DESIGN AND RETROSYNTHESIS

Inspired by the proposed biosynthesis, we envisioned that pyridine (**46**) could serve as a stable, inexpensive synthon for Δ^1-piperidine (**17**), and the remaining five carbons of the tetracyclic matrine framework could derive from glutaryl chloride (**47**, Fig. 1.11B).

Figure 1.11: *(A) Proposed biosynthesis of matrine (**4**). (B) Retrosynthetic analysis of isomatrine (**6**). (C) Late-stage isomerization to access matrine (**4**), allomatrine (**7**), sophoridine (**8**) and isosophoridine (**9**).*

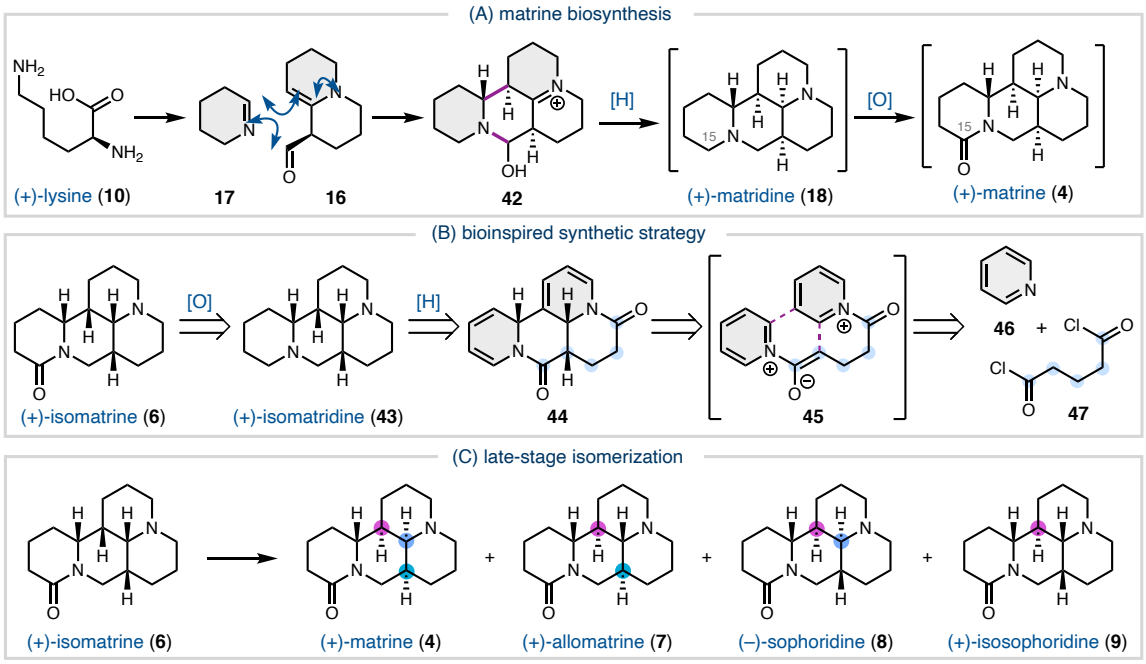

In the key step, we proposed a dearomative annulation via bis-acyl pyridinium salt **45** to form tetracycle **44**, a molecule that contains all the carbon and nitrogen atoms of **4**.[19]

Tetracycle **44** could be elaborated to **6** by global reduction followed by a site-selective oxidation of isomatridine **43**) reminiscent of the proposed biosynthesis of matrine (**4**).

Isomatrine (**6**) is the least thermodynamically stable lupin alkaloid and its isomerization to both matrine (**4)** and allomatrine (**7)** has been previously reported and was also deployed in the 2022 Sherburn synthesis of several matrine alkaloids.[16,20] We therefore anticipated that access to **6** could enable the synthesis of additional lupin alkaloids.[21] In contrast to previous syntheses that construct the tetracyclic framework in a linear, stepwise manner, this approach enables the early generation of molecular complexity and provides streamlined access to the core carbocyclic structure of matrine-type alkaloids — an intermediate that could be valuable beyond natural product synthesis, *i.e.* as starting point for SAR studies.

1.3 DEAROMATIVE PYRIDINE CYCLIZATION

1.3.1 Tetracycle Formation

Figure 1.12: *Diastereoselective pyridine dearomatization with glutaryl chloride.*

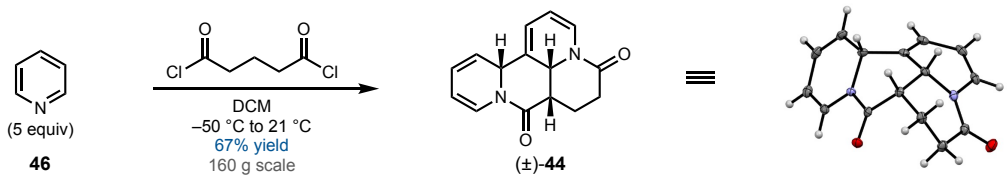

Our studies commenced with the investigation of the dearomative annulation (Figure 1.12). Addition of glutaryl chloride (**47**) to pyridine (**46**) in dichloromethane at –50 °C followed by warming to 21 °C resulted in clean formation of a (±)-tetracycle **44** in 62% yield and as a single diastereomer (10 g scale). The reaction was highly robust and

could be carried out on one mole scale to produce over 160 grams (67% yield) of (±)-tetracycle **44** in a single batch. The product was isolated by precipitation from the crude reaction mixture, alleviating the need for a workup or column chromatography. Given the cost of pyridine ($7/mol), glutaryl chloride ($211/mol), and all solvents ($31/mol), the raw materials cost $398/mol of product formed.[56] Recrystallization of (±)-**44** enabled single crystal X-ray diffraction, which confirmed the *syn-syn* relative stereochemistry.

1.3.2 Mechanistic Investigation

To elucidate the reaction pathway, mechanistic and computational studies were undertaken. Monitoring the reaction between glutaryl chloride **47** and pyridine **46** by ^{1}H NMR determined that the major species at –40 °C was bis-acyl pyridinium salt **48** (Figure 1.13). After warming to 25 °C, acid chloride **49** resulting from mono-cyclization was observed. Presumably the acyl pyridinium salt **Int1a** and acyl chloride **49** are in equilibrium, but the acyl chloride is the major species at 25 °C. A second, minor species assigned as the acid chloride resulting from **Int1b** (*vide infra*) was also observed; this species was consumed as the reaction progressed to full conversion. Although deprotonation of acyl pyridinium salts or acyl chlorides can give rise to ketene intermediates,[57] no such species was detected by ^{1}H NMR or by reactIR. Attempts to calculate a pathway involving ketene intermediates failed to locate a transition state (TS) for a concerted [2+2] cycloaddition. Similarly, no TS for the concerted [4+2] cycloaddition of bis-acyl pyridinium salt **45** could be located. Investigation of a stepwise pathway determined that the lowest-energy TS for the first cyclization involves a boat-like conformation to form the *syn* product (**TS1a**, ΔG_{TS} = 7.3 kcal/mol) (Figure 1.14). Attempts

to find the analogous chair-like TS were unsuccessful and led instead to conversion to the boat-like TS. The pathways leading to the *anti* mono-cyclization product (**Int1b**) are higher in energy (see **TS1b** and **TS1c**). The preference for the *syn* boat compared to the *anti* boat TS is likely due to favorable dispersive interactions between the heteroaryl ring and the oxygen-bearing carbon of the enolate, as well as minimization of the dipole moment in the *syn* TS.

Figure 1.13: *Proposed mechanism for the diastereoselective cyclization.*

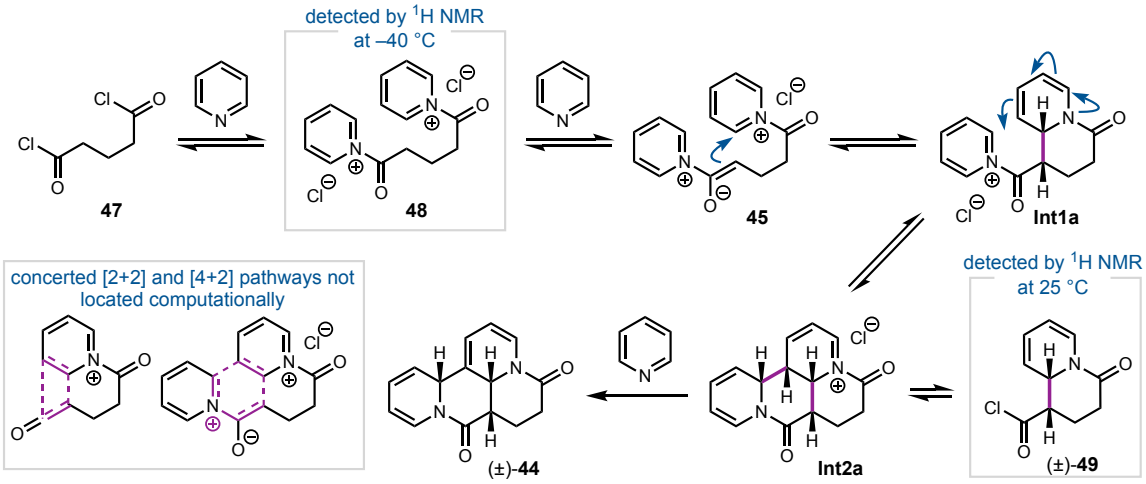

To test the importance of dispersive interactions in these TSs, the TSs were recomputed with B3LYP, a functional known to lack dispersion. Indeed, with this functional, the difference between the two transition states was only 0.1 kcal/mol. Inclusion of dispersion with Grimme's D3 correction restored the energy difference to 1.4 kcal/mol in favor of the *syn* boat transition state. These TSs lead to two intermediates: *syn* intermediate **Int1a** (–12.6 kcal/mol) and *anti* intermediate **Int1b** (–10.7 kcal/mol). The TS for the second C–C bond formation (**TS2a**) is most favorable for the *syn-syn* inter-mediate (**Int2a**), with a barrier of 20.2 kcal/mol. The second lowest-energy pathway proceeds via

TS2b leading to **Int2b**, which gives rise to the *anti-syn-anti* configuration at the ring fusions. The transition states leading to the other four potential diastereomers are higher in energy.

Figure 1.14: *Reaction coordinate diagram.*

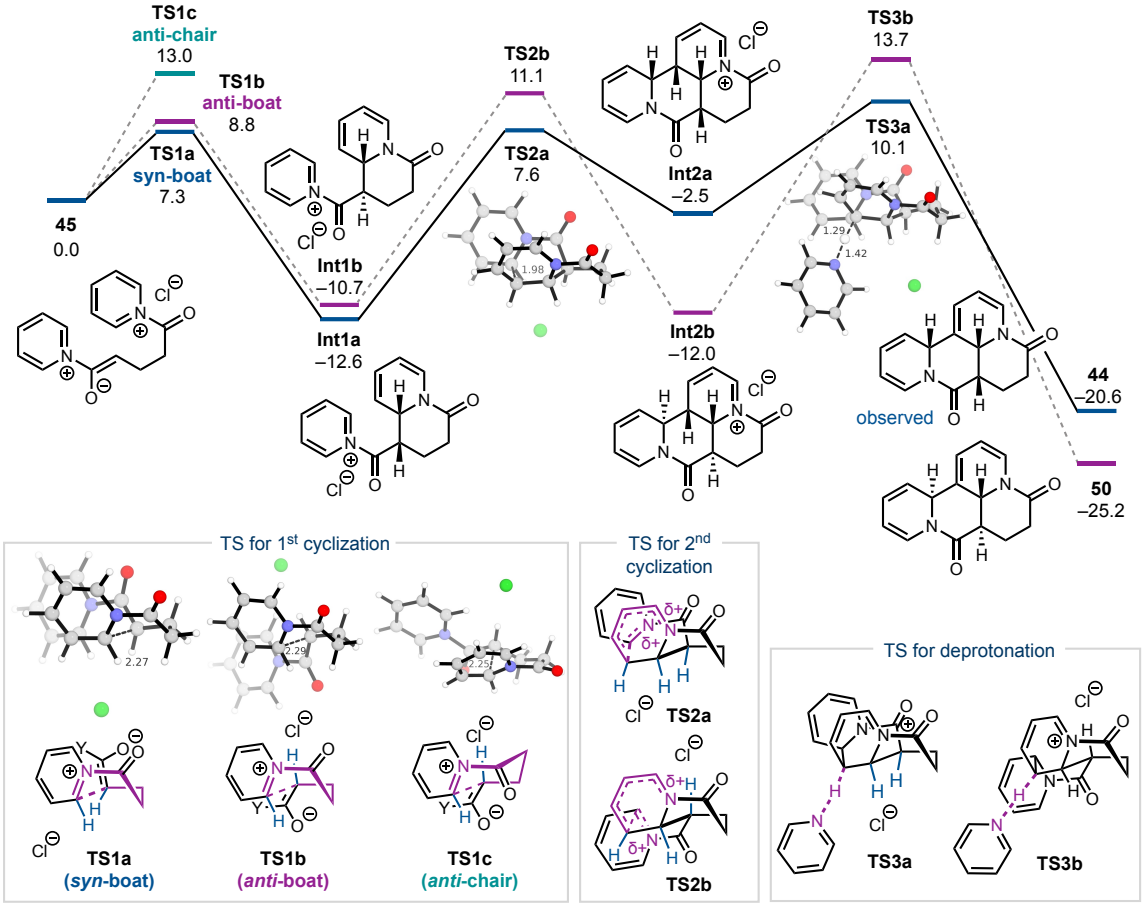

Formation of **Int2a** and **Int2b** is followed by deprotonation by pyridine. While **Int2b** is lower in energy than **Int2a**, the deprotonation of **Int2a** to give *syn-syn* (±)-**44** follows the lowest-energy pathway. Thus, the selectivity-determining step is the final deprotonation (**TS3a**) and *syn-syn* (±)-**44** is favored, even though it is thermodynamically less stable than *anti-anti* **50**. These results are consistent with the experimentally observed

formation of product (±)-**44** as a single diastereomer, despite the initial mixture of monocyclization products.

1.3.3 Studies on the Enantioselective Cyclization

Attempts to induce enantioselectivity in the cyclization reaction between pyridine and glutaryl chloride were unsuccessful. A range of additives—including PyBOX ligands, chiral bases, and anion-binding catalysts—were evaluated, but none had a discernible effect on the reaction outcome. When enantiopure (R)-2-methylpentandioyl chloride (**52**) was employed, C3-methyl tetracycle (+)-**51** was obtained in 66% yield as a single diastereomer and in >99% *ee* (Figure 1.15). This stereochemical outcome is consistent with the calculations, where the pathway initiating with a *syn* boat transition state bearing the methyl group in a pseudo-equatorial position is favored. When (S)-2-phthaloyl glutaryl chloride **53** was used, the product was obtained with a 27% yield, but there was a significant loss of enantiomeric excess. Efforts to use methoxyprolinol to ring-open glutaric anhydride (**55**) *in situ*, followed by amide and carboxylic acid activation with triflic anhydride, and subsequent reduction achieved cyclization with 94% enantiomeric excess. However, despite extensive optimization, the yield of compound **56** could not be improved beyond 12%. Since classical resolution of isomatridine (**43**) (*vide infra*) gave 24% material recovery we opted for this approach.

***Figure 1.15**: Studies towards formation of an enantioenriched tetracycle.*

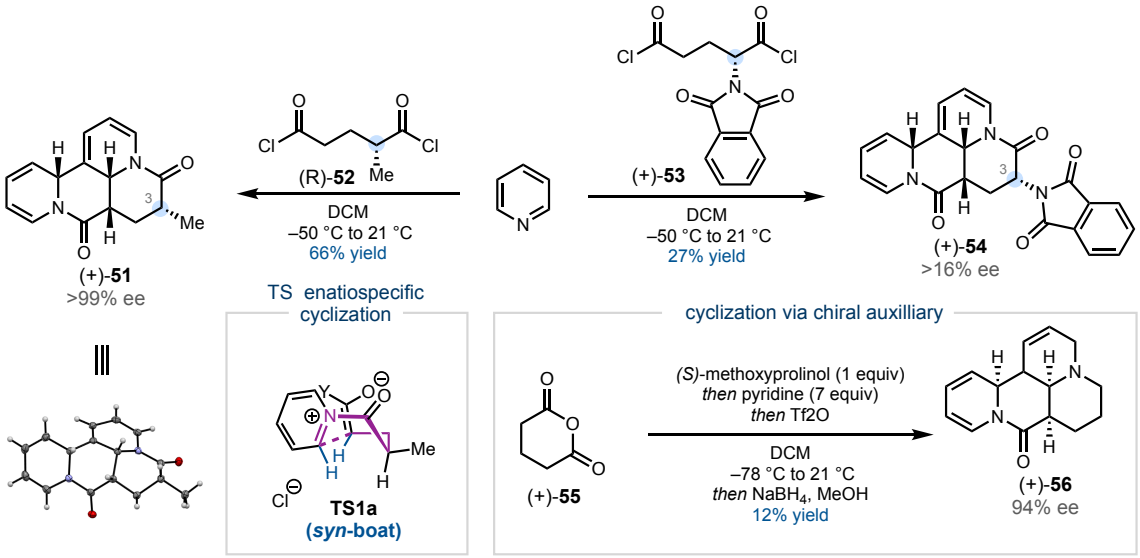

1.4 REDUCTION OF THE DIAMIDE

1.4.1 Investigations on Catalytic Reductions

Enabled by the complexity-building dearomative annulation reaction, we established access to large quantities of cyclization product **44** which enabled the investigation of the subsequent reduction to isomatridine (**43**). To access compound **43** from **44**, global hydrogenation of the alkenes and reduction of both amides to the corresponding amines were required. It was envisioned that both transformations could potentially be achieved in a one-pot global reduction to access isomatridine **43** directly from tetracycle **44**. Initially investigations found that hydrogenation of **44** with 5% Rh/C gave saturated diamide **57** cleanly in 97% yield with the desired diastereoselectivity.

***Figure 1.16**: Rh-catalyzed hydrogenation of cyclization product **57**.*

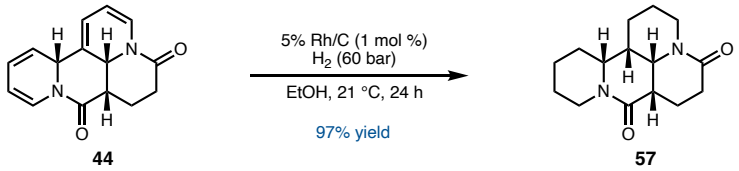

1.4.1.1 Global Reduction via Hydrogenation

Given that the alkene reduction of **44** proceeds smoothly and with the correct diastereoselectivity, concurrent amide reduction under hydrogenation conditions would be ideal. However, amide hydrogenations are generally considered challenging and usually requires high pressures and temperatures which can be only accessed with specialized set ups.[58] A recent report from Kaneda and coworkers found that a Pt/V coated hydroxy apatite (HAP) catalyst (Pt/V/HAP) was able to catalyze the hydrogenation of tertiary amines at room temperature under only 30 bar of hydrogen.[59] However, evaluation of this catalyst as well as other well-known hydrogenation catalysts under elevated temperatures did not lead to formation of significant amounts of amine **43** (Table 1.1, entry 1-5). Attempts to reduce the saturated diamide **43** using the Pt/V/hydroxyapatite catalyst gave only recovered starting material. It became obvious that amide hydrogenation would require further increase in temperatures and pressure, which led us to investigate alternative options for a global reduction protocol.

Table 1.1: *Investigation of one-pot alkene and amid hydrogenation catalysts.*

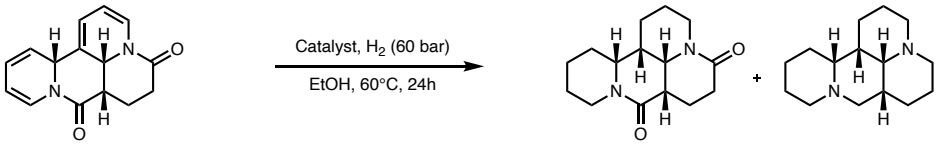

44 **57** **43**

Entry	Catalyst	% Yield 57	% Yield 43
1	5% Rh/C (10 mol%)	62	2
2	10% Pd/C (10 mol%)	91	11
3	PtO_2 (10 mol%)	66	3
4	Raney Ni (10 mol%)	0	0
5	Pt/V/hydroxyapatite[a]	66	3

[a]run in DME with 4 Å molsieves.

1.4.1.2 Silane-mediated Transition Metal-catalyzed Reductions

Transition metal-catalyzed silane reductions have been proven to be powerful reactions for the reduction of amides.[60–65] It was envisioned that similar conditions could be employed for a silane-mediated alkene reductions, therefore enabling a streamlined reduction protocol.[66]

Table 1.2: *Investigation of Ir-catalyzed silane reductions of cyclization product* ***44****.*

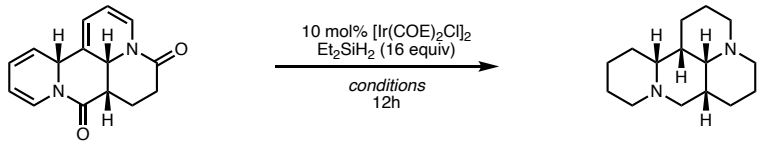

44 **43**

Entry	Conditions	Results
1	neat in silane, 21°C	complex mixture
2	DCM (0.1M), 21°C	complex mixture
3	neat in silane, 80°C	complex mixture

Initial attempts to reduce the unsaturated cyclization product **44** gave complex mixtures of the partially reduced structures which complicated the development of an

efficient assay for reaction optimization (Table 1.2). Therefore, subsequent studies focused on the reduction of saturated diamide **57**. It was found that nickel and iron[64,65] catalysts were unable to facilitate amide reduction and gave complex mixtures or decomposition (Table 1.3, entry 1 and 2). In contrast, rhodium[63] and iridium[61] catalysts gave diamine **43** in a 16% and 37% yield, respectively (Table 1.3, entry 3 and 4) and were selected for further optimization efforts. Unfortunately, neither an increase in temperature nor changing the silane identity improved the reaction outcome under rhodium catalysis (Table 1.4, entry 3). In most cases, enamine **58** was found to be the major side product.

Table 1.3: *Transition metal-catalyzed amide reductions.*

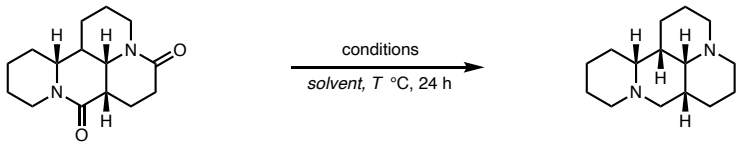

57 **43**

Entry	Conditions	% Yield
1	$NiCl_2$•dme (10 mol %), $PhSiH_3$ (4.0 equiv), toluene, 115 °C	complex mixture
2	Fe_3CO_{12} (10 mol %), PMHS (5.0 equiv), toluene, 100 °C	complex mixture
3	$HRh(PPh_3)_4$ (5 mol %), Ph_2SiH_2 (5.0 equiv), DCM, 50 °C	16
4	$[Ir(COE)_2Cl]_2$ (0.5 mol %), $PhSiH_3$ (8.0 equiv), DCM, 21 °C	4

Subsequent evaluation of iridium loadings from 0.5 to 10 mol% showed that a loading of 5 mol% $[Ir(COE)_2Cl]_2$ resulted in the best reaction profile and gave product **43** in 59% yield (Table 1.5 entry 3). As observed in the rhodium catalyzed reaction, enamine **58** was identified as major side product. Attempts to improve the reaction by raising the

temperature from 21°C to 110°C as had been previously reported did not improve the yield significantly and only lead to a more complex reaction profile (entry 6 and 7).[61]

***Table 1.4**: Investigation of the rhodium-catalyzed silane reduction.*

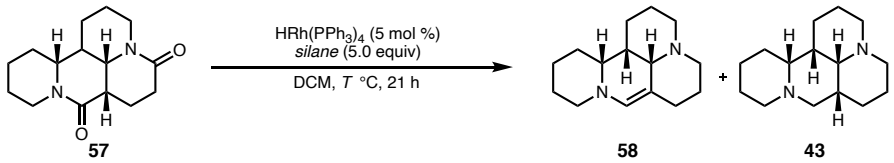

57 **58** **43**

Entry	Silane	Temperature	% Yield 58	% Yield 43	Ratio 58 : 43
1	Ph_2SiH_2	20 °C	0	0	/
2	Ph_2SiH_2	50 °C	46	16	2.9 : 1.0
3	Ph_2SiH_2	80 °C	46	17	2.7 : 1.0
4	Ph_2SiH_2	110 °C	38	22	1.5 : 1.0
5	$PhSiH_3$	20 °C	5	18	1.0 : 3.6
6	$(EtO)_3SiH$	20 °C	0	0	/

At low iridium catalyst loadings of 0.5 mol% selective monoreduction of the C2 amide **59** was observed in 73% yield (Table 1.5, entry 1). At these lower catalyst loadings, reduction of the second amide was no longer observed. While full conversion could be achieved at higher loadings, we aimed to optimize the reaction under more efficient conditions to gain insight into the factors governing reactivity and selectivity. We hypothesized that the identity of the silane or inclusion of specific additives might restore reactivity, especially given the unexpected selectivity observed under these conditions. Increasing the silane loading from 8.0 to 70 equivalents did not increase the efficiency of the first reduction significantly or reduced the second amide (Table 1.6, entry 1–4).

Table 1.5: *Influence of the $[Ir(COE)_2Cl]_2$ loading and temperature.*

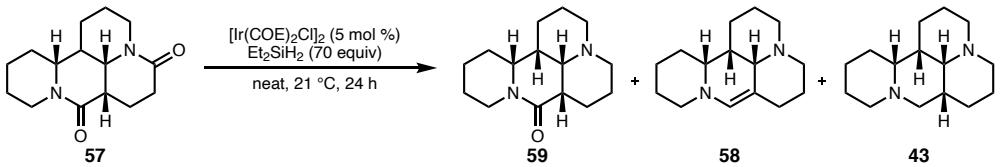

57 **59** **58** **43**

Entry	Devitation	% Yield 59	% Yield 58	% Yield 43	Ratio 58 : 43
1	0.5 mol % $[Ir(COE)_2Cl]_2$	73	2	0	/
2	1 mol % $[Ir(COE)_2Cl]_2$	0	55	37	1.5 : 1.0
3	5 mol % $[Ir(COE)_2Cl]_2$	0	43	59	1.0 : 1.4
4	7.5 mol % $[Ir(COE)_2Cl]_2$	0	64	29	2.2 : 1.0
5	10 mol % $[Ir(COE)_2Cl]_2$	0	43	40	1.1 : 1.0
6	60 °C	0	49	68[a]	1.0 : 1.4
7	110 °C	0	45	67[a]	1.0 : 1.5

[a]Inflated to to formation of unidentified product.

It was also found that neither phenyl silane, tetramethyldisiloxane (TMDS) nor polymethylhydrosiloxane (PMHS) could initiate the second reduction or outperform diethyl silane (Table 1.6, entry 5-7). Further attempts to activate the amide towards reduction by employing triflic anhydride or BF_3•Et_2O led to decomposition (entry 8-10).

While these conditions demonstrated that global amide reduction is feasible, they consistently produced significant amounts of partially reduced intermediates, such as monoamide **59** and enamine **58**. We therefore investigated alternative strategies aimed at achieving complete reduction more selectively and efficiently.

Table 1.6: *Influence of the silane loading and various silanes on the iridium-catalyzed amide reduction.*

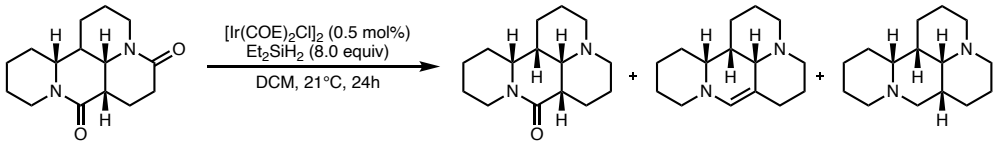

57 **59** **58** **43**

Entry	Devitation	% Yield 59	% Yield 58	% Yield 43	Comments
1	Et_2SiH_2 (8 equiv)	66	4	0	/
2	Et_2SiH_2 (16 equiv)	63	4	0	/
3	Et_2SiH_2 (32 equiv)	63	3	0	/
4	Et_2SiH_2 (70 equiv)	73	2	0	/
5	$PhSiH_3$[a]	51	0	4	/
6	TMDS[a]	0	0	0	/
7	PMHS[a]	0	0	0	/
8	Tf_2O (1.0 equiv)**	51	0	4	decomposition
9	Tf_2O, 2-Cl-pyridine	0	0	0	decomposition

[a]1 %mol $[Ir(COE)_2Cl]_2$, 70 equiv silane.
[b]run neat in Et_2SiH_2 (70 equiv).

1.4.1.3 Attempted Enamine Reductions

To mitigate issues of enamine formation, methods to reduce the enamine *in situ* were explored. Attempts to activate enamine **58** towards silane reduction using trifluoroacetic acid (TFA) or boron trifluoride etherate (BF_3•Et_2O) led to decomposition (Table 8). Employing $[Ir(COE)_2Cl]_2$ as a dual catalyst for the silane reduction and subsequent hydrogenation failed to give product (Figure 1.17, entry 4). Furthermore, a one pot silane sodium borohydride reduction reduced enamine **58**, however no increase in the yield of the desired product could be observed due to a messy reaction profile (Figure 1.17, entry 2). Reduction of isolated enamine **58** with sodium borohydride proceeded readily but predominantly yielded the undesired diastereomer **60**. The difficulty in achieving full reduction to diamine **43** prompted us to investigate the origin of the observed partial

reduction at the C17 amide, especially given that complete reduction of the C2 amide proceeds readily.

.

Figure 1.17: *Enamine reduction studies.*

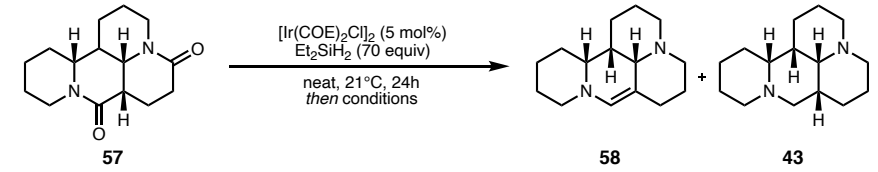

Entry	Conditions	% Yield 58	% Yield 43	Ratio 58 : 43
1	BF_3•Et_2O	0	0	/
2	TFA	35	7	5.0 : 1.0
3	$NaBH_3CN$, AcOH, MeOH	0	33	/
4	BF_3•Et_2O	0	8	/
5	rac-BINAP, H_2 (1 atm), MeOH	28	/	/

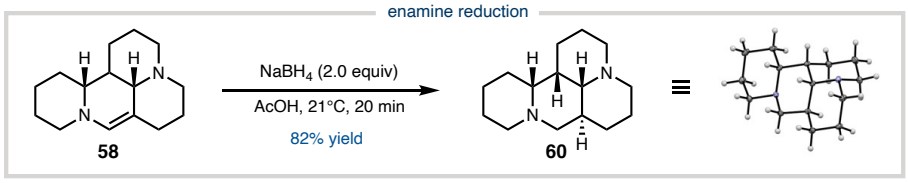

1.4.1.4 Investigations on the Observed Selectivity

Previous results had shown that reduction of diamide **57** to monoamide **59** proceeded readily in a 73% yield with loadings as low as 0.5 mol% $[Ir(COE)_2Cl]_2$ (Table 1.5, entry 4) showcasing that the first reduction is more facile than the second one. Before continuing our studies, we found that diluting the reaction mixture with toluene was preferable to using neat silane, as the starting material was not soluble in the silane alone. Performing the reaction in toluene using 8 equivalents of diethylsilane gave a 28% and 50 % yield for enamine **58** and diamine **43**, respectively (Figure 1.18, top). Furthermore, we could observe that reduction of the carbonyl at C2 proceeded smoothly to give

monoamide **59** in a 67% yield after 5 minutes with only minor formation of the C9/C8 enamine **61** (Figure 1.18, bottom).

Figure 1.18: *Reduction studies.*

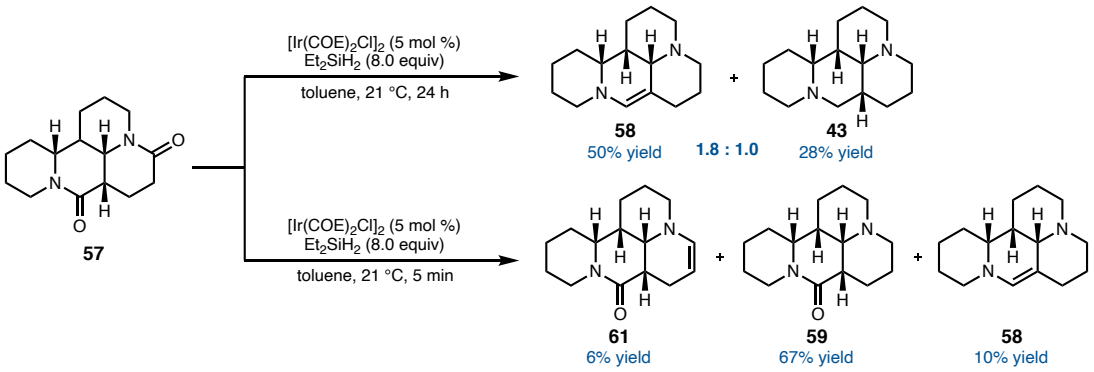

We hypothesized that successful reduction of the C2 amide generates a basic amine, and that the resulting monoamide **59** or diamine **43** could coordinate to iridium, potentially leading to catalyst poisoning. Diamine **43** was expected to be a strong ligand, as previous studies demonstrated its ability to form isolable copper and palladium complexes, highlighting its propensity to coordinate metal centers (Figure 1.19, top). However, when a 2:1 mixture of diamide **57** and diamine **43** was subjected to the reaction conditions only an insignificant decrease to a 55% and 20% yield for enamine **58** and amine **43**, respectively was observed (Figure 1.19, bottom).

Figure 1.19: *Product poisoning study.*

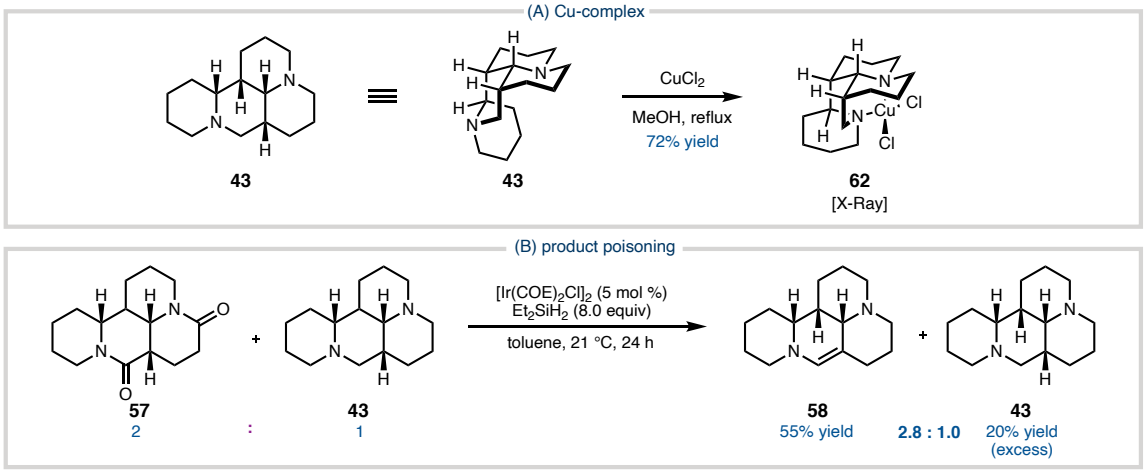

Intrigued by this result, we ought to identify if the variance in reactivity is caused by steric and electronic differences of between the two amides. To influence the reactivity, understanding of the modified Chalk-Harrod cycle which is believed to be the operative catalytic cycle for transition metal-catalyzed hydrosilations is crucial (Figure 1.20).[67] Nagashima proposed[68] that iridium-catalyzed hydrosilylations of amides to enamines (see Figure 1.21A) proceed via initial oxidative addition of the silanes Si–H bond (**64**) to the Ir-metal center (**63**) to generate an H–Ir–Si intermediate **65** (Figure 1.20). The amide carbonyl is activated by said complex and subsequent amide insertion into the Ir–Si bond gives intermediate **68**, which undergoes reductive elimination to yield the silylhemiaminal product **69**. These intermediates can eliminate silanol under thermal or acidic conditions to form an iminium ion (**70**), which can either be further reduced to the amine or undergo E1-type elimination to yield an enamine.

Figure 1.20: *Proposed mechanism (Chalk-Harrod cycle) for the transition metal-catalyzed reduction of amides.*[62]

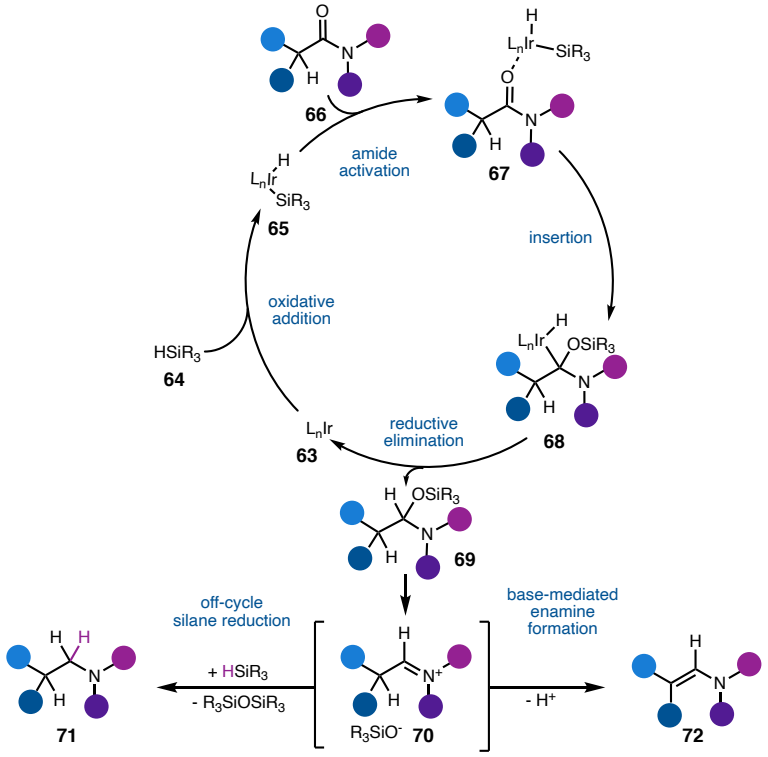

The nature of the in oxidative addition complex **65** and the amide influence the feasibility of the reduction. The amide's reactivity toward the oxidative addition complex is enhanced when the zwitterionic resonance form **66b** is favored, as this increases the partial negative charge on the oxygen atom, promoting stronger coordination to the iridium center (Figure 1.21C). *N,N*-dialkylamides, which favor such resonance form, are highly reactive and undergo efficient conversion even with less electrophilic catalysts like Vaska's complex (**74**). In contrast, amides with adjacent aryl groups favor the neutral resonance form **66a** due to delocalization of the nitrogen lone pair into the π-system, reducing their reactivity under the same conditions. For less intuitive systems the contribution the zwitterionic structure – and hence their reactivity – can be estimated by determining the

amide carbonyl stretching frequency (ν_{CO}(amide)) via IR. Due to the decreased bond order in zwitterionic resonance structure **66b**, lower ν_{CO} indicate higher contribution of the zwitterionic form and therefore enhanced activation towards reduction.

***Figure 1.21**: Mechanistic considerations. (A) Nagashima's studies on Ir-catalyzed reduction of amides to enamines.[68] (B) Carbonyl stretching frequencies (ν_{CO}) of **57** and **59**. (C) Trends in amide reactivity. (D) Reactivity regimes of Ir-catalyzed amide reductions.*

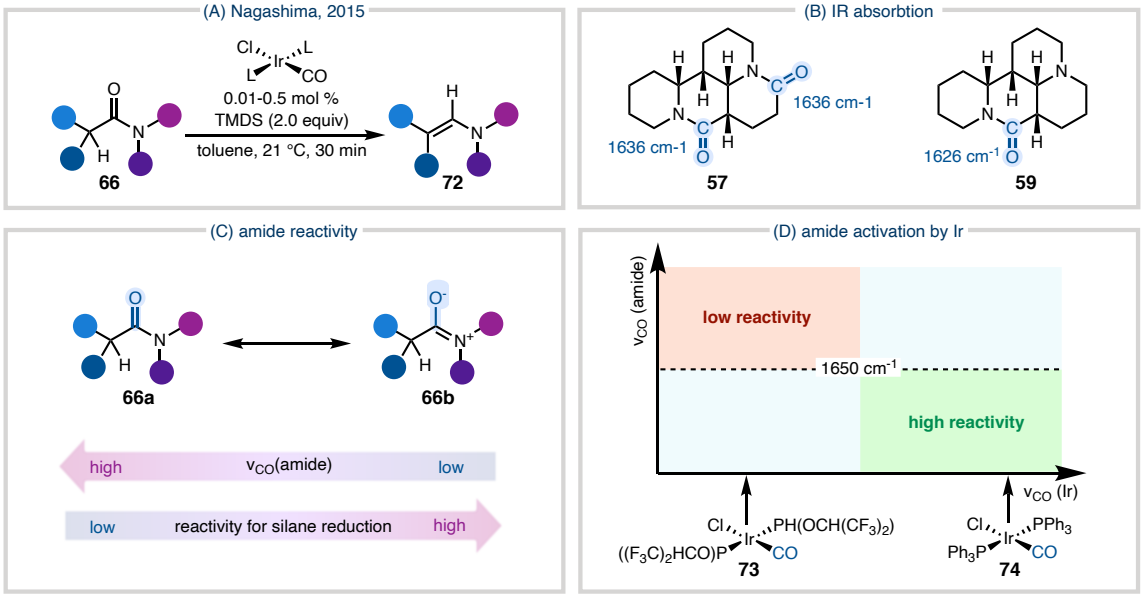

The electronics of Ir-complex **65** also affects the reaction. The Si–Ir bonds in oxidative addition complex **65** are polarized, with silicon carrying partial positive charge ($Si^{\delta+}$) and iridium partial negative charge ($Ir^{\delta-}$), due to their difference in electronegativity. In some cases, this bond can fully dissociate, generating a highly electrophilic silyl cation (R_3Si^+) and a nucleophilic iridium hydride ($[Ir–H]^-$). Electron-withdrawing phosphine ligands—such as $P(NC_4H_4)_3$, $P(OC_6F_5)_3$, and $P[O(CHCF_3)_2]_3$—stabilize the hydride and further enhance the electrophilicity of the silyl cation which activates the complex for

reduction. Mechanistic studies on the silane-mediated reduction of amides to enamines with derivatives of Vaska's complex showed that electron-deficient iridium center were more active towards amide reduction (Figure 1.21D).[62] While Nagashima studied amide reductions to the enamine, overreduction to the amine was observed when highly electron-deficient catalysts were used for the reduction of activated amides.[62]

For carbonyl Ir-complexes which are common catalysts for silane-mediated amide reductions, ν_{CO}(Ir-CO) can be used to estimate their reactivity since it inversely correlates with the electron density of the Ir-center. The degree of reduction (*i.e.* enamine vs amine) can therefore be influenced by matching the reactivity of the amide/catalyst pair which is estimated by the carbonyl stretching frequencies of the Ir-complex and amide (Figure 1.21D). Nagashima classified the pairs into high (overreduction to amine) and low reactivity regimes (no/sluggish reduction) and defined ν_{CO}(amide) of 1650 cm^{-1} as threshold for activated amides. The IR spectra of diamide **57** revealed that both carbonyls gave the same signal at 1636 cm^{-1} and were therefore considered as "activated" substrates by Nagashima's definition (Figure 1.21C).[62] Surprisingly, difficult to reduce monoamide **59** exhibits an even lower ν_{CO} of 1626 cm^{-1} which would suggest that reduction by Ir-catalysis should be even more facile.

This contrasts with the previously observed reactivity and hinted that the origin of the sluggish second reduction is potentially not grounded in the inherent reducibility of the second amide. Despite this, we anticipated a more electron-deficient catalyst should promote full reduction to diamine **43**. Replacement of triphenyl phosphine with phosphite ligands gave a more electrophilic derivative of Vaska's complex [$IrCOCl(OPPh_3)_2$] which was synthesized in 2 steps.[62] Previous results had revealed that 10 mol % Vaska's complex

(**74**) gave the diamine **43** in a 14% yield (Figure 1.22, top). As expected, the more electron rich catalyst **75** gave diamine **43** in a 31% yield and 1.0:1.4 selectivity at a lower silane and catalyst loading compared to Vaska's complex (Figure 1.22, bottom). However, **75** was not able to outperform previous results with $[Ir(COE)_2Cl]_2$.

***Figure 1.22**: Reaction of electron deficient Ir-catalysts.*

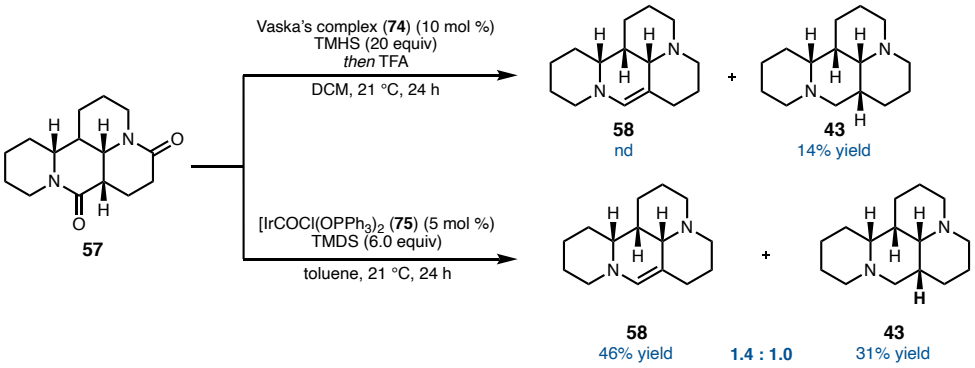

Given the inconsistency of the observed sluggish reduction of C10 amide **59** and its predicted increased reducibility we wondered if the observed enamine formation does not stem from differences in the amide activation process but rather arises from the fate of the resulting iminium ion. It has been shown that transition metal-catalyzed hydrosilane reductions of amides to amines proceeds via transition metal-catalyzed reduction to the iminium ion followed by an off-cycle reduction by silane.[61] However – if a base is present – the iminium ion could also undergo base-mediated elimination to give the enamine **42**. As the first, facile amide reduction of **57** generates a basic amine, we wondered if monoreduction product **59** could promote elimination of the iminium intermediate of the second reduction causing the undesired enamine formation.

Figure 1.23: *Reduction studies on the monoamide. (A) Reduction of the ammonium salt of monoamide* ***59****. (B) In situ formation and reduction of ammonium BF_3 salt* ***76****.*

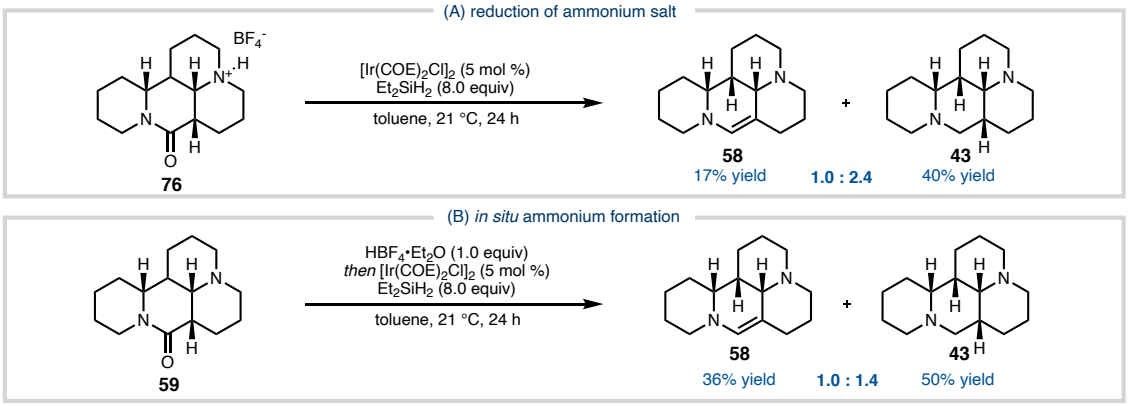

To test this hypothesis, monoamide **59** was prepared by $LiAlH_4$ reduction and reacted with HBF_4 to generate ammonium tetrafluoroborate salt **76**. Masking the basic amine as an ammonium salt was anticipated to prevent deprotonation of the iminium ion and increase the selectivity for reduction. When the ammonium salt **76** was subjected to the reaction conditions it was observed that the selectivity increased to 2.4:1.0 in favor for desired product giving diamine **29** in a 40% yield (Figure 1.23A). Pleasingly, the reaction could be performed without preformation of the conjugated acid by *in situ* preparation of the ammonium salt. Addition of HBF_4 to the reaction mixture before the catalyst was added gave diamine **29** in a 50% yield, however a reduced selectivity of 1.4:1.0 was observed (Figure 1.23B). Schreiner's thiourea catalyst **77**, which had been reported to assist iminium ion formation from hemiaminals by anion binding was evaluated, but the desired product **43** was not observed (Scheme 14A).[69]

***Figure 1.24**: Amide reduction with Schreiner's thiourea catalyst **77**.*

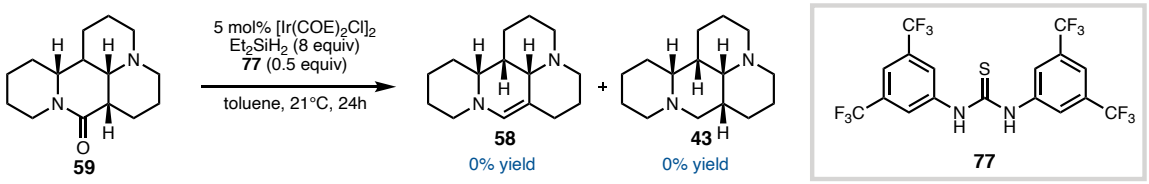

Intrigued by the increase in selectivity upon addition of acid for the reduction of monoamide **59**, the influence of acid additives on the reduction of diamide **57** was investigated. In contrast to previous results, addition of HBF_4 did not result in an improvement of the reaction but prevented the formation of diamine **43** (Table 1.7, entries 2-4). Gas evolution was observed upon addition of the acid to the reaction mixture leading to the conclusion that strong acids can quench the silane under the reaction conditions. A similar behavior was observed when the reaction was performed with AcOH and formation of the product could not be detected (Table 1.7, entries 5 and 6). It was noted that the ammonium tetrafluoroborate salt **76** performed well under the reaction conditions and thus, ammonium acids were investigated next. However, even a catalytic amount of triethylammonium chloride completely shut down reactivity (Table 1.7, entries 7 and 8). Switching the counterion to non-coordinating tetrafluoroborate suppressed the formation of enamine **58** and gave diamine **43** in a 37% yield with a 12:1.0 selectivity (Table 1.7, entry 10). While we were able to improve the selectivity of the reaction, yields were still only moderate, which prompted us to investigate alternative reduction protocols in parallel.

Table 1.7: *Influence of acid additives on the reduction of the diamide.*

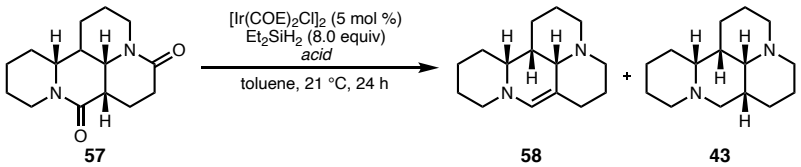

57 **58** **43**

Entry	Acid	Equivalents	% Yield 58	% Yield 43	Ratio 58 : 43
1	none	/	50	28	1.8 : 1.0
2	$HBF_4 \cdot Et_2O$	0.9	13	0	/
3	$HBF_4 \cdot Et_2O$	1.8	3	0	/
4	$HBF_4 \cdot Et_2O$	3.6	0	0	/
5	AcOH	2.0	4	0	/
6	AcOH[a]	2.0	4	0	/
7	$HNEt_3Cl$	0.2	3	0	/
8	$HNEt_3Cl$[a]	0.2	2	0	/
9	$HNEt_3BF_4$	1.0	43	39	1.1 : 1.0
10	$HNEt_3BF_4$	2.0	3	37	1.0 : 12

[a]$HRhCO(PPh_3)_3$ (5 % mol), Ph_2SiH_2 (5.0 equiv).

1.4.1.5 Investigation of Stoichiometric Reductants

Table 1.8*: Attempts towards triflic acid-mediated amid reduction.*

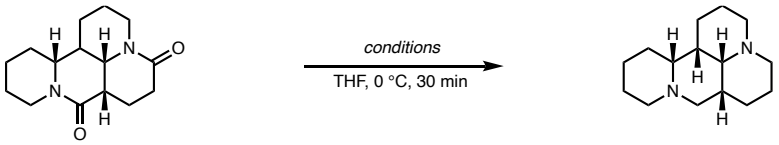

57 **43**

Entry	Conditions	Results
1	Tf_2O (2.2 equiv), then $NaBH_4$	no reaction
2	Tf_2O (2.2 equiv), $LiAlH_4$	complex mixture
3	Tf_2O (2.2 equiv), TMDS[a]	complex mixture
4	Tf_2O (2.2 equiv), Hantzsch ester[a]	complex mixture

[a]run in DCM.

During our optimization campaign, several canonical reducing agents such as metal hydrides were explored. Initial attempts to reduce bis-amide **57** using lithium aluminum hydride (LAH) led only to partial reduction, yielding the monoamide **59** in 36% yield.

Refluxing the reaction in LAH gave isomatridine (**43**) in a modest 42% yield. Huang and coworkers had previously reported that treatment with triflic acid can activate amides for the reduction with various reductants.[70] Unfortunately, attempts to reduce diamide **57** with metal hydride, TMDS and Hantschz ester after activation with triflic acid only gave decomposition (Table 1.8). However, addition of $AlCl_3$ to LAH (to generate alane (AlH_3)) significantly improved the outcome, affording isomatridine in 68% yield in a single step, or 60% over two step alkene hydrogenation-amide reduction protocol without requiring purification of intermediate **57**. Purification of isomatridine **43** was conveniently achieved by forming its hydrogen oxalate salt, followed by trituration in acetone—eliminating the need for column chromatography. Enantiomeric resolution of racemic isomatridine (±)-**43** was accomplished via recrystallization of the di-*p*-toluoyl tartaric acid salt, delivering (+)-isomatridine **43** in 90% ee and a 24% recovery (46% of theoretical yield).

Figure 1.25: *Stepwise reduction sequence towards the diamine **43**.*

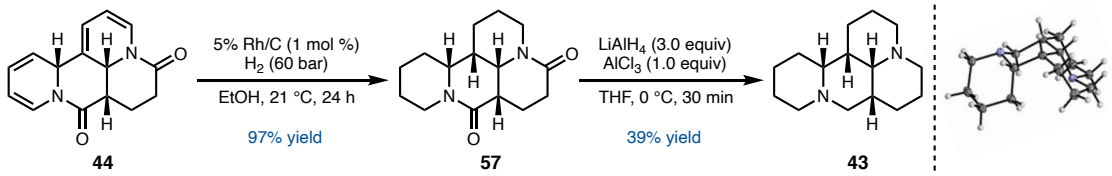

This sequence provided short reaction times, enabled the use of cost-effective reductants, offered a practicable purification protocol and facilitated the synthesis of **43** on multigram scale which led us to favor this approach over the previously discussed Ir-catalyzed conditions.

1.5 *DEVELOPMENT OF A SELECTIVE C15 OXIDATION*

The developed sequence enabled access to diamine **43** on multigram scale, paving the road for the development of the late-stage oxidation of C15. The major challenge of the transformation was anticipated to be selectivity, as diamine **43** possesses four potential sites for α-oxidation which are chemically equivalent. Several strategies to address this challenge are discussed in the following section.

1.5.1 Bioinspired Enzymatic Oxidation

Cytochrome P450 enzymes (P450s or CYPs) are a superfamily of heme-containing monooxygenases that catalyze the oxidation of a wide array of substrates, including steroids, fatty acids, and xenobiotics. They function primarily by introducing an oxygen atom into non-activated hydrocarbons, facilitating reactions such as hydroxylation, epoxidation, and oxidation of α-amine CH oxidations.[71,72] Given their broad substrate scope and regioselectivity, P450s have been extensively studied for their potential in selective C–H bond oxidation. Notably, certain P450 enzymes have demonstrated the ability to hydroxylate specific positions on steroid frameworks. For instance, CYP106A2 is known to catalyze 15β-hydroxylation of progesterone, and through targeted mutagenesis, its activity was redirected to achieve hydroxylation at the C11 position.[73]

Inspired by these precedents and the proposed biosynthetic pathway of our target molecule, we initially explored the enzymatic oxidation of (+)-**43** to synthesize (+)-**6**, focusing on achieving selective oxidation at the C15 position. In collaboration with the Arnold group, over 180 bacterially derived P450 enzymes were screened, encompassing

both wild-type and engineered variants known for their diverse regioselective oxidation capabilities. Despite this extensive screening, liquid chromatography-mass spectrometry (LC-MS) analysis did not detect any C15 oxidation products. Consequently, we redirected our efforts toward developing non-enzymatic methodologies to achieve the desired C15 oxidation.

1.5.2 Structural Analysis of the Diamine

Figure 1.26: *Structural analysis of diamine* ***43***.

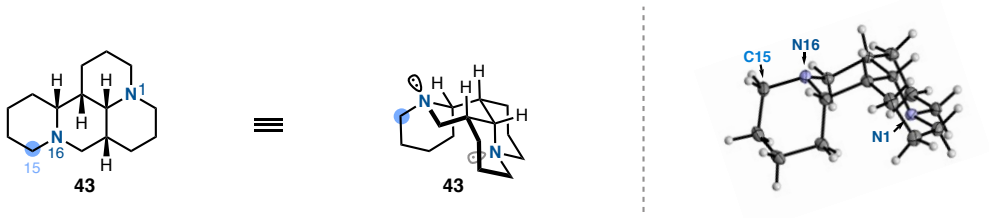

Developing a method for the selective oxidation of C15, in preference to other chemically similar amine-adjacent methylene positions, was expected to be a significant challenge. It was hypothesized that steric factors—rather than electronic differences—could be exploited to achieve site-selectivity. Based on the X-ray crystal structure of diamine **43**, it was observed that the D-ring region, which includes C15, is the most sterically accessible, suggesting that oxidation at this site should be favored (Figure 1.26). The crystal structure also revealed a key distinction: the lone pair on N16 is exposed and accessible, while the lone pair on N1 is positioned within the molecule's concave interior, making it more sterically hindered. This spatial arrangement supported the conclusion that chemical oxidation—guided by steric accessibility—would be more suitable than enzymatic methods for achieving selective C15 functionalization.

1.5.3 Alternative Approaches

Exposure of compound **43** to singlet oxygen in the presence of trimethylsilyl cyanide furnished α-aminonitrile **95**, though in only 20% yield (Scheme 2.4).[27]. Attempts to selectively functionalize the less hindered nitrogen using photoredox conditions instead resulted in epimerization at neighboring stereocenters, producing diastereomers **96** and **97**.[28] Direct oxidation of isomatridine with molecular iodine under basic conditions provided the conjugated iminium ion **98** in 29% yield.[29] Furthermore, recently reported protocols for C–N bond cleavage proved ineffective in this context, delivering a poorly separable mixture of **99** and **100** in low yield.[30]

Figure 1.27: *Attempted C-H oxidations.*

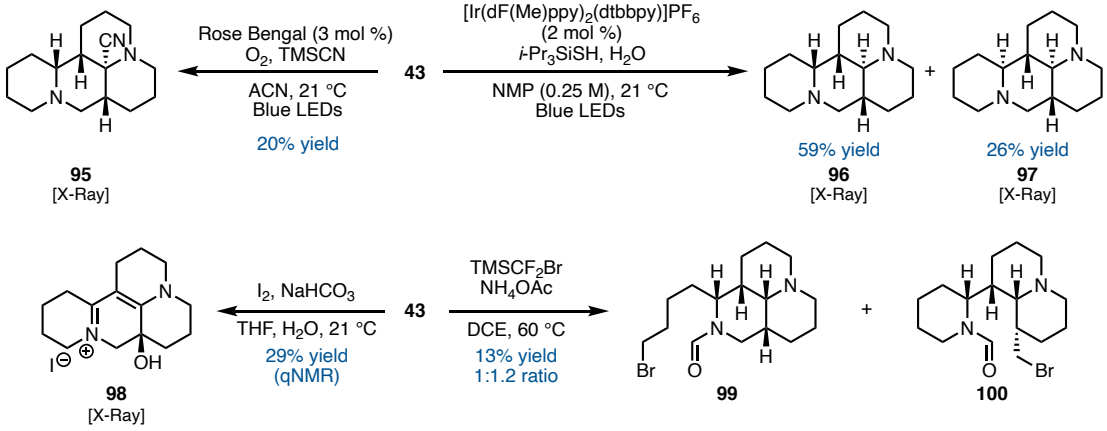

1.5.4 Selectivity via N-Oxidation: N-Oxide Rearrangements

Based on our conformational analysis, it was expected that more accessible nitrogen would be preferentially functionalized. Oxidation to the *N*-oxide was anticipated to occur at N16.

Figure 1.28: *Imminium ion formation by Polonovski reaction.*

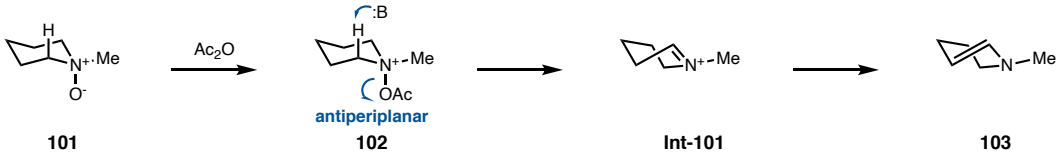

It was envisioned that oxidative functionalization of C15 could be achieved by Polonovski reaction of such *N*-oxide. Successful iminium ion formation could be followed by elimination to form the enamine or addition of a nucleophile (Figure 1.28). Excitingly, in agreement with our conformational analysis, N16 was selectively oxidized with peracetic acid, which proved superior compared to other peroxides, to yield *N*-oxide **104** in a 54% yield. A slight excess of oxidant was required; higher amounts of oxidant, however, gave lower yields of **104** due to double oxidation of N16 and N1.

.

Figure 1.29*: Oxidation to the N-oxide* ***104.***

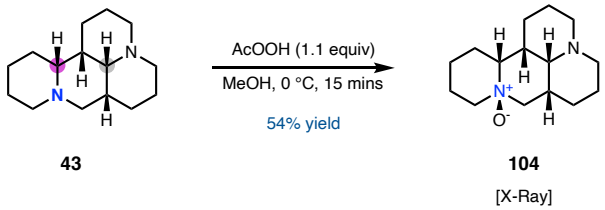

With access to the N-oxide **104** in hand we investigated Polonovski conditions to achieve C15 oxidation (Figure 1.30).

Figure 1.30: *Attempts towards a Polonovski reaction.*

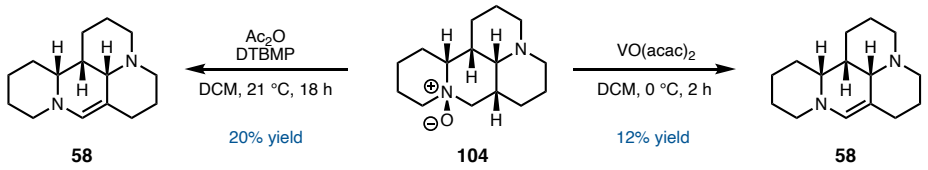

Conditions employing acetic anhydride were unsuccessful, instead isomeric enamine **58** was isolated. Subsequent reduction with $NaBH_4$ led to formation of a previously detected reduced *syn-syn-syn-anti* isomer. Additional attempts to use Burgess reagent to facilitate elimination towards the desired regioisomer failed.

In the crystal structure of N-oxide **104** the measured dihedral angle of the C-17 C-H bond is 177°, which is the required anti-periplanar alignment relative to the the N–O bond to undergo elimination and was observed experimentally.

Figure 1.31: *Conformational considerations for the Polonovski reaction of* ***104****.*

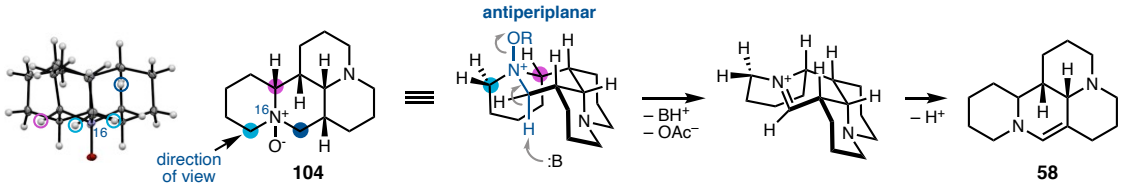

In contrast, the two hydrogen atoms on C15, and the hydrogen atom on C11 have dihedral angles of 51°, 65°, and 53° respectively relative to the N–O bond which precludes their elimination under Polonovski conditions. To circumvent the issue of C–H bond geometry, a complementary approach inspired by Okazaki and coworkers was explored (*Figure 1.32*)[74]

Figure 1.32: *Siloxyammonium rearrangement upon treatment with methyl lithium.*

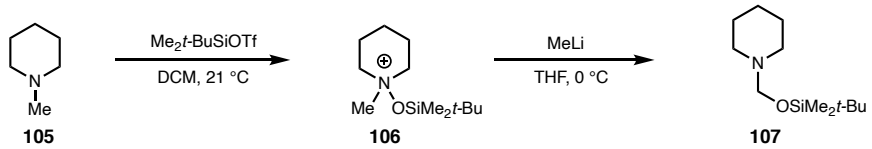

Okazaki and coworkers reported in 1984 that siloxyammonium salt **106** rearranges to α-siloxyamine **107** under basic conditions. It was hypothesized that the regioselectivity of this reaction could be controlled by the base identity exploiting selectivity for the sterically most accessible hydrogens on C15.

Figure 1.33: *Attempts towards a base-mediated siloxyammonium rearrangement.*

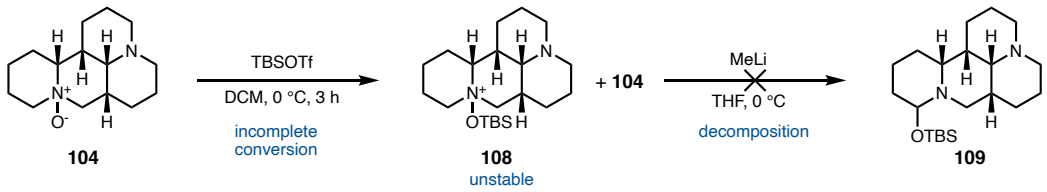

Silylation of *N*-oxide **104** proved to be challenging. An NMR study showed that the reaction stalled at incomplete conversion; Longer reaction times however led to decomposition of product **108** under the reaction conditions. Subjecting a mixture of starting material **104** and silyl ammonium triflate **108** to the required solvent switch for the base-mediated rearrangement led to decomposition. Given the unfavored orbital alignment and the sensitivity of *N*-oxide **108**, it was decided to investigate alternative approaches to activate the amine towards oxidation.

1.5.5 Selectivity via α-Amine Deprotonation

Our previous studies confirmed that N16 is more activated towards reaction and functionalization of N16 can occur with high selectivity. It was anticipated that site-selective reaction of the desired amine, *i.e.,* by a lewis acid, could activate said amine for subsequent reactions. Subsequently, sterics could be used to distinguish the two α-positions (C15 and C16) to establish the desired selectivity towards C15-oxidation. We became interested in a report by Kessar and coworkers demonstrating that amine–BF_3 adducts could undergo deprotonation using mixtures of *tert*-butyl lithium (*t*-BuLi) and potassium *tert*-butoxide (*t*-BuOK).[27] Furthermore, Singh and coworkers had reported a protocol for the α-lithiation of amine BF_3•Et_2O complexes and subsequent trapping with electrophiles to access α-functionalized substrates.[75] It was hypothesized that formation of the BF_3-complex of would activate diamine **43** for lithiation at C15 upon treatment with a strong base. Upon treatment with BF_3•Et_2O N16 would preferably react as it was observed for the oxidation with peroxides. The selectivity of the subsequent lithiation could then be steered with a bulky base favoring deprotonation of the more accessible C15 methylene group.

To evaluate this hypothesis, the complexation-deprotonation sequence was studied via a ^{1}H-NMR assay. Consistent with the selectivity in the *N*-oxide formation, treatment of diamine (+)-**43** with $BF_3 \cdot OEt_2$ quantitatively formed the Lewis acid-base complex. Diamine **43** was first subjected to BF_3•Et_2O, then base, and was subsequently quenched with deuterated methanol to investigate the selectivity of the deprotonation (Table 1.9). Whereas Hauser base derivatives and *t*-BuLi were unable to facilitate the deprotonation (Table 11, entries 1-4), Schlosser's base was successful (Table 1.9, entry 5). The selectivity

of the reaction is influenced by the steric demand of the base. If less sterically demanding *n*-BuLi/*t*-BuOK was employed the undesired product was favored (Table 1.9, entry 5). However, use of *t*-BuLi/*t*-BuOK favors the desired deuteration product in a 26% yield (Table 1.9, entry 7).

Table 1.9: *Influence of base identity on the selectivity of the deprotonation.*

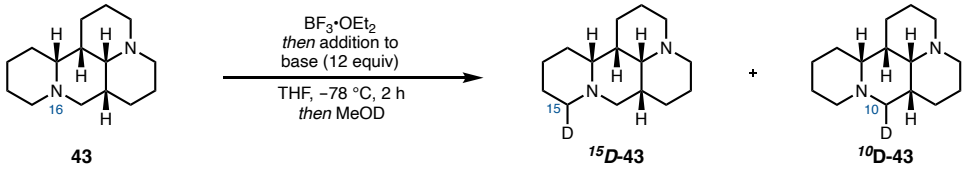

43 **^{15}D-43** **^{10}D-43**

Entry	Base	Ratio C15:C10	% Yield ^{15}D-43	% Conversion
1	$Zn(TMP)_2$•LiCl	/	0	0
2	$(iPr)_2NMgCl$•LiCl	/	0	0
3	TMPMgCl•LiCl	/	0	0
4	*t*-BuLi	/	0	0
5	*n*-BuLi/*t*-BuOK	1.0 : 2.5	21	75
6	*s*-BuLi/*t*-BuOK	1.5 : 1.0	25	42
7	*t*-BuLi/*t*-BuOK	2.0 : 1.0	26	39
8	NpI/*t*-BuOK	1.5 : 1.0	6	10

Next, the influence of the solvent was investigated. Hexanes, a non-coordinating solvent, was found to be unsuitable for the reaction (Table 1.10, entry 2). The reaction in ethereal solvents gave the desired product, however with low selectivity and low conversion (Table 1.10, entries 1, 3 and 4). A literature review revealed that ethereal solvents can decompose under strongly basic conditions.[76]

Table 1.10: *Influence of the solvent.*

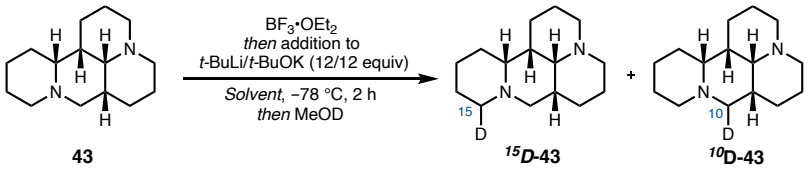

43 **^{15}D-43** **^{10}D-43**

Entry	Solvent	Ratio C15:C10	% Yield ^{15}D-43	% Yield ^{10}D-43
1	Et_2O	1.0 : 2.5	26	88
2	Hexane	/	0	0
3	2-Me-THF	1.0 : 1.3	4	9
4	THF	2.0 : 1.5	26	39
5	THF-d_8	2.0 : 1.0	44	81
6	THP[a]	2.4 : 1.0	31	44
7	THF/TMEDA (12 equiv)	1.8 : 1.0	39	61
8	Et_2O/TMEDA (12 equiv)	1.3 : 1.0	50	90
9	TMEDA	nd	0	0
10	TMEDA[b]	5.0 : 1.0	45	54

It was hypothesized that base-mediated decomposition would be slowed in deuterated tetrahydrofuran (d-THF) due to a kinetic isotope effect for the deprotonation, and pleasingly, higher conversions were observed (Table 1.9, entry 5). Tetrahydropyran (THP) is known to extend the half-life for alkyl lithium species compared to THF. Tetramethyldiamine (TMEDA) has also been used as an additive to allow for longer half-lifes.[77,78] Furthermore, it has been reported to reduce the degree of aggregation for alkyl lithium increasing the reactivity and enhancing reaction rates.[79–81] As expected, running the reaction in THP gave better selectivity and conversion comparable to those observed in d^8-THF (Table 1.10, entry 6). Furthermore, addition of TMEDA proved to be highly beneficial for yield and selectivity. This can be seen most drastically when TMEDA is used as a cosolvent with ether, completely reversing the ratio in favor of the desired product (Table 1.10, entries 7-8). Running the reaction in neat TMEDA as solvent gave initially no reaction, however it was hypothesized that a large excess of TMEDA outcompetes the

substrate in BF_3 complexation (Table 1.10, entry 9). Hence, it was concluded that preformation of the amine BF_3 complex (**110**) could be beneficial (Table 1.11). Reaction of diamine **43** with BF_3•Et_2O in ether gave amine BF_3 complex (**110**) in a quantitative yield without the need for purification. Subjection of the complex to the reaction conditions in TMEDA increased the yield to 55% and selectivity to 5.0 : 1.0 (Table 1.11, entry 10).

Table 1.11: *Influence of the t-BuLi/t-BuOK ratio.*

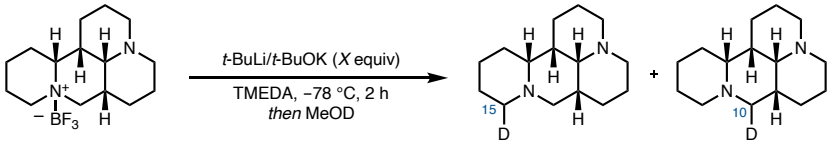

110 **^{15}D-43** **^{10}D-43**

Entry	Base	Ratio C15:C10	% Yield ^{15}D-43	% Yield ^{10}D-43
1	*t*-BuLi/*t*-BuOK (6/12 equiv)	10.0 : 1.0	80	88
2	*t*-BuLi/*t*-BuOK (12/24 equiv)	3.7 : 1.0	70	89

The concentration of alkoxide salts was also reported to have a large impact on the formation of alkyl lithium aggregates in ethereal solution.[82] Hence, the influence of the *t*-BuLi to *t*-BuOK ratio was investigated. It was found that an increased ratio of *t*-BuOK toalkyl lithium (12 to 6 equivalents) increased the selectivity to 10 : 1 with conversion of 88% (Table 1.11, entry 1). Notably, this result enables lowering the amount of alkyl lithium base to 6 equivalents and at the same time achieving higher conversions.

1.5.6 Development of an Electrophile Trapping-Oxidation Sequence

Table 1.12: *Electrophile trapping of different electrophiles.*

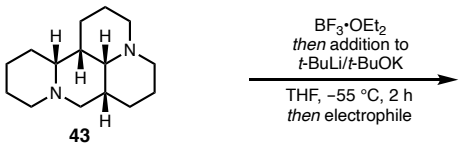

Entry	Electrophile	Result
1	TBSOOTBS	complex mixture
2	BzOOBz	complex mixture
3	Davis reagent (**111**)	complex mixture
4	**112**	complex mixture
5	O_2	unidentified product
6	BzCl	complex mixture
7	$ClP(O)(OEt_2)$	complex mixture
8	BrCN	complex mixture
9	BzCl then O_2	complex mixture

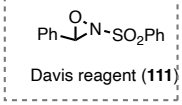

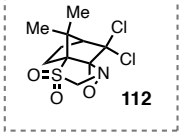

Having established a highly selective deprotonation protocol, the subsequent trapping of oxygen electrophiles was then investigated (Table 1.12). Neither silyl peroxides nor other peroxides gave detectable amounts of product but only gave complex mixtures (Table 1.12, entry 1 and 2). Reaction with other oxygen electrophiles such as oxaziridines and molecular oxygen did not give rise to the desired product (Table 1.12, entry 3,4 and 5).

Figure 1.34: *Successful electrophiles for the trapping of the lithiated intermediate.*

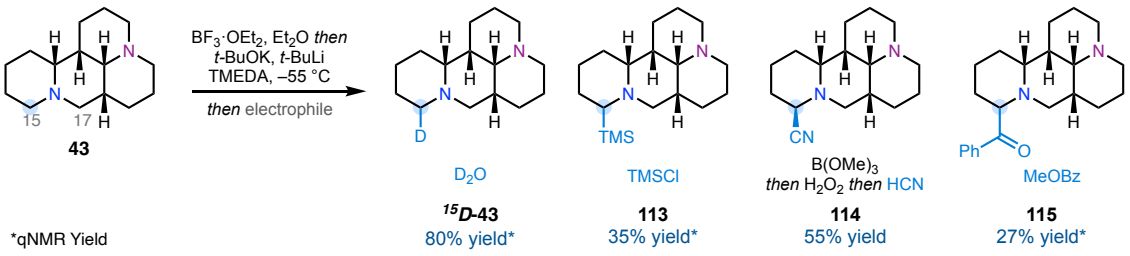

Reaction with non-oxygen electrophiles such as chlorophosphite and BrCN only gave complex mixtures (Table 1.12, entry 7-10), while quenching with TMSCl provided silylated diamine **113** in only 35% yield. Eventually, it was found that reaction with methyl benzoate gave unstable phenyl ketone **115** in 27% yield with methyl benzoate (**115**) proceeded in a 27% yield (Figure 1.34).

Figure 1.35: *Additionally investigated electrophiles.*

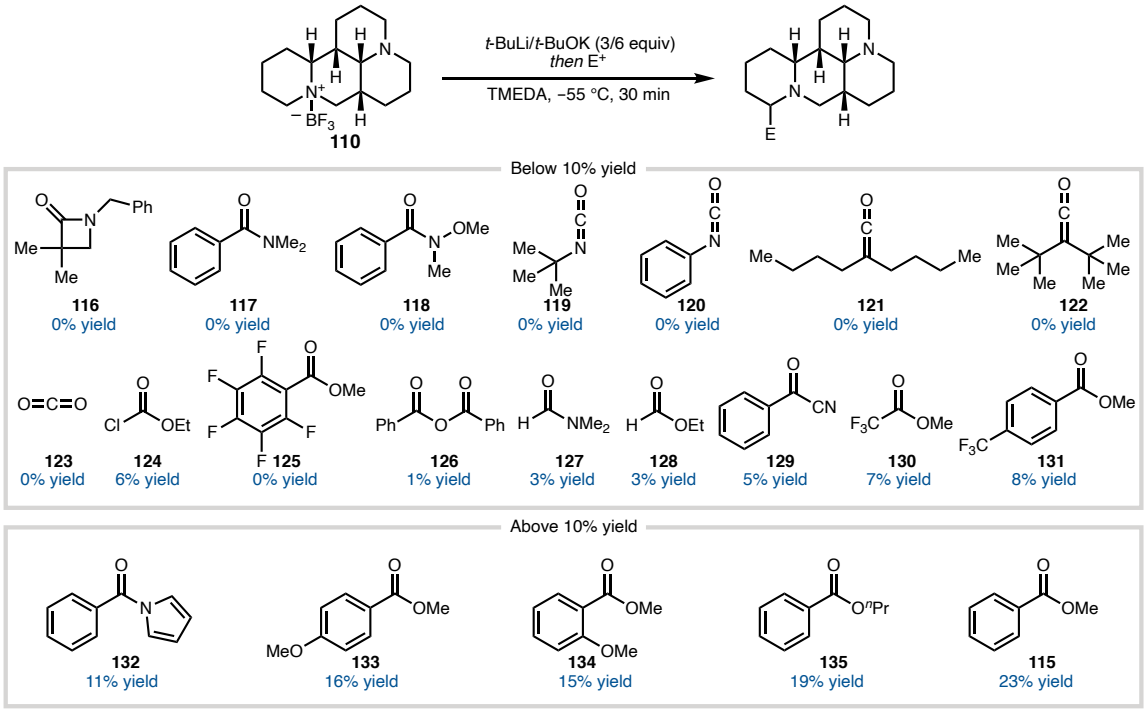

Subsequently, other carbonyl electrophiles were also evaluated, however none was able to outperform methyl benzoate (Figure 1.35). Vicente and coworkers previously reported that α-aminoketones can be oxidized with molecular oxygen.[83] Excitingly, the oxidation of α-amino ketone **63** with molecular oxygen proceeded smoothly to give isomatrine (**6**) in a 48% yield (Scheme 17). The best yield of C15-functionalized product

was obtained when 11 was deprotonated and then trapped with trimethyl borate; oxidation with hydrogen peroxide and trapping of the resultant enamine with HCN gave aminonitrile **114** in 55% yield. Aerobic oxidation of **115** provided isomatrine in 46% yield (25% yield over three steps from **43**). Additionally, it was found that isomatrine (**7**) could be obtained from BF_3-complex **110** in a one pot procedure featuring a deprotonation, electrophile trapping and oxidation sequence. Further optimization showed that the amount of *t*-BuLi and methyl benzoate could be lowered to 3.0 and 8.0 equivalents, respectively (Table 1.13, entry 6). Furthermore, it was found that addition of methyl benzoate in CPME instead of TMEDA gave the best result obtaining isomatrine in a 32% yield and a 61% yield based on remaining starting material (Table 1.13, entry 1, 5 and 6).

Table 1.13: *Final optimization of the one-pot oxidation.*

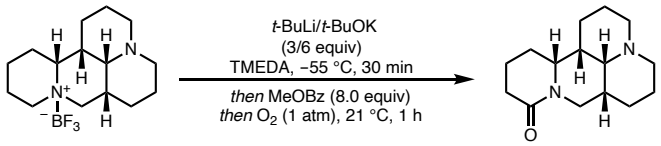

110 (±)-Isomatrine (**6**)

Entry	MeOBz Equiv	Solvent	% Yield	% Yield BRSM
1	25	TMEDA	15	43
2	4	Hexanes	26	45
3	4	Et_2O	26	49
4	4	PhMe	29	50
5	4	CPME	28	50
6	8	CPME	32	61
7	12	CPME	28	43

To date, >1 gram of (+)-isomatrine has been prepared with this protocol, to give (+)-**6** directly in 18–26% yield, depending on the scale. This route provides access to (±)-isomatrine in four steps, and (+)-isomatrine can be easily accessed by incorporating the resolution of diamine **43**.

1.6 Divergent Isomerization

Having a route to isomatrine in hand, the previously published isomerization to matrine and allomatrine was tested (Figure 1.36).[55] Initial attempts to reproduce Okuda's Pt-catalyzed isomerization of (+)-isomatrine failed to provide the reported yields of (+)-matrine (**4**) and (+)-allomatrine (**7**), and instead produced a mixture of five compounds.[20]

Figure 1.36: *Time dependent product distribution of the divergent isomerization with different catalysts.*

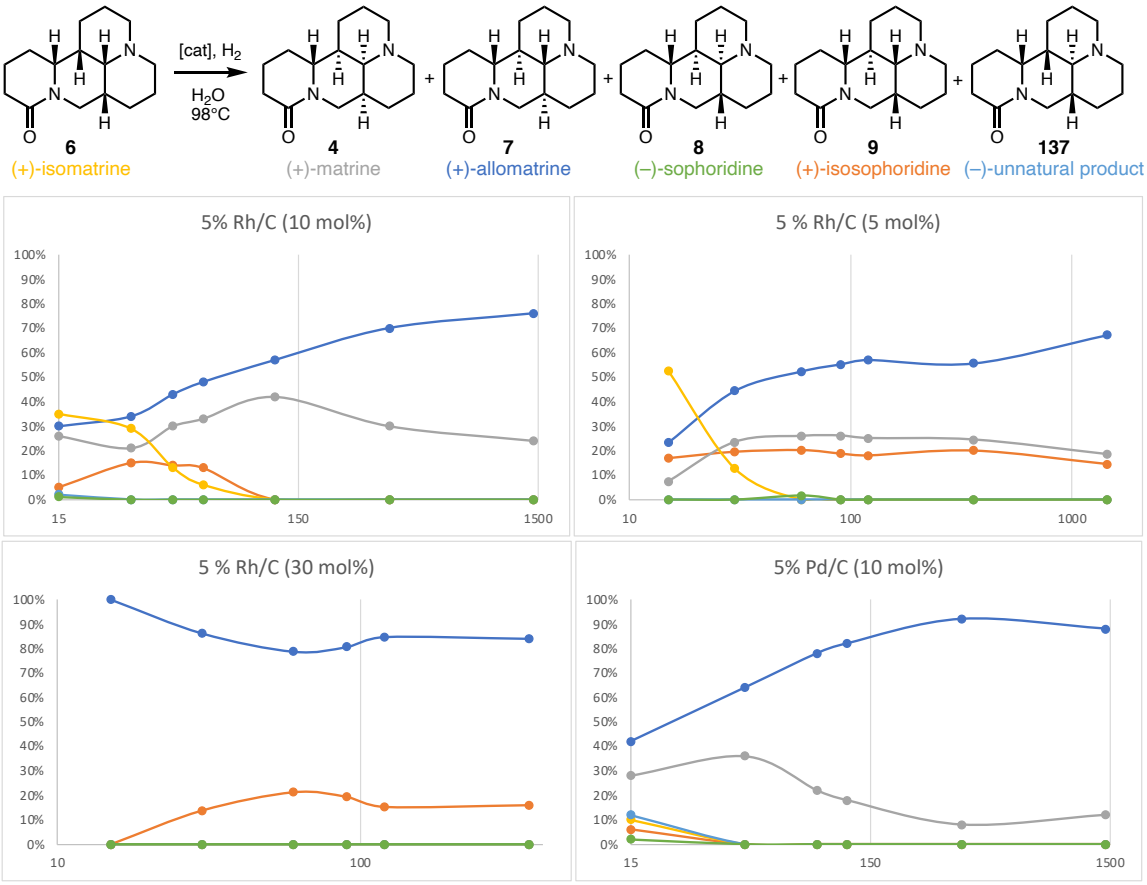

To improve the yield of **4** and **7**, while also broadening the synthetic access to other congeners, an investigation of several isomerization catalysts was carried out (Figure 1.36). The optimized results are summarized in Figure 1.37. After 15 min, use of 5% Rh/C with a 10 mol% loading provided the best yields of (+)-**4** (32% yield), while (+)-**3** could be obtained in 83% yield when Pd/C was used. Isomerization with 10 % Pt/C provided (+)-isosophoridine (**5**) in 55% yield. Finally, use of PtO_2 at 98 °C for 15 minutes furnished (–)-sophoridine (**4**) in 10% yield, together with the other isomers. When the reaction with PtO_2 was conducted at 80 °C for 24 hours, (–)-isomer **137** was isolated in 40% yield. To our knowledge, **137** has not yet been isolated from natural sources. In all cases, the mass balance consisted of other isomers in varying ratios.

Figure 1.37: *Optimized conditions for the synthesis of matrine and related lupin alkaloids.*

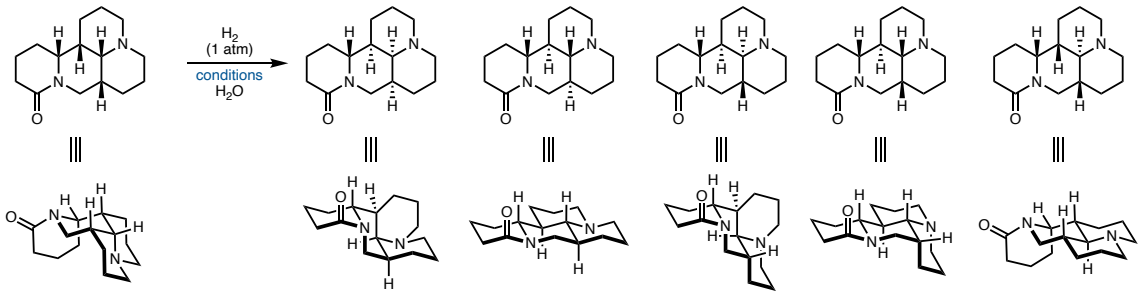

6 (+)-isomatrine	conditions	**4** (+)-matrine	**7** (+)-allomatrine	**8** (–)-sophoridine	**9** (+)-isosophoridine	**137** (–)-unnatural product
	10 mol% Rh/C, 98 °C, 1 h	**32%**	60%	0%	0%	0%
	10 mol% Pd/C, 98 °C, 2 h	15%	**83%**	0%	0%	0%
	110 mol% PtO_2, 98 °C, 15 min	6%	10%	**10%**	29%	14%
	10 mol% Pt/C, 98 °C, 15 min	0%	11%	0%	**55%**	19%
	110 mol% PtO_2, 80 °C, 24 h	0%	18%	0%	33%	**40%**

The proposed mechanism proceeds through a series of metal-catalyzed dehydrogenation and hydrogenation steps, guided by the relative thermodynamic stabilities

of the lupin alkaloid products.[14] The sequence begins with coordination of (+)-isomatrine to the metal catalyst, forming intermediate **Int4**. Subsequent dehydrogenation generates iminium ion **Int5**. Direct hydrogenation of **Int5** leads to the unnatural diastereomer (–)-**137**. Alternatively, **Int5** can isomerize to enamine **Int6**, which upon hydrogenation yields (–)-sophoridine (**137**). Further dehydrogenation of **Int6** produces intermediate **Int7**, which can undergo hydrogenation from either face to afford either (+)-isosophoridine (**9**) or (+)-matrine (**4**). A final dehydrogenation produces **Int8**, and subsequent hydrogenation furnishes the most thermodynamically stable product, (+)-allomatrine (**7**).

Figure 1.38: *Proposed mechanism of the divergent isomerization.*

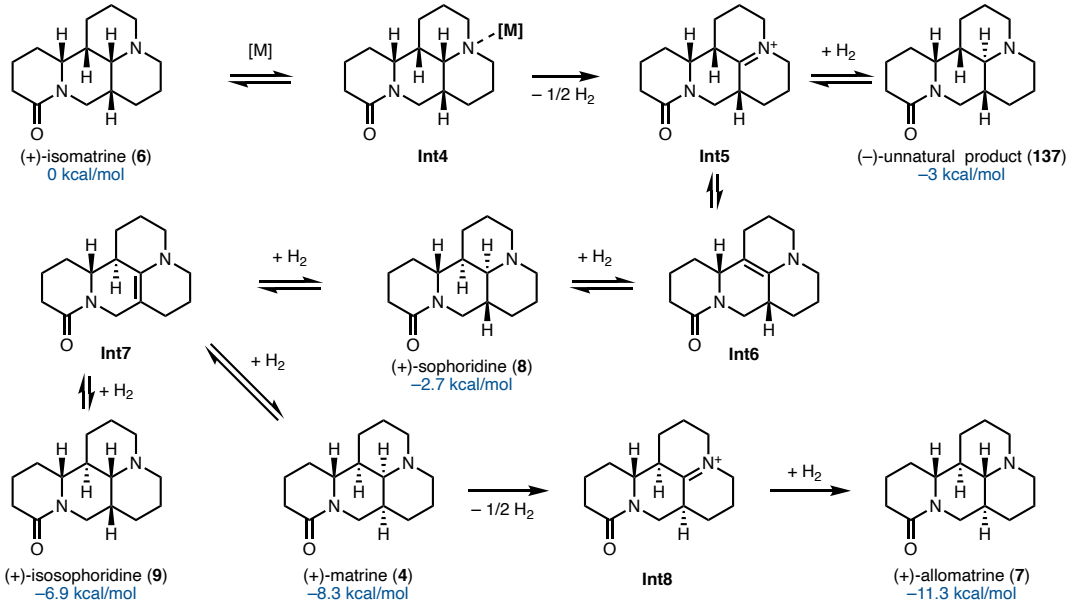

1.7 *CONCLUDING REMARKS*

The bioinspired dearomative annulation between pyridine and glutaryl chloride developed in this work has enabled the first total synthesis of (–)-sophoridine and the shortest reported syntheses of (+)-isomatrine, (+)-matrine, (+)-allomatrine, and (+)-isosophoridine. Central to the conciseness of these routes is a pyridine dearomative cascade that rapidly constructs the core carbocyclic framework of the lupin alkaloids in a single step. The initial annulation product can be subjected to hydrogenation and subsequent alane-mediated reduction to furnish isomatridine, a scaffold of interest not only as a synthetic intermediate but also as a gram-scale-accessible, structurally novel ligand.

Efforts to achieve C15-selective oxidation of isomatridine have led to the development of conditions capable of functionalizing multiple positions on the framework, thereby opening avenues for structure–activity relationship (SAR) studies that were previously inaccessible using the natural product directly. A regioselective deprotonation–electrophile trapping–oxidation cascade enabled the total synthesis of (+)-isomatrine in just four steps from pyridine, with more than a gram of material produced to date.

This dearomative platform has also been extended to the total syntheses of lupinine and sparteine.[84] Mechanistic studies revealed that the annulation proceeds via two kinetically distinct cyclization events. Quenching the monocyclized intermediate (Figure 1.14, **Int1a**) with methanol allows selective access to an isolable quinolizidine intermediate, which can be globally reduced to provide lupinine in three steps and 35% overall yield. Transformation of the same quinolizidine intermediate into sparteine has been achieved in five steps on gram scale, delivering a practical route to this synthetically and biologically significant natural product.

The ability to generate diverse lupin alkaloids and analogs from simple commodity starting materials highlights the broad utility of this methodology and its potential to support future pharmacological investigations.

1.8 EXPERIMENTAL SECTION

Unless otherwise stated, reactions were performed under an inert atmosphere (dry N_2) using freshly dried solvents and standard Schlenk techniques. Glassware was oven-dried at 120 °C for a minimum of four hours. Tetrahydrofuran (THF), methylene chloride (DCM), acetonitrile (ACN), methanol (MeOH), benzene (PhH), and toluene (PhMe) were dried by passing through activated alumina columns. CH_2Cl_2 (D150-4), benzene (PhH, OmniSolv, BX0212-1), acetonitrile (A998-4), pentane (P399-4), acetone (A18-20), hexanes (H292-20), and *n*-butanol (A399-4) were purchased from Fisher and used as received. Anhydrous *N*,*N*-dimethylformamide (DMF) was purchased from VWR (EM-DX1727-6) and used as received. All reactions were monitored by thin-layer chromatography using EMD/Merck silica gel 60 F254 pre-coated plates (0.25 mm) and were visualized by UV or by staining with *p*-anisaldehyde or potassium permanganate ($KMnO_4$). Flash column chromatography was performed as described by Still et al.[85] using silica gel (particle size 0.032–0.063) purchased from MilliporeSigma. ^1H and ^{13}C NMR spectra were recorded on a Bruker Avance III HD with Prodigy cryoprobe (at 400 MHz and 101 MHz, respectively), a Varian Inova 500 (at 500 MHz and 126 MHz, respectively), a Bruker 400 MHz Spectrometer with broadband iProbe, or a Varian Inova 600 (at 600 MHz and 150 MHz, respectively), and are reported relative to internal $CDCl_3$ (^1H, $\delta = 7.26$; ^{13}C, $\delta = 77.16$) or CD_2Cl_2 ^1H, $\delta = 5.32$; ^{13}C, $\delta = 53.84$). $CDCl_3$ was stored over anhydrous

potassium carbonate (K_2CO_3). Data for ^1H NMR spectra are reported as follows: chemical shift (δ ppm) (multiplicity, coupling constant (Hz), integration). Multiplicity and qualifier abbreviations are as follows: s = singlet, d = doublet, t = triplet, q = quartet, m = multiplet, br = broad. IR spectra were recorded on a Perkin Elmer Paragon 1000 spectrometer and are reported in frequency of absorption (cm^{-1}). HRMS data were acquired using an Agilent 6230 Series time-of-flight (TOF) mass spectrometer with an Agilent G1978A ion trap or by LC-MS using a Waters LCT Premier XE Electrospray TOF mass spectrometer interfaced with Waters UPLC chromatography, or by GC-MS interfaced with a JEOL JMS-T2000 GC AccuTOF GC-Alpha with Field Ionization. Molecular formulas of the compounds [M] are given, with the observed ion fragment in brackets, e.g. $[M+H]^+$. Optical rotations were measured on a Jasco P-2000 polarimeter using a 100 mm path-length cell at 589 nm. Melting points were determined using a Büchi B-545 capillary melting point apparatus, and the values reported are uncorrected. Photochemical experiments were performed using a 34 W Kessil H150 Blue LED light. Unless otherwise stated, chemicals and reagents were used as received. Reagents were purchased from commercial vendors as follows: Solid potassium *tert*-butoxide was purchased from STREM Chemicals Inc., stored in a glovebox, and used as received. TMEDA and trimethylborate were purchased from MilliporeSigma and were distilled over CaH_2 under N_2 prior to use. Glutaryl chloride was purchased from Oakwood Chemicals Inc. and was used as received. Anhydrous pyridine, rhodium on carbon (5%), palladium on carbon (10%), platinum dioxide, platinum on carbon (5%), trimethylsilyl cyanide, lithium aluminum hydride, aluminum trichloride, *tert*-butyl lithium solution in pentanes, rose bengal, peracetic acid, hydrogen peroxide, oxalyl chloride, $Rh(PPh_3)_3(CO)(H)$, sodium borohydride, $[Ir(dF(Me)ppy)_2(dtbbpy)]PF_6$,

triisopropylsilanethiol, (fluorodibromo)trimethylsilane, and *N*-phthaloyl-L-glutamic acid were purchased from MilliporeSigma and were used as received. Di-*p*-toluoyl-L-tartaric acid was purchased from Ambeed Inc. and was used as received. (*R*)-2-methylglutaric acid and racemic 2-methylglutaric acid were purchased from Combi-Blocks Inc. and were used as received. ^{1}H qNMR standards trimethylphenyl silane (99% purity) and pyrazine (≥99% purity) were purchased from MilliporeSigma and were used as received.

Preparation of (±)-tetracycle 44:

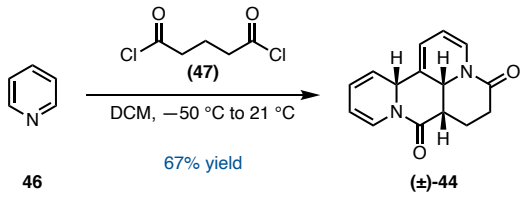

Large-Scale Procedure:

A 12 L oven-dried, N_2-flushed 3-neck flask equipped with an overhead stirrer, thermocouple, and rubber septum was charged with anhydrous DCM (8.0 L, 0.12 M) followed by glutaryl chloride (**47**) (126 mL, 980 mmol, 1.0 equiv). The solution was cooled to –50 °C on an acetone/dry ice bath. Pyridine (**46**) (396 mL, 4.90 mol, 5.0 equiv) was added via cannula at such a rate as to prevent the temperature from rising above –40 °C (*ca*. 1 hour). Following pyridine addition, the reaction was stirred at –50 °C for 15 minutes and then at 21 °C until complete, as judged by ^{1}H NMR in CD_2Cl_2 (*ca*. 24–36 hours). Upon completion, the reaction was concentrated under reduced pressure to yield a brown solid which was suspended in MeOH (800 mL). The solids were isolated via suction filtration, washed with MeOH (3 x 150 mL), and dried *in vacuo* to yield (±)-tetracycle **44** as a tan crystalline solid (165.9 g, 67% yield).

Medium-Scale Procedure:

A 3 L oven-dried, N_2-flushed 3-neck flask equipped with an overhead stirrer, thermocouple, and rubber septum was charged with anhydrous DCM (1.8 L, 0.1 M) followed by glutaryl chloride (**47**) (23 mL, 179 mmol, 1.0 equiv). The solution was cooled to –50 °C on an acetone/dry ice bath. Pyridine (**46**) (72 mL, 895 mmol, 5.0 equiv) was added via cannula at such a rate as to prevent the temperature from rising above –40 °C (*ca*. 30 minutes). Following pyridine addition, the reaction was stirred at –50 °C for 15 minutes then at 21 °C until complete, as judged by ^{1}H NMR in CD_2Cl_2 (*ca*. 24–36 hours). Upon completion, the reaction was concentrated under reduced pressure to yield a brown solid which was suspended in MeOH (200 mL). The solids were isolated via suction filtration, washed with MeOH (3 x 100 mL), and dried *in vacuo* to yield (±)-tetracycle **44** as a tan crystalline solid (31.1 g, 68% yield).

Small-Scale Procedure:

A 1 L oven-dried, N_2-flushed flask with a 36 mm x 18 mm x 18 mm egg-shaped stir bar was charged with anhydrous DCM (296 mL, 0.1 M) followed by glutaryl chloride (**47**) (3.78 mL, 29.6 mmol, 1.0 equiv). The solution was cooled to –50 °C on an acetone/dry ice bath. Pyridine (**46**) (12 mL, 148 mmol, 5.0 equiv) was added dropwise via syringe over the course of 10 minutes. Following pyridine addition, the reaction was stirred at –50 °C for 15 minutes then at 21 °C until complete, as judged by ^{1}H NMR in CD_2Cl_2 (*ca*. 24–36 hours). Upon completion, the reaction was concentrated under reduced pressure to yield a brown solid which was suspended in MeOH (40 mL). The solids were isolated via suction

filtration, washed with MeOH (3 x 50 mL), and dried *in vacuo* to yield (±)-tetracycle **44** as a tan crystalline solid (4.67 g, 62% yield).

(±)-Tetracycle 44:

^{1}H NMR (500 MHz, $CDCl_3$): δ 7.15 (d, *J* = 7.7 Hz, 1H), 7.03 (dq, *J* = 8.0, 1.0 Hz, 1H), 6.00 (dddd, *J* = 10.1, 5.8, 2.2, 1.0 Hz, 1H), 5.87 (dddd, *J* = 5.0, 2.4, 1.5, 0.6 Hz, 1H), 5.67 (dd, *J* = 7.7, 5.4 Hz, 1H), 5.61 (ddt, *J* = 10.1, 3.3, 1.2 Hz, 1H), 5.39 (t, *J* = 2.8 Hz, 1H), 5.15 (ddd, *J* = 8.0, 5.7, 1.1 Hz, 1H), 4.72 – 4.66 (m, 1H), 2.94 (ddd, *J* = 18.7, 13.3, 6.0 Hz, 1H), 2.86 (dt, *J* = 6.7, 3.4 Hz, 1H), 2.63 (ddt, *J* = 13.7, 5.8, 2.7 Hz, 1H), 2.47 (dddd, *J* = 18.1, 5.3, 2.4, 1.3 Hz, 1H), 2.00 (dddt, *J* = 18.5, 13.4, 9.9, 5.2 Hz, 1H).

^{13}C NMR (126 MHz, $CDCl_3$): δ 168.2, 168.0, 130.8, 126.1, 123.3, 122.4, 121.2, 118.0, 109.7, 102.8, 53.7, 53.2, 36.9, 28.6, 19.5.

FTIR (NaCl, thin film): 3087, 2960, 2365, 1668, 1655, 1583, 1407, 1287, 1266, 1244, 1184, 733 cm^{-1}.

HRMS: (ESI-TOF) calc'd for $C_{15}H_{14}N_2O_2$ $[M^{\bullet}]^+$ 254.1050, found 254.1038.

TLC (10% MeOH/90% PhH), **R_f:** 0.32 ($KMnO_4$).

M.P. 184.2 °C – 186.9 °C.

Figure 1.39. *X-Ray structure of (±)-**44**.*

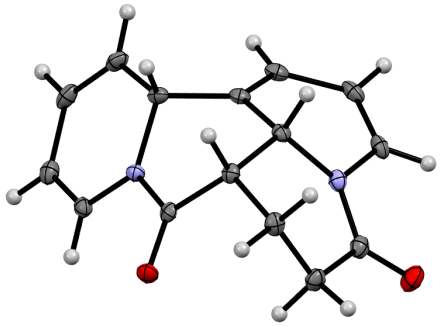

Preparation of (+)-3-methyltetracycle 51:

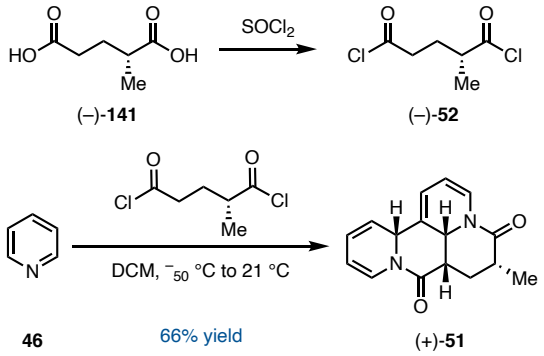

A 25 mL oven-dried, N_2 flushed flask was charged with (*R*)-2-methyl glutaric acid (1.00 g, 6.84 mmol, 1.0 equiv) and thionyl chloride (4.0 mL, 54.7 mmol, 8.0 equiv). The suspension was stirred for 24 hours at 21 °C under N_2, after which point it became a homogenous solution. The thionyl chloride was removed under vacuum (0.3 torr) on a Schlenk line at 21 °C to yield (*R*)-2-methylglutaryl chloride (**77**) as a clear, colorless liquid, which was used directly in the subsequent cyclization reaction.

A 100 mL oven-dried, N_2-flushed flask with a 36 mm x 18 mm x 18 mm egg-shaped stir bar was charged with DCM (26.4 mL, 0.125 M) and (*R*)-2-methylglutaryl chloride (605 mg, 3.31 mmol, 1.0 equiv). The solution was cooled to –50 °C, then pyridine (1.34 mL, 16.5 mmol, 5.0 equiv) was added dropwise over the course of 5 minutes. The reaction was allowed to warm to 21 °C and was stirred for 24 hours. The reaction was concentrated under reduced pressure and diluted in MeOH (20 mL). The solids were isolated by suction filtration, washed with MeOH (2 x 10 mL), and dried *in vacuo* to yield (+)-3-methyltetracycle **51** as a light orange crystalline solid (0.589 g, 66% yield).

(+)-3-methyltetracycle 51:

^{1}H NMR (500 MHz, $CDCl_3$): δ 7.17 (dt, *J* = 8.0, 1.0 Hz, 1H), 6.99 (dq, *J* = 8.1, 0.9 Hz, 1H), 6.04 (dddd, *J* = 10.1, 5.8, 2.2, 1.0 Hz, 1H), 5.78 (ddt, *J* = 5.8, 2.8, 1.0 Hz, 1H), 5.50 (ddt, *J* = 10.1, 3.4, 1.2 Hz, 1H), 5.32 (dd, *J* = 7.9, 5.7 Hz, 1H), 5.14 (ddd, *J* = 8.1, 5.7, 1.1 Hz, 1H), 5.09 (t, *J* = 2.9 Hz, 1H), 4.95 (ddt, *J* = 9.5, 2.6, 1.2 Hz, 1H), 2.96 (q, *J* = 9.5 Hz, 1H), 2.31 – 2.19 (m, 1H), 2.16 (dt, *J* = 9.3, 4.6 Hz, 1H), 2.03 (td, *J* = 13.8, 9.9 Hz, 1H), 1.29 (d, *J* = 6.6 Hz, 3H).

^{13}C NMR (126 MHz, $CDCl_3$): δ 173.9, 168.9, 129.6, 124.4, 123.7, 122.2, 120.9, 117.9, 103.7, 102.7, 54.0, 51.9, 41.5, 34.8, 25.5, 15.4.

FTIR (NaCl, thin film): 2946, 2835, 1652, 1456, 1113, 1033 cm^{-1}.

HRMS: (ESI-TOF) calc'd for $C_{16}H_{17}N_2O_2$ $[M+H]^+$ 269.1290, found 269.1278.

TLC (50% EtOAc /50% hexanes), **R_f:** 0.37 ($KMnO_4$).

M.P. 192.5 – 196.4 °C.

Specific Optical Rotation: $[\alpha]\frac{21}{D} = -1115$ (c 1.0, $CHCl_3$).

Figure 1.40. *X-Ray structure of (±)-**51**.*

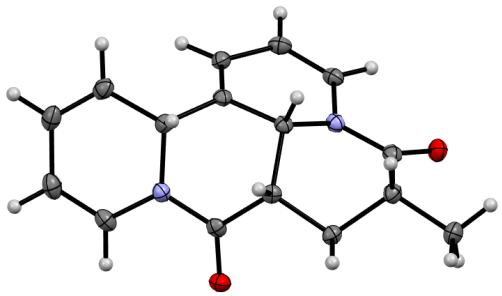

Chiral SFC: (IC, 2.5 mL/min, 45% IPA in CO_2, λ = 210 nm): t_R (major) = 7.6 min, t_R (minor) = 12.5 min.

Figure 1.41. *SFC trace of racemic* ***51***

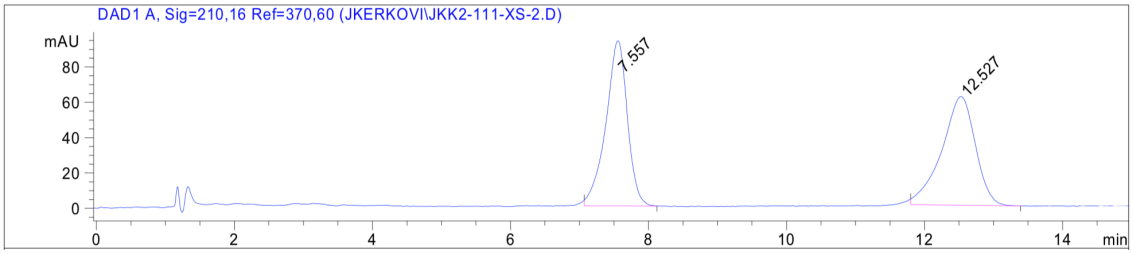

Signal 1: DAD1 A, Sig=210,16 Ref=370,60

Peak #	RetTime [min]	Type	Width [min]	Area [mAU*s]	Height [mAU]	Area %
1	7.557	BB	0.3214	2030.30872	93.47500	49.3078
2	12.527	BB	0.5080	2087.31201	61.50079	50.6922

Figure 1.42 *SFC trace of enantiopure* ***51***.

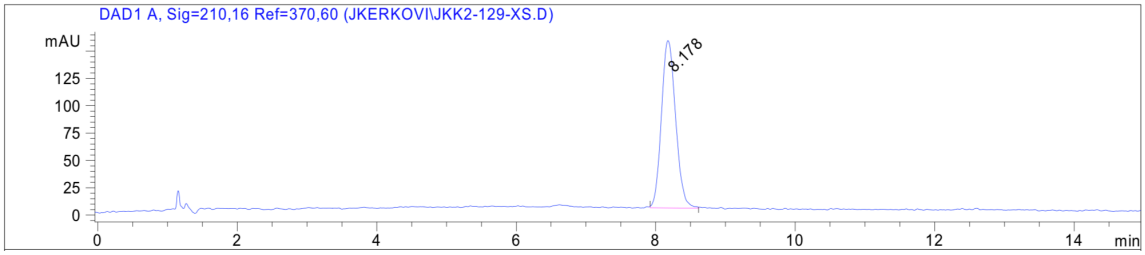

Signal 1: DAD1 A, Sig=210,16 Ref=370,60

Peak #	RetTime [min]	Type	Width [min]	Area [mAU*s]	Height [mAU]	Area %
1	8.178	BB	0.2207	2161.24438	153.12198	100.0000

Preparation of tetracycle (–)-56:

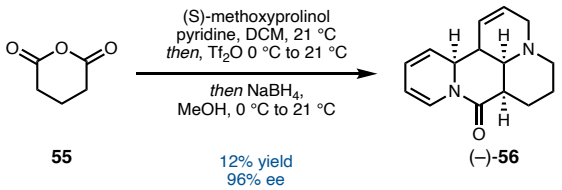

To a 100 mL flask in a glovebox was added the glutaric anhydride (100 mg, 876 umol, 1.0 equiv), pyridine (496 uL, 6.13 mmol, 7.0 equiv), DCM (8.76 mL, 0.1 M), and (*S*)-(+)-2-(methoxymethyl)pyrrolidine (108 uL, 876 umol, 1.0 equiv). The reaction was stirred for 30 minutes at 21 °C, then cooled to –78 °C. To the solution was added trifluoromethanesulfonic anhydride (302 uL, 1.80 mmol, 2.05 equiv). The reaction was then allowed to warm to 21 °C, and stirred for 4 hours. Then, the MeOH (8.76 mL, 0.1 M) was added and the solution cooled to 0 °C. The sodium borohydride (497 mg, 13.1 mmol, 15 equiv) was added next in portions. Once the addition was finished, the reaction was warmed to 21 °C and stirred for 30 minutes. The crude reaction mixture was concentrated under reduced pressure, made basic with sat. Na_2CO_3 (20 mL) and water (20 mL). The reaction mixture was extracted with DCM (3 x 30 mL). The combined organic layers were dried over anhydrous Na_2SO_4, filtered, and concentrated under reduced pressure. In a glovebox the crude material was treated with Et_2O (20 mL), which caused the product to crash out as an tan solid. The product was isolated via suction filtration in the glovebox to yield the product (–)-**56** as a light tan crystalline solid (25.5 mg, 12% yield, 96% ee).

(+)-tetracycle 56:

^{1}H NMR (600 MHz, $CDCl_3$): δ 7.11 (dd, *J* = 7.9, 1.3 Hz, 1H), 6.02 (ddt, *J* = 10.5, 5.7, 2.3 Hz, 1H), 5.94 (dddd, *J* = 10.0, 5.7, 2.3, 1.1 Hz, 1H), 5.90 (dtd, *J* = 10.2, 2.9, 0.9 Hz,

1H), 5.50 (ddt, *J* = 10.0, 3.5, 1.2 Hz, 1H), 5.01 (ddd, *J* = 7.9, 5.7, 1.1 Hz, 1H), 4.84 (dt, *J* = 5.8, 2.8 Hz, 1H), 3.09 (dd, *J* = 15.9, 5.9 Hz, 1H), 2.93 (ddt, *J* = 11.1, 3.8, 1.7 Hz, 1H), 2.83 (dd, *J* = 8.6, 3.6 Hz, 1H), 2.71 (dtd, *J* = 8.6, 4.5, 4.1, 1.8 Hz, 1H), 2.58 (ddt, *J* = 15.9, 3.9, 2.1 Hz, 1H), 2.42 (dtd, *J* = 12.6, 4.2, 2.3 Hz, 1H), 2.33 (q, *J* = 3.6 Hz, 1H), 2.24 – 2.05 (m, 2H), 1.55 – 1.45 (m, 2H).

^{13}C NMR (104 MHz, $CDCl_3$): δ 170.8, 128.5, 123.7, 123.4, 122.3, 121.3, 101.8, 58.1, 56.8, 55.7, 52.3, 41.0, 39.7, 24.2, 21.4.

FTIR (NaCl, thin film): 3054, 2986, 2339, 1675, 1655, 1420, 1265, 896, 738 cm^{-1}.

HRMS: (ESI-TOF) calc'd for $C_{15}H_{18}N_2O$ $[M+H]^+$ 243.1497, found 243.1509.

TLC (3% MeOH/97% $CHCl_3$ with 0.75% EtOH stabilizer), **R_f:** 0.27 ($KMnO_4$).

M.P. 175.7 °C – 178.1 °C.

Specific Optical Rotation: $[\alpha]_D^{21} = -94.0$ (c 1.0, $CHCl_3$).

Figure 1.43. *X-Ray structure of (+)-**56***.

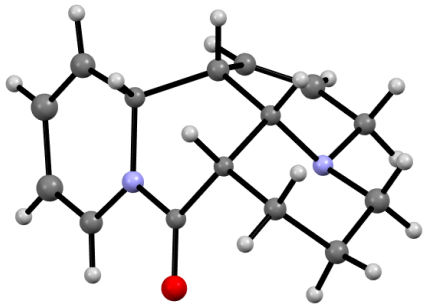

X-Ray ID placeholder: D21063.

Chiral SFC: (IC, 2.5 mL/min, 30% IPA in CO_2, λ = 280 nm): t_R (major) = 8.829 min, t_R (minor) = 9.437 min.

Figure 1.44. *SFC trace of racemic **56***.

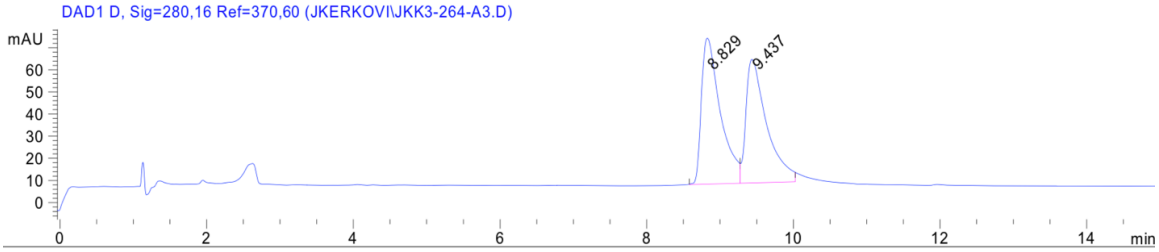

Peak #	RetTime [min]	Type	Width [min]	Area [mAU*s]	Height [mAU]	Area %
1	8.829	BV	0.2651	1182.97705	65.99975	51.8590
2	9.437	VB	0.2855	1098.16357	55.83330	48.1410

Figure 1.45. *SFC trace of enantioenriched* ***56****.*

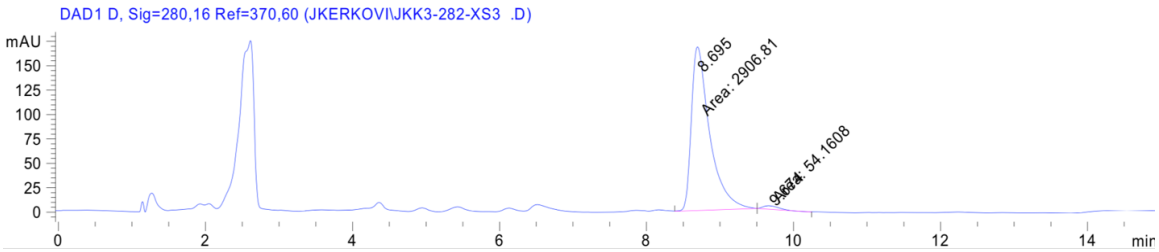

Signal 3: DAD1 D, Sig=280,16 Ref=370,60

Peak #	RetTime [min]	Type	Width [min]	Area [mAU*s]	Height [mAU]	Area %
1	8.695	MM	0.2889	2906.81177	167.67546	98.1708
2	9.674	MM	0.2538	54.16077	3.55604	1.8292

Preparation of 8-phthaloyltetracycle 54:

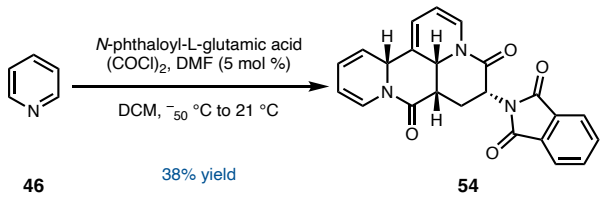

A 500 mL oven dried flask was charged with *N*-phthaloyl-L-glutamic acid (5.00 g, 18.0 mmol, 1.0 equiv), DMF (70 µL, 0.90 mmol, 5 mol %) and DCM (18 mL, 1 M).

The flask was equipped with a scrubber to remove HCl vapors, and to the suspension in the flask was added oxalyl chloride (3.36 mL, 39.7 mmol, 2.2 equiv). The reaction was stirred at ambient temperature for 5 hours which resulted in the formation of a clear colorless solution, progress of the reaction was monitored by NMR aliquots. The solution was diluted in DCM (180 mL, 0.1 M) and was cooled to –50 °C. To the solution was added pyridine (7.29 mL, 90.2 mmol, 5 equiv) over the course of 5 minutes. The slurry was stirred at –50 °C for 15 minutes then at ambient temperature for 15 hours. The reaction was concentrated under reduced pressure and suspended in MeOH (50 mL). The solids were isolated by suction filtration and dried in vacuo to yield the product as a brown powder (2.72 g, 38% yield). Using enantiopure *N*-phthaloyl-L-glutamic acid provided the product **54** with 16% ee.

8-phthaloyltetracycle 54:

^{1}H NMR (600 MHz, $CDCl_3$): δ 7.89 – 7.85 (m, 2H), 7.76 – 7.70 (m, 2H), 7.14 (d, *J* = 7.9 Hz, 1H), 7.01 (dt, *J* = 7.9, 1.0 Hz, 1H), 6.06 (dddd, *J* = 10.0, 5.8, 2.2, 0.9 Hz, 1H), 5.83 (ddt, *J* = 5.7, 2.7, 0.9 Hz, 1H), 5.53 (ddt, *J* = 10.1, 3.4, 1.2 Hz, 1H), 5.43 (dd, *J* = 7.9, 5.8 Hz, 1H), 5.17 (dd, *J* = 8.0, 5.8 Hz, 1H), 5.14 (t, *J* = 2.3 Hz, 1H), 5.12 (dd, *J* = 9.9, 2.8 Hz, 1H), 4.78 (dd, *J* = 13.7, 4.6 Hz, 1H), 3.33 (td, *J* = 13.7, 10.2 Hz, 1H), 3.12 (q, *J* = 9.6 Hz, 1H), 2.33 (ddd, *J* = 13.8, 9.1, 4.7 Hz, 1H).

^{13}C NMR (104 MHz, $CDCl_3$): δ 167.7, 166.9, 134.4, 134.0, 131.7, 129.3, 124.0, 123.7, 123.6, 122.2, 120.6, 117.5, 105.0, 102.8, 53.7, 51.6, 48.8, 40.3, 22.0.

FTIR (NaCl, thin film): 3053, 2986, 1720, 1672, 1610, 1421, 1390, 1266 cm^{-1}.

HRMS: (ESI-TOF) calc'd for $C_{23}H_{17}N_3O_4$ $[M+H]^+$ 400.1297, found 400.1292

TLC (60% EtOAc /40% ACN), $\mathbf{R_f}$**:** 0.50 ($KMnO_4$).

M.P. decomposed at 180 °C.

Figure 1.46. *X-Ray structure of (+)-**54**.*

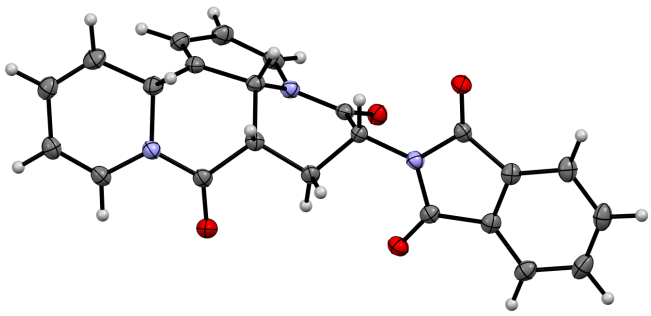

X-Ray ID: V19479.

Chiral SFC: (AD-H, 2.5 mL/min, 45% IPA in CO2, λ = 210 nm): tR (major) = 7.8 min, tR (minor) = 8.7 min.

Figure 1.47. *SFC trace of racemic **54**.*

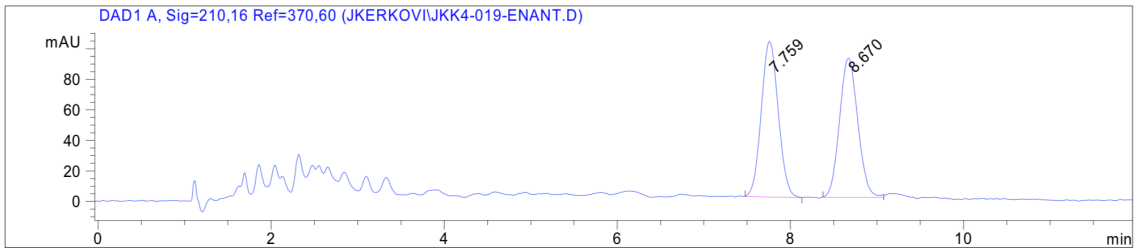

Peak #	RetTime [min]	Type	Width [min]	Area [mAU*s]	Height [mAU]	Area %
1	7.759	BB	0.2153	1390.96790	101.88776	50.9158
2	8.670	BB	0.2316	1340.93018	91.18265	49.0842

Figure 1.48. *SFC trace of scalemic* ***54****.*

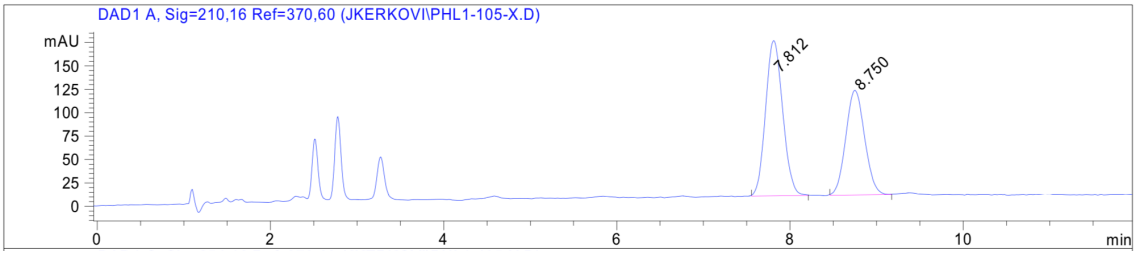


```
Signal 1: DAD1 A, Sig=210,16 Ref=370,60

Peak RetTime Type  Width     Area      Height     Area
  #   [min]       [min]   [mAU*s]     [mAU]       %
----|-------|----|-------|----------|----------|--------|
   1   7.812 BB    0.2122 2275.86987  165.71790  57.3807
   2   8.750 BB    0.2364 1690.39539  111.81298  42.6193
```

Cyclization NMR Study:

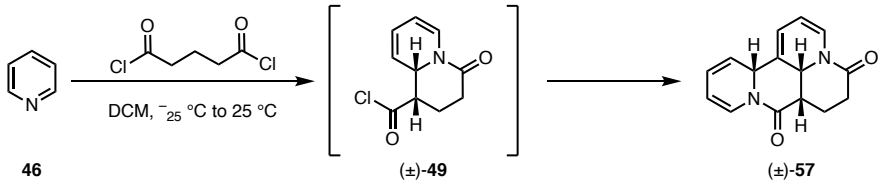

In a glovebox, an NMR tube was charged with CD_2Cl_2 (0.75 mL, 0.045 M), pyridine (34 µL, 0.42 mmol, 12.0 equiv), and $PhSiMe_3$ (5.1 mg, 0.034 mmol, 0.97 equiv). The solution was cooled in the glovebox freezer (–25 °C) for 15 minutes. To the cold solution was rapidly added glutaryl chloride (4.5 µL, 0.035 mmol, 1.0 equiv). The tube was capped and inverted to mix. Initially, a precipitate formed which dissolved after one minute of mixing. The reaction was then monitored by ^{1}H qNMR over the course of 24 hours ($PhSiMe_3$ internal standard).

Figure 1.49. *Cyclization of glutaryl chloride and pyridine ^{1}H NMR time-course study.*

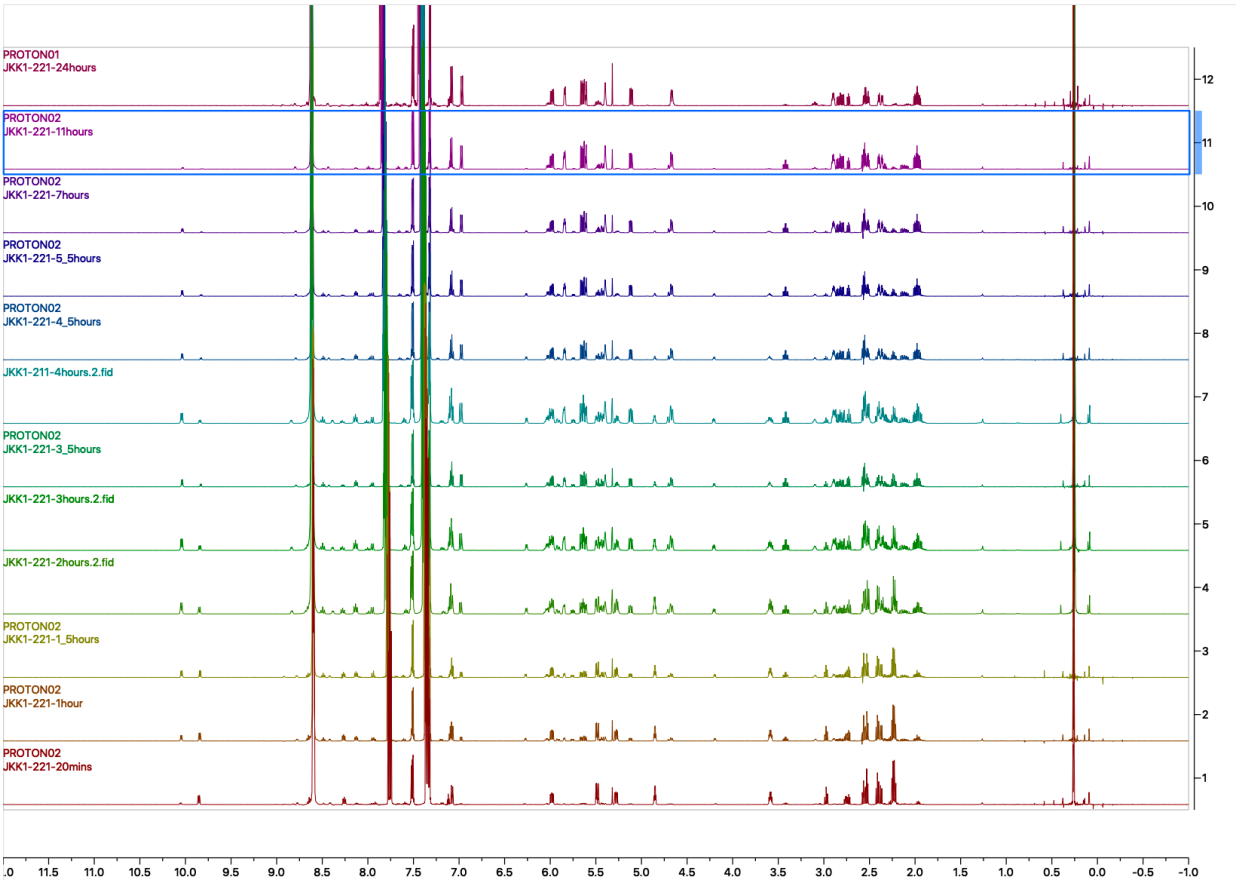

(±)-Acid chloride 73:

^{1}H NMR (600 MHz, $CDCl_3$): δ 7.08 (dt, *J* = 8.1, 0.9 Hz, 1H), 5.98 (dddd, *J* = 9.7, 5.6, 2.6, 1.0 Hz, 1H), 5.49 (ddt, *J* = 9.7, 2.9, 1.1 Hz, 1H), 5.28 (ddd, *J* = 7.7, 4.9, 1.0 Hz, 1H), 4.85 (dt, *J* = 5.0, 2.8 Hz, 1H), 3.59 (dt, *J* = 6.5, 4.8 Hz, 1H), 2.76 (td, *J* = 7.5, 4.8 Hz, 1H), 2.55 (dt, *J* = 17.1, 7.0 Hz, 1H), 2.40 (dt, *J* = 17.2, 7.2 Hz, 1H), 2.27 – 2.19 (m, 1H).

Figure 1.50. *Cyclization of glutaryl chloride and pyridine ^{1}H NMR time-course study trans isomer inset.*

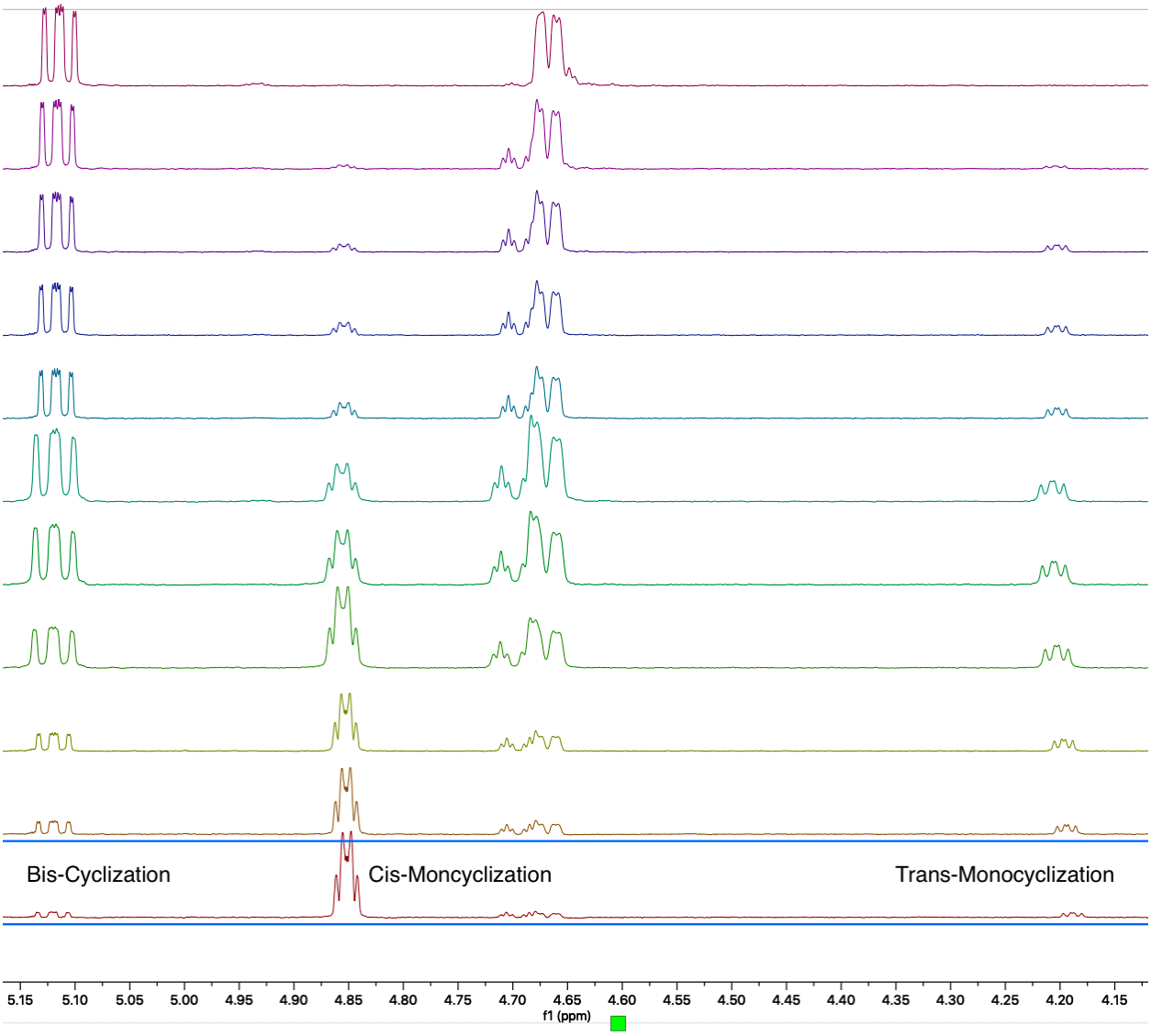

Preparation of alkenyl ester 141:

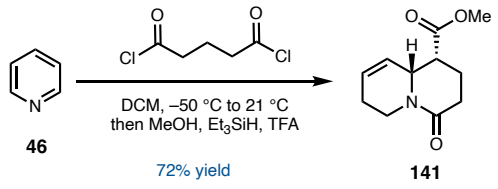

46 **141**

A 500 mL oven dried N_2 flushed flask was charged with glutaryl chloride (0.76 mL, 5.92 mmol, 1 equiv) and DCM (59 mL, 0.1 M). The solution was cooled to –50 °C, then pyridine (2.4 mL, 29.6 mmol, 5 equiv) was added dropwise. The thick slurry was stirred at –50 °C for 15 minutes and was then allowed to warm to ambient temperature. Once the reaction become homogenous (ca. 30-60 minutes) the methanol (0.48 mL, 11.8 mmol, 2 equiv) was added. The solution was cooled to 0 °C then triethylsilane (14.2 mL, 88.8 mmol, 15 equiv) was added followed by a dropwise addition trifluoroacetic acid (6.8 mL, 88.8 mmol, 15 equiv). The reaction was allowed to warm to ambient temperature and stir for 18 hours. Once complete, the reaction was made basic with sat. Na_2CO_3, and the aqueous layer was extracted with DCM (3 x 50 mL). The combined organic layers were dried over anhydrous Na_2SO_4, filtered, and concentrated under reduced pressure. The crude product was purified via SiO_2 column chromatography [160 g SiO_2, 55 mm diameter column, eluted with 60% Acetone/40% Hexanes] to yield the alkenyl methyl ester **141** as a pale yellow crystalline solid (895 mg, 72% yield).

Alkenyl Ester 141:

^{1}H NMR (500 MHz, $CDCl_3$): δ 6.04 – 5.89 (m, 1H), 5.50 (ddt, *J* = 10.1, 2.9, 1.4 Hz, 1H), 4.76 (ddt, *J* = 12.8, 5.8, 1.3 Hz, 1H), 4.37 (ddt, *J* = 6.9, 4.9, 2.4 Hz, 1H), 3.69 (s, 3H), 3.01 (dt, *J* = 6.6, 4.9 Hz, 1H), 2.73 (td, *J* = 12.2, 4.2 Hz, 1H), 2.61 (ddd, *J* = 17.7, 7.8, 6.7 Hz, 1H), 2.43 (dt, *J* = 17.6, 6.5 Hz, 1H), 2.33 (ddtd, *J* = 20.3, 11.9, 6.0, 2.5 Hz, 1H), 2.10 – 1.96 (m, 3H).

^{13}C NMR (104 MHz, $CDCl_3$): δ 172.0, 169.1, 129.1, 125.9, 55.8, 52.0, 43.1, 39.8, 30.4, 24.7, 21.6.

FTIR (NaCl, thin film): 3031, 2951, 2841, 1736, 1642, 1459, 1436, 1417, 1280, 1263, 1233, 1193, 1163, 1014, 988, 917 cm^{-1}.

HRMS: (FI-TOF) calc'd for $C_{11}H_{15}NO_3$ $[M]^+$ 209.10464, found 209.10482.

TLC (50% acetone/50% hexanes), **R_f:** 0.23 ($KMnO_4$).

M.P. 38.4 – 40.6 °C.

Preparation of (±)-bis-amide 57:

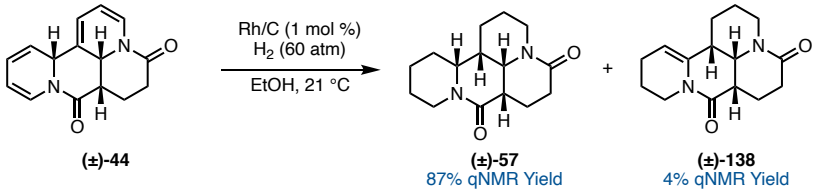

A Parr Instrument Company pressure vessel (600 mL volume, model 4760) containing a 50 mm x 6 mm x 6 mm rectangular stir bar was charged with (±)-tetracycle **44**, (22.0 g, 39.7 mmol, 1.0 equiv), 5% rhodium on carbon (817 mg, 0.397 mmol, 1 mol %), and EtOH (200 mL, 0.4 M). The vessel was flushed with argon then pressurized and vented with H_2 (3 x 7 atm). The vessel was pressurized with H_2 to 60 atm and was stirred at 1200 rpm at 21 °C for 20 hours. Upon completion, the reaction was carefully depressurized and filtered through celite that was subsequently washed with DCM. The solution was concentrated under reduced pressure to yield a yellow oil that solidified slowly on standing. (±)-Bis-amide **57** was obtained as a pale yellow, crystalline solid and was used directly in the next step without additional purification. Purity was measured via ^1H qNMR against pyrazine as an internal standard. An analytically pure sample was prepared via SiO_2 column chromatography [1 g of crude material, 120 g SiO_2, 50 mm

column diameter, 10% MeOH/90% ACN] to yield (±)-bis-amide **57** as a white crystalline solid.

(±)-Enamide **138** was produced in 4% qNMR yield (against pyrazine) during the reaction and an analytically pure sample was obtained via SiO_2 column chromatography of the crude reaction mixture [1 g of crude material, 120 g SiO_2, 50 mm column diameter, 10% MeOH/90% ACN] to yield (±)-enamide **138** as a white crystalline solid.

(±)-Bis-amide 57:

^{1}H NMR (500 MHz, $CDCl_3$): δ 4.81 (ddt, *J* = 12.8, 4.2, 2.1 Hz, 1H), 4.71 (dq, *J* = 12.3, 2.4, 1.4 Hz, 1H), 3.74 (dd, *J* = 7.6, 3.5 Hz, 1H), 3.39 (ddd, *J* = 12.5, 6.6, 2.4 Hz, 1H), 2.83 (qt, *J* = 4.1, 2.0 Hz, 1H), 2.64 (ddt, *J* = 13.1, 5.2, 2.7 Hz, 1H), 2.55 (td, *J* = 11.9, 3.3 Hz, 1H), 2.42 (td, *J* = 12.5, 2.3 Hz, 1H), 2.38 – 2.30 (m, 2H), 2.07 (ddd, *J* = 17.8, 14.2, 4.6 Hz, 1H), 1.92 (ddt, *J* = 15.1, 5.3, 2.9 Hz, 1H), 1.89 – 1.75 (m, 4H), 1.73 – 1.59 (m, 3H), 1.42 (qt, *J* = 12.4, 3.6 Hz, 1H), 1.37 – 1.25.

^{13}C NMR (125 MHz, $CDCl_3$): δ 169.7, 167.2, 61.5, 56.8, 45.6, 42.1, 38.1, 34.0, 32.1, 29.9, 26.1, 25.9, 25.1, 22.3, 21.6.

FTIR (NaCl, thin film): 2932, 2855, 1636, 1472, 750 cm^{-1}.

HRMS: (ESI-TOF) calc'd for $C_{15}H_{22}N_2O_2Na$ $[M+Na]^+$ 285.1573, found 285.1573

TLC (15% MeOH/85% ACN), **R_f:** 0.26 ($KMnO_4$).

M.P. 147.1 °C – 150.5 °C.

Figure 1.51. *X-Ray structure of (±)-**57**.*

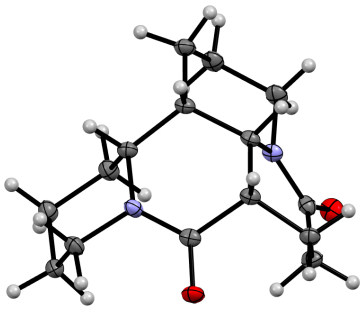

(±)-Enamide 138:

^{1}H NMR (400 MHz, $CDCl_3$): δ 4.93 (td, *J* = 4.1, 1.9 Hz, 1H), 4.76 (ddt, *J* = 13.3, 4.9, 1.9 Hz, 1H), 4.34 – 4.25 (m, 1H), 3.71 (dd, *J* = 6.1, 3.1 Hz, 1H), 3.21 (dddd, *J* = 13.1, 10.5, 3.2, 1.0 Hz, 1H), 2.92 (qd, *J* = 5.2, 4.6, 2.3 Hz, 1H), 2.65 (dh, *J* = 5.4, 2.7 Hz, 1H), 2.57 (dddd, *J* = 13.1, 5.4, 3.3, 2.2 Hz, 1H), 2.48 (td, *J* = 13.1, 3.5 Hz, 1H), 2.32 (ddtd, *J* = 17.5, 4.2, 2.1, 0.7 Hz, 1H), 2.23 (ddd, *J* = 16.9, 5.3, 2.8 Hz, 1H), 2.17 (dd, *J* = 13.9, 4.9 Hz, 1H), 2.11 (dddd, *J* = 9.5, 7.1, 6.1, 3.3 Hz, 2H), 1.91 – 1.79 (m, 2H), 1.79 – 1.63 (m, 4H), 1.53 (dq, *J* = 13.3, 3.0 Hz, 1H).

^{13}C NMR (104 MHz, $CDCl_3$): δ 170.2, 166.8, 133.1, 106.8, 57.0, 42.3, 41.0, 39.8, 36.5, 29.4, 25.9, 22.6, 22.6, 21.6, 20.1.

FTIR (NaCl, thin film): 3052, 2985, 2974, 2954, 2874, 1633, 1414, 1264 cm^{-1}.

HRMS: (ESI-TOF) calc'd for $C_{15}H_{21}N_2O_2$ $[M+H]^+$ 261.1603, found 261.1593.

TLC (15% MeOH/85% ACN), **R_f:** 0.37 ($KMnO_4$).

M.P. 76.6 °C – 83.1 °C.

General procedure for the optimization of the transition metal-catalyzed hydrosilylation reaction:

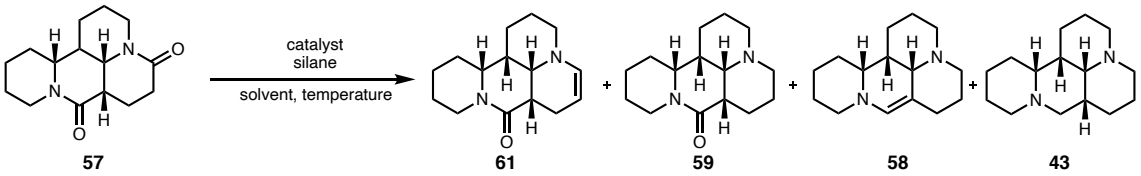

57 **61** **59** **58** **43**

In a nitrogen-filled glovebox, catalyst, silane and solvent were combined in a 1-dram vial equipped with a magnetic stir bar. The resulting solution was stirred for 15 min at room temperature, after which **57** was added to give a yellow solution. Subsequently, any additional reagents were added before the vial was sealed with a PTFE-lined septum cap, reinforced with Teflon tape, and removed from the glovebox. The reaction mixture was stirred at the specified temperature and for the specified time, then opened to air, and the solvent was removed under reduced pressure.

The resulting residue was dissolved in $CDCl_3$ containing 1,2,4,5-tetrachloro-3-nitrobenzene (TCNB) as an internal standard and analyzed by quantitative ^1H NMR spectroscopy.

The crude material could be purified by flash column chromatography on silica gel using chloroform with 2–5% ammonia in methanol as the eluent.

Figure 1.52. *NMR assignments for QNMR studies on the reduction of bisamide **57**.*

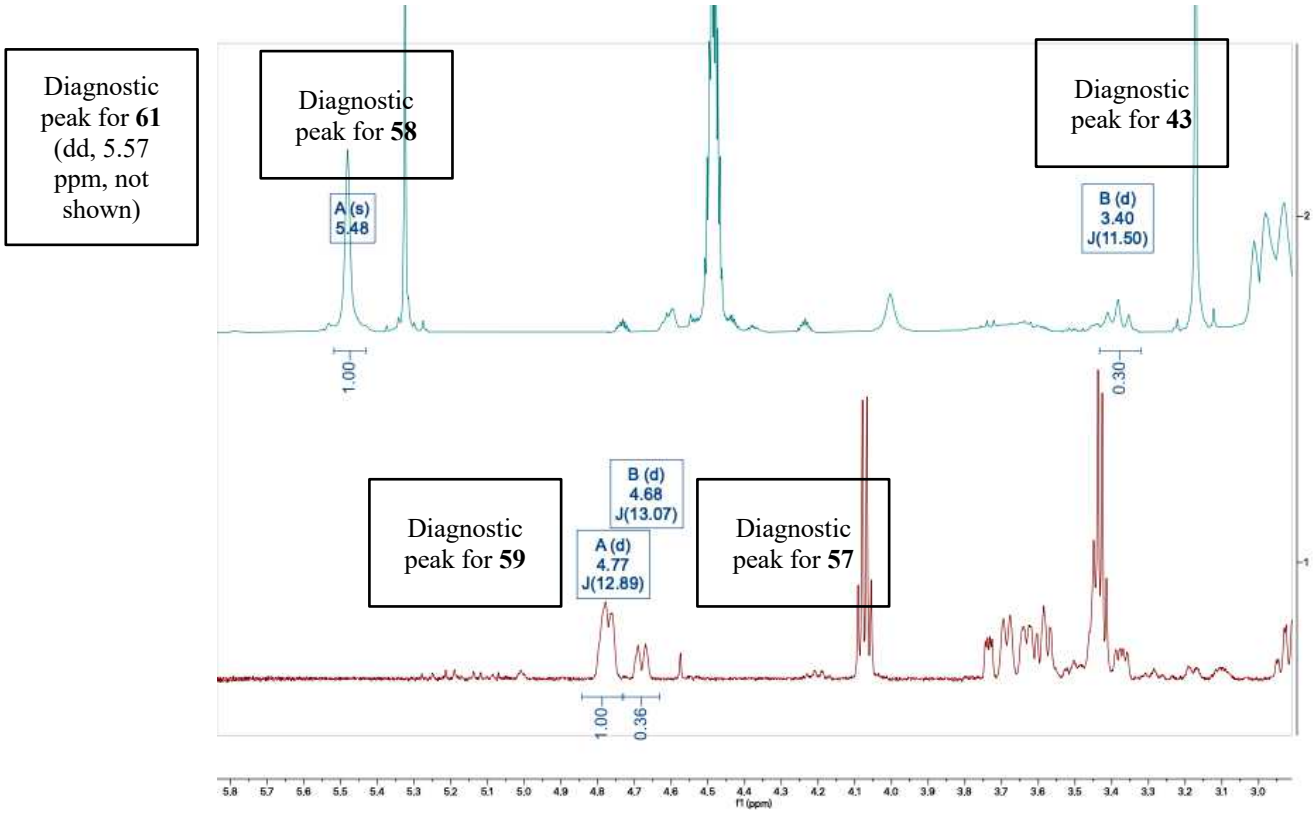

Preparation of mono-amide 59:

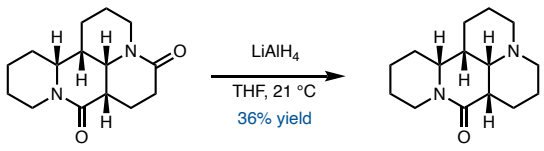

57 **59**

A 100 mL N_2 flushed flask was charged with bis-amide **57** (498 mg, 1.90 mmol, 1.0 equiv.), and THF (9.5 mL, 0.2 M). The solution was cooled to 0 °C, then $LiAlH_4$ (144 mg, 3.80 mmol, 2.0 equiv) was added to the flask in a single portion. The reaction was stirred at 0 °C for 5 minutes, then at ambient temperature until complete by TLC (*ca.* 18 hours). Upon completion the reaction was quenched with sat. Rochelles salt (20 mL). The

reaction mixture was extracted with DCM (3 x 20 mL). The combined organic layers were dried over anhydrous Na_2SO_4, filtered, and concentrated under reduced pressure. The crude product was purified via SiO_2 column chromatography [40 g SiO_2, 30 mm column diameter, eluted with 20% MeOH/80% ACN] to yield mono amide **59** as a white crystalline solid (171 mg, 36% yield).

Mono-amide 59:

^{1}H NMR (600 MHz, $CDCl_3$): δ 4.81 (ddq, *J* = 12.7, 3.6, 2.1 Hz, 1H), 3.39 (ddd, *J* = 11.3, 7.9, 2.5 Hz, 1H), 2.86 – 2.74 (m, 2H), 2.66 (ddt, *J* = 13.1, 4.0, 2.1 Hz, 1H), 2.43 – 2.29 (m, 2H), 2.27 – 2.16 (m, 2H), 2.07 (qd, *J* = 12.5, 3.7 Hz, 1H), 2.00 – 1.88 (m, 3H), 1.81 – 1.62 (m, 4H), 1.62 – 1.56 (m, 1H), 1.50 – 1.35 (m, 5H), 1.20 (dddd, *J* = 19.9, 8.1, 6.6, 3.6 Hz, 1H).

^{13}C NMR (104 MHz, $CDCl_3$): δ 168.9, 63.4, 62.5, 57.5, 57.0, 45.2, 40.8, 34.9, 33.1, 26.5, 25.9, 25.8, 25.7, 22.9, 22.6.

FTIR (NaCl, thin film): 2921, 2854, 2762, 2805, 1634, 1434, 1243, 1134 cm^{-1}.

HRMS: (ESI-TOF) calc'd for $C_{15}H_{24}N_2O$ $[M+H]^+$ 249.1961, found 249.1958.

TLC (10% 2 M NH_3 in MeOH/90% $CHCl_3$ with 0.75% EtOH stabilizer), **R_f:** 0.42 ($KMnO_4$).

M.P. 97.6 – 103.3 °C.

Figure 1.53. *X-Ray structure of (±)-**59**.*

X-Ray ID placeholder: V20006.

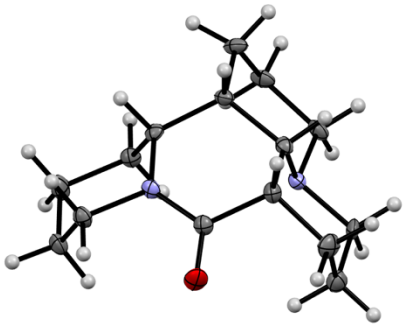

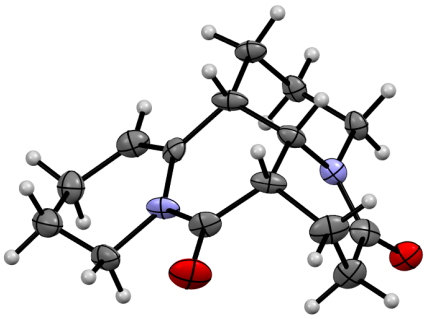

Preparation of (±)-diamine 43:

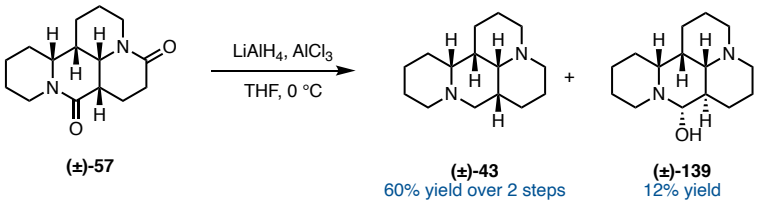

A 3 L oven-dried, N_2-flushed flask equipped with a thermocouple and a mechanical stirrer was charged with THF (856 mL, 0.1 M). The THF was cooled to 0 °C on an ice bath, then $AlCl_3$ (29.7 g, 223 mmol, 2.6 equiv) was added in a single portion, causing the solution to heat up to 30 °C. Upon dissolution of $AlCl_3$, lithium aluminum hydride (25.6 g, 642 mmol, 7.5 equiv) was added in portions at such a rate as to keep the internal temperature below 21 °C. Upon completion of the addition (*ca*. 10 minutes), the reaction

was allowed to stir for 30 minutes while cooling to 0 °C on an ice bath. A solution of unpurified (±)-bis-amide **57** (*ca.* 22.5 g, 85.6 mmol, 1.0 equiv) in THF (449 mL, 0.2 M) was added via cannula into the reaction flask at such a rate as to keep the internal temperature below 10 °C (*ca.* 30 minutes). Upon completion, the reaction was stirred for 1 hour at 0 °C. A 6 L Erlenmeyer flask in an ice bath was equipped with a mechanical stirrer and was charged with ice (1500 g), water (500 mL), and Rochelle's salt (200 g). The reaction was quenched by addition via cannula into the ice slurry (*ca*. 10 minutes). Liquid nitrogen was periodically added to purge hydrogen gas from the Erlenmeyer flask. Upon completion of the quench, 3 M NaOH (1 L) was added to the reaction mixture, which was then stirred at 21 °C until the aluminum salts transformed from a grey sediment into a white slurry (*ca.* 30 minutes). The organic layer was separated, and the aqueous layer was extracted with DCM (5 x 400 mL). The combined organic layers were concentrated under reduced pressure without drying. To the crude residue was added enough 12 M HCl (*ca.* 20–30 mL) to make the mixture acidic followed by enough 3 M NaOH (*ca*. 200 mL) to make the mixture basic. The resulting milky white suspension was extracted with DCM (5 x 120 mL). The combined organic layers were dried over anhydrous Na_2SO_4, filtered, and concentrated under reduced pressure. The crude product was dissolved in Et_2O (400 mL) and was concentrated under reduced pressure until crystallization of (±)-hemi-aminal **89** began. The mixture was diluted in Et_2O (total volume *ca.* 200–300 mL), and the solids were isolated via suction filtration. The solids were washed with Et_2O (3 x 30 mL) to yield (±)-hemi-aminal **139** as a white crystalline solid (2.49 g, 12% yield). The filtrate was concentrated under reduced pressure to yield crude (±)-diamine **43** as a yellow oil, which was allowed to crystallize under vacuum (0.3 torr) on a Schlenk line (13.55 g). To crude

(±)-diamine **43** was added anhydrous oxalic acid (6.76 g, 75.1 mmol, 1.0 equiv based on the mass of the obtained crude diamine) and MeOH (214 mL, 0.4 M). The mixture was heated to boiling, cooled to 21 °C, and concentrated under reduced pressure. The obtained solids were concentrated under reduced pressure from acetone (2 x 100 mL) and dried under vacuum (0.3 torr) on a Schlenk line on a warm water bath (40 °C). The solids were suspended in acetone with the aid of sonication and were isolated by suction filtration. The solids were washed with acetone (3 x 60 mL) and dried by pulling air through. The obtained crystals were dissolved in water (100 mL) and made basic with 3 M NaOH (*ca*. 50 mL), and the aqueous layer was extracted with DCM (5 x 100 mL). The combined organic layers were dried over anhydrous Na_2SO_4, filtered, and concentrated under reduced pressure. The resulting oil was concentrated under reduced pressure from Et_2O (3 x 100 mL) and suction filtered to remove precipitates. The obtained solution was concentrated under reduced pressure and was allowed to crystallize under vacuum (0.3 torr) on a Schlenk line to yield (±)-diamine **43** as a white crystalline solid (11.97 g, 60%).

Sodium borohydride reduction of hemi-aminal 139:

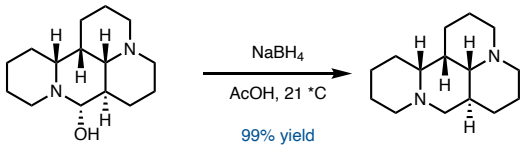

139 **60**

To a 250 mL flask was added the hemi-aminal **139** (500 mg, 2.00 mmol, 1.0 equiv), sodium borohydride (151 mg, 3.99 mmol, 2.0 equiv) and AcOH (10 mL, 0.2 M) at 21 °C. The reaction was stirred for 24 hours at 21 °C and was quenched with 3 M NaOH until basic by pH paper. The crude reaction mixture was extracted with DCM (3 x

50 mL), dried over anhydrous Na_2SO_4, filtered, and concentrated under reduced pressure. The crude product was allowed to crystallize under vacuum on a Schlenk line (0.3 torr, 30 minutes). The solids were dissolved in Et2O (30 mL) and the cloudy suspension was vacuum filtered. The clear colorless solution was concentrated under reduced pressure to yield the product diamine **60** as a white crystalline solid (468 mg, 99% yield) which did not require additional purification.

(±)-Diamine 60:

^{1}H NMR (600 MHz, $CDCl_3$): δ 2.99 – 2.91 (m, 3H), 2.83 (ddt, *J* = 11.5, 4.2, 2.0 Hz, 1H), 2.61 (dd, *J* = 11.3, 3.9 Hz, 1H), 2.52 (dd, *J* = 11.0, 4.7 Hz, 1H), 2.46 (dddd, *J* = 11.3, 4.0, 2.5, 1.2 Hz, 1H), 2.16 (qt, *J* = 11.3, 3.8 Hz, 1H), 1.87 – 1.79 (m, 3H), 1.79 – 1.70 (m, 2H), 1.70 – 1.53 (m, 5H), 1.54 – 1.40 (m, 4H), 1.37 (ddq, *J* = 13.0, 5.5, 2.8 Hz, 1H), 1.27 – 1.17 (m, 2H), 1.05 (tdd, *J* = 13.0, 11.7, 4.2 Hz, 1H).

^{13}C NMR (104 MHz, $CDCl_3$): δ 66.2, 64.0, 63.3, 57.2, 54.7, 45.8, 41.2, 30.2, 29.7, 26.3, 26.2, 26.0, 24.8, 20.1, 19.1.

FTIR (NaCl, thin film): 2927, 2850, 2750, 1440, 1131, 1110 cm^{-1}.

HRMS: (ESI-TOF) calc'd for $C_{15}H_{27}N_2$ $[M+H]^+$ 235.2169, found 235.2167.

TLC (40% 2 M NH_3 in MeOH/60% ACN), **R_f:** 0.32 ($KMnO_4$).

M.P. 82.3 – 83.3 °C.

Figure 1.54. *X-Ray structure of (±)-**60**.*.

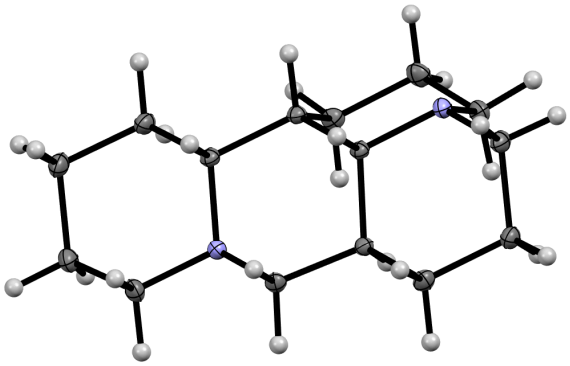

Preparation of copper complex 62:

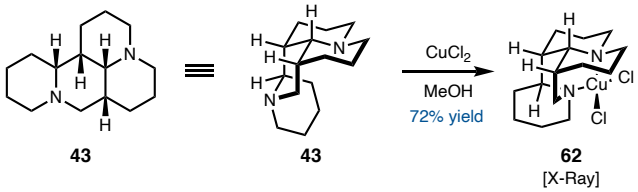

A 1-dram vial in a glovebox was charged anhydrous copper (II) chloride (57.7 mg, 429 umol, 1.0 equiv) and anhydrous MeOH (0.85 mL, 0.5 M) and was stirred until a homogenous solution was obtained. A separate 2-dram vial in a glovebox was charged with isomatridine (**43**) and MeOH (0.85 mL, 0.5 M) and was stirred until a homogenous solution was obtained. The two solutions were mixed, which initially produced a mixed blue/yellow precipitate. The mixture was heated to reflux for one minute, and then cooled to 21 °C at which point green crystals formed in a cloudy suspension. The supernatant was decanted, and the crystals were washed with MeOH (2 x 0.3 mL) and dried under vacuum (0.3 torr, 30 minutes) to yield the product **62** as a bright green crystalline solid (114 mg, 72% yield). The copper complex was found to be air stable but decomposed in aqueous solution. The copper complex could also be reduced to a copper (I) complex with zinc dust. The obtained crystals were directly used to obtain an X-ray structure.

X-ray placeholder: D19147

Figure 1.55. *X-Ray structure of (±)-**62**.*

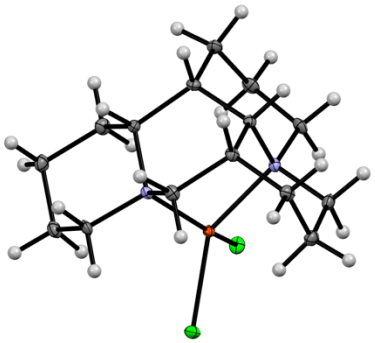

Resolution of (+)-diamine 43

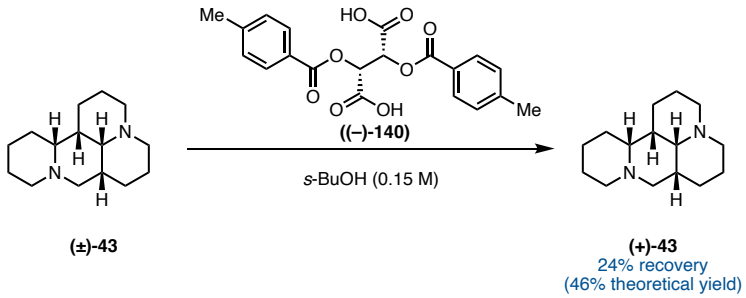

A 500 mL flask equipped with a 40 mm x 15 mm x 15 mm egg-shaped stir bar was charged with (±)-diamine **43** (11.97 g, 51.1 mmol, 1.0 equiv), (–)-di-*O,O'*-*p*-toluyl-L-tartaric acid (**126**) (19.7 g, 51.1 mmol, 1.0 equiv), and *s*-BuOH (341 mL, 0.15 M). The mixture was heated, with stirring, under N_2 until a homogenous solution was obtained. The mixture was cooled to 21 °C and was stirred at 300 rpm. Crystallization progress was monitored by ^{1}H NMR. Aliquots of the supernatant (250 μL), obtained by stopping stirring and allowing the solids to settle out of solution (*ca.* 10 minutes), were concentrated under

vacuum (0.3 torr) on a Schlenk line and then dissolved in $CDCl_3$. Crystallization was allowed to progress until 45% of diamine **43** had crystallized (*ca*. 25–45 hours), as measured relative to an aliquot taken before crystallization had begun. The crystals were isolated via suction filtration and were washed with *s*-BuOH (3 x 20 mL) then acetone (1 x 20 mL). The obtained crystalline solid was transferred into a separatory funnel with water (500 mL) and DCM (100 mL). The suspension was made basic with 3 M NaOH (*ca.* 50 mL) then the aqueous layer was extracted with DCM (4 x 150 mL). The combined organic layers were dried over anhydrous Na_2SO_4, filtered, and concentrated under reduced pressure. The residue was concentrated under reduced pressure from Et_2O (3 x 50 mL), suction filtered, and concentrated under reduced pressure. The resolution procedure was repeated a second time on the obtained diamine **43** (*ca*. 50-70% ee) to yield enantioenriched (+)-diamine **43** (2.82 g, 46% recovery of (+)-**43**, >90% ee) as a white to pale yellow crystalline solid. The optical activity of (+)-diamine **43** was assessed via ^{1}H NMR of its mono-(–)-di-*O,O′*-*p*-toluyl-L-tartaric acid salt (prepared in MeOH followed by concentration under vacuum (0.3 torr) on a Schlenk line for 30 minutes) in $CDCl_3$.

(+)-Diamine 43:

^{1}H NMR (600 MHz, $CDCl_3$): δ 3.40 (t, *J* = 11.5 Hz, 1H), 3.01 – 2.91 (m, 2H), 2.83 (ddd, *J* = 12.4, 5.7, 2.8 Hz, 1H), 2.80 – 2.70 (m, 2H), 2.10 (qd, *J* = 13.5, 3.3 Hz, 1H), 2.04 (dd, *J* = 11.0, 4.2 Hz, 1H), 1.96 – 1.78 (m, 6H), 1.78 – 1.66 (m, 3H), 1.65 – 1.48 (m, 4H), 1.44 – 1.31 (m, 4H), 1.11 (d, *J* = 14.5 Hz, 1H).

^{13}C NMR (104 MHz, $CDCl_3$): δ 63.1, 61.1, 58.0, 57.7, 55.5, 46.1, 38.6, 36.9, 29.0, 27.0, 26.3, 24.3, 23.0, 22.4, 19.2.

FTIR (NaCl, thin film): 2922, 2848, 2806, 2765, 2745, 2693, 2674, 2612, 2550, 2442, 1441, 1353, 1165, 1122, 1091, 1054 cm^{-1}.

HRMS: (ESI-TOF) calc'd for $C_{15}H_{27}N_2$ $[M+H]^+$ 235.2169, found 235.2164.

TLC (40% 2 M NH_3 in MeOH/60% ACN), **R*f*:** 0.37 ($KMnO_4$).

M.P. 64.1 °C – 66.7 °C.

Specific Optical Rotation: $[\alpha]\frac{21}{D} = +22.3$ (c 1.0, $CHCl_3$).

Figure 1.56. *X-Ray structure of (+)-**43**.*

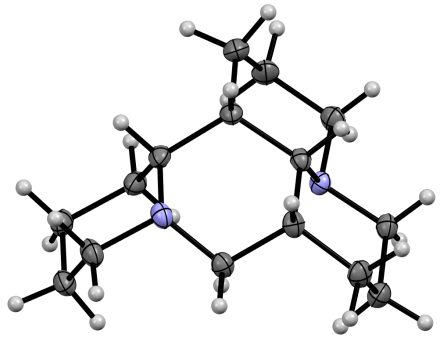

(±)-Hemi-aminal 89:

^{1}H NMR (400 MHz, $CDCl_3$): δ 4.83 (d, *J* = 11.8 Hz, 1H), 3.72 (d, *J* = 11.3 Hz, 1H), 3.01 (dd, *J* = 11.4, 8.8 Hz, 1H), 2.95 – 2.85 (m, 3H), 2.66 (dd, *J* = 11.3, 4.3 Hz, 1H), 2.49 (dt, *J* = 10.6, 2.9 Hz, 1H), 2.28 (dq, *J* = 13.2, 3.5 Hz, 1H), 2.07 (dt, *J* = 10.8, 3.0 Hz, 1H), 1.99 (s, 1H), 1.87 (tdd, *J* = 11.9, 8.9, 3.6 Hz, 1H), 1.81 – 1.36 (m, 11H), 1.35 – 1.21 (m, 2H), 1.14 (tdd, *J* = 13.2, 11.5, 4.1 Hz, 1H).

^{13}C NMR (104 MHz, $CDCl_3$): δ 92.8, 63.2, 60.8, 54.2, 52.9, 45.9, 40.8, 33.9, 29.8, 29.1, 26.1, 25.0, 25.0, 19.8, 18.8.

FTIR (NaCl, thin film): 2941, 2861, 2832, 1456, 1436, 1118, 1032 cm^{-1}.

HRMS: (ESI-TOF) calc'd for $C_{15}H_{27}N_2O$ $[M+H]^+$ 251.2123, found 251.2122.

TLC (40% 2 M NH_3 in MeOH/60% ACN), **R*f*:** 0.35 ($KMnO_4$).

M.P. 149.5 °C – 151.1 °C.

Figure 1.56. *X-Ray structure of (±)-**89**.*

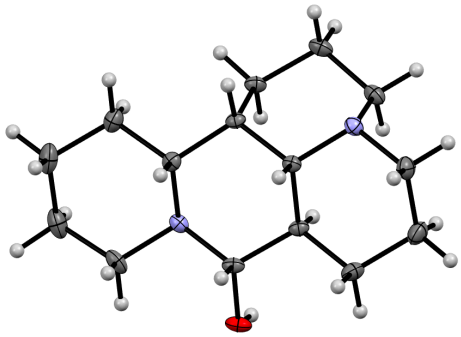

Figure 1.57. ^{1}H *NMR assay for determining enantiomeric excess.*

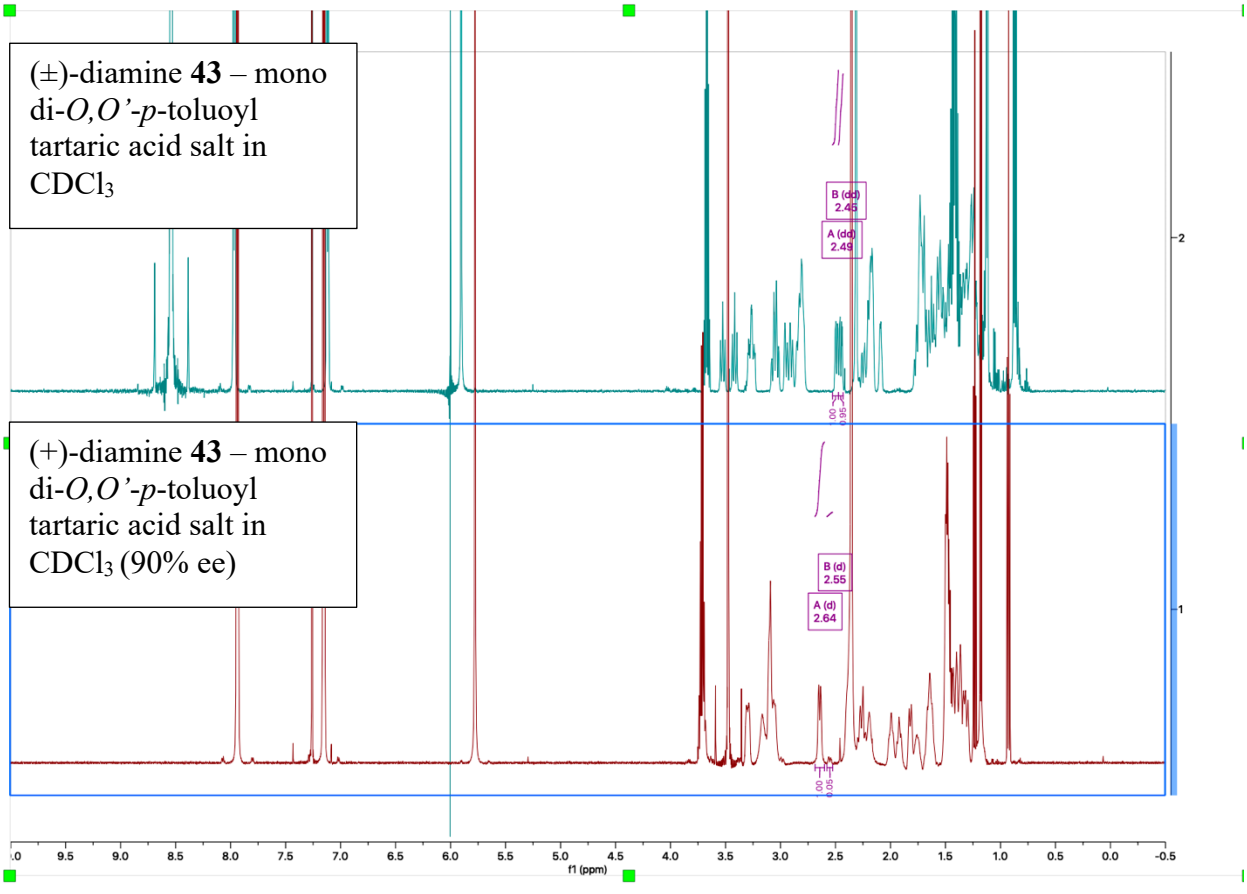

Figure 1.57. ^{1}H *NMR assay for determining enantiomeric excess close up.*

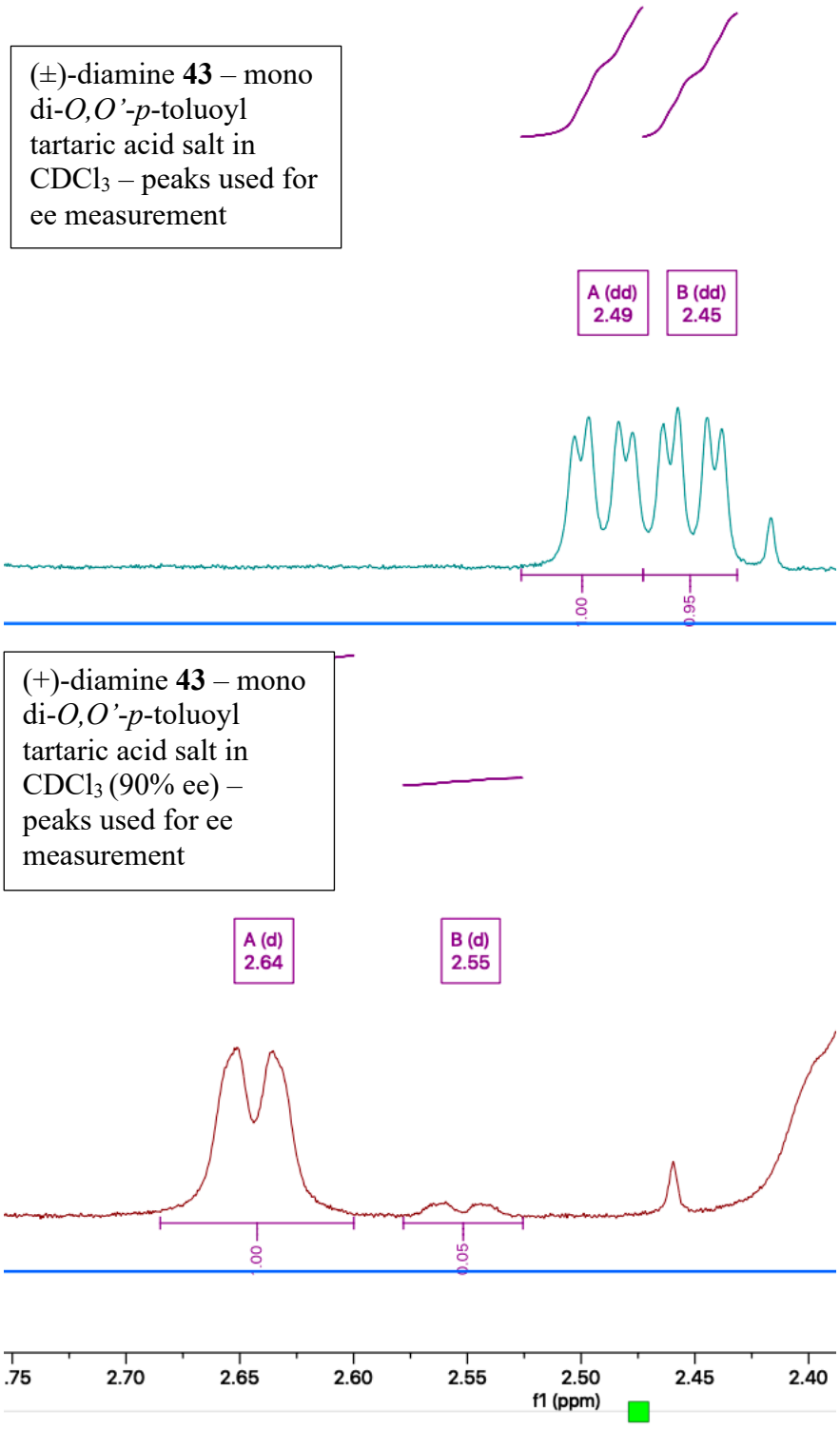

Preparation of α-aminonitrile 114:

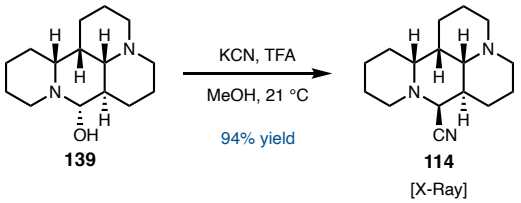

A 10 mL flask was charged with potassium cyanide (91.0 mg, 1.40 mmol, 7.0 equiv), hemi-aminal **89** (50.0 mg, 200 umol, 1.0 equiv), and MeOH (2.00 mL, 0.1 M). The flask was capped with a septa, then trifluoroacetic acid (153 uL, 2.00 mmol, 10 equiv) was added. The reaction was stirred while sealed at 21 °C for 1 hour. Upon completion the reaction was made basic with 3 M NaOH. The reaction mixture was extracted with DCM (3 x 20 mL), dried over anhydrous Na_2SO_4, filtered, and concentrated under reduced pressure. The product **114** was obtained as a white crystalline solid (48.7 mg, 94% yield) and did not require additional purification.

α-aminonitrile 114:

^{1}H NMR (600 MHz, $CDCl_3$): δ 3.60 (d, *J* = 4.5 Hz, 1H), 3.02 – 2.91 (m, 3H), 2.89 (td, *J* = 12.0, 2.9 Hz, 1H), 2.71 (d, *J* = 11.0 Hz, 1H), 2.51 – 2.40 (m, 3H), 2.38 (tt, *J* = 11.9, 4.7 Hz, 1H), 1.88 (qt, *J* = 13.2, 4.3 Hz, 1H), 1.80 – 1.57 (m, 7H), 1.57 – 1.40 (m, 4H), 1.35 (qd, *J* = 13.9, 13.5, 4.3 Hz, 1H), 1.31 – 1.21 (m, 2H).

^{13}C NMR (104 MHz, $CDCl_3$): δ 115.9, 62.5, 59.8, 59.1, 54.3, 54.2, 45.6, 40.3, 29.3, 28.7, 27.7, 25.9, 25.8, 24.0, 19.8, 18.4.

FTIR (NaCl, thin film): 3052, 2984, 2941, 2304, 1420, 1268, 895 cm^{-1}.

HRMS: (ESI-TOF) calc'd for $C_{16}H_{25}N_3$ $[M+H]^+$ 260.2121, found 260.2120.

TLC (10% 2 M NH_3 in MeOH /90% $CHCl_3$ stabilized with 0.75% EtOH), **R_f:** 0.35 ($KMnO_4$).

M.P. 180.2 °C – 181.1 °C

X-ray placeholder: V22045

Figure 1.58. *X-Ray structure of (±)-**114**.*

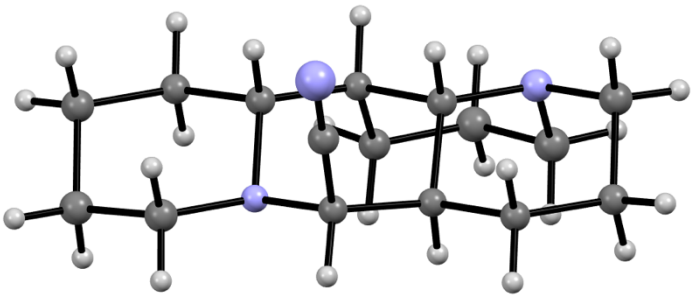

Preparation of conjugated iminium ion 98:

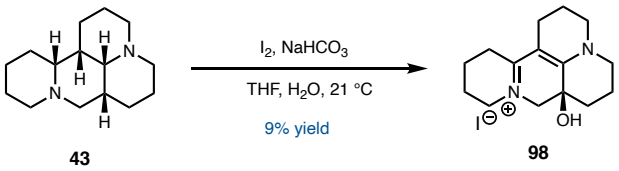

A 100 mL flask was charged with diamine **43** (200 mg, 0.85 mmol, 1 equiv), sodium bicarbonate (717 mg, 8.53 mmol, 10 equiv), THF (24 mL, 0.025 M), water (10 mL, 0.025 M), and iodine (1.62 g, 6.40 mmol, 7.5 equiv) and was stirred at ambient temperature for 20 hours. Upon completion the reaction was diluted in water (200 mL), and the reaction mixture was extracted with DCM (3 x 50 mL). The combined organic layers were dried over anhydrous Na_2SO_4, filtered, and concentrated under reduced pressure. A QNMR of the crude reaction revealed a 29% yield of iminium ion xx. An analytically pure sample was prepared by purification of the crude reaction mixture by SiO_2 column chromatography [20 g SiO_2, 20 mm column diameter, 10% 2 M NH_3 in

MeOH/90% $CHCl_3$ containing 0.75% EtOH as a stabilizer to 20% 2 M NH_3 in MeOH/90% $CHCl_3$ containing 0.75% EtOH in 2% increments] to yield a yellow oil. Trituration of the yellow oil from acetone yielded the iminium ion **98** as a pale yellow crystalline solid (18.7 mg, 9% yield). X-ray quality crystals were grown by slow evaporation from acetone under an atmosphere of N_2.

^{1}H NMR (400 MHz, $CDCl_3$): δ 4.85 (s, 1H), 3.93 (dt, *J* = 13.1, 6.1 Hz, 1H), 3.77 (d, *J* = 14.5 Hz, 1H), 3.52 – 3.34 (m, 5H), 3.24 (ddd, *J* = 13.4, 6.6, 4.3 Hz, 1H), 2.80 (dt, *J* = 18.8, 6.1 Hz, 1H), 2.65 – 2.39 (m, 3H), 2.27 – 1.70 (m, 9H), 1.51 (td, *J* = 13.6, 3.9 Hz, 1H).

^{13}C NMR (104 MHz, $CDCl_3$): δ 165.4, 157.3, 95.5, 63.7, 60.1, 52.2, 51.3, 50.5, 29.1, 28.0, 21.8, 21.1, 20.4, 18.5, 17.2.

FTIR (NaCl, thin film): 3053, 2986, 2685, 1605, 1554, 1422, 1273, 1261 cm^{-1}.

HRMS: (ESI-TOF) calc'd for $C_{15}H_{23}N_2O$ $[M]^+$ 247.1805, found 247.1805.

TLC (10% 2 M NH_3 in MeOH/90% $CHCl_3$ with 0.75% EtOH stabilizer), $\mathbf{R_f}$**:** 0.19 ($KMnO_4$).

M.P. 178.9 – 181.6 °C.

X-Ray ID placeholder: V22009.

Figure 1.59. *X-Ray structure of (±)-**98**.*

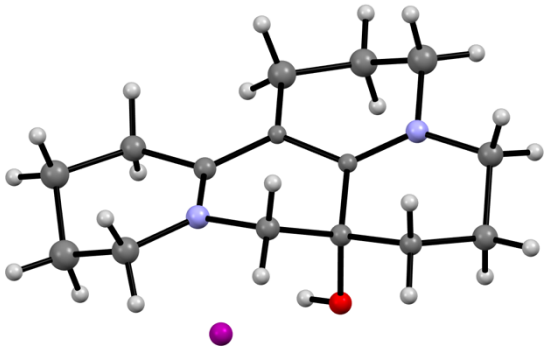

Preparation of α-aminonitrile 43:

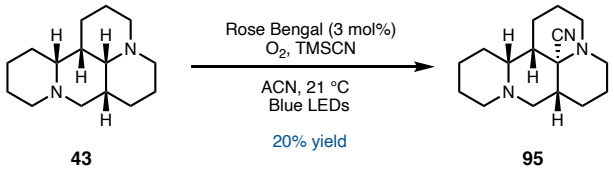

To a 4 mL vial was added the diamine **43** (50.5 mg, 0.22 mmol, 1.0 equiv), rose bengal (6.58 mg, 6.46 µmol, 3 mol %), trimethylsilyl cyanide 98 % (108 uL, 0.86 mmol, 4.0 equiv), and acetonitrile (2.15 mL, 0.1 M) The reaction was stirred vigorously under dry air while being The reaction was irradiated with a 34 W Kessil H150 Blue LED setup for 3 hours. Once the reaction was complete, K_2CO_3 was added, and the reaction was stirred for 10 minutes. The crude product was purified via SiO_2 column chromatography [5 g SiO_2, 10 mm column, 18% 2 M NH_3 in MeOH acetonitrile] to yield **95** as a light pink oil (11.0 mg, 20% yield).

α-aminonitrile 43:

^{1}H NMR (600 MHz, $CDCl_3$): δ 3.10 (t, *J* = 11.8 Hz, 1H), 3.01 – 2.91 (m, 3H), 2.67 (ddd, *J* = 12.2, 5.2, 2.1 Hz, 2H), 2.49 – 2.34 (m, 3H), 2.15 (qd, *J* = 13.2, 3.9 Hz, 1H), 1.97 (ddd, *J* = 12.5, 5.4, 3.3 Hz, 1H), 1.93 – 1.87 (m, 1H), 1.85 (dt, *J* = 11.8, 3.4 Hz, 1H),

1.76 – 1.60 (m, 4H), 1.60 – 1.51 (m, 2H), 1.51 – 1.41 (m, 2H), 1.35 (tt, J = 12.7, 3.7 Hz, 1H), 1.32 – 1.24 (m, 2H), 1.19 (d, J = 13.7 Hz, 1H).

^{13}C NMR (104 MHz, $CDCl_3$): δ 117.4, 64.2, 60.8, 54.9, 52.1, 51.5, 49.0, 45.5, 43.3, 25.5, 25.0, 25.0, 24.9, 24.5, 20.3, 20.0.

FTIR (NaCl, thin film): 2984, 2930, 2852, 2304, 1459, 1441, 1421, 1266 cm^{-1}.

HRMS: (ESI-TOF) calc'd for $C_{16}H_{25}N_3$ $[M+H]^+$ 260.2121, found 260.2120.

TLC (40% 2 M NH_3 in MeOH/60% ACN), **R_f:** 0.20 ($KMnO_4$).

M.P. 66.8 – 67.9 °C.

X-Ray ID placeholder: V21361.

Figure 1.60. *X-Ray structure of the dihydrate of (±)-**95**.*

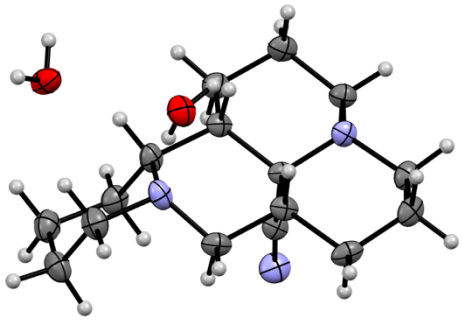

Preparation of diamine 96 and diamine 97:

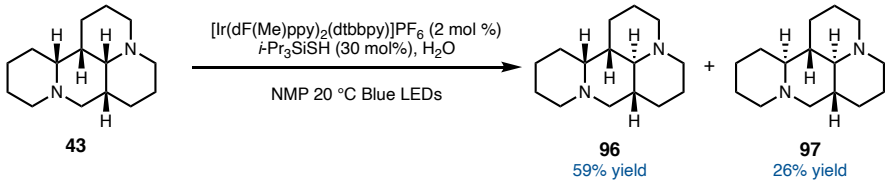

A one dram vial was charged with $[Ir(dF(Me)ppy)_2(dtbbpy)]PF_6$ (8.7 mg, 8.53 µmol, 2 mol %), diamine **43** (100 mg, 427 µmol, 1 equiv), NMP (1.7 mL, 0.25 M), triisopropylsilanethiol (27.5 µL, 128 µmol, 30 mol %), and water (77 µL, 50 equiv)

sequentially, then the vial was sparged with N_2 for 20 minutes. The reaction was irradiated with a 34 W Kessil H150 Blue LED setup for 24 hours. The reaction mixture was passed through a SiO_2 plug with DCM to elute the NMP, then 2 M NH_3 in MeOH to elute the products. The crude product mixture was purified via SiO_2 column chromatography [5 g SiO_2, 10 mm column, eluted with 40% 2 M NH_3 in MeOH/60% ACN] to yield the diamine **96** as a white crystalline solid (58.6 mg, 59% yield) and diamine **97** as a white crystalline solid (26.2 mg, 26% yield). X-Ray quality crystals were grown from slow evaporation of a solution of each diamine in ACN.

Diamine 96:

^{1}H NMR (400 MHz, $CDCl_3$): δ 3.06 – 2.73 (m, 6H), 2.38 (dd, *J* = 11.4, 3.9 Hz, 1H), 1.99 (td, *J* = 11.7, 3.3 Hz, 1H), 1.95 – 1.88 (m, 1H), 1.88 – 1.82 (m, 1H), 1.79 – 1.52 (m, 9H), 1.51 – 1.32 (m, 3H), 1.27 – 1.18 (m, 1H), 1.17 – 1.07 (m, 2H), 1.02 (qd, *J* = 12.9, 4.5 Hz, 1H).

^{13}C NMR (104 MHz, $CDCl_3$): δ 65.7, 60.6, 56.8, 56.5, 54.8, 51.0, 43.2, 41.3, 29.0, 27.7, 26.0, 25.5, 25.2, 19.2, 18.8.

FTIR (NaCl, thin film): 2930, 2856, 2802, 2750, 1265 cm^{-1}.

HRMS: (FI-TOF) calc'd for $C_{15}H_{26}N_2$ $[M]^+$ 234.20905, found 234.20943.

TLC (40% 2 M NH_3 in MeOH/60% ACN), **R_f:** 0.11 ($KMnO_4$).

M.P. 57.1 – 58.8 °C.

X-Ray ID placeholder: V20120.

Figure 1.61. *X-Ray structure of (±)-***96**.

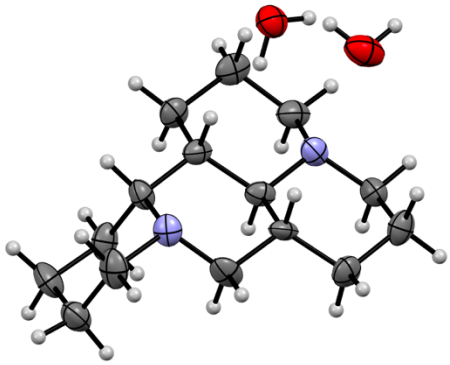

Diamine 97:

^{1}H NMR (400 MHz, $CDCl_3$): δ 2.89 – 2.75 (m, 3H), 2.68 (dd, *J* = 11.3, 3.5 Hz, 1H), 2.02 – 1.89 (m, 3H), 1.90 – 1.80 (m, 3H), 1.80 – 1.54 (m, 6H), 1.51 (td, *J* = 10.1, 2.2 Hz, 1H), 1.23 – 1.04 (m, 5H), 0.94 (qd, *J* = 12.5, 4.5 Hz, 1H), 0.88 – 0.74 (m, 3H).

^{13}C NMR (104 MHz, $CDCl_3$): δ 71.3, 66.7, 61.8, 56.8, 56.6, 56.2, 44.6, 39.3, 29.9, 29.5, 29.1, 27.0, 25.7, 25.1, 24.6.

FTIR (NaCl, thin film): 2935, 2854, 2802, 2754, 1264 cm^{-1}.

HRMS: (FI-TOF) calc'd for $C_{15}H_{26}N_2$ $[M]^+$ 234.20905, found 234.20976.

TLC (40% 2 M NH_3 in MeOH/60% ACN), **R_f:** 0.32 ($KMnO_4$).

M.P. 46.8 – 49.1 °C.

X-Ray ID placeholder: V20119.

Figure 1.62. *X-Ray structure of (±)-**97**.*

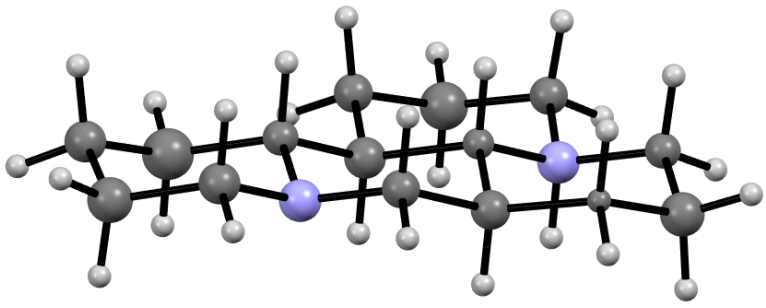

Preparation of alkyl bromides 99 and 100:

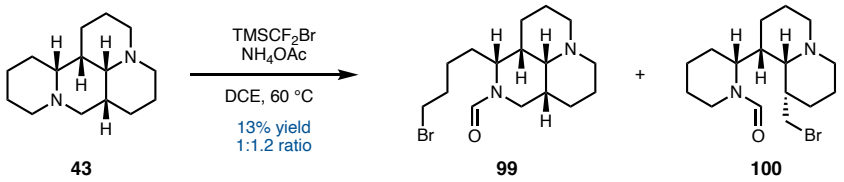

A 1-dram vial in a glovebox was charged with diamine **43** (46.9 mg, 200 μmol, 1 equiv), ammonium acetate (61.7 mg, 800 μmol, 4 equiv), dichloroethane (0.5 mL, 0.4 M) and lastly (bromodifluoromethyl)trimethylsilane (124 μL, 800 μmol, 4 equiv). The reaction was sealed and stirred at 60 °C for 12 hours. Upon completion the mixture was filtered through a pad of celite which was washed with EtOAc (3 x 10 mL). The solution was concentrated under reduced pressure and was purified via SiO_2 column chromatography on SiO_2 [5 g SiO_2, 10 mm column diameter, eluted with 5% 2 M NH_3 in MeOH/95% $CHCl_3$ containing 0.75% EtOH] to yield the mixture of products **99** and **100** as a clear colorless oil (11.8 mg, 13% yield).

alkyl bromides 99 and 100:

^{1}H NMR (400 MHz, $CDCl_3$): δ 8.07 (s, 1H), 8.03 (s, 1H), 4.39 (dt, *J* = 12.3, 5.1 Hz, 1H), 3.90 (dd, *J* = 12.7, 4.3 Hz, 1H), 3.49 (t, *J* = 12.8 Hz, 1H), 3.45 – 3.31 (m, 6H), 2.98 – 2.89 (m, 2H), 2.81 – 2.73 (m, 5H), 2.37 (dtd, *J* = 13.6, 11.4, 4.8 Hz, 1H), 2.29 (dddd, *J* = 13.8, 12.5, 10.2, 4.9 Hz, 1H), 2.08 (q, *J* = 3.3 Hz, 2H), 2.01 – 1.93 (m, 1H), 1.93 – 1.79 (m, 10H), 1.76 (ddt, *J* = 14.5, 11.4, 3.0 Hz, 3H), 1.72 – 1.58 (m, 10H), 1.58 – 1.49 (m, 3H), 1.45 (dddd, *J* = 13.1, 9.9, 5.1, 2.6 Hz, 4H), 1.41 – 1.31 (m, 2H), 1.31 – 1.23 (m, 2H), 1.23 – 1.14 (m, 1H).

^{13}C NMR (104 MHz, $CDCl_3$): δ 161.2, 160.8, 63.9, 63.8, 59.3, 57.7, 57.6, 57.5, 57.5, 51.6, 42.3, 39.1, 37.8, 37.2, 35.9, 35.8, 34.1, 33.6, 32.7, 32.7, 30.2, 30.0, 28.1, 28.1, 26.6, 26.5, 25.9, 25.3, 22.7, 22.6, 21.7, 21.6.

Preparation of (±)-*N*-oxide 104:

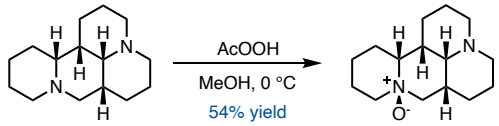

(±)-**43** (±)-**104**

A 1 L flask was charged with (±)-diamine **43** (2.50 g, 10.7 mmol, 1.0 equiv) and methanol (323 mL, 0.033 M). The solution was cooled to 0 °C, then peracetic acid (32% wt. % in dilute acetic acid, 2.42 mL, 11.7 mmol, 1.1 equiv) was added dropwise. The reaction was stirred for 15 minutes at 0 °C followed by removal of the solvent under reduced pressure. The residue was diluted in DCM (200 mL) and the organic layer washed with 3 M NaOH (50 mL). The aqueous layer was extracted with DCM (3 x 100 mL). The combined organic layers were dried over anhydrous Na_2SO_4, filtered, and concentrated under reduced pressure. The crude product was purified by crystallization from boiling hexanes (15 mL) and enough chloroform to ensure complete dissolution. The solution was allowed to cool to 21 °C then to –20 °C. The solution was decanted from the crystals, and the crystals were washed with a 5:1 mixture of hexanes/chloroform followed by drying *in vacuo* to yield (±)-*N*-oxide **104** as a white crystalline solid (1.44 g, 54% yield).

(±)-*N*-oxide 104:

^{1}H NMR (400 MHz, $CDCl_3$): δ 3.87 (dd, *J* = 12.7, 11.0 Hz, 1H), 3.47 (ddtd, *J* = 13.2, 4.0, 2.3, 0.3 Hz, 1H), 3.37 (td, *J* = 13.2, 4.4 Hz, 1H), 3.17 (dtd, *J* = 7.8, 6.0, 4.9, 2.8 Hz, 1H),

3.14 – 3.06 (m, 1H), 3.02 (dddd, J = 13.2, 5.4, 3.8, 1.3 Hz, 1H), 2.81 – 2.66 (m, 2H), 2.40 – 2.26 (m, 2H), 2.01 (t, J = 3.9 Hz, 1H), 1.98 – 1.32 (m, 15H).

^{13}C NMR (104 MHz, $CDCl_3$): δ 77.0, 72.2, 61.0, 57.6, 57.5, 57.4, 31.1, 29.2, 29.1, 27.3, 25.5, 23.8, 23.1, 22.6, 22.2.

FTIR (NaCl, thin film): 2985, 1420, 1268 cm^{-1}.

HRMS: (ESI-TOF) calc'd for $C_{15}H_{27}N_2O$ $[M+H]^+$ 251.2118, found 251.2116.

TLC (40% 2 M NH_3 in MeOH/60% ACN), **R_f:** 0.31 ($KMnO_4$).

M.P. 202.9 – 208.1 °C.

Figure 1.63. *X-Ray structure of the mono-chloroform adduct of (±)-**104**.*

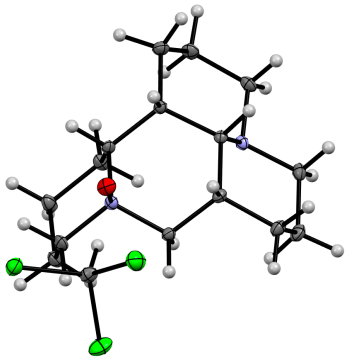

Preparation of (±)-diamine 60:

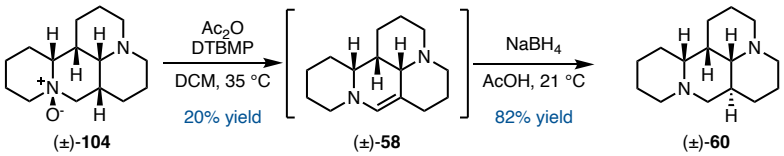

N-oxide elimination:

A 25 mL oven-dried, N_2-flushed flask was charged with (±)-*N*-oxide **104** (100 mg, 0.399 mmol, 1.0 equiv), 2,6-di-*tert*-butyl-4-methylpyridine (147 mg, 0.718 mmol, 1.8 equiv), DCM (10 mL, 0.04 M), and acetic anhydride (0.38 mL, 3.99 mmol, 10.0 equiv).

The reaction was stirred at 35 °C until complete consumption of the starting material, as judged by TLC (*ca.* 24 hours). The reaction was concentrated under reduced pressure and then the crude product was partially purified via SiO_2 column chromatography (20 g SiO_2, 20 mm column diameter, 40% 2 M NH_3 in MeOH/60% can) to yield (±)-enamine **58** as a brown oil (18.4 mg, 20% yield) which was unstable to storage and was immediately subjected to reduction.

Sodium borohydride reduction:

A 25 mL flask was charged with partially purified (±)-enamine **58** (107 mg, 0.46 mmol, 1.0 equiv), sodium borohydride (34.8 mg, 0.92 mmol, 2.0 equiv), and acetic acid (4.6 mL, 0.1 M). The reaction was stirred at 21 ºC until complete consumption of the starting material, as judged by TLC (*ca.* 20 minutes). Upon completion, the reaction was diluted in DCM (50 mL) and was neutralized with 3 M NaOH (50 mL). The aqueous layer was extracted with DCM (3 x 30 mL). The combined organic layers were dried over anhydrous Na_2SO_4, filtered, and concentrated under reduced pressure. The crude product was purified via SiO_2 column chromatography (20 g SiO_2, 20 mm column diameter, 40% 2 M NH_3 in MeOH/60% can) to yield (±)-diamine **60** as a white crystalline solid (88.3 mg, 82% yield). X-ray-quality crystals were grown by allowing a solution of **60** in acetonitrile to slowly evaporate at 21 °C. See above for full characterization data.

Preparation of (±)-isomatrine (6) and (+)-isomatrine (6):

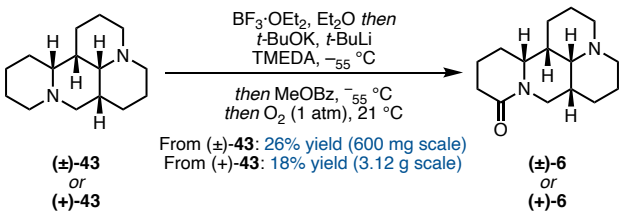

Small scale racemic procedure:

A 250 mL oven-dried flask equipped with a 40 mm x 15 mm x 15 mm egg-shaped stir bar was charged with (±)-diamine **43** (600 mg, 2.56 mmol, 1.0 equiv), then the flask was evacuated and backfilled three times with N_2. Diethyl ether (2.6 mL, 1 M) was added, resulting in a clear, colorless solution. To the solution at 21 °C was added boron trifluoride diethyl etherate (319 uL, 2.59 mmol, 1.01 equiv). The resulting white slurry was stirred at 21 °C for five minutes followed by removal of the diethyl ether under vacuum (0.3 torr) on a Schlenk line; the solids were allowed to dry for an additional 30 minutes. After backfilling the flask with N_2, a thermocouple was introduced into the flask through the rubber septum. The flask was cooled to –60 °C and maintained at this temperature using an acetone/dry ice bath. A solution of potassium *tert*-butoxide (1.72 g, 15.4 mmol, 6.0 equiv) in tetramethylethylenediamine (TMEDA) (12.8 mL, 0.2 M), prepared by dissolving potassium *tert*-butoxide in TMEDA in an inert atmosphere followed by clarification of the suspension via syringe filtration, was added via syringe, allowing the solution to flow down the side of the flask to pre-cool it before it encountered the solids. To the resulting suspension between –55 °C to –60 °C was added *tert*-butyl lithium (1.6 M in pentane, 4.8 mL, 7.68 mmol, 3.0 equiv) via syringe at such a rate as to prevent the internal reaction temperature from increasing above –40 °C (*ca.* 2 to 4 minutes). Once the addition was

complete, the reaction was stirred for 30 minutes at –55 °C to –60 °C. Subsequently, a solution of methyl benzoate (2.56 mL, 20.5 mmol, 8.0 equiv) in cyclopentyl methyl ether (10.2 mL, 0.25 M) was added at such a rate as to prevent the internal reaction temperature from increasing above –40 °C (*ca*. 4 to 8 minutes). Once the addition was complete, the reaction was allowed to stir at –55 °C to –60 °C for 30 minutes, then methanol (311 uL, 7.68 mmol, 3.0 equiv) was added. The thermocouple was removed, and the rubber septum was replaced with a new rubber septum. **Caution!** Traces of solid *tert*-butyl lithium tend to get stuck on the inside of the rubber septum, and it should be replaced before oxygen is introduced into the flask. The flask was purged with O_2 (balloon) at –55 °C then was allowed to warm to 21 °C. The resulting orange suspension was stirred vigorously (1500 rpm) for 2 hours. Upon completion, the yellow suspension was diluted in water (50 mL) and treated with sat. aq. $Na_2S_2O_3$ (15 mL) and 3 M NaOH (15 mL). The reaction mixture was extracted with DCM (4 x 50 mL). The combined organic layers were dried over anhydrous Na_2SO_4, filtered, and concentrated under reduced pressure. The crude product was purified via SiO_2 column chromatography (30 g SiO_2, 30 mm column diameter, 3% 2 M NH_3 in MeOH/97% $CHCl_3$ containing 0.75% EtOH as a stabilizer). The obtained product underwent a final purification by crystallization from boiling hexanes (*ca*. 5 mL). After dissolution in boiling hexanes, the solution was allowed to slowly cool to 21 °C then to –20 °C. The supernatant was decanted and the crystals washed with cold hexanes (3 x 1 mL). The obtained crystals were dried *in vacuo* to yield (±)-isomatrine (**6**) as white crystalline needles (167 mg, 26% yield).

Large Scale Enantiopure Procedure:

A 1 L oven-dried, N_2-flushed flask equipped with a 40 mm x 15 mm x 15 mm egg-shaped stir bar was charged with (+)-diamine **43** (3.12 g, 13.3 mmol, 1.0 equiv), then the flask was evacuated and backfilled three times with N_2. Diethyl ether (14 mL, 1 M) was added, which created a clear pale yellow solution. To the solution at 21 °C was added boron trifluoride diethyl etherate (1.66 mL, 13.4 mmol, 1.01 equiv). The resulting white slurry was stirred at 21 °C for five minutes followed by removal of the diethyl ether under vacuum (0.3 torr) on a Schlenk line; the solids were allowed to dry for an additional 30 minutes. After backfilling the flask with N_2, a thermocouple was introduced into the flask through the rubber septum. The flask was cooled to –60 °C and maintained at this temperature using an acetone/dry ice bath. A solution of potassium *tert*-butoxide (8.96 g, 79.9 mmol, 6.0 equiv) in TMEDA (67 mL, 0.2 M), prepared by dissolving potassium *tert*-butoxide in TMEDA in an inert atmosphere followed by clarification of the suspension via syringe filtration, was added via syringe, allowing the solution to flow down the side of the flask to pre-cool it before it encountered the solids. To the resulting suspension at –55 °C to –60 °C was added *tert*-butyl lithium (1.6 M in pentane, 25 mL, 39.9 mmol, 3.0 equiv) via cannula at such a rate as to prevent the reaction temperature from increasing above –40 °C (*ca.* 5 to 10 minutes). Once the addition was complete, the reaction was stirred for 30 minutes at –55 °C to –60 °C. Subsequently, a solution of methyl benzoate (13.3 mL, 106 mmol, 8.0 equiv) in cyclopentyl methyl ether (53 mL, 0.25 M) was added at such a rate as to prevent the reaction temperature from increasing above –40 °C (*ca*. 5 to 12 minutes). Once the addition was complete, the reaction was allowed to stir at –55 °C for 30 minutes, then methanol (1.62 mL, 39.9 mmol, 3.0 equiv) was added. The thermocouple was

removed, and the rubber septum was replaced with a new rubber septum. **Caution!** Traces of solid *tert*-butyl lithium tend to get stuck on the inside of the rubber septum, and it should be replaced before oxygen is introduced. The flask was purged with O_2 (balloon) at –55 °C then was allowed to warm to 21 °C. The resulting orange suspension was stirred vigorously (1500 rpm) for 2 hours. Upon completion, the yellow suspension was diluted in water (150 mL) and treated with sat. aq. $Na_2S_2O_3$ (50 mL) and 3 M NaOH (50 mL). The reaction mixture was extracted with DCM (4 x 150 mL). The combined organic layers were dried over anhydrous Na_2SO_4, filtered, and concentrated under reduced pressure. The crude product was purified via SiO_2 column chromatography (120 g SiO_2, 50 mm column diameter, eluting with 3% 2 M NH_3 in MeOH/97% $CHCl_3$ containing 0.75% EtOH as a stabilizer). The product underwent a final purification by crystallization from boiling hexanes (*ca*. 15 mL). After dissolution in boiling hexanes, the solution was allowed to slowly cool to 21 °C then to –20 °C. The supernatant was decanted and the crystals washed with cold hexanes (3 x 2 mL). The obtained crystals were dried *in vacuo* to yield (+)-isomatrine (**6**) as white crystalline needles (589 mg, 18% yield, >99% ee). An X-ray structure was acquired directly from the obtained crystals.

(+)-Isomatrine (6):

^{1}H NMR (600 MHz, $CDCl_3$): δ 3.77 (p, *J* = 4.4 Hz, 1H), 3.62 (t, *J* = 13.0 Hz, 1H), 3.52 (dd, *J* = 12.8, 4.1 Hz, 1H), 2.71 (d, *J* = 9.2 Hz, 1H), 2.67 (td, *J* = 11.2, 2.6 Hz, 1H), 2.45 – 2.39 (m, 1H), 2.35 – 2.26 (m, 2H), 2.22 – 2.15 (m, 1H), 2.05 (dt, *J* = 11.5, 8.0 Hz, 1H), 1.99 – 1.90 (m, 2H), 1.90 – 1.81 (m, 2H), 1.75 – 1.59 (m, 5H), 1.56 (dt, *J* = 13.4, 5.4 Hz, 1H), 1.53 – 1.47 (m, 1H), 1.47 – 1.36 (m, 3H).

^{13}C NMR (104 MHz, $CDCl_3$): δ 170.5, 61.3, 55.9, 52.8, 52.1, 43.2, 39.3, 32.8, 30.8, 27.4, 26.8, 21.6, 21.4, 20.3, 18.2.

FTIR (NaCl, thin film): 2983, 2952, 2887, 2795, 2684, 1618, 1421, 1276, 1265, 1170 cm^{-1}.

HRMS: (FI-TOF) calc'd for $C_{15}H_{24}N_2O$ $[M]^+$ 248.1883, found 248.1886.

TLC (10% 2 M NH_3 in MeOH/90% $CHCl_3$ with 0.75% EtOH stabilizer), **R_f:** 0.36 ($KMnO_4$).

M.P. 99.1 °C – 100.3 °C.

Specific Optical Rotation: $[\alpha]\frac{21}{D} = +35.5$ (c 1.0, $CHCl_3$).

Literature Specific Optical Rotation: $[\alpha]\frac{21}{D} = +44$ (c 1.0, $CHCl_3$).[86]

Chiral SFC: (OB-H, 2.5 mL/min, 15% IPA in CO_2, λ = 210 nm): t_R (major) = 3.388 min, t_R (minor) = 4.523 min.

Figure 1.64. *SFC trace of racemic isomatrine.*

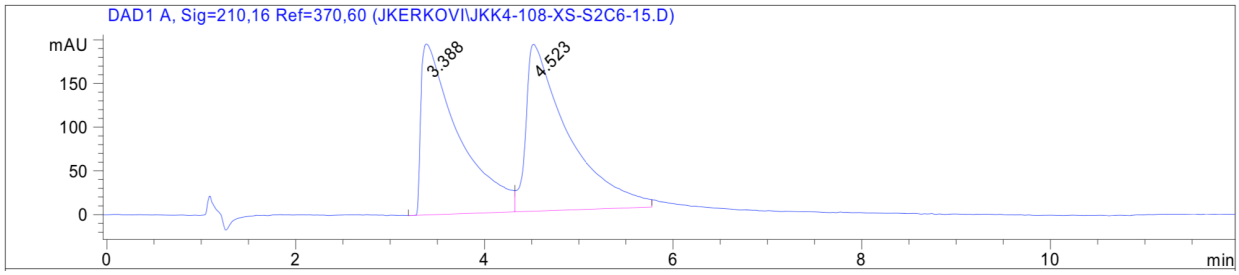

Signal 1: DAD1 A, Sig=210,16 Ref=370,60

Peak #	RetTime [min]	Type	Width [min]	Area [mAU*s]	Height [mAU]	Area %
1	3.388	BV	0.3695	5387.90967	195.53056	47.3900
2	4.523	VB	0.4174	5981.39648	190.98810	52.6100

Figure 1.65. *SFC trace of enantiopure isomatrine.*

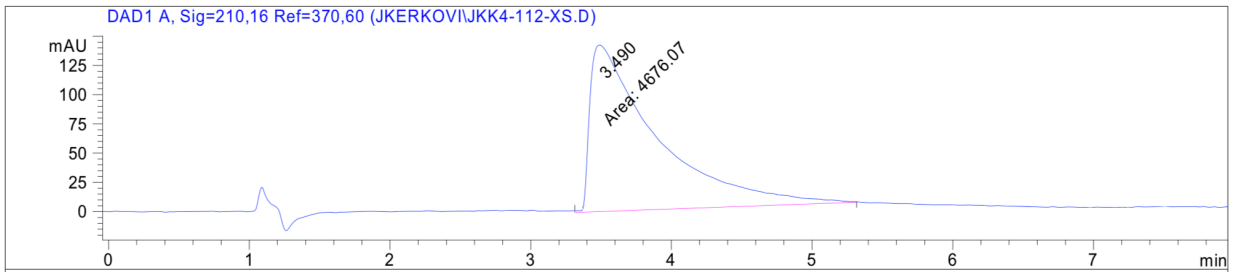

Signal 1: DAD1 A, Sig=210,16 Ref=370,60

Peak #	RetTime [min]	Type	Width [min]	Area [mAU*s]	Height [mAU]	Area %
1	3.490	MM	0.5466	4676.07227	142.58051	100.0000

Figure 1.66. *X-Ray structure of (+)-isomatrine ((+)-**6**).*

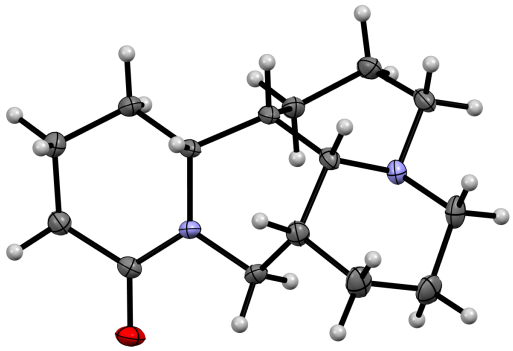

Table 2.13. *^{1}H NMR data for authentic vs synthetic (+)-isomatrine.*

The X-ray structure of (+)-isomatrine has been previously published.[87]

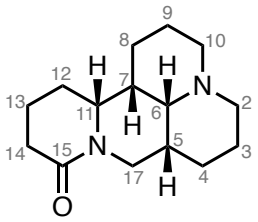

Isomatrine Literature ^{1}H δ ppm (220 MHz, $CDCl_3$)[87]	Isomatrine Recorded ^{1}H δ ppm (600 MHz, $CDCl_3$)
3.78 (m, 1H)	3.77, (p, *J* = 4.4 Hz, 1H)
3.63 (dd, *J* = 13.5, 12.8 Hz, 1 H)	3.62 (t, *J* = 13.0 Hz, 1H)
3.51 (dd, 13.5, 4.6 Hz, 1H)	3.52 (dd, *J* = 12.8, 4.1 Hz, 1H)
2.93 – 2.64 (m, 2H)	2.71 (d, *J* = 9.2 Hz, 1H)
	2.67 (td, *J* = 11.2, 2.6 Hz, 1H)
2.50 – 1.30 (m, 19H)	2.45 – 2.39 (m, 1H)
	2.35 – 2.26 (m, 2H)
	2.22 – 2.15 (m, 1H)
	2.05 (dt, *J* = 11.5, 8.0 Hz, 1H)
	1.99 – 1.90 (m, 2H)
	1.90 – 1.81 (m, 2H)
	1.75 – 1.59 (m, 5H)
	1.56 (dt, *J* = 13.4, 5.4 Hz, 1H)
	1.53 – 1.45 (m, 1H)
	1.45 – 1.36 (m, 3H)

Table 2.14. *^{13}C NMR data for authentic vs synthetic (+)-isomatrine.*

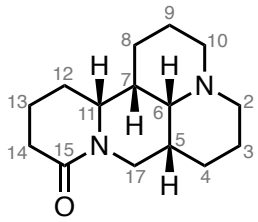

Carbon No. isomatrine	Isomatrine Literature ^{13}C δ ppm (75 MHz, $CDCl_3$)[87]	Isomatrine Recorded ^{13}C δ ppm (101 MHz, $CDCl_3$)	Δ δ
2	55.7	55.9	0.2
3	21.2	21.4	0.2
4	21.2	21.6	0.3
5	30.6	30.8	0.2
6	61.0	61.3	0.3
7	39.1	39.3	0.2
8	26.7	26.8	0.1
9	20.2	20.3	0.1
10	51.9	52.1	0.2
11	52.6	52.8	0.2
12	27.1	27.4	0.3
13	18.2	18.2	0.0
14	32.6	32.8	0.2
15	170.4	170.6	0.2
17	43.1	43.2	0.1

Preparation of (±)-aminonitrile 114:

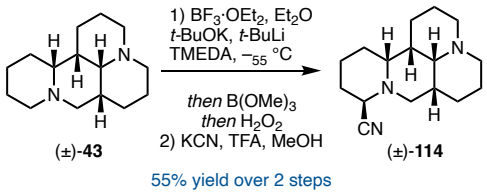

A 50 mL flask was charged with (±)-diamine **43** (200 mg, 0.66 mmol, 1.0 equiv). The flask was evacuated and backfilled three times with N_2. Diethyl ether (0.9 mL, 1 M) was added, resulting in a clear, colorless solution. To the solution at 21 °C was added boron trifluoride diethyl etherate (106 uL, 0.86 mmol, 1.01 equiv). The resulting white suspension was stirred at 21 °C for five minutes followed by removal of the diethyl ether under vacuum (0.3 torr) on a Schlenk line; the solids were allowed to dry for an additional 30 minutes. The flask was backfilled with N_2, and a thermocouple was introduced into the flask through the septum. The flask was cooled to –60 °C and maintained at this temperature using an acetone/dry ice bath. A solution of potassium *tert*-butoxide (446 mg, 3.97 mmol, 6.0 equiv) in TMEDA (3.3 mL, 0.2 M), prepared by dissolving potassium *tert*-butoxide in TMEDA in an inert atmosphere followed by clarification of the suspension via syringe filtration, was added via syringe by allowing the solution to flow down the side of the flask to pre-cool it before it encountered the solids. To the resulting suspension at –55 °C to –60 °C was added *tert*-butyl lithium (1.6 M in pentane, 1.24 mL, 1.99 mmol, 3.0 equiv) via syringe at such a rate as to prevent the reaction temperature from increasing above –40 °C (*ca.* 1 to 2 minutes). Once the addition was complete, the reaction was stirred for 30 minutes at –55 °C to –60 °C. After 30 minutes, trimethylborate (0.59 mL, 5.29 mmol, 8.0 equiv) was added at such a rate as to prevent the reaction temperature from increasing above –40 °C

(*ca*. 5 to 8 minutes). Once the addition was complete, the reaction was allowed to stir at –55 °C for 30 minutes. Subsequently, 30% aqueous hydrogen peroxide (0.68 mL, 6.62 mmol, 10.0 equiv) was added at –55 °C, then the reaction was allowed to warm to 21 °C and stir for one hour. After one hour, the reaction was treated with 3 M NaOH (10 mL) and sat. aq. $Na_2S_2O_3$ (10 mL). The aqueous layer was extracted with DCM (3 x 25 mL). The combined organic layers were dried over anhydrous Na_2SO_4, filtered, and concentrated under reduced pressure to yield a yellow oil. A 25 mL flask was charged with the crude reaction mixture, potassium cyanide (302 mg, 4.63 mmol, 7.0 equiv), and methanol (6.6 mL, 0.1 M). The flask was capped with a rubber septum, and trifluoroacetic acid (1.0 mL, 13.2 mmol, 20.0 equiv) was added (**Caution!** HCN vapors are produced!) The reaction was stirred until complete consumption of the starting material, as judged by TLC (*ca*. 2 hours). Upon completion, the reaction was quenched with 3 M NaOH (50 mL). The aqueous layer was extracted with DCM (3 x 25 mL). The combined organic layers were dried over anhydrous Na_2SO_4, filtered, and concentrated under reduced pressure. The crude reaction was purified via SiO_2 column chromatography (20 g SiO_2, 20 mm column diameter, 4% 2 M NH_3 in MeOH/96% $CHCl_3$ containing 0.75% EtOH) to yield (±)-aminonitrile **114** as a white crystalline solid (94.5 mg, 55% yield). X-ray-quality crystals were grown by allowing a solution of (±)-aminonitrile **114** in diethyl ether to slowly evaporate at 21 °C.

(±)-Aminonitrile 114:

^{1}H NMR (600 MHz, $CDCl_3$): δ 3.93 (dt, *J* = 3.5, 1.7 Hz, 1H), 3.34 (dd, *J* = 11.9, 10.6 Hz, 1H), 3.19 (ddd, *J* = 12.5, 5.6, 2.9 Hz, 1H), 2.73 (ddd, *J* = 9.3, 7.4, 4.9 Hz, 2H), 2.10 (qd, *J* = 13.1, 4.1 Hz, 1H), 2.03 (dd, *J* = 10.5, 4.3 Hz, 1H), 1.97 (dt, *J* = 13.7, 4.5 Hz, 1H), 1.94 –

1.90 (m, 2H), 1.90 – 1.83 (m, 2H), 1.82 – 1.71 (m, 3H), 1.70 – 1.58 (m, 3H), 1.53 (dt, J = 12.9, 4.5 Hz, 2H), 1.49 (h, J = 1.4 Hz, 1H), 1.48 – 1.45 (m, 1H), 1.45 – 1.38 (m, 3H).

^{13}C NMR (104 MHz, $CDCl_3$): δ 120.0, 62.8, 57.8, 57.6, 57.1, 54.7, 46.9, 38.0, 36.4, 28.6, 26.7, 23.5, 22.9, 22.3, 22.2, 21.8.

FTIR (NaCl, thin film): 2928, 2858, 2804, 2762, 2676, 2240, 1462, 1359, 1123 cm^{-1}.

HRMS: (ESI-TOF) calc'd for $C_{15}H_{26}N_3$ $[M+H]^+$ 260.2121, found 260.2122.

TLC (10% 2 M NH_3 in MeOH/90% $CHCl_3$ containing 0.75% EtOH), **R_f:** 0.42 ($KMnO_4$).

M.P. 134.5 – 138.3 °C.

Table 2.20. *X-Ray structure of (±)-**114**.*

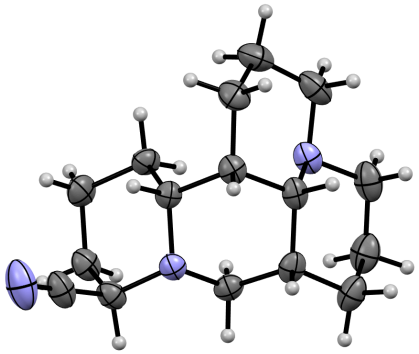

Preparation of (±)-isomatrine (6) from (±)-aminonitrile 114:

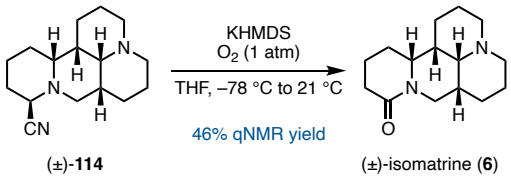

An oven-dried, N_2-flushed 10 mL flask was charged with (±)-aminonitrile **114** (20 mg, 77 μmol, 1.0 equiv), and THF (0.77 mL, 0.1 M). The solution was cooled to –78 °C, then potassium hexamethyldisilazide (0.5 M in PhMe, 278 μL, 139 μmol, 1.8 equiv) was added dropwise. The yellow solution was stirred at –78 °C for 30 minutes, then the flask

was purged with dry O_2 (balloon) at –78 °C. The solution was stirred vigorously (1500 rpm) and was allowed to warm to 21 °C then stirred for an additional 30 minutes. Upon completion, the reaction was treated with 3 M NaOH (10 mL) and sat. aq. $Na_2S_2O_3$ (10 mL). The aqueous phase was extracted with DCM (3 x 15 mL). The combined organic layers were dried over anhydrous Na_2SO_4, filtered, and concentrated under reduced pressure. The yield of (±)-isomatrine (**6**) was measured by ^{1}H qNMR (46% yield, pyazine internal standard).

Preparation of (+)-matrine (4):

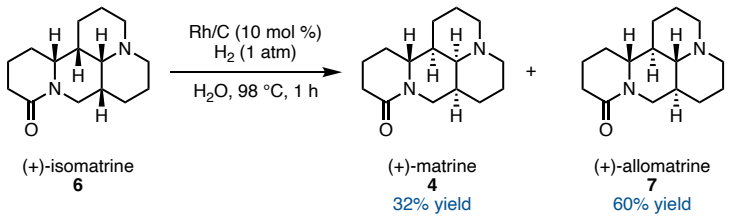

A 50 mL flask with a 20 mm x 8 mm x 8 mm egg-shaped stir bar was charged with (+)-isomatrine (50.0 mg, 201 μmol, 1.0 equiv), 5% rhodium on carbon (41.4 mg, 20.1 μmol, 10 mol %), and water (5 mL, 0.04 M). The reaction was purged with N_2 (balloon) followed by H_2 (balloon). The reaction was not stirred during the gas purge. Once the flask was under an atmosphere of H_2, it was placed into a preheated oil bath at 98 °C, and the mixture was stirred at 1500 rpm for 1 hour. Upon completion, the flask was removed from the oil bath and was cooled to 21 °C. The catalyst was removed via filtration through a syringe filter, then the filter was washed with water (3 x 5 mL). The obtained aqueous solution was concentrated under reduced pressure. The crude product was purified by SiO_2 column chromatography (20 g SiO_2, 20 mm column diameter, 3% 2 M NH_3 in MeOH/97%

$CHCl_3$ containing 0.75% EtOH as a stabilizer) to yield (+)-matrine (**4**) as a white crystalline solid (16.1 mg, 32% yield) along with (+)-allomatrine (**7**) as a white crystalline solid (29.8 mg, 60% yield).

(+)-Matrine (4):

^{1}H NMR (600 MHz, $CDCl_3$): δ 4.40 (dd, *J* = 12.8, 4.4 Hz, 1H), 3.81 (td, *J* = 9.8, 5.8 Hz, 1H), 3.04 (t, *J* = 12.7 Hz, 1H), 2.83 (ddt, *J* = 11.4, 4.3, 2.2 Hz, 1H), 2.78 (dp, *J* = 11.6, 2.1 Hz, 1H), 2.42 (dtd, *J* = 17.1, 4.7, 1.8 Hz, 1H), 2.24 (ddd, *J* = 16.9, 11.0, 5.5 Hz, 1H), 2.12 – 2.04 (m, 2H), 1.99 – 1.91 (m, 2H), 1.89 (dt, *J* = 14.3, 2.5 Hz, 1H), 1.84 – 1.77 (m, 1H), 1.77 – 1.55 (m, 5H), 1.51 (tt, *J* = 13.6, 4.9 Hz, 1H), 1.47 – 1.34 (m, 5H).

^{1}H NMR (600 MHz, C_6D_6): δ 4.76 (dd, *J* = 12.5, 4.4 Hz, 1H), 3.57 (q, *J* = 7.8 Hz, 1H), 3.05 (t, *J* = 12.6 Hz, 1H), 2.58 (d, *J* = 10.9 Hz, 1H), 2.52 (d, *J* = 11.3 Hz, 1H), 2.39 (dtd, *J* = 16.8, 4.7, 1.9 Hz, 1H), 2.09 (ddd, *J* = 16.6, 10.9, 5.5 Hz, 1H), 1.74 – 1.61 (m, 3H), 1.61 – 1.45 (m, 4H), 1.45 – 1.31 (m, 2H), 1.33 – 1.19 (m, 2H), 1.18 – 0.97 (m, 5H), 0.88 (q, *J* = 11.6 Hz, 1H).

^{13}C NMR (104 MHz, $CDCl_3$): δ 169.5, 63.9, 57.5, 57.4, 53.3, 43.4, 41.6, 35.5, 33.0, 27.9, 27.3, 26.6, 21.3, 20.9, 19.2.

^{13}C NMR (104 MHz, C_6D_6): δ 168.0, 63.9, 57.5, 57.5 53.0, 43.5, 41.6, 35.9, 33.3, 28.2, 27.3, 26.7, 21.5, 21.0, 19.3.

FTIR (NaCl, thin film): 2985, 2944, 2683, 1624, 1464, 1420, 1263, 1168 cm^{-1}.

HRMS: (ESI-TOF) calc'd for $C_{15}H_{25}N_2O$ $[M+H]^+$ 249.1961, found 249.1961.

TLC (10% 2 M NH_3 in MeOH/90% $CHCl_3$ with 0.75% EtOH stabilizer), **R_f:** 0.46 ($KMnO_4$).

M.P. 69.6 – 71.4 °C.

Specific Optical Rotation: $[\alpha]\frac{21}{D} = +42.8$ (c 1.0, $CHCl_3$).

Literature Specific Optical Rotation: $[\alpha]\frac{21}{D} = +38$ (c 1.0, H_2O).**Error! Bookmark not defined.**

Figure 1.67. *X-Ray structure of the monohydrate of (+)-matrine ((+)-**4**).*

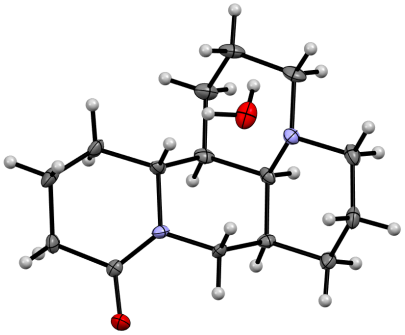

Table 2.15. *^{1}H NMR data for authentic vs synthetic (+)-matrine.*

The X-ray structure of matrine has been previously published (CCDC: 1209643).[88]

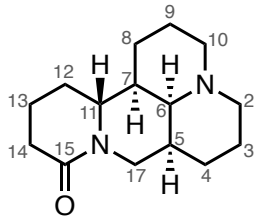

Matrine Literature ^{1}H δ ppm (400 MHz, $CDCl_3$)[89]	Matrine Recorded ^{1}H δ ppm (600 MHz $CDCl_3$)
4.40 (dd, *J* = 12.7, 4.3 Hz, 1H)	4.40 (dd, *J* = 12.8, 4.4 Hz, 1H)
3.82 (dt, *J* = 10.1, 7.7 Hz, 1H)	3.81 (td, *J* = 9.8, 5.8 Hz, 1H)
3.05 (t, *J* = 12.7 Hz, 1H)	3.04 (t, *J* = 12.7 Hz, 1H)
2.80 (m, 2H)	2.83 (ddt, *J* = 11.4, 4.3, 2.2 Hz, 1H)
	2.78 (dp, *J* = 11.6, 2.1 Hz)
2.43 (m, 1H)	2.42 (dtd, *J* = 17.1, 4.7, 1.8 Hz, 1H)
2.25 (m, 1H)	2.24 (ddd, *J* = 16.9, 11.0, 5.5 Hz, 1H)
2.09 (m, 3H)	2.12 – 2.04 (m, 2H)
	1.99 – 1.91 (m, 2H)
1.94 (m, 4H)	1.89 (dt, *J* = 17.1, 4.7, 1.8 Hz, 1H)
1.87 (m, 1H)	1.84 – 1.77 (m, 1H)
1.85 – 1.50 (m, 9H)	1.77 – 1.55 (m, 5 H)
	1.51 (tt, *J* = 13.6, 4.9 Hz, 1H)
	1.47 – 1.34 (m, 5H)

Table 2.16. *^{13}C NMR data for authentic vs synthetic (+)-matrine.*

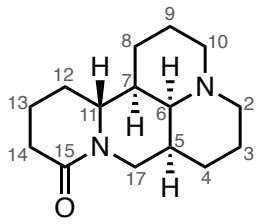

Carbon No. matrine	Matrine Literature ^{13}C δ ppm (101 MHz, $CDCl_3$)	Matrine Recorded ^{13}C δ ppm (101 MHz, $CDCl_3$)	Δ δ
2	57.6	57.5	–0.1
3	21.4	21.3	–0.1
4	27.9	27.9	0.0
5	35.6	35.5	–0.1
6	64.0	63.9	–0.1
7	43.4	43.4	0.0
8	26.6	26.6	0.0
9	21.0	20.9	–0.1
10	57.4	57.4	0.0
11	53.4	53.3	–0.1
12	27.4	27.3	–0.1
13	19.2	19.2	0.0
14	33.0	33.0	0.0
15	169.7	169.5	–0.2
17	41.7	41.6	–0.1

Table 2.17. *^{1}H NMR data for authentic vs synthetic (+)-matrine in C_6D_6.*

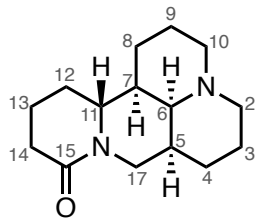

Matrine Literature ^{1}H δ ppm (500 MHz, C_6D_6)[90*]	Matrine Recorded ^{1}H δ ppm (600 MHz, C_6D_6)
4.73 (dd, *J* = 12.6, 4.4 Hz, 1H)	4.76 (dd, *J* = 12.5, 4.4 Hz, 1H)
3.57 (ddd, *J* = 9.5, 9.2, 5.8 Hz, 1H)	3.57 (q, *J* = 7.8 Hz, 1H)
3.03 (dd, *J* = 12.6, 12.4 Hz, 1H)	3.05 (t, *J* = 12.6 Hz, 1H)
2.57 (ddd, *J* = 11.1, 4.2, 2.1 Hz, 1H)	2.58 (d, *J* = 10.9 Hz, 1H)
2.52 (dd, *J* = 11.0, 4.0, 2.1 Hz, 1H)	2.52 (d, *J* = 11.3 Hz, 1H)
2.38 (ddd, *J* = 17.0, 4.8, 2.0 Hz, 1H)	2.39 (dtd, *J* = 16.8, 4.7, 1.9 Hz, 1H)
2.08 (dd, *J* = 17.0, 10.7, 5.5 Hz, 1H)	2.09 (ddd, *J* = 16.6, 10.9, 5.5 Hz, 1H)
1.71 (m, 1H)	1.74 – 1.61 (m, 3H)
1.70 (ddd, *J* = 11.9, 11.1, 2.8, 1H)	
1.67 (ddd, *J* = 12.9, 11.0, 2.8 Hz, 1H)	
1.55 (dddt, *J* = 13.6, 13.3, 12.9, 4.0 4.0 Hz, 1H)	1.61 – 1.45 (m, 4H)
1.50 (d, *J* = 11.4 Hz, 1H)	
1.49 (ddd, *J* = 12.4, 4.9, 4.4 Hz, 1H)	
1.49 (m, 1H)	
1.42 (d, *J* = 13.7 Hz, 1H)	1.45 – 1.31 (m, 2H)
1.36 (dtt, *J* = 12.7, 11.9, 4.3, 4.2 Hz, 1H)	
1.28 (d, *J* = 12.7 Hz, 1H)	1.33 – 1.19 (m, 2H)
1.22 (dddd, *J* = 13.7, 13.6, 4.9, 4.7 Hz, 1H)	
1.13 (ddddd, *J* = 13.4, 12.7, 10.7, 4.8, 3.0 Hz, 1H)	1.18 – 0.97 (m, 5H)
1.09 (d, *J* = 13.3 Hz, 1H)	
1.07 (d, *J* = 12.7 Hz, 1H)	
1.02 (m, 1H)	
1.02 (m, 1H)	
0.88 (dddd, *J* = 13.4, 11.4, 9.2, 3.2 Hz, 1H)	0.88 (q, *J* = 11.6 Hz, 1H)

*The literature report of the ^{1}H NMR of matrine in C_6D_6 utilized HMQC, HMQC-TOCSY and MAXY to measure the coupling constants of overlapping multiplets.

Table 2.18. *^{13}C NMR data for authentic vs synthetic (+)-matrine in C_6D_6.*

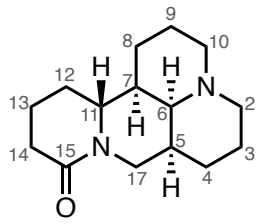

Carbon No. matrine	Matrine Literature ^{13}C δ ppm (126 MHz, C_6D_6)	Matrine Recorded ^{13}C δ ppm (101 MHz, C_6D_6)	Δ δ
2	57.0	57.5	0.5
3	21.0	21.5	0.5
4	27.7	28.2	0.5
5	35.4	35.9	0.5
6	63.4	63.9	0.5
7	43.0	43.5	0.5
8	26.2	26.7	0.5
9	20.5	21.0	0.5
10	57.0	57.5	0.5
11	52.5	53.0	0.5
12	26.7	26.7	0.0
13	18.8	19.3	0.5
14	32.8	33.3	0.5
15	167.6	168.0	0.4
17	41.1	41.6	0.5

Preparation of (+)-allomatrine (7):

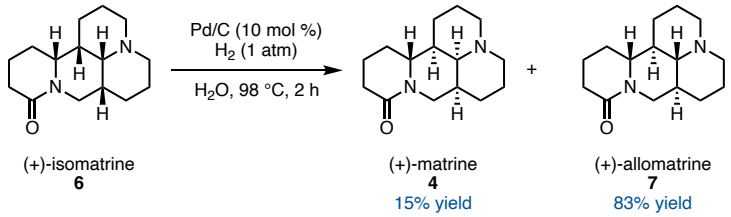

A 50 mL flask with a 20 mm x 8 mm x 8 mm egg-shaped stir bar was charged with (+)-isomatrine (50.0 mg, 201 μmol, 1.0 equiv), 10% palladium on carbon (21.4 mg, 20.1 μmol, 10 mol %), and water (5 mL, 0.04 M). The reaction was purged with N_2 (balloon) followed by H_2 (balloon). The reaction was not stirred during the gas purge. Once the flask was under an atmosphere of H_2, it was placed into a preheated oil bath at 98 °C, and the mixture was stirred at 1500 rpm for 2 hours. Upon completion, the flask was removed from the oil bath and cooled to 21 °C. The catalyst was removed via filtration through a syringe filter, then the filter was washed with water (3 x 5 mL). The obtained aqueous solution was concentrated under reduced pressure. The crude product was purified by SiO_2 column chromatography (20 g SiO_2, 20 mm column diameter, 3% 2 M NH_3 in MeOH/97% $CHCl_3$ containing 0.75% EtOH as a stabilizer) to yield (+)-allomatrine (**7**) as a white crystalline solid (41.5 mg, 83% yield) along with (+)-matrine (**4**) as a white crystalline solid (7.3 mg, 15% yield).

(+)-Allomatrine (7):

^{1}H NMR (600 MHz, $CDCl_3$): δ 4.68 (dd, *J* = 13.3, 3.9 Hz, 1H), 2.98 (td, *J* = 9.5, 5.4 Hz, 1H), 2.87 – 2.77 (m, 2H), 2.40 (dtd, *J* = 17.3, 4.6, 1.9 Hz, 1H), 2.26 (ddd, *J* = 17.1, 11.3, 5.6 Hz, 1H), 2.15 (t, *J* = 12.4 Hz, 1H), 2.06 (dtt, *J* = 13.6, 5.4, 2.5 Hz, 1H), 2.00 – 1.90 (m, 2H), 1.86 – 1.77 (m, 2H), 1.73 – 1.61 (m, 5H), 1.57 (dddd, *J* = 23.5, 11.9, 4.8, 2.8 Hz, 1H),

1.49 – 1.37 (m, 2H), 1.42 – 1.36 (m, 1H), 1.32 (t, J = 9.6 Hz, 1H), 1.27 – 1.19 (m, 1H), 0.98 – 0.82 (m, 2H).

^{13}C NMR (126 MHz, $CDCl_3$): 169.3, 70.8, 60.3, 56.6, 55.9, 46.3, 46.2, 39.1, 32.9, 28.4, 27.5, 26.9, 24.8, 24.8, 19.4.

FTIR (NaCl, thin film): 2986, 1628, 1422, 1260 cm^{-1}.

HRMS: (ESI-TOF) calc'd for $C_{15}H_{25}N_2O$ $[M+H]^+$ 249.1961, found 249.1961.

TLC (10% 2 M NH_3 in MeOH/90% $CHCl_3$ with 0.75% EtOH stabilizer), **R_f:** 0.34 ($KMnO_4$).

M.P. 88.5 – 94.8 °C.

Specific Optical Rotation: $[\alpha]\frac{21}{D} = +40.5$ (c 1.0, $CHCl_3$).

Literature Specific Optical Rotation: $[\alpha]\frac{21}{D} = +51.2$ (c 1.07, $CHCl_3$).[91]

Figure 1.68. *X-Ray structure of (+)-allomatrine ((+)-**7**).*

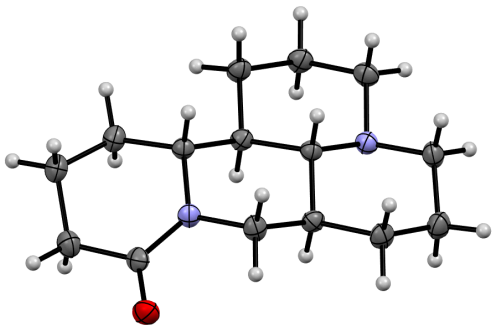

Table 2.19. *^{1}H NMR data for authentic vs synthetic (+)-allomatrine.*

The X-ray structure of allomatrine has been previously published (CCDC: 11022140).[92]

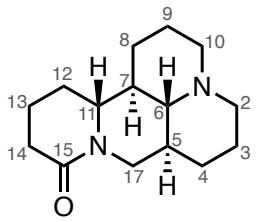

Allomatrine Literature ^{1}H δ ppm (400 MHz, $CDCl_3$)[92]	Allomatrine Recorded ^{1}H δ ppm (600 MHz, $CDCl_3$)
4.69 (dd, *J* = 12.9, 3.9 Hz, 1H)	4.68 (dd, *J* = 13.3, 3.9 Hz, 1H)
3.00 (td, *J* = 9.4, 5.4 Hz, 1H)	2.98 (td, *J* = 9.5, 5.4 Hz, 1H)
2.85 (m, 2H)	2.87 – 2.77 (m, 2H)
2.42 (m, 1H)	2.40 (dtd, *J* = 17.3, 4.6, 1.9 Hz, 1H)
2.27 (ddd, *J* = 17.0, 11.1, 5.5 Hz, 1H)	2.26 (ddd, *J* = 17.1, 11.3, 5.6 Hz, 1H)
2.17 (t, *J* = 12.9 Hz, 1H)	2.15 (t, *J* = 12.4 Hz, 1H)
2.11 – 1.92 (m, 3H)	2.06 (dtt, *J* = 13.6, 5.4, 2.5 Hz, 1H)
	2.00 – 1.90 (m, 2H)
1.89 – 1.78 (m, 2H)	1.86 – 1.77 (m, 2H)
1.75 – 1.58 (m, 5H)	1.73 – 1.61 (m, 5H)
1.58 (m, 1H)	1.57 (dddd, *J* = 23.5, 11.9, 4.8, 2.8 Hz, 1H)
1.52 – 1.39 (m, 2H)	1.49 – 1.37 (m, 2H)
1.35 (t, *J* = 9.4 Hz, 1H)	1.32 (t, *J* = 9.6 Hz, 1H)
1.27 (m, 1H)	1.27 – 1.19 (m, 1H)
1.03 – 0.83 (m, 2H)	0.98 – 0.82 (m, 2H)

Table 2.20. *^{13}C NMR data for authentic vs synthetic (+)-allomatrine.*

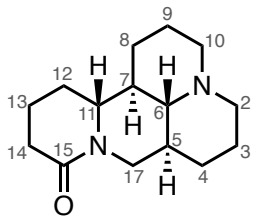

Carbon No. allomatrine	Allomatrine Literature ^{13}C δ ppm (101 MHz, $CDCl_3$)[92]	Allomatrine Recorded ^{13}C δ ppm (101 MHz, $CDCl_3$)	Δ δ
2	55.8	55.9	0.1
3	24.5	24.8	0.3
4	27.4	27.6	0.2
5	38.9	39.1	0.2
6	70.7	70.9	0.2
7	46.0	46.3	0.3
8	26.7	26.9	0.2
9	24.5	24.8	0.3
10	56.4	56.6	0.2
11	60.1	60.3	0.2
12	28.2	28.4	0.2
13	19.3	19.5	0.2
14	32.7	32.9	0.2
15	169.1	169.3	0.2
17	46.1	46.3	0.2

Preparation of (–)-sophoridine (8):

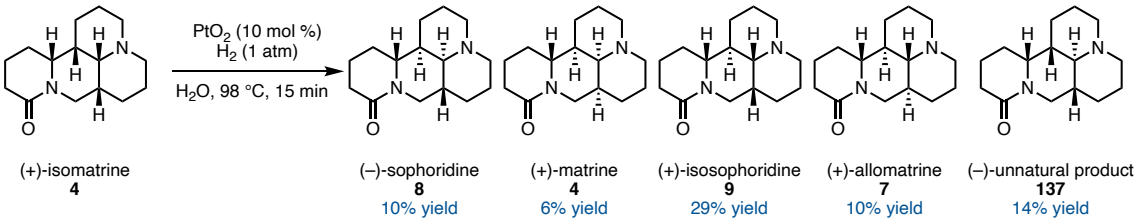

A 50 mL flask with a 20 mm x 8 mm x 8 mm egg-shaped stir bar was charged with (+)-isomatrine (50.0 mg, 201 μmol, 1.0 equiv), PtO_2 (4.6 mg, 20.1 μmol, 10 mol %) and water (5 mL, 0.04 M). The reaction was purged with N_2 (balloon) followed by H_2 (balloon).

The reaction was not stirred during the gas purge. Once the flask was under an atmosphere of H_2, it was put into a preheated oil bath at 98 °C, and the mixture was stirred at 1500 rpm for 15 minutes. Upon completion, the flask was removed from the oil bath and cooled to 21 °C. The catalyst was removed via filtration through a syringe filter, then the filter was washed with water (3 x 5 mL). The obtained aqueous solution was concentrated under reduced pressure. The crude product was purified by SiO_2 column chromatography (20 g SiO_2, 20 mm column diameter, 3% 2 M NH_3 in MeOH/97% $CHCl_3$ containing 0.75% EtOH as a stabilizer to 15% 2 M NH_3 in MeOH/85% $CHCl_3$ containing 0.75% EtOH as a stabilizer in 2% increments) to yield (–)-sophoridine (**8**) as a white crystalline solid (5.0 mg, 10% yield); (+)-isosophoridine (**9**) as a white crystalline solid (14.6 mg, 29% yield); a mixture of (+)-allomatrine (**7**) and (–)-unnatural product **137** in a 40:60 ratio (12.1 mg, 24% combined yield) as a clear, colorless oil; and a mixture of (+)-isomatrine (**6**) and (+)-matrine (**4**) in a 80:20 ratio (15.5 mg, 31% combined yield) as a white crystalline solid.

(–)-Sophoridine (8):

^{1}H NMR (400 MHz, $CDCl_3$): δ 3.42 (t, *J* = 11.6 Hz, 1H), 3.34 (t, *J* = 10.0 Hz, 1H), 3.26 (t, *J* = 12.6 Hz, 1H), 2.86 (d, *J* = 12.1 Hz, 1H), 2.76 (t, *J* = 10.8 Hz, 1H), 2.39 (dt, *J* = 17.6, 5.6 Hz, 1H), 2.31 (ddd, *J* = 17.5, 9.2, 5.7 Hz, 1H), 2.25 – 2.09 (m, 2H), 2.08 – 1.37 (m, 14H), 1.05 (qd, *J* = 12.8, 3.8 Hz, 1H).

^{13}C NMR (104 MHz, $CDCl_3$): δ 170.1, 63.5, 56.0, 55.8, 50.4, 47.7, 41.1, 32.6, 30.9, 30.3, 28.2, 23.8, 21.9, 21.6, 19.0.

FTIR (NaCl, thin film): 2986, 2938, 1622, 1420, 1272, 1263 cm^{-1}.

HRMS: (ESI-TOF) calc'd for $C_{15}H_{25}N_2O$ $[M+H]^+$ 249.1961, found 249.1960.

TLC (10% 2 M NH_3 in MeOH/90% $CHCl_3$ with 0.75% EtOH stabilizer), **R_f:** 0.24 ($KMnO_4$).

M.P. 61.2 – 64.2 °C.

Specific Optical Rotation: $[\alpha]\frac{21}{D} = -57.3$ (c 1.0, $CHCl_3$).

Specific Optical Rotation: $[\alpha]\frac{21}{D} = -60.9$ (c 1.0, H_2O).

Literature Specific Optical Rotation: $[\alpha]\frac{21}{D} = -64$ (c 1.0, H_2O).[86]

Table 2.46. *^1H NMR data for authentic vs synthetic (+)-sophoridine.*

The X-ray structure of sophoridine has been previously published (CCDC: 1261174).[93]

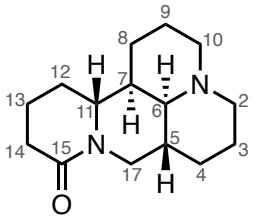

Sophoridine Literature ^1H δ ppm	Sophoridine Recorded ^1H δ ppm (600 MHz, $CDCl_3$)
unpublished	3.42 (dd, *J* = 11.6 Hz, 1H)
	3.34 (br t, *J* = 10.0 Hz, 1H)
	3.26 (t, *J* = 12.6 Hz, 1H)
	2.86 (d, *J* = 12.1 Hz, 1H)
	2.76 (t, *J* = 10.8 Hz, 1H)
	2.39 (dt, *J* = 17.6, 5.6 Hz, 1H)
	2.31 (ddd, *J* = 17.5, 9.2, 5.7 Hz, 1H)
	2.25 – 2.09 (m, 2H)
	2.08 – 1.37 (m, 14H)
	1.05 (qd, *J* = 12.8, 3.8 Hz, 1H)

Table 2.47. *^{13}C NMR data for authentic vs synthetic (+)-sophoridine.*

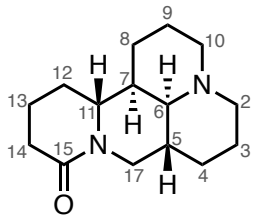

Carbon No. sohporidine	Sophoridine Literature ^{13}C δ ppm (101 MHz, $CDCl_3$)[94]	Sophoridine Recorded ^{13}C δ ppm (101 MHz, $CDCl_3$)	Δ δ
2	50.2	50.4	0.2
3	21.6	21.9	0.3
4	23.5	23.8	0.3
5	30.6	31.0	0.4
6	63.2	63.5	0.3
7	40.8	41.1	0.3
8	30.1	30.3	0.2
9	21.5	21.6	0.1
10	55.8	56.0	0.2
11	55.7	55.8	0.1
12	28.0	28.2	0.2
13	18.8	19.0	0.2
14	32.5	32.6	0.1
15	169.9	170.1	0.2
17	47.4	47.7	0.3

Preparation of (+)-isosophoridine (9):

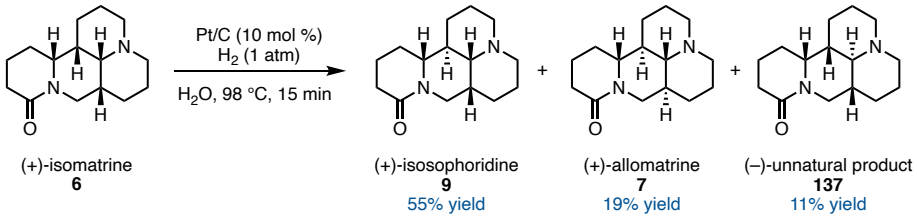

A 50 mL flask with a 20 mm x 8 mm x 8 mm egg-shaped stir bar was charged with (+)-isomatrine (50.0 mg, 201 μmol, 1.0 equiv), 10% platinum on carbon (78.5 mg, 20.1 μmol, 10 mol %), and water (5 mL, 0.04 M). The reaction was purged with N_2 (balloon) followed by H_2 (balloon). The reaction was not stirred during the gas purge. Once the flask was under an atmosphere of H_2, it was put into a preheated oil bath at 98 °C, and the mixture was stirred at 1500 rpm for 15 minutes. Upon completion, the flask was removed from the oil bath and cooled to 21 °C. The catalyst was removed via filtration through a syringe filter, then the filter was washed with water (3 x 5 mL). The obtained aqueous solution was concentrated under reduced pressure. The crude product was purified by SiO_2 column chromatography (20 g SiO_2, 20 mm column diameter, 3% 2 M NH_3 in MeOH/97% $CHCl_3$ with 0.75% EtOH stabilizer to 15% 2 M NH_3 in MeOH/85% $CHCl_3$ with 0.75% EtOH stabilizer as a gradient in 2% increments) to yield (+)-isosophoridine (**9**) as a white crystalline solid (27.5 mg, 55% yield) along with a mixture of (+)-allomatrine (**7**) and (–)-unnatural product **137** in a 36:64 ratio (14.9 mg, 30% combined yield).

(+)-Isosophoridine (9):

^{1}H NMR (600 MHz, $CDCl_3$): δ 4.67 (dd, *J* = 13.3, 1.9 Hz, 1H), 3.00 – 2.82 (m, 4H), 2.75 (dd, *J* = 10.8, 4.7 Hz, 1H), 2.63 (dd, *J* = 13.4, 3.6 Hz, 1H), 2.46 (dt, *J* = 11.6, 3.6 Hz, 1H), 2.40 (dtd, *J* = 17.3, 5.2, 1.7 Hz, 1H), 2.28 (ddd, *J* = 17.2, 9.8, 5.4 Hz, 1H), 2.07 – 1.95 (m,

1H), 1.93 – 1.70 (m, 5H), 1.86 – 1.75 (m, 3H), 1.73 (ddt, *J* = 15.9, 6.1, 3.6 Hz, 1H), 1.66 – 1.55 (m, 2H), 1.55 – 1.48 (m, 2H), 1.38 – 1.28 (m, 2H), 1.04 (qd, *J* = 12.7, 4.2 Hz, 1H).

^{13}C NMR (104 MHz, $CDCl_3$): δ 169.9, 62.4, 60.1, 54.2, 46.9, 45.2, 36.1, 33.4, 33.0, 28.1, 26.7, 26.0, 23.1, 19.3, 19.2.

FTIR (NaCl, thin film): 2934, 2856, 1632, 1265, 1168 cm^{-1}.

HRMS: (ESI-TOF) calc'd for $C_{15}H_{25}N_2O$ $[M+H]^+$ 249.1961, found 249.1963.

TLC (10% 2 M NH_3 in MeOH/90% $CHCl_3$ with 0.75% EtOH stabilizer), **R_f:** 0.24 ($KMnO_4$).

M.P. 111.0 – 114.1 °C.

Specific Optical Rotation: $[\alpha]_D^{21} = +94.0$ (c 1.0, $CHCl_3$).

Specific Optical Rotation: $[\alpha]_D^{21} = +98.7$ (c 1.0, EtOH).

Literature Specific Optical Rotation: $[\alpha]_D^{21} = +101$ (c 1.0, EtOH).[86]

Figure 1.69. *X-Ray structure of (±)-isosophoridine ((±)-**9**).*

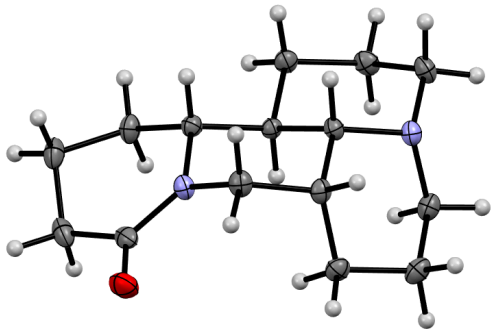

Table 2.44. *^{1}H NMR data for authentic vs synthetic (+)-isosophoridine.*

The X-ray structure of isosophoridine has been previously published (CCDC: 1180978 and 1180979).[95,96]

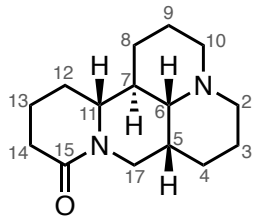

Isosophoridine Literature ^{1}H δ ppm (400 MHz, $CDCl_3$)[97]	Isosophoridine Recorded ^{1}H δ ppm (600 MHz, $CDCl_3$)
4.69 (dd, *J* = 13.4, 1.9 Hz, 1H)	4.67 (dd, *J* = 13.3, 1.9 Hz, 1H)
3.02 – 2.85 (m, 4H)	3.00 – 2.82 (m, 4H)
2.77 (dd, *J* = 10.6, 4.7, Hz, 1H)	2.75, (dd, *J* = 10.8, 4.7 Hz, 1H)
2.65 (dd, *J* = 13.4, 3.5 Hz, 1H)	2.63 (dd, *J* = 13.4, 3.6 Hz, 1H)
2.52 – 2.37 (m, 2H)	2.46 (dt, *J* = 11.6, 3.6 Hz, 1H)
	2.40 (dtd, *J* = 17.3, 5.2, 1.7 Hz, 1H)
2.35 –2.24 (m, 1H)	2.28 (ddd, *J* = 17.2, 9.8, 5.4 Hz, 1H)
2.09 – 1.99 (m, 1H)	2.07 – 1.95 (m, 1H)
1.95 – 1.71 (m, 5H)	1.93 – 1.70 (m, 6H)
1.71 – 1.49 (m, 4H)	1.66 – 1.47 (m, 4H)
1.41 – 1.23 (m, 3H)	1.38 – 1.29 (m, 2H)
1.05 (qd, *J* = 12.4, 4.2 Hz, 1H)	1.04 (qd, *J* = 12.7, 4.2 Hz, 1H)

Table 2.43. *^{13}C NMR data for authentic vs synthetic (+)-isosophoridine.*

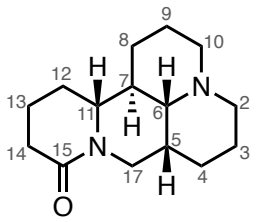

Carbon No. isosohporidine	Isosophoridine Literature ^{13}C δ ppm (101 MHz, $CDCl_3$)[97]	Isosophoridine Recorded ^{13}C δ ppm (101 MHz, $CDCl_3$)	Δ δ
2	45.0	45.2	0.2
3	25.6	26.0	0.4
4	22.7	23.1	0.4
5	35.8	36.1	0.3
6	62.1	62.4	0.3
7	33.3	33.4	0.1
8	26.6	26.7	0.1
9	19.0	19.3	0.3
10	53.9	54.2	0.3
11	59.9	60.2	0.3
12	27.8	28.1	0.3
13	18.9	19.2	0.3
14	32.8	33.0	0.2
15	169.9	169.9	0.0
17	46.6	46.9	0.3

Preparation of (–)-unnatural product 137:

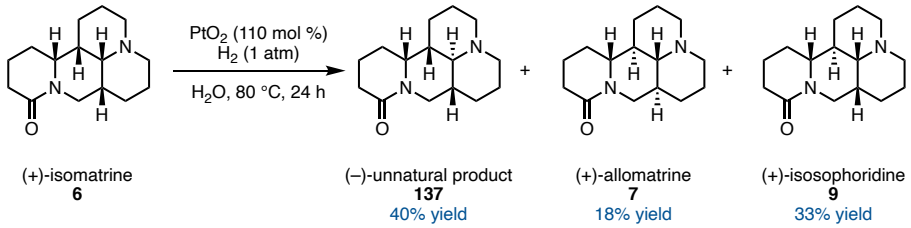

A 50 mL flask with a 20 mm x 8 mm x 8 mm egg-shaped stir bar was charged with (+)-isomatrine (30.0 mg, 121 μmol, 1.0 equiv.), PtO_2 (30.2 mg, 133 μmol, 110 mol %), and water (3 mL, 0.04 M). The reaction was purged with N_2 (balloon) followed by H_2 (balloon). The reaction was not stirred during the gas purge. Once the flask was under an atmosphere of H_2, it was put into a preheated oil bath at 80 °C, and the mixture was stirred at 1500 rpm for 24 hours. Upon completion, the flask was removed from the oil bath and cooled to 21 °C. The catalyst was removed via filtration through a syringe filter, then the filter was washed with water (3 x 5 mL). The obtained aqueous solution was concentrated under reduced pressure. The crude product was purified by SiO_2 column chromatography (5 g SiO_2, 10 mm column diameter, 5% 2 M NH_3 in MeOH/95% $CHCl_3$ containing 0.75% EtOH to 10% 2 M NH_3 in MeOH/90% $CHCl_3$ containing 0.75% EtOH as a gradient in 1% increments) to yield (+)-isosophoridine (**9**) as a white crystalline solid (9.9 mg, 33% yield) along with a mixture of (+)-allomatrine (**3**) and (–)-unnatural product **137**. The separation of the (–)-unnatural product was carried out via HPLC reverse phase chromatography (Eclipse XDB-C8 – 9.4 mm x 250 mm column, 8% ACN/92% H_2O with 0.2% TFA, flow rate: 5 mL/min, t_r ((–)-unnatural product **137**) = 5.06 min, t_r ((+)-allomatrine (**7**)) = 6.29 min) to yield (–)-unnatural product **137** as a white crystalline solid (12.0 mg, 40% yield) along with (+)-allomatrine (**7**) as a white crystalline solid (5.4 mg, 18% yield). X-ray-

quality crystals of (–)-unnatural product **137** were prepared via slow evaporation of a hexanes solution at –20 °C open to air.

(–)-Unnatural Product 137:

^{1}H NMR (400 MHz, $CDCl_3$): δ 3.75 (ddd, *J* = 9.5, 8.2, 4.6 Hz, 1H), 3.47 (dd, *J* = 13.5, 6.9 Hz, 1H), 3.35 (dd, *J* = 13.6, 10.0 Hz, 1H), 2.83 (d, *J* = 10.6 Hz, 2H), 2.45 – 2.24 (m, 2H), 2.10 – 1.96 (m, 2H), 1.88 – 1.52 (m, 11H), 1.38 (t, *J* = 10.2 Hz, 1H), 1.30 (dd, *J* = 12.7, 5.1 Hz, 1H), 1.24 (dd, *J* = 12.5, 3.4 Hz, 1H), 1.13 – 0.98 (m, 1H).

^{13}C NMR (104 MHz, $CDCl_3$): δ 172.7, 65.4, 56.1, 55.9, 54.5, 46.7, 42.4, 35.8, 32.1, 30.3, 27.3, 25.8, 24.8, 24.4, 19.3.

FTIR (NaCl, thin film): 2922, 2798, 2740, 1638, 1179, 1142, 1126 cm^{-1}.

HRMS: (ESI-TOF) calc'd for $C_{15}H_{25}N_2O$ $[M+H]^+$ 249.1961, found 249.1960.

TLC (10% 2 M NH_3 in MeOH/90% $CHCl_3$ with 0.75% EtOH stabilizer), **R_f:** 0.34 ($KMnO_4$).

M.P. 63.2 – 66.5 °C.

Specific Optical Rotation: $[\alpha]\frac{21}{D} = -53.0$ (c 1.0, $CHCl_3$).

Figure 1.70. *X-Ray structure of (–)-unnatural product ((–)-**137**).*

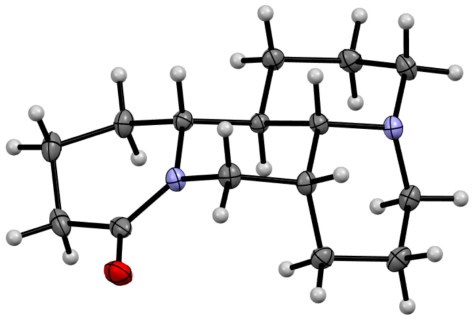

Table 2.6. *Isomatrine isomerization optimization.*

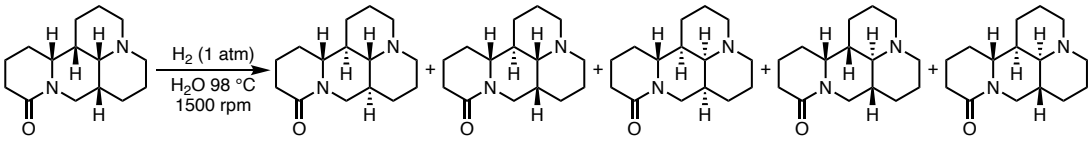

(+)-isomatrine **5** | (+)-allomatrine **7** | (+)-isosophoridine **9** | (+)-matrine **4** | (–)-unnatural product **137** | (–)-sophoridine **8**

Entry	Catalyst (loading)	Time	Recovered SM	allomatrine	isosophoridine	matrine	unnatural isomer	sophoridine
1	PtO_2 (10 mol%)	0.25 h	57%	6%	15%	3%	9%	10%
2[a]	PtO_2 (10 mol %)	0.25 h	100%	0%	0%	0%	0%	0%
3[b]	PtO_2 (10 mol %)	0.25 h	87%	3%	5%	2%	0%	2%
4[c]	PtO_2 (10 mol%)	0.25 h	95%	1%	1%	0%	1%	1%
5	Rh/C (10 mol%)	0.25 h	35%	30%	5%	26%	2%	1%
6	Pd/C (10 mol%)	0.25 h	10%	42%	6%	28%	12%	2%
7	Ru/C (10 mol%)	0.25 h	100%	0%	0%	0%	0%	0%
8	Ir/C (10 mol%)	0.25 h	7%	10%	59%	2%	11%	11%
9	RuO_2 (10 mol%)	0.25 h	100%	0%	0%	0%	0%	0%
10	Pt/C (10 mol%)	0.25 h	0%	12%	67%	0%	21%	0%
11[d]	PtO_2 (10 mol%)	0.25 h	100%	0%	0%	0%	0%	0%
12	PtO_2 (5 mol%)	24 h	100%	0%	0%	0%	0%	0%
13[c]	PtO_2 (5 mol%)	24 h	73%	10%	5%	11%	0%	0%
14[c]	PtO_2 (110 mol%)	24 h	5%	36%	9%	3%	48%	0%
15[c]	PtO_2 (5 mol%)	0.25 h	99%	0%	1%	0%	0%	0%
16	PtO_2 (110 mol%)	0.25 h	0%	20%	55%	2%	21%	1%

reported yields are qNMR yields against a pyrazine internal standard

Table 2.4. *Isomatrine isomerization optimization with Rh/C.*

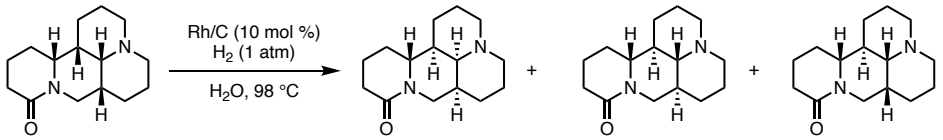

(+)-isomatrine **6** | (+)-matrine **4** | (+)-allomatrine **7** | (+)-isosophoridine **9**

Entry	Time	Recovered SM	allomatrine	isosophoridine	matrine	unnatural product	sophoridine
1	0.5 h	35	30%	5%	26%	2%	1%
2	0.75 h	39	23%	10%	28%	0%	0%
3	1 h	18	30%	10%	42%	0%	0%
4	1.5 h	8	35%	9%	48%	0%	0%
5	2 h	0	57%	0%	42%	0%	0%
6	6 h	0	70%	0%	30%	0%	0%
7	24 h	0	76%	0%	24%	0%	0%

all yields are qNMR yields against pyrazine internal standard

Table 2.7. *Isomatrine isomerization optimization with Pd/C.*

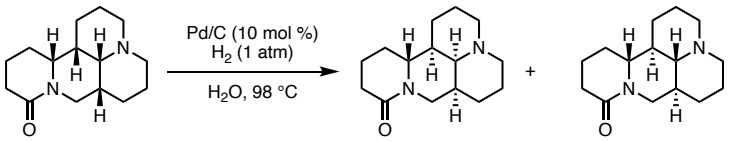

(+)-isomatrine **6** (+)-matrine **4** (+)-allomatrine **7**

Entry	Time	Recovered SM	allomatrine	isosophoridine	matrine	unnatural product	sophoridine
1	0.25 h	10	42%	6%	28%	0%	2%
2	0.75 h	0	64%	6%	36%	0%	2%
3	1 h	0	87%	0%	13%	0%	0%
4	1.5 h	0	78%	0%	22%	0%	0%
5	2 h	0	82%	0%	18%	0%	0%
6	6 h	0	92%	0%	8%	0%	0%
7	24 h	0	88%	0%	12%	0%	0%

all yields are qNMR yields against pyrazine internal standard

1.8.1 X-RAY CRYSTALLOGRAPHY REPORTS

Low-temperature diffraction data (φ- and ω-scans) were collected on a Bruker AXS D8 VENTURE KAPPA diffractometer coupled to either a PHOTON 100 CMOS detector with Mo-Kα radiation (λ = 0.71073 Å) or a PHOTON II CPAD detector with either Mo-Kα radiation (λ = 0.71073 Å) or Cu-Kα radiation (λ = 1.54178 Å) from a fine-focus sealed X-ray tube. All diffractometer manipulations, including data collection integration, and scaling were carried out using the Bruker APEXII software.[98] Absorption corrections were applied using SADABS.[99] The structure was solved by intrinsic phasing using SHELXT[100] and refined against F2 on all data by full-matrix least squares with SHELXL-2014[101] using established refinement techniques.[102] All non-hydrogen atoms were refined anisotropically. All hydrogen atoms were included into the model at geometrically calculated positions and refined using a riding model. The isotropic displacement parameters of all hydrogen atoms were fixed to 1.2 times the U value of the atoms they are

linked to (1.5 times for methyl and hydroxyl groups). Absolute configuration was determined by anomalous dispersion[103] and confirmed by Bayesian statistical analysis using the program PLATON.[104] Graphical representation of the structure with 50% probability thermal ellipsoids was generated using Mercury visualization software.[105]

Crystallographic Analysis of (±)-114.

Special Refinement Details

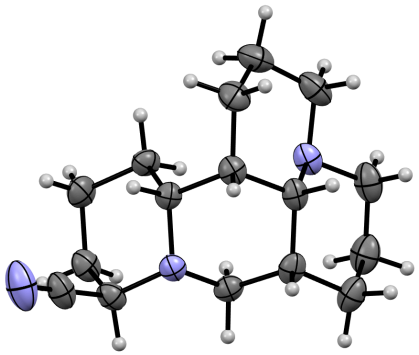

Compound (±)-**114** crystallizes in the triclinic space group P-1 with two molecules in the asymmetric unit. CCDC number: 2159774

Table 2.32. *Crystal data and structure refinement for (±)-**114**.*

Identification code	V22048
Empirical formula	$C_{16}H_{25}N_3$
Formula weight	259.39
Temperature/K	200.0
Crystal system	triclinic
Space group	P-1
a/Å	10.3418(10)
b/Å	11.0488(9)
c/Å	13.5340(12)
α/°	71.002(5)
β/°	75.301(7)

γ/°	89.676(5)
Volume/Å^3	1409.4(2)
Z	4
ρ_{calc}g/cm^3	1.222
μ/mm^{-1}	0.560
F(000)	568.0
Crystal size/mm^3	0.3 × 0.15 × 0.15
Radiation	CuKα (λ = 1.54178)
2Θ range for data collection/°	7.166 to 150.084
Index ranges	-12 ≤ h ≤ 12, -13 ≤ k ≤ 13, -16 ≤ l ≤ 16
Reflections collected	32777
Independent reflections	5743 [R_{int} = 0.0603, R_{sigma} = 0.0397]
Data/restraints/parameters	5743/0/343
Goodness-of-fit on F^2	1.051
Final R indexes [I>=2σ (I)]	R_1 = 0.0497, wR_2 = 0.1416
Final R indexes [all data]	R_1 = 0.0579, wR_2 = 0.1522
Largest diff. peak/hole / e Å^{-3}	0.34/-0.22

Crystallographic Analysis of (–)-137 monohydrate.

Special Refinement Details

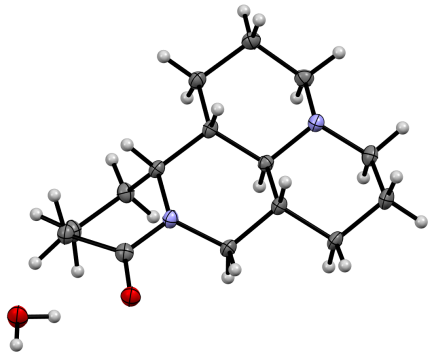

Compound (–)-**137** monohydrate crystallizes in the monoclinic space group $P2_1$ with one molecule in the asymmetric unit. Absolute configuration was determined by anomalous dispersion (Flack = 0.09(15). Bayesian statistics further confirm the absolute

stereochemistry: P2(true) = 1.000, P3(true) = 0.992, P3(rac-twin) = 0.008, and P3(false) = $0.1x10^{-10}$. CCDC number: 2163777

Table 2.33. *Crystal data and structure refinement for (–)-**137** monohydrate.*

Identification code	V22047
Empirical formula	$C_{15}H_{28}N_2O_3$
Formula weight	266.38
Temperature/K	100.0
Crystal system	monoclinic
Space group	$P2_1$
a/Å	6.5987(12)
b/Å	14.549(5)
c/Å	7.3792(15)
α/°	90
β/°	99.85(2)
γ/°	90
Volume/$Å^3$	698.0(3)
Z	2
$\rho_{calc}g/cm^3$	1.267
μ/mm^{-1}	0.665
F(000)	292.0
Crystal size/mm^3	0.15 × 0.1 × 0.05
Radiation	CuKα (λ = 1.54178)
2Θ range for data collection/°	12.166 to 148.87
Index ranges	$-7 \leq h \leq 8$, $-18 \leq k \leq 17$, $-9 \leq l \leq 9$
Reflections collected	10516
Independent reflections	2832 [R_{int} = 0.0508, R_{sigma} = 0.0415]
Data/restraints/parameters	2832/1/175
Goodness-of-fit on F^2	0.895
Final R indexes [I>=2σ (I)]	R_1 = 0.0357, wR_2 = 0.1073
Final R indexes [all data]	R_1 = 0.0396, wR_2 = 0.1131
Largest diff. peak/hole / e $Å^{-3}$	0.22/-0.18
Flack parameter	0.09(15)

Crystallographic Analysis of (+)-7.

Special Refinement Details

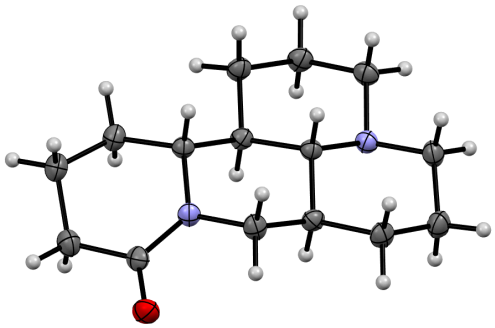

Compound (+)-**7** crystallizes in the monoclinic space group $P2_1$ with one molecule in the asymmetric unit. Absolute configuration was determined by anomalous dispersion (Flack = -0.16(18). Bayesian statistics further confirm the absolute stereochemistry: P2(true) = 1.000, P3(true) = 0.988, P3(rac-twin) = 0.012, and P3(false) = $0.2x10^{-8}$. CCDC number: 2159773

Table 2.34. *Crystal data and structure refinement for (+)-**7**.*

Identification code	V22044
Empirical formula	$C_{15}H_{24}N_2O$
Formula weight	248.36
Temperature/K	100.0
Crystal system	monoclinic
Space group	$P2_1$
a/Å	6.6233(8)
b/Å	8.0886(11)
c/Å	12.9022(19)
α/°	90
β/°	103.235(9)
γ/°	90
Volume/$Å^3$	672.85(16)
Z	2

$\rho_{calc}g/cm^3$	1.226
μ/mm^{-1}	0.599
F(000)	272.0
Crystal size/mm^3	0.3 × 0.15 × 0.15
Radiation	CuKα (λ = 1.54178)
2Θ range for data collection/°	7.038 to 159.11
Index ranges	$-8 \leq h \leq 8$, $-10 \leq k \leq 10$, $-16 \leq l \leq 14$
Reflections collected	11330
Independent reflections	2847 [R_{int} = 0.0738, R_{sigma} = 0.0617]
Data/restraints/parameters	2847/1/163
Goodness-of-fit on F^2	1.056
Final R indexes [I>=2σ (I)]	R_1 = 0.0485, wR_2 = 0.1361
Final R indexes [all data]	R_1 = 0.0527, wR_2 = 0.1420
Largest diff. peak/hole / e $Å^{-3}$	0.36/-0.25
Flack parameter	-0.16(18)

Crystallographic Analysis of (±)-9.

Special Refinement Details

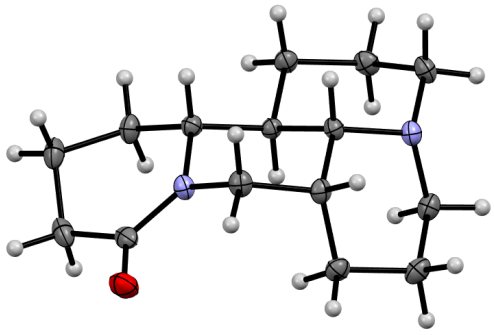

Compound (±)-**9** crystallizes in the monoclinic space group $P2_1/n$ with one molecule in the asymmetric unit. CCDC number: 2159772

Table 2.35. *Crystal data and structure refinement for (±)-**9**.*

Identification code	V22037
Empirical formula	$C_{15}H_{24}N_2O$

Formula weight	248.36
Temperature/K	100.0
Crystal system	monoclinic
Space group	$P2_1/n$
a/Å	7.700(3)
b/Å	22.520(9)
c/Å	8.384(2)
α/°	90
β/°	116.574(15)
γ/°	90
Volume/Å^3	1300.4(8)
Z	4
ρ_{calc}g/cm^3	1.269
μ/mm^{-1}	0.620
F(000)	544.0
Crystal size/mm^3	0.3 × 0.2 × 0.1
Radiation	CuKα (λ = 1.54178)
2Θ range for data collection/°	7.852 to 148.692
Index ranges	$-8 \leq h \leq 9$, $-22 \leq k \leq 27$, $-8 \leq l \leq 10$
Reflections collected	9620
Independent reflections	2589 [R_{int} = 0.0383, R_{sigma} = 0.0318]
Data/restraints/parameters	2589/0/163
Goodness-of-fit on F^2	0.971
Final R indexes [I>=2σ (I)]	R_1 = 0.0368, wR_2 = 0.1194
Final R indexes [all data]	R_1 = 0.0462, wR_2 = 0.1291
Largest diff. peak/hole / e Å^{-3}	0.25/-0.18

Crystallographic Analysis of (+)-6.

Special Refinement Details

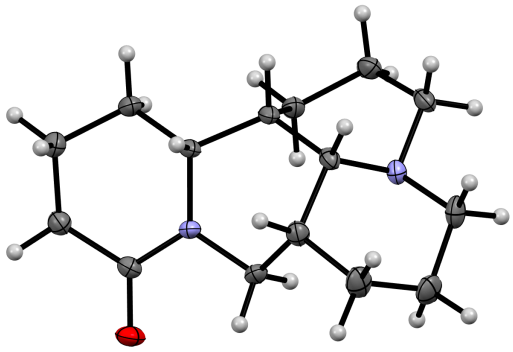

Compound (+)-**6** crystallizes in the orthorhombic space group $P2_12_12_1$ with one molecule in the asymmetric unit. Absolute configuration was determined by anomalous dispersion (Flack = -0.11(11). Bayesian statistics further confirm the absolute stereochemistry: P2(true) = 1.000, P3(true) = 1.000, P3(rac-twin) = $0.1x10^{-8}$, and P3(false) = $0.4x10^{-30}$. CCDC number: 2159771

Table 2.36. *Crystal data and structure refinement for (+)-**6**.*

Identification code	V22027
Empirical formula	$C_{15}H_{24}N_2O$
Formula weight	248.36
Temperature/K	100.0
Crystal system	orthorhombic
Space group	$P2_12_12_1$
a/Å	7.4690(6)
b/Å	11.4564(13)
c/Å	15.6304(13)
α/°	90
β/°	90
γ/°	90
Volume/Å^3	1337.5(2)
Z	4
ρ_{calc}g/cm^3	1.233
μ/mm^{-1}	0.602
F(000)	544.0

Crystal size/mm^3	0.4 × 0.15 × 0.15
Radiation	CuKα (λ = 1.54178)
2Θ range for data collection/°	9.572 to 149.208
Index ranges	-8 ≤ h ≤ 9, -14 ≤ k ≤ 13, -19 ≤ l ≤ 19
Reflections collected	19281
Independent reflections	2724 [R_{int} = 0.0440, R_{sigma} = 0.0240]
Data/restraints/parameters	2724/0/163
Goodness-of-fit on F^2	0.973
Final R indexes [I>=2σ (I)]	R_1 = 0.0341, wR_2 = 0.1044
Final R indexes [all data]	R_1 = 0.0346, wR_2 = 0.1052
Largest diff. peak/hole / e Å^{-3}	0.18/-0.24
Flack parameter	-0.11(11)

Crystallographic Analysis of (±)-89.

Special Refinement Details

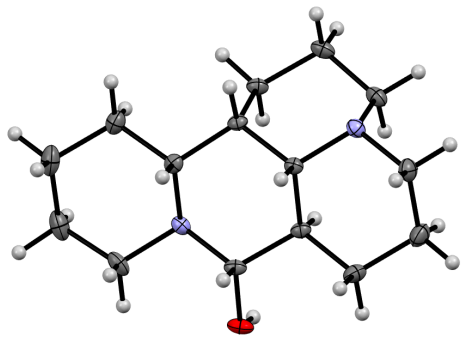

Compound (±)-**89** crystallizes in the triclinic space group P-1 with two molecules in the asymmetric unit. CCDC number: 2159770

Table 2.37. *Crystal data and structure refinement for (±)-**89**.*

Identification code	V21098
Empirical formula	$C_{15}H_{26}N_2O$
Formula weight	250.38

Temperature/K	100.0
Crystal system	triclinic
Space group	P-1
a/Å	10.6426(13)
b/Å	10.6776(12)
c/Å	13.7940(13)
α/°	107.937(7)
β/°	108.100(5)
γ/°	101.232(6)
Volume/Å^3	1342.4(3)
Z	4
ρ_{calc}g/cm^3	1.239
μ/mm^{-1}	0.601
F(000)	552.0
Crystal size/mm^3	0.2 × 0.15 × 0.15
Radiation	CuKα (λ = 1.54178)
2Θ range for data collection/°	7.34 to 149.188
Index ranges	-12 ≤ h ≤ 13, -13 ≤ k ≤ 13, -17 ≤ l ≤ 17
Reflections collected	14327
Independent reflections	5244 [R_{int} = 0.0274, R_{sigma} = 0.0317]
Data/restraints/parameters	5244/0/327
Goodness-of-fit on F^2	1.057
Final R indexes [I>=2σ (I)]	R_1 = 0.0379, wR_2 = 0.1033
Final R indexes [all data]	R_1 = 0.0395, wR_2 = 0.1047
Largest diff. peak/hole / e Å^{-3}	0.26/-0.26

Crystallographic Analysis of (+)-51.

Special Refinement Details

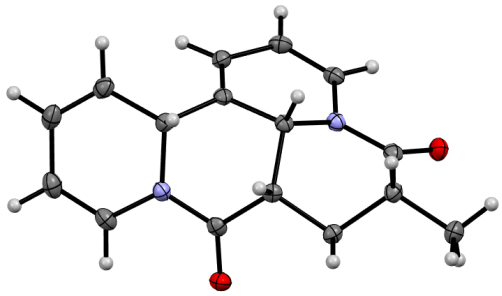

Compound (+)-**51** crystallizes in the orthorhombic space group $P2_12_12_1$ with one molecule in the asymmetric unit. Absolute configuration was determined by anomalous dispersion (Flack = 0.13(8). Bayesian statistics further confirm the absolute stereochemistry: P2(true) = 1.000, P3(true) = 1.000, P3(rac-twin) = $0.7x10^{-5}$, and P3(false) = $0.4x10^{-34}$. CCDC number: 2159768

Table 2.38. *Crystal data and structure refinement for (+)-**51**.*

Identification code	V19453
Empirical formula	$C_{16}H_{16}N_2O_2$
Formula weight	268.31
Temperature/K	100.0
Crystal system	orthorhombic
Space group	$P2_12_12_1$
a/Å	8.8059(15)
b/Å	11.451(2)
c/Å	12.474(3)
α/°	90
β/°	90
γ/°	90
Volume/Å^3	1257.9(4)
Z	4
ρ_{calc}g/cm^3	1.417
μ/mm^{-1}	0.764
F(000)	568.0

Crystal size/mm^3	? × ? × ?
Radiation	CuKα (λ = 1.54178)
2Θ range for data collection/°	12.302 to 149.394
Index ranges	-11 ≤ h ≤ 10, -14 ≤ k ≤ 14, -15 ≤ l ≤ 15
Reflections collected	23931
Independent reflections	2557 [R_{int} = 0.0554, R_{sigma} = 0.0245]
Data/restraints/parameters	2557/0/182
Goodness-of-fit on F^2	1.027
Final R indexes [I>=2σ (I)]	R_1 = 0.0329, wR_2 = 0.1071
Final R indexes [all data]	R_1 = 0.0339, wR_2 = 0.1113
Largest diff. peak/hole / e Å^{-3}	0.17/-0.20
Flack parameter	0.13(8)

Crystallographic Analysis of (±)-43.

Special Refinement Details

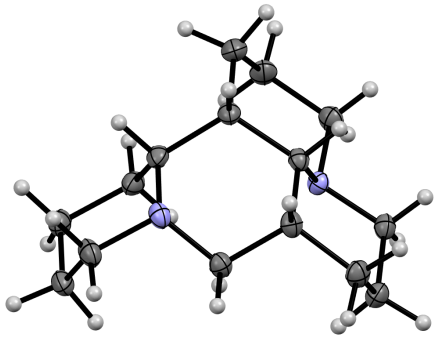

Compound (±)-**43** crystallizes in the monoclinic space group $P2_1/c$ with two molecules in the asymmetric unit. CCDC number: 2159767

Table. 2.39. *Crystal data and structure refinement for (±)-**43**.*

Identification code	V19355
Empirical formula	$C_{15}H_{26}N_2$

Formula weight	234.38
Temperature/K	100
Crystal system	monoclinic
Space group	$P2_1/c$
a/Å	10.738(2)
b/Å	17.591(4)
c/Å	14.316(3)
α/°	90
β/°	103.629(10)
γ/°	90
Volume/Å^3	2627.8(9)
Z	8
ρ_{calc}g/cm^3	1.185
μ/mm^{-1}	0.521
F(000)	1040.0
Crystal size/mm^3	0.22 × 0.08 × 0.03
Radiation	CuKα (λ = 1.54178)
2Θ range for data collection/°	8.102 to 161.38
Index ranges	$-13 \leq h \leq 12$, $-21 \leq k \leq 22$, $-17 \leq l \leq 17$
Reflections collected	38183
Independent reflections	5498 [R_{int} = 0.0594, R_{sigma} = 0.0296]
Data/restraints/parameters	5498/0/307
Goodness-of-fit on F^2	1.029
Final R indexes [I>=2σ (I)]	R_1 = 0.0455, wR_2 = 0.1109
Final R indexes [all data]	R_1 = 0.0542, wR_2 = 0.1175
Largest diff. peak/hole / e Å^{-3}	0.27/-0.26

Crystallographic Analysis of (±)-44.

Special Refinement Details

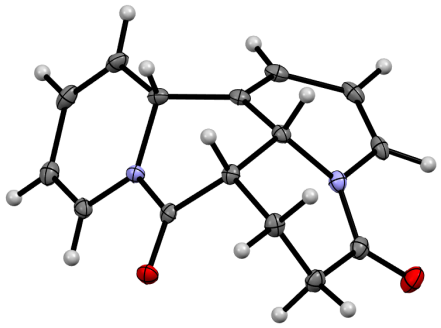

Compound (±)-**44** crystallizes in the monoclinic space group $P2_1/c$ with two molecules in the asymmetric unit. CCDC number: 2159766

Table 2.40. *Crystal data and structure refinement for (±)-**44**.*

Identification code	V18405_a
Empirical formula	$C_{15}H_{14}N_2O_2$
Formula weight	254.24
Temperature/K	99.97
Crystal system	monoclinic
Space group	$P2_1/c$
a/Å	7.0167(3)
b/Å	15.8509(6)
c/Å	20.6888(9)
α/°	90
β/°	91.261(2)
γ/°	90
Volume/Å^3	2300.47(17)
Z	46
ρ_{calc}g/cm^3	1.468
μ/mm^{-1}	0.099
F(000)	1072.5
Crystal size/mm^3	0.51 × 0.41 × 0.32
Radiation	Mo Kα (λ = 0.71073)
2Θ range for data collection/°	4.7 to 55.02
Index ranges	$-9 \leq h \leq 9$, $-20 \leq k \leq 20$, $-26 \leq l \leq 26$

Reflections collected	40432
Independent reflections	5233 [R_{int} = 0.0603, R_{sigma} = 0.0348]
Data/restraints/parameters	5233/0/343
Goodness-of-fit on F^2	1.049
Final R indexes [I>=2σ (I)]	R_1 = 0.0463, wR_2 = 0.0897
Final R indexes [all data]	R_1 = 0.0608, wR_2 = 0.0929
Largest diff. peak/hole / e $Å^{-3}$	0.48/-0.51

Crystallographic Analysis of (±)-140.

Special Refinement Details

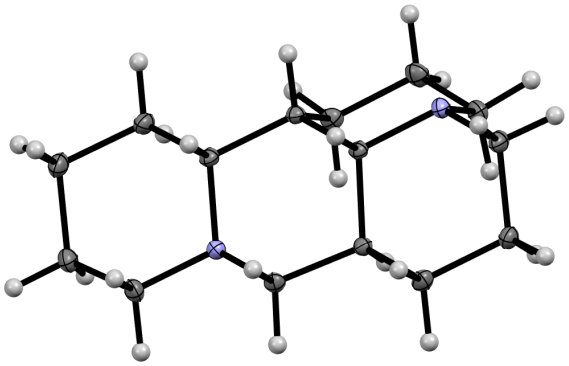

Compound (±)-**140** crystallizes in the triclinic space group P-1 with one molecule in the asymmetric unit. CCDC number: 2159765

Table 2.41. *Crystal data and structure refinement for (±)-**140**.*

Identification code	d20015
Empirical formula	$C_{15}H_{26}N_2$
Formula weight	234.38
Temperature/K	100
Crystal system	triclinic
Space group	P-1

a/Å	5.129(5)
b/Å	9.175(10)
c/Å	14.500(7)
α/°	106.65(3)
β/°	93.82(3)
γ/°	92.81(6)
Volume/Å^3	650.7(10)
Z	2
ρ_{calc}g/cm^3	1.196
μ/mm^{-1}	0.070
F(000)	260.0
Crystal size/mm^3	0.47 × 0.18 × 0.05
Radiation	MoKα (λ = 0.71073)
2Θ range for data collection/°	2.942 to 74.252
Index ranges	-8 ≤ h ≤ 8, -15 ≤ k ≤ 15, -24 ≤ l ≤ 24
Reflections collected	41718
Independent reflections	6408 [R_{int} = 0.0428, R_{sigma} = 0.0339]
Data/restraints/parameters	6408/0/155
Goodness-of-fit on F^2	1.034
Final R indexes [I>=2σ (I)]	R_1 = 0.0465, wR_2 = 0.1095
Final R indexes [all data]	R_1 = 0.0753, wR_2 = 0.1238
Largest diff. peak/hole / e Å^{-3}	0.41/-0.24

Crystallographic Analysis of (±)-104 mono-chloroform adduct.

Special Refinement Details

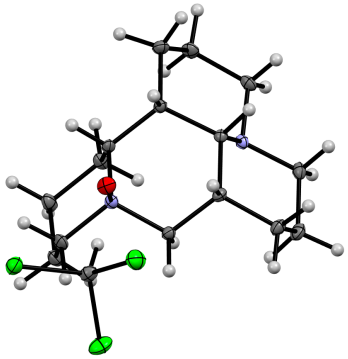

Compound (±)-**104** mono-chloroform adduct crystallizes in the monoclinic space group $P2_1/n$ with one molecule in the asymmetric unit. CCDC number: 2159764

Table 2.42. *Crystal data and structure refinement for (±)-**104** mono-chloroform adduct.*

Identification code	D20014
Empirical formula	$C_{16}H_{27}Cl_3N_2O$
Formula weight	369.74
Temperature/K	100
Crystal system	monoclinic
Space group	$P2_1/n$
a/Å	5.771(4)
b/Å	13.008(10)
c/Å	23.438(6)
α/°	90
β/°	96.271(16)
γ/°	90
Volume/Å^3	1748.9(17)
Z	4
ρ_{calc}g/cm^3	1.404
μ/mm^{-1}	0.528
F(000)	784.0
Crystal size/mm^3	0.45 × 0.4 × 0.32
Radiation	MoKα (λ = 0.71073)
2Θ range for data collection/°	3.496 to 79.03
Index ranges	$-10 \leq h \leq 10$, $-23 \leq k \leq 23$, $-39 \leq l \leq 41$
Reflections collected	113231
Independent reflections	10352 [R_{int} = 0.0335, R_{sigma} = 0.0183]
Data/restraints/parameters	10352/0/199
Goodness-of-fit on F^2	1.042
Final R indexes [I>=2σ (I)]	R_1 = 0.0342, wR_2 = 0.0843
Final R indexes [all data]	R_1 = 0.0442, wR_2 = 0.0886
Largest diff. peak/hole / e Å^{-3}	0.95/-0.85

Crystallographic Analysis of (±)-90.

Special Refinement Details

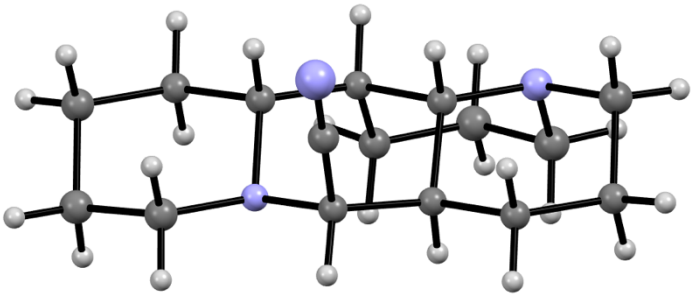

Compound (±)-**90** mono-chloroform adduct crystallizes in the triclinic space group P-1 with one molecule in the asymmetric unit.

Table 2.43. *Crystal data and structure refinement for (±)-**90**.*

Identification code	V22045
Empirical formula	$C_{16}H_{25}N_3$
Formula weight	259.39
Temperature/K	100.0
Crystal system	triclinic
Space group	P-1
a/Å	5.0835(7)
b/Å	11.3220(13)
c/Å	12.058(2)
α/°	94.182(7)
β/°	94.487(11)
γ/°	95.227(12)
Volume/Å^3	686.75(18)
Z	2
ρ_{calc}g/cm^3	1.254
μ/mm^{-1}	0.575
F(000)	284.0

Crystal size/mm^3	0.4 × 0.1 × 0.1
Radiation	CuKα (λ = 1.54178)
2Θ range for data collection/°	7.866 to 99.416
Index ranges	-4 ≤ h ≤ 2, -4 ≤ k ≤ 10, -2 ≤ l ≤ 11
Reflections collected	475
Independent reflections	474 [R_{int} = 0.0376, R_{sigma} = 0.0211]
Data/restraints/parameters	474/0/77
Goodness-of-fit on F^2	1.113
Final R indexes [I>=2σ (I)]	R_1 = 0.0377, wR_2 = 0.1220
Final R indexes [all data]	R_1 = 0.0488, wR_2 = 0.1389
Largest diff. peak/hole / e Å^{-3}	0.07/-0.08

Crystallographic Analysis of (–)-56.

Special Refinement Details

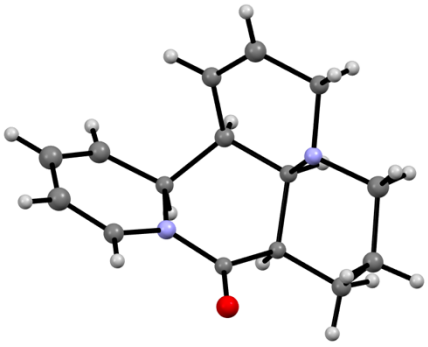

Compound (–)-**56** crystallizes in the monoclinic space group Cc with one molecule in the asymmetric unit. Absolute configuration was determined by anomalous dispersion (Flack = -2.3(10). Bayesian statistics further supports the absolute stereochemistry: P2(true) = -0.630, P3(true) = 0.422, P3(rac-twin) = 0.330, and P3(false) = 0.248.

Table 2.44. *Crystal data and structure refinement for (–)-**56**.*

Identification code	D21063
Empirical formula	$C_{17}H_{19}N_3O$

Formula weight	281.35
Temperature/K	296.15
Crystal system	monoclinic
Space group	Cc
a/Å	5.201(3)
b/Å	14.167(7)
c/Å	16.404(18)
α/°	90
β/°	98.21(3)
γ/°	90
Volume/Å^3	1196.4(16)
Z	4
ρ_{calc}g/cm^3	1.562
μ/mm^{-1}	0.100
F(000)	600.0
Crystal size/mm^3	0.4 × 0.25 × 0.1
Radiation	MoKα (λ = 0.71073)
2Θ range for data collection/°	5.018 to 53.262
Index ranges	$-5 \leq h \leq 5$, $-15 \leq k \leq 15$, $-19 \leq l \leq 19$
Reflections collected	3029
Independent reflections	1770 [R_{int} = 0.0862, R_{sigma} = 0.1507]
Data/restraints/parameters	1770/2/163
Goodness-of-fit on F^2	0.978
Final R indexes [I>=2σ (I)]	R_1 = 0.0563, wR_2 = 0.0893
Final R indexes [all data]	R_1 = 0.1330, wR_2 = 0.1092
Largest diff. peak/hole / e Å^{-3}	0.22/-0.26
Flack parameter	-2.3(10)

Crystallographic Analysis of (±)-59.

Special Refinement Details

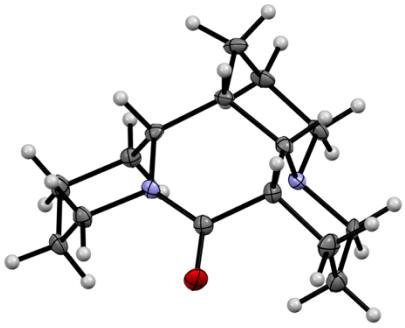

Compound (±)-**59** crystallizes in the monoclinic space group $P2_1/n$ with one molecule in the asymmetric unit.

Table 2.47. *Crystal data and structure refinement for (±)-**59**.*

Identification code	V20006
Empirical formula	$C_{16}H_{24}NO$
Formula weight	246.36
Temperature/K	99.99
Crystal system	monoclinic
Space group	$P2_1/n$
a/Å	5.4330(11)
b/Å	13.383(4)
c/Å	18.052(2)
α/°	90
β/°	90.171(11)
γ/°	90
Volume/Å^3	1312.6(5)
Z	4
ρ_{calc}g/cm^3	1.247
μ/mm^{-1}	0.077
F(000)	540.0
Crystal size/mm^3	? × ? × ?
Radiation	MoKα (λ = 0.71073)
2Θ range for data collection/°	5.444 to 72.732

Index ranges	$-9 \leq h \leq 9, -22 \leq k \leq 22, -30 \leq l \leq 30$
Reflections collected	34154
Independent reflections	6337 [R_{int} = 0.0685, R_{sigma} = 0.0544]
Data/restraints/parameters	6337/0/163
Goodness-of-fit on F^2	1.123
Final R indexes [I>=2σ (I)]	R_1 = 0.2513, wR_2 = 0.5841
Final R indexes [all data]	R_1 = 0.2577, wR_2 = 0.5904
Largest diff. peak/hole / e $Å^{-3}$	1.01/-1.12

Crystallographic Analysis of (±)-62.

Special Refinement Details

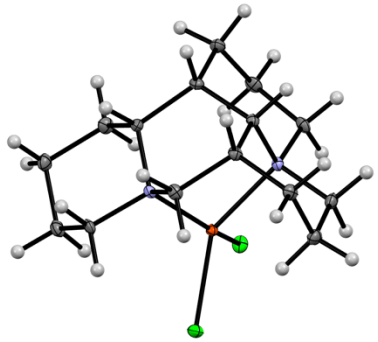

Compound (±)-**62** crystallizes in the monoclinic space group $P2_1/n$ with one molecule in the asymmetric unit.

Table 2.48. *Crystal data and structure refinement for (±)-**62**.*

Identification code	d19147
Empirical formula	$C_{15}H_{26}Cl_2CuN_2$
Formula weight	368.82
Temperature/K	99.98
Crystal system	monoclinic
Space group	$P2_1/n$
a/Å	8.918(4)

b/Å	13.094(9)
c/Å	13.774(9)
α/°	90
β/°	105.34(5)
γ/°	90
Volume/Å^3	1551.1(17)
Z	4
ρ_{calc}g/cm^3	1.579
μ/mm^{-1}	1.744
F(000)	772.0
Crystal size/mm^3	0.44 × 0.2 × 0.08
Radiation	MoKα (λ = 0.71073)
2Θ range for data collection/°	4.368 to 75.22
Index ranges	$-15 \leq h \leq 15$, $-22 \leq k \leq 22$, $-23 \leq l \leq 23$
Reflections collected	69103
Independent reflections	7997 [R_{int} = 0.0372, R_{sigma} = 0.0240]
Data/restraints/parameters	7997/0/182
Goodness-of-fit on F^2	1.013
Final R indexes [I>=2σ (I)]	R_1 = 0.0244, wR_2 = 0.0512
Final R indexes [all data]	R_1 = 0.0361, wR_2 = 0.0543
Largest diff. peak/hole / e Å^{-3}	0.49/-0.49

Crystallographic Analysis of (±)-98.

Special Refinement Details

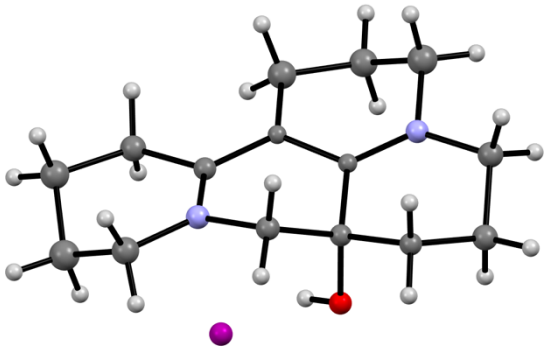

Compound (±)-**98** crystallizes in the monoclinic space group $P2_1/n$ with one molecule in the asymmetric unit.

Table 2.49. *Crystal data and structure refinement for (±)-**98**.*

Identification code	V22009
Empirical formula	$C_{15}H_{24}N_2OI$
Formula weight	280.42
Temperature/K	100.0
Crystal system	monoclinic
Space group	$P2_1/n$
a/Å	12.8228(19)
b/Å	8.3093(12)
c/Å	14.078(2)
α/°	90
β/°	95.136(13)
γ/°	90
Volume/Å^3	1494.0(4)
Z	4
ρ_{calc}g/cm^3	1.247
μ/mm^{-1}	1.870
F(000)	608.0
Crystal size/mm^3	? × ? × 0.15
Radiation	CuKα (λ = 1.54178)
2Θ range for data collection/°	8.938 to 148.562
Index ranges	$-14 \leq h \leq 14$, $-10 \leq k \leq 9$, $-15 \leq l \leq 8$
Reflections collected	4460

Independent reflections	1887 [R_{int} = 0.0649, R_{sigma} = 0.0726]
Data/restraints/parameters	1887/0/78
Goodness-of-fit on F^2	1.075
Final R indexes [I>=2σ (I)]	R_1 = 0.0738, wR_2 = 0.2057
Final R indexes [all data]	R_1 = 0.0886, wR_2 = 0.2214
Largest diff. peak/hole / e $Å^{-3}$	3.40/-4.19

Crystallographic Analysis of (±)-97.

Special Refinement Details

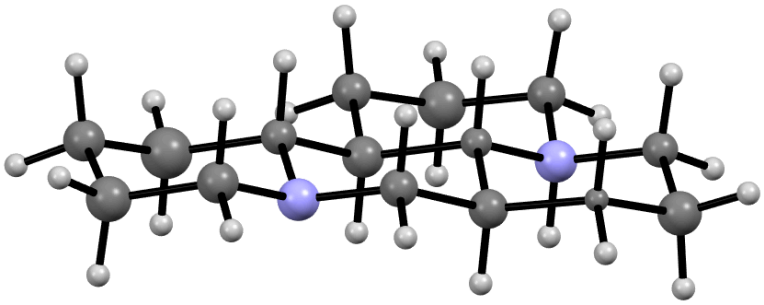

Compound (±)-**97** crystallizes in the triclinic space group P1 with two molecules in the asymmetric unit.

Table 2.50. *Crystal data and structure refinement for (±)-**97**.*

Identification code	V20119
Empirical formula	$C_{15}H_{26}N_2$
Formula weight	234.38
Temperature/K	100.0
Crystal system	triclinic
Space group	P1
a/Å	4.6048(5)
b/Å	10.8544(11)

c/Å	13.5496(16)
α/°	91.728(14)
β/°	90.179(10)
γ/°	102.239(8)
Volume/Å^3	661.52(13)
Z	2
ρ_{calc}g/cm^3	1.177
μ/mm^{-1}	0.517
F(000)	260.0
Crystal size/mm^3	0.2 × 0.08 × 0.07
Radiation	CuKα (λ = 1.54178)
2Θ range for data collection/°	6.526 to 159.182
Index ranges	-5 ≤ h ≤ 5, -13 ≤ k ≤ 13, -16 ≤ l ≤ 16
Reflections collected	14702
Independent reflections	4817 [R_{int} = 0.0688, R_{sigma} = 0.0680]
Data/restraints/parameters	4817/3/134
Goodness-of-fit on F^2	3.790
Final R indexes [I>=2σ (I)]	R_1 = 0.2362, wR_2 = 0.5409
Final R indexes [all data]	R_1 = 0.2639, wR_2 = 0.5655
Largest diff. peak/hole / e Å^{-3}	2.67/-0.95
Flack parameter	0.4(4)

Crystallographic Analysis of (±)-96 dihydrate.

Special Refinement Details

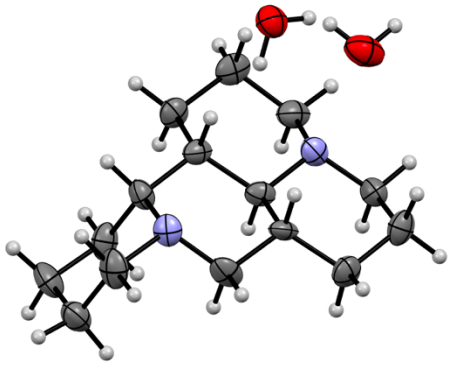

Compound (±)-**96** dihydrate crystallizes in the orthorhombic space group Pbcn with one molecule in the asymmetric unit.

Table 2.51. *Crystal data and structure refinement for (±)-**96** dihydrate.*

Identification code	v20120
Empirical formula	$C_{15}H_{26}N_2O_{0.13}$
Formula weight	236.38
Temperature/K	100.0
Crystal system	orthorhombic
Space group	Pbcn
a/Å	22.990(9)
b/Å	6.991(2)
c/Å	19.007(6)
α/°	90
β/°	90
γ/°	90
Volume/Å^3	3054.8(18)
Z	8
ρ_{calc}g/cm^3	1.028
μ/mm^{-1}	0.458
F(000)	1048.0
Crystal size/mm^3	? × ? × ?
Radiation	CuKα (λ = 1.54178)
2Θ range for data collection/°	9.306 to 99.616
Index ranges	-14 ≤ h ≤ 22, -2 ≤ k ≤ 6, -18 ≤ l ≤ 12
Reflections collected	3454

Independent reflections	1343 [R_{int} = 0.0459, R_{sigma} = 0.0553]
Data/restraints/parameters	1343/0/178
Goodness-of-fit on F^2	1.239
Final R indexes [I>=2σ (I)]	R_1 = 0.1127, wR_2 = 0.2674
Final R indexes [all data]	R_1 = 0.1385, wR_2 = 0.2786
Largest diff. peak/hole / e $Å^{-3}$	0.33/-0.28

Crystallographic Analysis of (±)-133.

Special Refinement Details

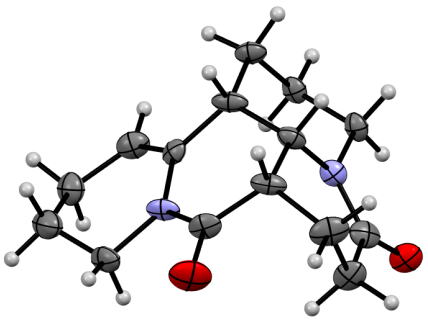

Compound (±)-**133** crystallizes in the monoclinic space group $P2_1/n$ with one molecule in the asymmetric unit.

Table 2.52. *Crystal data and structure refinement for (±)-**133**.*

Identification code	V21317
Empirical formula	$C_{15}H_{20}N_3O_2$
Formula weight	274.34
Temperature/K	100.0
Crystal system	monoclinic
Space group	$P2_1/n$
a/Å	12.249(11)
b/Å	8.778(6)
c/Å	12.919(13)

α/°	90
β/°	98.75(3)
γ/°	90
Volume/Å^3	1373(2)
Z	4
ρ_{calc}g/cm^3	1.327
μ/mm^{-1}	0.090
F(000)	588.0
Crystal size/mm^3	0.2 × 0.15 × 0.1
Radiation	MoKα (λ = 0.71073)
2Θ range for data collection/°	4.976 to 72.256
Index ranges	-13 ≤ h ≤ 16, -11 ≤ k ≤ 14, -18 ≤ l ≤ 15
Reflections collected	9867
Independent reflections	3365 [R_{int} = 0.1918, R_{sigma} = 0.2293]
Data/restraints/parameters	3365/0/176
Goodness-of-fit on F^2	1.682
Final R indexes [I>=2σ (I)]	R_1 = 0.2035, wR_2 = 0.5010
Final R indexes [all data]	R_1 = 0.3340, wR_2 = 0.5603
Largest diff. peak/hole / e Å^{-3}	4.93/-0.56

Crystallographic Analysis of (±)-57.

Special Refinement Details

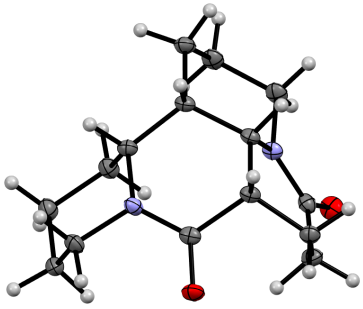

Compound (±)-**57** crystallizes in the monoclinic space group $P2_1/c$ with one molecule in the asymmetric unit.

Table 2.53. *Crystal data and structure refinement for (±)-**57**.*

Identification code	V19018
Empirical formula	$C_{15}H_{22}N_2O_2$
Formula weight	262.34
Temperature/K	99.99
Crystal system	monoclinic
Space group	$P2_1/c$
a/Å	13.8942(11)
b/Å	9.0952(9)
c/Å	10.4946(9)
α/°	90
β/°	105.846(4)
γ/°	90
Volume/Å^3	1275.8(2)
Z	4
ρ_{calc}g/cm^3	1.366
μ/mm^{-1}	0.726
F(000)	568.0
Crystal size/mm^3	? × ? × ?
Radiation	CuKα (λ = 1.54178)
2Θ range for data collection/°	6.612 to 148.632
Index ranges	$-13 \leq h \leq 15$, $-10 \leq k \leq 11$, $-10 \leq l \leq 12$
Reflections collected	4850
Independent reflections	2197 [R_{int} = 0.0557, R_{sigma} = 0.0566]
Data/restraints/parameters	2197/0/77
Goodness-of-fit on F^2	1.054
Final R indexes [I>=2σ (I)]	R_1 = 0.0745, wR_2 = 0.1975
Final R indexes [all data]	R_1 = 0.0771, wR_2 = 0.2008
Largest diff. peak/hole / e Å^{-3}	0.51/-0.67

Crystallographic Analysis of (±)-4 monohydrate.

Special Refinement Details

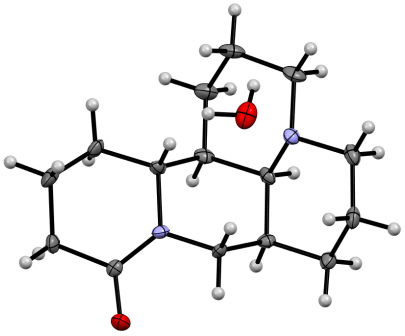

Compound (±)-**4** monohydrate crystallizes in the tetragonal space group $P4_32_12$ with one molecule in the asymmetric unit.

Table 2.54. *Crystal data and structure refinement for (±)-**4** monohydrate.*

Identification code	V22034
Empirical formula	$C_{15}H_{24}N_2O$
Formula weight	248.36
Temperature/K	100.0
Crystal system	tetragonal
Space group	$P4_32_12$
a/Å	11.6747(9)
b/Å	11.6747(9)
c/Å	21.878(5)
α/°	90
β/°	90
γ/°	90
Volume/Å^3	2981.9(8)
Z	8

ρ_{calc}g/cm^3	1.106
μ/mm^{-1}	0.540
F(000)	1088.0
Crystal size/mm^3	0.45 × 0.4 × 0.3
Radiation	CuKα (λ = 1.54178)
2Θ range for data collection/°	8.584 to 148.596
Index ranges	$-10 \leq h \leq 8$, $-7 \leq k \leq 13$, $-23 \leq l \leq 14$
Reflections collected	7045
Independent reflections	2250 [R_{int} = 0.0371, R_{sigma} = 0.0286]
Data/restraints/parameters	2250/0/175
Goodness-of-fit on F^2	2.458
Final R indexes [I>=2σ (I)]	R_1 = 0.0896, wR_2 = 0.2715
Final R indexes [all data]	R_1 = 0.0939, wR_2 = 0.2742
Largest diff. peak/hole / e Å^{-3}	2.50/-0.40
Flack parameter	0.10(15)

Crystallographic Analysis of (±)-95 dihydrate.

Special Refinement Details

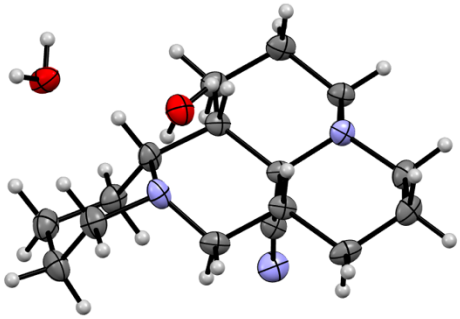

Compound (±)-**95** dihydrate crystallizes in the monoclinic space group C2/c with one molecule in the asymmetric unit.

Table 2.55. *Crystal data and structure refinement for (±)-**95** dihydrate.*

Identification code	V21361
Empirical formula	$C_{16}H_{25}N_3O_{0.13}$
Formula weight	261.39
Temperature/K	100.0
Crystal system	monoclinic
Space group	C2/c
a/Å	23.605(6)
b/Å	7.0420(12)
c/Å	19.453(5)
α/°	90
β/°	97.767(14)
γ/°	90
Volume/Å^3	3203.9(13)
Z	8
ρ_{calc}g/cm^3	1.084
μ/mm^{-1}	0.502
F(000)	1144.0
Crystal size/mm^3	0.25 × 0.05 × 0.05
Radiation	CuKα (λ = 1.54178)
2Θ range for data collection/°	7.56 to 148.54
Index ranges	-21 ≤ h ≤ 24, -6 ≤ k ≤ 8, -13 ≤ l ≤ 17
Reflections collected	3621
Independent reflections	1967 [R_{int} = 0.0441, R_{sigma} = 0.0533]
Data/restraints/parameters	1967/0/196
Goodness-of-fit on F^2	1.214
Final R indexes [I>=2σ (I)]	R_1 = 0.0638, wR_2 = 0.1738
Final R indexes [all data]	R_1 = 0.0893, wR_2 = 0.1877
Largest diff. peak/hole / e Å^{-3}	0.46/-0.25

Crystallographic Analysis of (±)-79.

Special Refinement Details

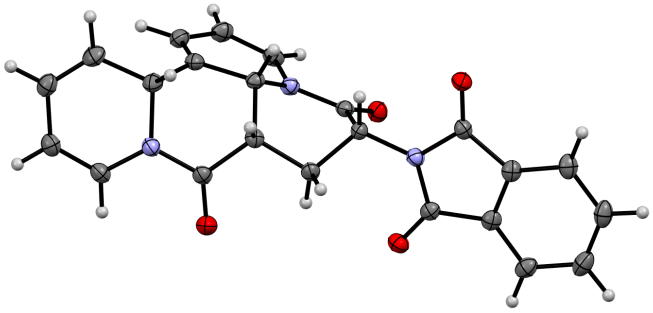

Compound (±)-**79** crystallizes in the monoclinic space group $P2_1$ with one molecule in the asymmetric unit.

Table 2.56. *Crystal data and structure refinement for (±)-**79**.*

Identification code	V19479
Empirical formula	$C_{23}H_{17}N_3O_4$
Formula weight	399.39
Temperature/K	99.99
Crystal system	monoclinic
Space group	$P2_1$
a/Å	5.1166(7)
b/Å	15.6750(16)
c/Å	11.2761(15)
α/°	90
β/°	102.567(9)
γ/°	90
Volume/Å^3	882.71(19)
Z	2
ρ_{calc}g/cm^3	1.503
μ/mm^{-1}	0.864
F(000)	416.0
Crystal size/mm^3	0.15 × 0.1 × 0.05
Radiation	CuKα (λ = 1.54178)
2Θ range for data collection/°	8.032 to 149.378

Index ranges	$-6 \leq h \leq 6, -19 \leq k \leq 19, -14 \leq l \leq 14$
Reflections collected	9371
Independent reflections	3529 [$R_{int} = 0.0436$, $R_{sigma} = 0.0431$]
Data/restraints/parameters	3529/1/271
Goodness-of-fit on F^2	1.032
Final R indexes [I>=2σ (I)]	$R_1 = 0.0325$, $wR_2 = 0.0787$
Final R indexes [all data]	$R_1 = 0.0355$, $wR_2 = 0.0804$
Largest diff. peak/hole / e $Å^{-3}$	0.20/-0.17
Flack parameter	0.23(11)

1.8.2 COMPUTATIONAL METHODS

Density functional theory (DFT) calculations were performed with Gaussian 16.[106] A comprehensive conformer search was performed for each intermediate and transition state using the CREST program.[107] Geometry optimizations, frequency calculations, and energy calculations were performed using the ωB97XD[108] functional and def2-TZVP basis set.[109,110] Dichloromethane solvation was modeled using the SMD solvation model.[111] A chloride anion was included when necessary to create a neutral species. Frequency calculations confirmed the optimized structures as minima (zero imaginary frequencies) or transition state structures (one imaginary frequency) on the potential energy surface. A quasi-harmonic correction was applied using the GoodVibes program.[112] PyMOL was used to render visualizations of structures.[113] Initial structures were made using GaussView.[114] For calculations analyzing the effects of dispersion on the transition states, the B3LYP-D3/def2-TZVP/SMD(DCM) and B3LYP/def2-TZVP/SMD(DCM) levels of theory were used.

Figure 1.71. *Second C–C Bond Formation Energies.*

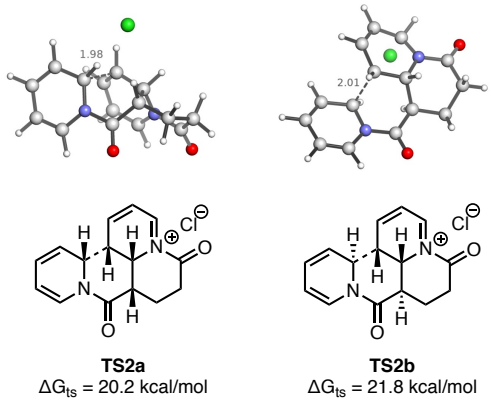

Figure 1.72. *Deprotonation of Int2a with Pyridine Energies.*

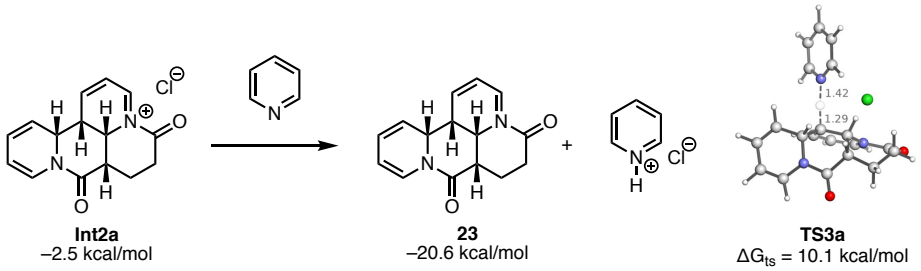

Figure 1.73. *Initial C–C Bond Formation with an acyl-Cl/acyl-pyridinium Starting Material.*

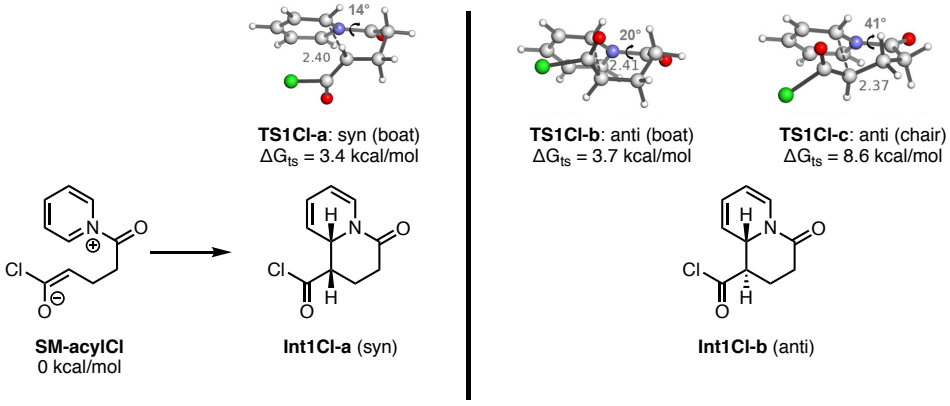

Figure 1.74. *C–C Bond Formation with a Ketene Starting Material Resulting in the Formation of a Cyclobutanone Intermediate.*

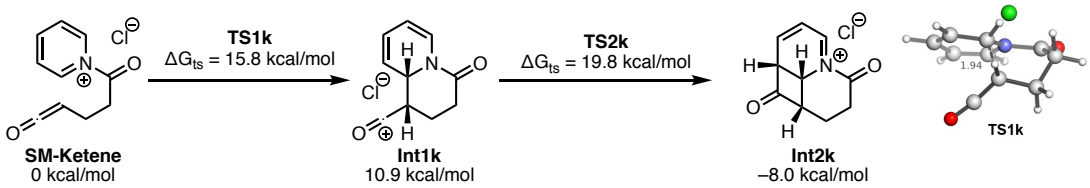

Figure 1.75. *Relative Energy of Starting Material Species.*

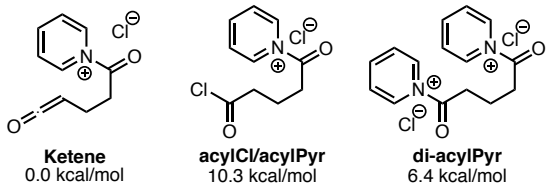

Table 1.76. *Summary of Energies.*

Structure	E (au)	qh-H (au)	qh-S (au)	qh-G(T) (au)	qh-G(T) (kcal/mol)	ΔG relative to SM (kcal/mol)
Figure 2.						
1. 65	-1300.829	-1300.542	0.064877	-1300.606	-816142.2	0.0
2. TS1a	-1300.820	-1300.532	0.062761	-1300.595	-816134.9	7.3
3. TS1b	-1300.816	-1300.529	0.063230	-1300.592	-816133.4	8.8
4. TS1c	-1300.809	-1300.519	0.066721	-1300.586	-816129.2	13.0
5. Int1a	-1300.853	-1300.563	0.062907	-1300.626	-816154.8	-12.6
6. Int1b	-1300.849	-1300.560	0.063824	-1300.623	-816152.9	-10.7
7. TS2a	-1300.823	-1300.534	0.060381	-1300.594	-816134.6	7.6
8. TS2b	-1300.820	-1300.530	0.058511	-1300.589	-816131.1	11.1
9. Int2a	-1300.851	-1300.553	0.057899	-1300.610	-816144.7	-2.5
10. Int2b	-1300.859	-1300.567	0.058893	-1300.626	-816154.2	-12.0
11. TS3a	-1549.130	-1548.752	0.073312	-1548.825	-971901.5	10.1
12. TS3b	-1549.125	-1548.746	0.073075	-1548.819	-971897.9	13.7
13. Int3a	-840.012	-839.736	0.055476	-839.791	-526976.5	-20.6
14. Int3b	-840.020	-839.743	0.055101	-839.798	-526981.1	-25.2
15. Pyr	-248.294	-248.202	0.032670	-248.235	-155769.4	
16. Pyr·HCl	-709.151	-709.044	0.039009	-709.083	-444955.7	
SI						
17. SM-acylCl	-1052.506	-1052.313	0.053085	-1052.366	-660369.2	0.0

18. TS1Cl-a	-1052.502	-1052.310	0.051096	-1052.361	-660365.8	3.4
19. TS1Cl-b	-1052.501	-1052.309	0.051295	-1052.360	-660365.5	3.7
20. TS1Cl-c	-1052.492	-1052.301	0.051695	-1052.352	-660360.6	8.6
46. SM-ketene	-1052.514	-1052.321	0.056199	-1052.378	-660376.4	0.0
47. TS1k	-1052.491	-1052.300	0.052884	-1052.352	-660360.7	15.8
44. Int1k	-1052.499	-1052.307	0.053175	-1052.360	-660365.5	10.9
43. TS2k	-1052.485	-1052.294	0.052200	-1052.346	-660356.6	19.8
6. Int2k	-1052.537	-1052.341	0.049466	-1052.390	-660384.4	-8.0
SM species						
4. di-acylPyr	-2009.980	-2009.586	0.084118	-2009.670	-1261086.0	6.4
7. acylCl/acylPyr	-2009.971	-2009.579	0.085215	-2009.664	-1261082.1	10.3
8. ketene	-2009.984	-2009.592	0.087969	-2009.680	-1261092.4	0.0

Table 1.77. *Coordinates.*

1

C	4.241804	-0.634410	0.109065
C	3.688490	-1.777624	-0.447706
C	2.395767	-1.735813	-0.913047
N	1.679201	-0.606082	-0.849794
C	2.187084	0.505890	-0.299249
C	3.475550	0.516688	0.186345
H	3.855962	1.425019	0.631595
H	1.539952	1.375440	-0.225545
C	0.246192	-0.667665	-1.377307
C	-0.198668	0.478885	-1.948167
C	-1.602848	0.566770	-2.450576
H	-1.673252	1.340472	-3.215910
H	-1.910565	-0.374284	-2.914120
C	-2.674652	0.939926	-1.385415
C	-2.930778	-0.180457	-0.436496
O	-3.799951	-0.987369	-0.550315
N	-2.016018	-0.344090	0.728848
C	-1.133729	0.605773	1.086228
C	-0.277851	0.395257	2.143310
C	-0.331500	-0.801107	2.833221
C	-1.255398	-1.768014	2.451870
C	-2.083311	-1.516970	1.393619
H	-2.811344	-2.222896	1.026827
H	-1.326928	-2.716355	2.963574
H	0.336807	-0.984056	3.664458
H	0.411799	1.187375	2.397192
H	-1.103624	1.538158	0.542790

Cl	0.564792	3.540088	0.616096
H	-2.389871	1.858833	-0.877126
H	-3.627096	1.109665	-1.885869
H	0.431524	1.351535	-2.021092
O	-0.305276	-1.769418	-1.200954
H	1.883731	-2.583965	-1.342729
H	4.248509	-2.698586	-0.522547
H	5.255553	-0.645123	0.487474

2

C	4.267561	-0.697170	0.058179
C	3.568186	0.491891	0.179673
C	2.274329	0.569424	-0.279421
N	1.685644	-0.498367	-0.845175
C	2.346432	-1.661597	-0.962186
C	3.640909	-1.788773	-0.522173
C	0.251226	-0.489595	-1.355875
C	-0.424308	0.720658	-1.285486
C	-1.110646	0.461671	0.866266
C	-0.073093	0.149509	1.777280
C	-1.751713	0.827168	-1.978595
C	-2.997817	1.018098	-1.069379
C	-3.210914	-0.161917	-0.185934
N	-2.113019	-0.456669	0.693185
C	-2.023818	-1.716474	1.232741
C	-0.990557	-2.058491	2.028902
C	0.002656	-1.089550	2.327196
O	-4.156391	-0.902702	-0.216378
O	-0.168008	-1.582892	-1.708201
H	5.286523	-0.773905	0.414137
H	4.008670	1.368130	0.633325
H	1.703333	1.485636	-0.169012
H	1.785195	-2.461989	-1.419214
H	4.145154	-2.737292	-0.636660
H	0.097654	1.644379	-1.090643
H	-1.348426	1.500150	0.713311
H	0.625436	0.939396	2.013768
H	-1.735420	1.690928	-2.644661
H	-1.920081	-0.057705	-2.593480
H	-3.887324	1.117447	-1.686940
H	-2.894426	1.930635	-0.479691
H	-2.828592	-2.383756	0.966917
H	-0.943717	-3.055128	2.441984
H	0.797220	-1.331050	3.021434

Cl	0.710884	3.543824	0.705226
3			
C	4.302610	0.418756	-0.601979
C	4.056378	-0.902940	-0.942663
C	2.903867	-1.503525	-0.500635
N	2.015849	-0.829208	0.248533
C	2.239670	0.448457	0.597732
C	3.379996	1.094547	0.178126
C	0.759246	-1.590272	0.649824
C	-0.332857	-0.811317	0.996101
C	-1.048406	-0.494707	-1.159738
C	-0.143437	0.318341	-1.874353
C	-1.536193	-1.486154	1.589505
C	-2.645547	-1.934500	0.595469
C	-3.233296	-0.770273	-0.121882
N	-2.276064	0.024923	-0.852232
C	-2.546957	1.356006	-1.031904
C	-1.646907	2.173958	-1.620294
C	-0.422485	1.633784	-2.077346
O	-4.372583	-0.399635	-0.059350
O	0.832172	-2.803807	0.505707
H	5.204394	0.913303	-0.938503
H	4.749049	-1.470781	-1.546793
H	2.639366	-2.527817	-0.714284
H	1.507840	0.961247	1.215295
H	3.529611	2.122346	0.476766
H	-0.228453	0.248654	1.176443
H	-0.989427	-1.566909	-1.250131
H	0.770908	-0.130938	-2.235064
H	-1.232341	-2.389812	2.119761
H	-1.993933	-0.817563	2.320008
H	-3.455085	-2.416124	1.138818
H	-2.238525	-2.660116	-0.110635
H	-3.509619	1.681147	-0.669379
H	-1.878923	3.221213	-1.742754
H	0.281270	2.266384	-2.602271
Cl	0.145562	2.713079	2.115411
4			
C	-4.205066	-1.070480	0.044850
C	-2.969470	-1.504960	0.494098
C	-1.925442	-0.613877	0.582838
N	-2.096472	0.674570	0.239034

C	-3.287750	1.111669	-0.200170
C	-4.361273	0.261652	-0.304878
C	-0.975128	1.710350	0.277398
C	0.245454	1.257766	0.737967
C	1.012873	0.576880	-1.268333
C	0.062071	-0.105233	-2.059039
C	1.373269	2.233396	0.906695
C	2.747434	1.561086	0.935995
C	3.148278	0.527943	-0.083422
N	2.106400	-0.128466	-0.846344
C	2.195901	-1.482296	-1.009507
C	1.245119	-2.164876	-1.687703
C	0.159566	-1.450486	-2.241231
O	4.271081	0.135751	-0.211430
O	-1.271578	2.793599	-0.213295
H	-5.036054	-1.759529	-0.030652
H	-2.796732	-2.531931	0.782802
H	-0.956259	-0.935435	0.948737
H	-3.322773	2.159245	-0.457047
H	-5.306513	0.648031	-0.657511
H	0.334449	0.324518	1.278095
H	1.153856	1.638272	-1.405160
H	-0.738838	0.471757	-2.499029
H	1.337737	2.992939	0.122022
H	1.275718	2.779283	1.849846
H	3.542024	2.306907	0.947791
H	2.846176	0.999182	1.873213
H	3.061487	-1.946197	-0.563146
H	1.333623	-3.234796	-1.799824
H	-0.583116	-1.972684	-2.830734
Cl	0.764392	-2.016958	2.313895

5

C	-3.745491	-1.648673	0.203284
C	-3.537248	-0.299075	-0.023961
C	-2.330493	0.265979	0.311767
N	-1.370984	-0.490876	0.875609
C	-1.557791	-1.803463	1.122063
C	-2.738064	-2.408771	0.783847
H	-2.862686	-3.464660	0.974027
H	-0.731012	-2.326016	1.578154
C	-0.045302	0.075192	1.243725
O	0.496693	-0.409299	2.185363
C	0.515801	1.118199	0.328335

C	1.677239	1.878352	0.991240
H	1.527949	2.944501	0.827807
H	1.663989	1.709363	2.066148
C	3.056776	1.483141	0.434746
C	3.182849	0.012141	0.147739
O	4.107595	-0.681144	0.522706
N	2.129990	-0.496870	-0.589330
C	2.024542	-1.867909	-0.791571
C	1.013510	-2.410171	-1.474451
C	-0.003651	-1.548150	-2.053937
C	0.011758	-0.237387	-1.825036
C	1.049293	0.422651	-0.967662
H	1.473728	1.246080	-1.547119
H	-0.723988	0.428264	-2.258602
H	-0.768108	-1.982354	-2.686281
H	0.972384	-3.481010	-1.610105
H	2.826402	-2.441047	-0.350725
H	3.848808	1.761589	1.125356
H	3.239415	2.014629	-0.504193
H	-0.262435	1.820736	0.017201
H	-2.127784	1.322645	0.138490
H	-4.297800	0.328638	-0.465231
H	-4.685970	-2.109648	-0.068612
Cl	-1.922507	3.510219	-0.675623

6

C	-4.857986	0.466590	-0.175803
C	-4.677088	-0.894401	0.036356
C	-3.410199	-1.378132	0.218048
N	-2.347791	-0.546190	0.184096
C	-2.499041	0.777098	-0.021578
C	-3.755602	1.303363	-0.200653
C	-1.003206	-1.161691	0.393207
C	0.164845	-0.358346	-0.071714
C	1.485961	-0.991582	0.422116
C	1.635276	-0.881643	1.913493
C	0.129001	-0.250659	-1.624452
C	1.341110	-0.933881	-2.256311
C	2.612722	-0.389519	-1.667093
N	2.607085	-0.353519	-0.290932
C	3.646424	0.285390	0.378266
C	3.703633	0.357277	1.707630
C	2.651595	-0.256196	2.499781
O	3.545411	0.018976	-2.332271

O	-0.981157	-2.258065	0.853248
H	-5.852726	0.868042	-0.318021
H	-5.511363	-1.580062	0.060844
H	-3.191933	-2.420457	0.391828
H	-1.619653	1.421969	-0.012532
H	-3.851547	2.368760	-0.352705
H	0.112977	0.653788	0.341556
H	1.469758	-2.052890	0.155124
H	0.856748	-1.352071	2.499792
H	-0.778636	-0.692828	-2.036127
H	0.121315	0.806517	-1.889706
H	1.364021	-0.764484	-3.330263
H	1.300513	-2.014027	-2.086686
H	4.383909	0.722423	-0.277663
H	4.522585	0.877199	2.182532
H	2.704983	-0.203251	3.580114
Cl	-0.080278	3.141767	0.256717

7

C	-3.767925	-0.993200	-0.038669
C	-3.095201	-1.945482	0.788089
C	-1.896272	-1.637303	1.316089
N	-1.288982	-0.431096	1.036466
C	-1.795519	0.399564	0.050407
C	-3.142264	0.148615	-0.383756
C	0.001519	-0.172682	1.569234
C	0.761564	0.892602	0.828566
C	0.857915	0.510899	-0.684578
C	-0.459273	0.283766	-1.409477
C	2.165855	1.128569	1.404634
C	3.291355	0.800310	0.412381
C	3.066263	-0.513571	-0.268541
N	1.762850	-0.648182	-0.790847
C	1.344626	-1.851310	-1.235161
C	0.118115	-2.051152	-1.795948
C	-0.722029	-0.947582	-1.982540
O	3.872459	-1.405378	-0.362075
O	0.423677	-0.843280	2.475012
H	-4.781225	-1.188820	-0.364528
H	-3.552746	-2.893554	1.030073
H	-1.345348	-2.283221	1.982063
H	-1.531849	1.452399	0.132670
H	-3.611258	0.905955	-0.996454
H	0.192859	1.825624	0.853399

H	1.343536	1.360672	-1.161199
H	-0.856697	1.168183	-1.893668
H	2.263392	2.170562	1.703318
H	2.294342	0.518585	2.297214
H	4.255898	0.761609	0.912309
H	3.350467	1.571577	-0.361587
H	2.071575	-2.646085	-1.134409
H	-0.152420	-3.035417	-2.146030
H	-1.625855	-1.059561	-2.569625
Cl	-0.963130	3.682556	-0.490044

8

C	-3.964636	-1.480477	0.080184
C	-4.417582	-0.109300	-0.026496
C	-3.543100	0.890485	0.113174
N	-2.189332	0.658689	0.355252
C	-1.673254	-0.676493	0.390688
C	-2.670835	-1.738853	0.294007
C	-1.312723	1.731762	0.281415
C	0.145805	1.350110	0.303601
C	0.546923	0.410920	-0.875055
C	-0.438959	-0.689620	-1.194519
C	1.085299	2.557552	0.323561
C	2.403541	2.284102	-0.423033
C	2.873033	0.859244	-0.299474
N	1.897315	-0.078645	-0.569206
C	2.171996	-1.429765	-0.284959
C	1.289948	-2.397669	-0.970360
C	0.087190	-2.030708	-1.403513
O	4.003782	0.542605	0.013267
O	-1.713923	2.874548	0.180973
H	-4.683312	-2.286559	0.005506
H	-5.458755	0.116439	-0.206394
H	-3.808964	1.933875	0.047978
H	-0.942383	-0.836028	1.177764
H	-2.302908	-2.750762	0.403236
H	0.302599	0.757476	1.207910
H	0.629604	1.035212	-1.766997
H	-1.161235	-0.377820	-1.942490
H	0.591113	3.411936	-0.135947
H	1.299460	2.828645	1.356971
H	3.200574	2.930703	-0.064576
H	2.271944	2.490451	-1.489080
H	3.228154	-1.623682	-0.426014

H	1.657849	-3.410008	-1.066425
H	-0.555686	-2.750753	-1.895700
Cl	1.997725	-1.767905	1.581335

9

C	2.735216	1.173874	1.868249
C	3.889893	0.833559	1.046585
C	3.702411	0.286072	-0.163828
N	2.392512	0.191710	-0.651262
C	1.510357	1.263082	-0.202598
C	1.532765	1.312371	1.300689
C	1.933704	-0.975721	-1.201786
C	0.483306	-1.342783	-0.924969
C	-0.528429	-0.177539	-0.865556
C	0.179150	1.177575	-0.940268
C	0.546327	-2.144040	0.384243
C	-0.846738	-2.543611	0.811026
C	-1.733986	-1.356080	1.029402
N	-1.452528	-0.228636	0.285003
C	-2.408889	0.814394	0.357231
C	-1.893266	2.153746	-0.011870
C	-0.705902	2.320017	-0.568984
O	-2.656075	-1.376654	1.822428
O	2.680868	-1.771956	-1.736397
H	2.867069	1.255645	2.940292
H	4.890488	0.912461	1.448627
H	4.485318	-0.160779	-0.759525
H	1.982841	2.190928	-0.557212
H	0.629610	1.501586	1.866882
H	0.183832	-2.027045	-1.717233
H	-1.154404	-0.244579	-1.758611
H	0.438802	1.304280	-1.996736
H	1.165802	-3.026588	0.230210
H	1.014483	-1.543199	1.168351
H	-0.840279	-3.120535	1.734324
H	-1.319908	-3.162062	0.041053
H	-2.872329	0.806888	1.336169
H	-2.540007	2.990916	0.216200
H	-0.336735	3.317532	-0.780126
Cl	-3.867548	0.451907	-0.767205

10

C	3.985624	-1.682300	-0.428108
C	4.485129	-0.543943	0.324597

C	3.694954	0.513043	0.511481
N	2.391699	0.562189	0.024629
C	1.758583	-0.585430	-0.656919
C	2.736605	-1.699799	-0.885836
C	1.602439	1.644595	0.328628
C	0.191366	1.502729	-0.181582
C	-0.445823	0.208728	0.339488
C	0.523860	-0.992446	0.188672
C	-0.712238	2.673797	0.125399
C	-1.995853	2.483996	-0.665384
C	-2.552195	1.080014	-0.706730
N	-1.738529	0.021173	-0.340093
C	-2.361064	-1.245989	-0.274902
C	-1.431850	-2.388472	-0.423317
C	-0.127143	-2.258006	-0.255520
O	-3.687742	0.886268	-1.096968
O	2.008661	2.615475	0.937638
H	4.651294	-2.511434	-0.633779
H	5.490948	-0.538917	0.718475
H	3.995853	1.399279	1.049539
H	1.399774	-0.258489	-1.639165
H	2.378649	-2.527567	-1.483286
H	0.273425	1.407435	-1.271516
H	-0.648700	0.338807	1.406018
H	0.927959	-1.193410	1.186062
H	-0.915667	2.712127	1.197599
H	-0.238378	3.614887	-0.149764
H	-1.831616	2.757730	-1.712262
H	-2.800250	3.122037	-0.301126
H	-3.176835	-1.277332	-0.985879
H	-1.881751	-3.342252	-0.666496
H	0.511681	-3.124295	-0.375629
Cl	-3.258253	-1.467010	1.359076

11

C	0.237787	4.103224	-0.394699
C	1.687977	4.156135	-0.313066
C	2.399864	3.037553	-0.466354
N	1.804567	1.803378	-0.699750
C	0.337947	1.634775	-0.669749
C	-0.387456	2.941213	-0.562230
C	2.585544	0.668449	-0.729341
C	1.802730	-0.621869	-0.848866
C	0.618322	-0.718386	0.150590

C	0.014561	0.654064	0.462143
C	2.697691	-1.858592	-0.780381
C	1.943165	-3.053093	-0.193673
C	1.567020	-2.748346	1.218913
N	1.010574	-1.446467	1.376777
C	0.840563	-0.953164	2.602342
C	0.363512	0.311547	2.858123
C	0.073283	1.130817	1.780673
O	1.735386	-3.464415	2.170891
O	3.799445	0.715490	-0.673053
H	-0.328696	5.023953	-0.330043
H	2.196487	5.093309	-0.139747
H	3.477861	3.004951	-0.418143
H	0.028123	1.156316	-1.603927
H	-1.465921	2.880346	-0.641949
H	1.313564	-0.605262	-1.828369
H	-0.133273	-1.330832	-0.351432
H	-1.259592	0.462876	0.366292
H	3.055436	-2.112072	-1.776696
H	3.575768	-1.646626	-0.169260
H	2.548814	-3.956168	-0.191955
H	1.036674	-3.243993	-0.779595
H	1.141553	-1.619130	3.401159
H	0.290002	0.655479	3.877896
H	-0.174755	2.173951	1.953451
C	-5.351113	-0.208741	0.062401
C	-4.516300	-0.787218	-0.880302
C	-3.152429	-0.576855	-0.784785
C	-3.431435	0.727773	1.104121
C	-4.801855	0.563752	1.075526
H	-6.422048	-0.358515	0.010046
H	-4.909013	-1.396887	-1.682377
H	-2.446595	-1.010802	-1.490538
H	-2.938228	1.320260	1.867899
H	-5.420817	1.030587	1.829099
N	-2.641235	0.167592	0.193868
Cl	-0.696331	-2.212946	-2.831124

12

C	-2.340245	2.746351	0.974425
C	-2.354254	3.128932	-0.427939
C	-1.355009	2.746004	-1.222430
N	-0.288820	1.974785	-0.763270
C	-0.141646	1.610143	0.662680

C	-1.326719	2.046049	1.474118
C	0.702195	1.618031	-1.648523
C	1.740952	0.694696	-1.044185
C	0.941504	-0.448727	-0.388729
C	0.145156	0.099147	0.797834
C	2.772127	0.179180	-2.049340
C	2.619263	-1.320402	-2.313389
C	2.659457	-2.096753	-1.032212
N	1.836719	-1.558074	-0.024627
C	1.851486	-2.100868	1.209888
C	1.156436	-1.587239	2.258188
C	0.443199	-0.396651	2.066046
O	3.328820	-3.081695	-0.835796
O	0.695799	1.966091	-2.813442
H	-3.160482	3.048694	1.613400
H	-3.162865	3.720415	-0.832057
H	-1.300370	2.988760	-2.272668
H	0.749882	2.111016	1.061238
H	-1.300674	1.785748	2.524097
H	2.246023	1.231937	-0.235031
H	0.241480	-0.847896	-1.130518
H	-1.024553	-0.463965	0.643985
H	2.670446	0.720812	-2.988007
H	3.774389	0.367976	-1.665991
H	3.410184	-1.696445	-2.957924
H	1.662748	-1.522486	-2.806082
H	2.499742	-2.960686	1.312230
H	1.250121	-2.034679	3.235077
H	0.032133	0.103238	2.933794
C	-4.616293	-2.264282	-0.363869
C	-4.192267	-1.151898	-1.074970
C	-2.984989	-0.572162	-0.737623
C	-2.630001	-2.123614	0.936776
C	-3.824206	-2.760321	0.660186
H	-5.557862	-2.740757	-0.605235
H	-4.784989	-0.736065	-1.877775
H	-2.603823	0.302561	-1.250107
H	-1.966655	-2.458503	1.725646
H	-4.122951	-3.624756	1.236571
N	-2.233258	-1.059124	0.245970
Cl	2.791281	1.638418	2.523597

13		.com	
C	3.245896	1.162020	1.416122

C	4.002511	0.299044	0.522034
C	3.345878	-0.470762	-0.354889
N	1.955542	-0.341393	-0.477247
C	1.465081	1.017483	-0.232777
C	1.984460	1.471837	1.112970
C	1.201169	-1.441175	-0.763603
C	-0.295485	-1.346014	-0.575665
C	-0.885101	0.028107	-0.858560
C	-0.012130	1.186347	-0.442601
C	-0.646216	-1.815884	0.836925
C	-2.154355	-1.944267	0.932187
C	-2.885563	-0.689230	0.538058
N	-2.213669	0.207357	-0.254430
C	-2.796639	1.455794	-0.505714
C	-2.009516	2.529373	-0.634643
C	-0.582300	2.394204	-0.413026
O	-4.021193	-0.462403	0.918480
O	1.714267	-2.504294	-1.066836
H	3.704088	1.497633	2.338372
H	5.073707	0.198068	0.626747
H	3.807573	-1.248945	-0.944126
H	1.966467	1.638719	-0.990449
H	1.345555	2.061087	1.757810
H	-0.721515	-2.063201	-1.278250
H	-1.031824	0.109228	-1.944615
H	-0.172947	-2.776642	1.037392
H	-0.273624	-1.098633	1.573702
H	-2.479041	-2.191829	1.942153
H	-2.504464	-2.746822	0.275759
H	-3.875667	1.488378	-0.516594
H	-2.445507	3.500363	-0.822808
H	0.003360	3.283156	-0.207416

14

C	3.897890	1.166846	-0.302606
C	4.149551	-0.123847	0.318559
C	3.158823	-1.009378	0.421002
N	1.871051	-0.744959	-0.038341
C	1.523341	0.533750	-0.707613
C	2.692388	1.472685	-0.771374
C	0.896244	-1.704088	0.106538
C	-0.481671	-1.238682	-0.312613
C	-0.731850	0.098022	0.377582
C	0.289152	1.121069	-0.060971

C	-1.592995	-2.209430	0.018876
C	-2.899588	-1.641712	-0.514035
C	-3.161663	-0.188934	-0.191889
N	-2.087709	0.601171	0.149994
C	-2.309965	1.921362	0.551291
C	-1.299706	2.795305	0.611964
C	0.018438	2.410479	0.131195
O	-4.284210	0.277686	-0.262938
O	1.118447	-2.807928	0.564539
H	4.710573	1.877310	-0.389742
H	5.129928	-0.371262	0.698821
H	3.271745	-1.983527	0.872294
H	1.243470	0.290312	-1.742723
H	2.506295	2.419136	-1.261397
H	-0.463057	-1.071476	-1.396878
H	-0.618444	-0.059342	1.461686
H	-1.400733	-3.186142	-0.422937
H	-1.647650	-2.347383	1.101284
H	-3.761104	-2.200493	-0.150066
H	-2.920400	-1.711810	-1.606345
H	-3.336701	2.173128	0.769923
H	-1.490275	3.809982	0.931493
H	0.728735	3.189337	-0.115226

15

C	1.404367	0.000028	0.000000
C	0.711314	1.202450	-0.000003
C	-0.662196	1.177712	-0.000002
C	-0.662147	-1.177737	0.000002
C	0.711370	-1.202419	0.000002
H	2.486537	0.000057	-0.000001
H	1.226688	2.151364	-0.000005
H	-1.282237	2.061832	-0.000004
H	-1.282142	-2.061889	0.000004
H	1.226776	-2.151315	0.000004
N	-1.297291	-0.000030	0.000001
H	-2.310834	-0.000050	0.000001

16

C	-2.622139	0.000083	0.000080
C	-1.927526	1.201096	0.000008
C	-0.551697	1.170062	-0.000017
C	-0.551845	-1.170138	-0.000019
C	-1.927674	-1.201022	0.000012

H	-3.704419	0.000163	-0.000033
H	-2.442262	2.150711	-0.000021
H	0.069207	2.054928	0.000012
H	0.068971	-2.055060	0.000004
H	-2.442525	-2.150573	-0.000020
N	0.088106	-0.000065	-0.000074
H	1.155017	-0.000189	-0.000300
Cl	3.068504	-0.000001	0.000029

17

C	1.524973	0.672122	-0.548227
C	1.376658	1.567821	0.461239
C	0.293776	2.598766	0.361342
H	0.556647	3.468347	0.965870
H	0.185253	2.950529	-0.668083
C	-1.127189	2.177768	0.849798
C	-1.743979	1.143180	-0.025880
O	-2.513813	1.358740	-0.909364
N	-1.342838	-0.277776	0.181864
C	-0.607787	-0.664227	1.241045
C	-0.214788	-1.975703	1.374361
C	-0.579096	-2.892808	0.406870
C	-1.345105	-2.476953	-0.676676
C	-1.709201	-1.163184	-0.769155
H	-2.282711	-0.760379	-1.588762
H	-1.645526	-3.163504	-1.454123
H	-0.272256	-3.926860	0.492171
H	0.374982	-2.259314	2.233279
H	-0.360685	0.078922	1.976657
H	-1.091626	1.862790	1.891136
H	-1.791136	3.038683	0.783846
H	2.028817	1.545243	1.319297
O	0.936019	0.447174	-1.587458
Cl	3.006523	-0.544590	-0.194004

18

C	-1.349532	-0.985439	-0.605617
C	-0.647112	-1.571458	0.434124
C	0.310441	0.507842	1.155634
C	-0.641851	1.531469	1.285877
C	0.624901	-2.305987	0.130060
C	1.947667	-1.699350	0.690218
C	2.274523	-0.402402	0.038070
N	1.287556	0.637450	0.212669

C	1.283617	1.682686	-0.673932
C	0.344226	2.650356	-0.598303
C	-0.641701	2.576256	0.411960
O	3.217187	-0.193737	-0.675302
O	-1.063991	-0.719346	-1.745583
H	-1.170997	-1.789458	1.351968
H	0.509158	-0.150440	1.979346
H	-1.363052	1.457744	2.085924
H	0.570681	-3.313667	0.546230
H	0.743698	-2.414039	-0.949431
H	2.773898	-2.372669	0.473242
H	1.882286	-1.590591	1.774036
H	2.067873	1.657372	-1.414107
H	0.359517	3.464149	-1.307967
H	-1.379055	3.363050	0.503264
Cl	-3.074325	-0.433693	-0.045451

19

C	2.081258	-0.726876	-0.005772
C	0.948504	-0.760497	0.786676
C	-0.378466	0.476404	-0.796527
C	0.007691	1.825594	-0.823910
C	0.131441	-2.021063	0.824277
C	-0.920008	-2.223962	-0.309268
C	-2.017918	-1.228441	-0.203862
N	-1.586900	0.153221	-0.257484
C	-2.335148	1.083440	0.409668
C	-1.935626	2.374813	0.474856
C	-0.746370	2.760776	-0.180404
O	-3.170752	-1.463012	0.029468
O	2.473412	-1.427378	-0.905307
H	0.852139	-0.044839	1.587601
H	0.050594	-0.225331	-1.490335
H	0.914020	2.086084	-1.349142
H	0.784102	-2.894633	0.765358
H	-0.392590	-2.082951	1.779561
H	-1.376041	-3.206993	-0.215483
H	-0.427364	-2.175750	-1.281296
H	-3.240262	0.708184	0.861535
H	-2.541033	3.092515	1.008495
H	-0.444926	3.800005	-0.181418
Cl	3.146837	0.801950	0.368813

20

C	-2.067551	-0.824881	0.121624
C	-0.862228	-1.119170	-0.475966
C	0.400263	0.345183	0.893386
C	-0.215854	1.590109	1.094253
C	-0.051268	-2.286253	0.016728
C	1.439623	-2.189664	-0.315909
C	2.251049	-0.953336	-0.036332
N	1.549949	0.304780	0.166783
C	2.012986	1.399474	-0.503081
C	1.374489	2.590381	-0.404391
C	0.244526	2.690805	0.433863
O	3.444150	-0.921522	-0.096522
O	-2.608656	-1.187993	1.137068
H	-0.641943	-0.697100	-1.445447
H	0.232286	-0.467979	1.580543
H	-1.066252	1.637765	1.758119
H	-0.185489	-2.406849	1.095090
H	-0.394640	-3.227367	-0.424958
H	1.986956	-3.018970	0.132401
H	1.567235	-2.300925	-1.400445
H	2.900723	1.241905	-1.096593
H	1.752241	3.444538	-0.946289
H	-0.245111	3.647103	0.563974
Cl	-2.976225	0.554979	-0.838429

21

C	3.429695	-1.032600	0.374830
O	3.271354	-2.123448	0.744326
C	3.604092	0.187344	-0.052530
C	2.600179	1.306749	0.098455
C	1.205195	0.864498	0.511055
C	0.467220	0.168492	-0.585557
O	0.790421	0.089619	-1.725257
N	-0.807804	-0.500997	-0.196529
C	-1.420558	-0.224377	0.968618
C	-2.602198	-0.845006	1.293223
C	-3.161959	-1.744032	0.402382
C	-2.521269	-2.004176	-0.802395
C	-1.343845	-1.364905	-1.081169
H	-0.788560	-1.510491	-1.994331
H	-2.929205	-2.697341	-1.523132
H	-4.093616	-2.239864	0.641308
H	-3.077656	-0.605997	2.232879
H	-0.958617	0.501104	1.614620

H	1.227308	0.231735	1.402102
H	0.593414	1.742179	0.755138
H	2.956998	2.014369	0.849443
H	2.542010	1.853952	-0.843315
H	4.560271	0.378632	-0.525490
Cl	-1.671249	2.837494	-0.008679

22

C	-0.209404	-1.381284	1.723882
C	-0.879176	-0.438611	1.036751
C	0.091812	-0.306925	-0.642725
C	0.605525	-1.576906	-1.091817
C	-0.957098	0.984337	1.576920
C	-0.810005	2.028171	0.453134
C	0.581285	2.004585	-0.097981
N	1.028899	0.704349	-0.463399
C	2.380571	0.427870	-0.403915
C	2.848852	-0.800479	-0.679549
C	1.930636	-1.821603	-1.080567
O	1.334909	2.939331	-0.142887
O	0.435065	-2.209520	2.161695
H	-1.817063	-0.824170	0.599356
H	-0.845103	0.002668	-1.099304
H	-0.116545	-2.313942	-1.414997
H	-1.929337	1.120260	2.046863
H	-0.191608	1.150507	2.334591
H	-0.989093	3.024289	0.850068
H	-1.547690	1.833919	-0.329947
H	3.002854	1.266916	-0.132373
H	3.909849	-0.994089	-0.627139
H	2.310177	-2.781358	-1.406677
Cl	-3.332147	-0.409933	-1.087759

23

C	0.744234	-0.731256	-1.648078
C	0.888986	0.116748	-0.561922
C	-0.081457	-0.291140	0.622289
C	-0.151570	-1.765311	0.857712
C	0.768852	1.621000	-0.927407
C	-0.091177	2.342794	0.115840
C	-1.443948	1.694271	0.237139
N	-1.385768	0.321004	0.418690
C	-2.528884	-0.449242	0.222153
C	-2.514321	-1.778550	0.332866

C	-1.282330	-2.451167	0.702641
O	-2.495330	2.285767	0.122532
O	0.658790	-1.452860	-2.503643
H	1.958470	-0.090569	-0.156671
H	0.413440	0.178025	1.474662
H	0.775075	-2.236558	1.159248
H	1.770128	2.045232	-0.947126
H	0.323786	1.747642	-1.913131
H	-0.236903	3.378396	-0.180850
H	0.411326	2.338454	1.086238
H	-3.408413	0.124397	-0.028310
H	-3.421145	-2.340570	0.165529
H	-1.295951	-3.519591	0.877049
Cl	3.603093	-0.022589	0.874237

24

C	0.698443	0.931322	1.384832
C	0.864082	-0.185122	0.482605
C	-0.063852	0.225710	-0.659648
C	-0.026111	1.723888	-0.538844
C	0.617272	-1.575265	1.093476
C	-0.248204	-2.368003	0.111539
C	-1.553782	-1.661121	-0.144125
N	-1.412920	-0.306313	-0.419876
C	-2.528220	0.501507	-0.514004
C	-2.444325	1.840501	-0.549269
C	-1.150166	2.461777	-0.483146
O	-2.639489	-2.191710	-0.072436
O	0.740531	1.572934	2.311001
H	1.931723	-0.076896	0.106296
H	0.326957	-0.140590	-1.611118
H	0.951200	2.182825	-0.648739
H	1.572422	-2.072196	1.247213
H	0.112838	-1.502484	2.056555
H	-0.470609	-3.356644	0.505073
H	0.284047	-2.492014	-0.836375
H	-3.467316	-0.032606	-0.506804
H	-3.343177	2.436359	-0.590790
H	-1.080796	3.537810	-0.381667
Cl	3.722000	-0.162372	-0.906443

25

C	2.129317	-1.089080	0.022144
C	1.924846	0.226309	0.763776

C	0.442847	-0.197033	0.946111
C	0.795639	-1.645535	0.543480
C	2.177341	1.549615	0.055260
C	0.940588	2.433784	0.205008
C	-0.289169	1.764668	-0.354091
N	-0.405661	0.424792	-0.058814
C	-1.510081	-0.298726	-0.565025
C	-1.220403	-1.733394	-0.841899
C	-0.143113	-2.343408	-0.369704
O	-1.106653	2.344183	-1.042178
O	2.943698	-1.481887	-0.757396
H	2.431720	0.168938	1.729136
H	0.024309	-0.068889	1.943163
H	1.002296	-2.245234	1.433786
H	3.049868	2.054447	0.466487
H	2.373540	1.377082	-1.005083
H	1.057210	3.384264	-0.311418
H	0.760471	2.648018	1.263351
H	-1.892412	0.213765	-1.440554
H	-1.936292	-2.247582	-1.469896
H	0.065555	-3.374151	-0.628874
Cl	-2.957640	-0.222692	0.611637

26

C	0.167617	0.622901	0.074598
C	-0.564210	1.686746	0.377092
C	-2.962518	-0.388146	0.840838
C	-2.839966	-1.519425	1.611049
C	-1.323759	2.459308	-0.653236
C	-2.822020	2.094261	-0.752868
C	-3.016211	0.745063	-1.370030
N	-2.857487	-0.461258	-0.496847
C	-2.653269	-1.638709	-1.115508
C	-2.533811	-2.795801	-0.391962
C	-2.630408	-2.739303	0.991944
O	-3.175618	0.541377	-2.529645
O	0.240472	0.030387	-1.107880
H	-0.626953	1.997686	1.411421
H	-3.154816	0.577457	1.271717
H	-2.932003	-1.434254	2.683576
H	-1.278273	3.519130	-0.401360
H	-0.860626	2.336946	-1.633037
H	-3.311704	2.788809	-1.432704
H	-3.316469	2.180296	0.210475

H	-2.592543	-1.600751	-2.191856
H	-2.370590	-3.728248	-0.911846
H	-2.543726	-3.642508	1.581521
Cl	3.049711	3.549372	0.720273
H	1.217259	-0.240546	-1.318082
C	0.794295	-1.386279	1.252011
C	1.477170	-2.056282	2.231357
C	2.313450	-1.342511	3.082013
C	2.449173	0.023473	2.914654
C	1.746376	0.657952	1.914593
N	0.927128	-0.051126	1.120838
H	2.862895	-1.855212	3.860413
H	0.132089	-1.870321	0.550010
H	1.352216	-3.125043	2.326095
H	3.110959	0.609443	3.535824
H	1.866957	1.713976	1.677877
Cl	-5.899091	0.602838	0.085231
C	3.161715	-1.760615	-1.962456
C	4.503002	-2.077993	-2.064980
C	5.439179	-1.138442	-1.659976
C	4.999652	0.080477	-1.170512
C	3.638195	0.317839	-1.103784
N	2.738805	-0.587750	-1.491654
H	6.497979	-1.355350	-1.725845
H	2.393836	-2.462682	-2.266086
H	4.803819	-3.041051	-2.454398
H	5.692904	0.843104	-0.842728
H	3.256391	1.261285	-0.719760

27

C	-1.859240	2.417850	0.492574
C	-0.779964	3.174522	0.652239
C	0.464757	0.486030	-0.814784
C	0.167585	-0.197703	-1.970496
C	0.155453	3.000353	1.812601
C	1.272165	1.952416	1.590613
C	0.747041	0.555534	1.655174
N	0.435949	-0.147523	0.371416
C	0.151778	-1.464110	0.452498
C	-0.123916	-2.188511	-0.674150
C	-0.128640	-1.546764	-1.906918
O	0.524949	-0.047184	2.656434
O	-2.271686	1.491179	1.340179
H	-0.553093	3.924051	-0.091651

H	0.770720	1.523836	-0.848630
H	0.197293	0.338214	-2.907746
H	0.660019	3.947590	2.001633
H	-0.393664	2.739155	2.718757
H	1.975528	2.015652	2.420437
H	1.817082	2.160974	0.670168
H	0.164079	-1.887552	1.444356
H	-0.339386	-3.242806	-0.583602
H	-0.352652	-2.101182	-2.808765
Cl	-2.893123	2.646461	-0.920406
H	-2.675892	0.678988	0.881759
C	-3.136918	-1.772459	1.201979
C	-3.410502	-3.083022	0.854408
C	-3.718513	-3.366736	-0.466661
C	-3.743653	-2.330690	-1.386215
C	-3.459011	-1.049024	-0.948808
N	-3.159310	-0.774312	0.318801
H	-3.937129	-4.381430	-0.774703
H	-2.886005	-1.505438	2.222345
H	-3.381989	-3.859903	1.606363
H	-3.981324	-2.506181	-2.426632
H	-3.466177	-0.210133	-1.634670
Cl	2.459744	3.019986	-1.791850
C	3.659557	-0.335074	-0.376381
C	4.079398	-1.349131	-1.223890
C	4.253755	-2.620916	-0.702835
C	4.004312	-2.827686	0.644875
C	3.584476	-1.752134	1.411154
N	3.408880	-0.527588	0.918395
H	4.579819	-3.437404	-1.335409
H	3.500353	0.671643	-0.757263
H	4.262655	-1.137769	-2.269217
H	4.130271	-3.802372	1.097798
H	3.372675	-1.880014	2.467977

28

C	5.604905	-1.261563	-0.255488
O	6.186759	-2.201250	-0.607473
C	4.963611	-0.195110	0.139634
C	3.789715	0.388975	-0.608227
H	3.785504	0.047616	-1.643372
C	2.443808	0.079596	0.037992
C	2.035538	-1.339720	-0.161871
O	2.646751	-2.193368	-0.717346

N	0.701592	-1.720829	0.390618
C	0.103616	-2.797067	-0.151099
C	-1.116657	-3.217856	0.309324
C	-1.727310	-2.519881	1.340768
C	-1.096951	-1.410045	1.879066
C	0.121612	-1.020749	1.381164
H	0.647308	-0.161587	1.782339
H	-1.539497	-0.837027	2.680594
H	-2.692686	-2.834050	1.715151
H	-1.584283	-4.077621	-0.147066
H	0.638094	-3.281797	-0.952821
Cl	0.085672	-0.163617	-2.555358
H	1.648768	0.679404	-0.414005
H	2.466989	0.319752	1.104559
H	3.902368	1.473368	-0.633800
H	5.294584	0.237539	1.076351
Cl	1.272091	1.810659	3.133342
H	0.425961	2.521796	1.489201
N	-0.004001	2.879362	0.596469
C	-1.296357	2.641927	0.364939
C	-1.878907	3.100668	-0.794053
C	-1.099084	3.796392	-1.704871
C	0.243930	4.022164	-1.436764
C	0.772732	3.547825	-0.259973
H	1.805015	3.678826	0.031929
H	0.876403	4.555324	-2.131261
H	-1.534951	4.157684	-2.626944
H	-2.924089	2.898932	-0.977146
H	-1.834430	2.076564	1.112829
C	-4.716529	-0.267095	0.940064
N	-3.668906	0.310821	0.353852
C	-3.205506	-0.240180	-0.767210
C	-3.763785	-1.370346	-1.345032
C	-4.852921	-1.962646	-0.728413
C	-5.338900	-1.401060	0.442519
H	-6.186740	-1.828088	0.962070
H	-5.314802	-2.847038	-1.149885
H	-3.339176	-1.772766	-2.255393
H	-2.334320	0.221170	-1.223954
H	-5.076232	0.198394	1.852077

1.9 *NOTES AND REFERENCES*

(1) Kerkovius, J. K.; Stegner, A.; Turlik, A.; Lam, P. H.; Houk, K. N.; Reisman, S. E. A Pyridine Dearomatization Approach to the Matrine-Type Lupin Alkaloids. *J. Am. Chem. Soc.* **2022**, *144* (35), 15938–15943.
(2) Cely-Veloza, W.; Kato, M. J.; Coy-Barrera, E. Quinolizidine-Type Alkaloids: Chemodiversity, Occurrence, and Bioactivity. *ACS Omega* **2023**, *8* (31), 27862–27893.
(3) Ohmiya, S.; Saito, K.; Murakoshi, I. Chapter 1 Lupine Alkaloids. In *The Alkaloids: Chemistry and Pharmacology*; Cordell, G. A., Ed.; Academic Press, 1995; Vol. 47, pp 1–114.
(4) Li, J.; Wei, S.; Marabada, D.; Wang, Z.; Huang, Q. Research Progress of Natural Matrine Compounds and Synthetic Matrine Derivatives. *Molecules* **2023**, *28* (15), 5780.
(5) Chuzel, O.; Riant, O. Sparteine as a Chiral Ligand for Asymmetric Catalysis. In *Chiral Diazaligands for Asymmetric Synthesis*; Lemaire, M., Mangeney, P., Eds.; Topics in Organometallic Chemistry; Springer: Berlin, Heidelberg, 2005; pp 59–92.
(6) Boschin, G.; Resta, D. Alkaloids Derived from Lysine: Quinolizidine (a Focus on Lupin Alkaloids). In *Natural Products*; Ramawat, K. G., Mérillon, J.-M., Eds.; Springer Berlin Heidelberg: Berlin, Heidelberg, 2013; pp 381–403.
(7) Senges, J.; Ehe, L. Antiarrhythmic Action of Sparteine on Direct and Indirect Models of Cardiac Fibrillation. *Naunyn. Schmiedebergs Arch. Pharmacol.* **1973**, *280* (3), 265–274.
(8) Wu, S.; Lee, S.; Beak, P. Asymmetric Deprotonation by BuLi/(−)-Sparteine: Convenient and Highly Enantioselective Syntheses of (S)-2-Aryl-Boc-Pyrrolidines. *J. Am. Chem. Soc.* **1996**, *118* (4), 715–721.
(9) Dhurandhar, Y.; Tomar, S.; Das, A.; Singh, A. P.; Prajapati, J. L.; Bodakhe, S. H.; Namdeo, K. P. Unlocking the Potential of Oxymatrine: A Comprehensive Review of Its Neuroprotective Mechanisms and Therapeutic Prospects in Neurological Disorders. *ACS Chem. Neurosci.* **2024**, *15* (23), 4245–4257.
(10) Zhang, H.; Chen, L.; Sun, X.; Yang, Q.; Wan, L.; Guo, C. Matrine: A Promising Natural Product With Various Pharmacological Activities. *Front. Pharmacol.* **2020**, *11*, 588.
(11) Cui, L.; Cai, Y.; Cheng, W.; Liu, G.; Zhao, J.; Cao, H.; Tao, H.; Wang, Y.; Yin, M.; Liu, T.; Liu, Y.; Huang, P.; Liu, Z.; Li, K.; Zhao, B. A Novel, Multi-Target Natural Drug Candidate, Matrine, Improves Cognitive Deficits in Alzheimer's Disease Transgenic Mice by Inhibiting A Beta Aggregation and Blocking the RAGE/A Beta Axis. *Mol. Neurobiol.* **2017**, *54* (3), 1939–1952.
(12) Wang. *Efficacy of compound Kushen injection plus radiotherapy on nonsmall-cell lungcancer: A systematic review and meta-analysis*.
(13) Ao, M.; Xiao, X.; Li, Q. Efficacy and Safety of Compound Kushen Injection Combined with Chemotherapy on Postoperative Patients with Breast Cancer. *Medicine (Baltimore)* **2019**, *98* (3).

(14) Boiteau, L.; Boivin, J.; Liard, A.; Quiclet-Sire, B.; Zard, S. Z. A Short Synthesis of (±)-Matrine. *Angew. Chem. Int. Ed.* **1998**, *37* (8), 1128–1131.
(15) Mandell, L.; Singh, K. P.; Gresham, J. T.; Freeman, W. J. The Total Syntheses of d,l-Matrine and d,l-Leontine [1]. *J. Am. Chem. Soc.* **1965**, *87* (22), 5234–5236.
(16) Tsuda, K.; Saeki, S.; Imura, S.-I.; Okuda, S.; Sato, Y.; Mishima, H. Studies on the Synthesis of Matrine. I. The Total Synthesis of Nordehydro-a-Matrinidine and Dehydro-a-Matrinidine. **1956**, *21*, 6.
(17) Tsuda, K.; Mishima, H. Studies on the Synthesis of Matrine. II. The Synthesis of Octadehydromatrine and Allomatridine [1]. *J. Org. Chem.* **1958**, *23* (8), 1179–1183.
(18) Chen, J.; Browne, L. J.; Gonnela, N. C. Total Synthesis of (±)-Matrine. *J Chem Soc Chem Commun* **1986**, No. 12, 905–907.
(19) Magann, N. L.; Westley, E.; Sowden, M. J.; Gardiner, M. G.; Sherburn, M. S. Total Synthesis of Matrine Alkaloids. *J. Am. Chem. Soc.* **2022**, *144* (43), 19695–19699.
(20) Li, J.-C.; Zhang, Z.-J.; Liu, D.; Jiang, M.-Y.; Li, R.-T.; Li, H.-M. Quinolizidine Alkaloids from the Roots of *Sophora Flavescens*. *Nat. Prod. Res.* **2022**, *36* (7), 1781–1788.
(21) Wang, Q.; Li, Y.; Li, K.-W.; Zhou, C.-Z. Sophoridine: A Review of Its Pharmacology, Pharmacokinetics and Toxicity. *Phytomedicine* **2022**, *95*, 153756.
(22) Mancinotti, D.; Frick, K. M.; Geu-Flores, F. Biosynthesis of Quinolizidine Alkaloids in Lupins: Mechanistic Considerations and Prospects for Pathway Elucidation. *Nat. Prod. Rep.* **2022**, 10.1039.D1NP00069A.
(23) Bunsupa, S.; Katayama, K.; Ikeura, E.; Oikawa, A.; Toyooka, K.; Saito, K.; Yamazaki, M. Lysine Decarboxylase Catalyzes the First Step of Quinolizidine Alkaloid Biosynthesis and Coevolved with Alkaloid Production in Leguminosae. *Plant Cell* **2012**, *24* (3), 1202–1216.
(24) Yang, T.; Nagy, I.; Mancinotti, D.; Otterbach, S. L.; Andersen, T. B.; Motawia, M. S.; Asp, T.; Geu-Flores, F. Transcript Profiling of a Bitter Variety of Narrow-Leafed Lupin to Discover Alkaloid Biosynthetic Genes. *J. Exp. Bot.* **2017**, *68* (20), 5527–5537.
(25) Golebiewski, W. M.; Spenser, I. D. Biosynthesis of the Lupine Alkaloids. I. Lupinine. *Can. J. Chem.* **1985**, *63* (10), 2707–2718.
(26) Leeper, F. J.; Grue-Sørensen, G.; Spenser, I. D. Biosynthesis of the Quinolizidine Alkaloids. Incorporation of Δ^{1}-Piperideine into Matrine. *Can. J. Chem.* **1981**, *59* (1), 106–115.
(27) Abdusalamov, B. A. Biosynthesis and Metabolism of Some Matrine Alkaloids inGoebelia Pachycarpa. *Chem. Nat. Compd.* **1984**, *20* (1), 1–9.
(28) Zhang, J.; Liu, Y.-Q.; Fang, J. The Biological Activities of Quinolizidine Alkaloids. In *The Alkaloids: Chemistry and Biology*; Elsevier, 2023; Vol. 89, pp 1–37.
(29) Zhang, S.; Li, W.; Nie, H.; Liao, M.; Qiu, B.; Yang, Y.; Chen, Y. Five New Alkaloids from the Roots of *Sophora Flavescens*. *Chem. Biodivers.* **2018**, *15* (3), e1700577.
(30) Villalpando-Vargas, F.; Medina-Ceja, L. Sparteine as an Anticonvulsant Drug: Evidence and Possible Mechanism of Action. *Seizure* **2016**, *39*, 49–55.
(31) De La Vega, R.; Gutierrez, M. P.; Sanz, C.; Calvo, R.; Robredo, L. M.; De La Cuadra, C.; Muzquiz, M. Bactericide-like Effect of Lupinus Alkaloids. *Ind. Crops Prod.* **1996**, *5* (2), 141–148.

(32) Bermúdez-Torres, K.; Martínez Herrera, J.; Figueroa Brito, R.; Wink, M.; Legal, L. Activity of Quinolizidine Alkaloids from Three Mexican Lupinus against the Lepidopteran Crop Pest Spodoptera Frugiperda. *BioControl* **2009**, *54* (3), 459–466.
(33) Rouden, J.; Lasne, M.-C.; Blanchet, J.; Baudoux, J. (−)-Cytisine and Derivatives: Synthesis, Reactivity, and Applications. *Chem. Rev.* **2014**, *114* (1), 712–778.
(34) Fedorova, V. A.; Kadyrova, R. A.; Slita, A. V.; Muryleva, A. A.; Petrova, P. R.; Kovalskaya, A. V.; Lobov, A. N.; Zileeva, Z. R.; Tsypyshev, D. O.; Borisevich, S. S.; Tsypysheva, I. P.; Vakhitova, J. V.; Zarubaev, V. V. Antiviral Activity of Amides and Carboxamides of Quinolizidine Alkaloid (−)-Cytisine against Human Influenza Virus A (H1N1) and Parainfluenza Virus Type 3. *Nat. Prod. Res.* **2021**, *35* (22), 4256–4264.
(35) Yu, L.; Wang, X.; Chen, Z.-F.; Jiang, B.; Shang, D.-Y.; Sun, Y.-X.; Yang, J.-H.; Zhang, L.-F.; Ji, Y.-B. Cytisine Induces Apoptosis of HepG2 Cells. *Mol. Med. Rep.* **2017**, *16* (3), 3363–3370.
(36) Wang, R.; Deng, X.; Gao, Q.; Wu, X.; Han, L.; Gao, X.; Zhao, S.; Chen, W.; Zhou, R.; Li, Z.; Bai, C. *Sophora Alopecuroides* L.: An Ethnopharmacological, Phytochemical, and Pharmacological Review. *J. Ethnopharmacol.* **2020**, *248*, 112172.
(37) Wang, Q.; Du, H.; Geng, G.; Zhou, H.; Xu, M.; Cao, H.; Zhang, B.; Song, G.; Hu, T. Matrine Inhibits Proliferation and Induces Apoptosis via BID-Mediated Mitochondrial Pathway in Esophageal Cancer Cells. *Mol. Biol. Rep.* **2014**, *41* (5), 3009–3020.
(38) Rashid, H. ur; Xu, Y.; Muhammad, Y.; Wang, L.; Jiang, J. Research Advances on Anticancer Activities of Matrine and Its Derivatives: An Updated Overview. *Eur. J. Med. Chem.* **2019**, *161*, 205–238.
(39) Wei, Y. P.; Wang, X. H.; Liu, G.; Zhang, J. F.; Yang, Y. X.; Zhang, J.; Song, X. L.; Li, Z. D.; Zhao, L. D. Matrine Exerts Inhibitory Effects in Melanoma through the Regulation of miR-19b-3p/PTEN. *Int. J. Oncol.* **2018**, *53* (2), 791–800.
(40) Jiang, J.-H.; Pi, J.; Jin, H.; Yang, F.; Cai, J.-Y. Chinese Herb Medicine Matrine Induce Apoptosis in Human Esophageal Squamous Cancer KYSE-150 Cells through Increasing Reactive Oxygen Species and Inhibiting Mitochondrial Function. *Pathol. - Res. Pract.* **2018**, *214* (5), 691–699.
(41) Wu, X.; Zhou, J.; Cai, D.; Li, M. Matrine Inhibits the Metastatic Properties of Human Cervical Cancer Cells via Downregulating the P38 Signaling Pathway. *Oncol. Rep.* **2017**, *38* (2), 1312–1320.
(42) Zhang, Y.; Liu, M.; Sun, H.; Yin, K. Matrine Improves Cognitive Impairment and Modulates the Balance of Th17/Treg Cytokines in a Rat Model of A B1-42 - Induced Alzheimer's Disease. *Cent. Eur. J. Immunol.* **2015**, *4*, 411–419.
(43) Sun, D.; Wang, J.; Yang, N.; Ma, H. Matrine Suppresses Airway Inflammation by Downregulating SOCS3 Expression via Inhibition of NF-κB Signaling in Airway Epithelial Cells and Asthmatic Mice. *Biochem. Biophys. Res. Commun.* **2016**, *477* (1), 83–90.
(44) Guo, S.; Gao, C.; Xiao, W.; Zhang, J.; Qu, Y.; Li, J.; Ye, F. Matrine Protects Cardiomyocytes From Ischemia/Reperfusion Injury by Regulating HSP70 Expression Via Activation of the JAK2/STAT3 Pathway: *SHOCK* **2018**, *50* (6), 664–670.

(45) Yang, Y.; Dong, Q.; Li, R. Matrine Induces the Apoptosis of Fibroblast-like Synoviocytes Derived from Rats with Collagen-Induced Arthritis by Suppressing the Activation of the JAK/STAT Signaling Pathway. *Int. J. Mol. Med.* **2017**, *39* (2), 307–316.
(46) Niu, Y.; Dong, Q.; Li, R. Matrine Regulates Th1/Th2 Cytokine Responses in Rheumatoid Arthritis by Attenuating the NF-κB Signaling: Matrine Regulates Th1/Th2 Cytokine Responses. *Cell Biol. Int.* **2017**, *41* (6), 611–621.
(47) Chen, Y.; Qi, Z.; Qiao, B.; Lv, Z.; Hao, Y.; Li, H. Oxymatrine Can Attenuate Pathological Deficits of Alzheimer's Disease Mice through Regulation of Neuroinflammation. *J. Neuroimmunol.* **2019**, *334*, 576978.
(48) Jiao-Yan, Y.; Qing-Qing, L.; Xi, L.; Mei, Z.; Ting, S.; Na, H.; Wei, J.; Rui-Tao, Z.; Peng, Y.; Qi, Y. Oxymatrine Improves Blood-Brain Barrier Integrity after Cerebral Ischemia-Reperfusion Injury by Downregulating CAV1 and MMP9 Expression. *Phytomedicine* **2021**, *84*, 153505.
(49) Fan, H.; Li, L.; Zhang, X.; Liu, Y.; Yang, C.; Yang, Y.; Yin, J. Oxymatrine Downregulates TLR4, TLR2, MyD88, and NF- κ B and Protects Rat Brains against Focal Ischemia. *Mediators Inflamm.* **2009**, *2009*, 1–10.
(50) Zhu, L.; Huang, S.; Li, J.; Chen, J.; Yao, Y.; Li, L.; Guo, H.; Xiang, X.; Deng, J.; Xiong, J. Sophoridine Inhibits Lung Cancer Cell Growth and Enhances Cisplatin Sensitivity through Activation of the P53 and Hippo Signaling Pathways. *Gene* **2020**, *742*, 144556.
(51) Xu, Z.; Zhang, F.; Bai, C.; Yao, C.; Zhong, H.; Zou, C.; Chen, X. Sophoridine Induces Apoptosis and S Phase Arrest via ROS-Dependent JNK and ERK Activation in Human Pancreatic Cancer Cells. *J. Exp. Clin. Cancer Res.* **2017**, *36* (1), 124.
(52) Liang, L.; Wang, X.-Y.; Zhang, X.-H.; Ji, B.; Yan, H.-C.; Deng, H.-Z.; Wu, X.-R. Sophoridine Exerts an Anti-Colorectal Carcinoma Effect through Apoptosis Induction in Vitro and in Vivo. *Life Sci.* **2012**, *91* (25–26), 1295–1303.
(53) Zhuang, H.; Dai, X.; Zhang, X.; Mao, Z.; Huang, H. Sophoridine Suppresses Macrophage-Mediated Immunosuppression through TLR4/IRF3 Pathway and Subsequently Upregulates CD8+ T Cytotoxic Function against Gastric Cancer. *Biomed. Pharmacother.* **2020**, *121*, 109636.
(54) OKUDA, SHIGENOBU.; Yoshimoto, M.; TSUDA, KYOSUKE. *Chem. Pharm. Bull.* **1966**, *14* (3), 275–279.
(55) Ueno, A.; Morinaga, K.; Fukushima, S.; Iitaka, Y.; Koiso, Y.; Okuda, S. Studies on Lupin Alkaloids. VI. Isolation and Structure of (+)-Isomatrine. *Chem. Pharm. Bull. (Tokyo)* **1975**.
(56) *MilliporeSigma; Pyridine. Product No. P57506-4L (accessed June 16, 2022). Oakwood Chemical; Glutaryl chloride. Product No. 095828-100g (accessed June 16, 2022). Fischer Scientific; Dichloromethane. Product No. D37-20 (accessed June 16, 2022) Fischer Scientific; Methanol. Product No. A412SK-20 (accessed June 16, 2022)*.
(57) Paull, D. H.; Weatherwax, A.; Lectka, T. Catalytic, Asymmetric Reactions of Ketenes and Ketene Enolates. *Tetrahedron* **2009**, *65* (34), 6771–6803.

(58) Cabrero-Antonino, J. R.; Adam, R.; Papa, V.; Beller, M. Homogeneous and Heterogeneous Catalytic Reduction of Amides and Related Compounds Using Molecular Hydrogen. *Nat. Commun.* **2020**, *11* (1), 3893.
(59) Mitsudome, T.; Miyagawa, K.; Maeno, Z.; Mizugaki, T.; Jitsukawa, K.; Yamasaki, J.; Kitagawa, Y.; Kaneda, K. Mild Hydrogenation of Amides to Amines over a Platinum-Vanadium Bimetallic Catalyst. *Angew. Chem. Int. Ed.* **2017**, *56* (32), 9381–9385.
(60) Trowbridge, A.; Walton, S. M.; Gaunt, M. J. New Strategies for the Transition-Metal Catalyzed Synthesis of Aliphatic Amines. *Chem. Rev.* **2020**, *120* (5), 2613–2692.
(61) Cheng, C.; Brookhart, M. Iridium-Catalyzed Reduction of Secondary Amides to Secondary Amines and Imines by Diethylsilane. *J. Am. Chem. Soc.* **2012**, *134* (28), 11304–11307.
(62) Tahara, A.; Miyamoto, Y.; Aoto, R.; Shigeta, K.; Une, Y.; Sunada, Y.; Motoyama, Y.; Nagashima, H. Catalyst Design of Vaska-Type Iridium Complexes for Highly Efficient Synthesis of π-Conjugated Enamines. *Organometallics* **2015**, *34* (20), 4895–4907.
(63) Kuwano, R.; Takahashi, M.; Ito, Y. Reduction of Amides to Amines via Catalytic Hydrosilylation by a Rhodium Complex. *Tetrahedron Lett.* **1998**, *39* (9), 1017–1020.
(64) Zhou, S.; Junge, K.; Addis, D.; Das, S.; Beller, M. A Convenient and General Iron-Catalyzed Reduction of Amides to Amines. *Angew. Chem. Int. Ed.* **2009**, *48* (50), 9507–9510.
(65) Simmons, B. J.; Hoffmann, M.; Hwang, J.; Jackl, M. K.; Garg, N. K. Nickel-Catalyzed Reduction of Secondary and Tertiary Amides. *Org. Lett.* **2017**, *19* (7), 1910–1913.
(66) Larson, G. L.; Fry, J. L. Ionic and Organometallic-Catalyzed Organosilane Reductions. In *Organic Reactions*; American Cancer Society, 2008; pp 1–737.
(67) Nakatani, N.; Hasegawa, J.; Sunada, Y.; Nagashima, H. Platinum-Catalyzed Reduction of Amides with Hydrosilanes Bearing Dual Si–H Groups: A Theoretical Study of the Reaction Mechanism. *Dalton Trans.* **2015**, *44* (44), 19344–19356.
(68) Nagashima, H. Efficient Transition Metal-Catalyzed Reactions of Carboxylic Acid Derivatives with Hydrosilanes and Hydrosiloxanes, Afforded by Catalyst Design and the Proximity Effect of Two Si–H Groups. *Synlett* **2015**, *26* (07), 866–890.
(69) Juste-Navarro, V.; Prieto, L.; Delso, I.; Manzano, R.; Tejero, T.; Reyes, E.; Vicario, J. L.; Merino, P. A Case Study of Thiourea-Assisted Iminium Formation by Hydroxyl Anion Binding: Kinetic, Spectroscopic and Computational Evidences. *Adv. Synth. Catal.* **2017**, *359* (23), 4122–4128.
(70) Xiang, S.-H.; Xu, J.; Yuan, H.-Q.; Huang, P.-Q. Amide Activation by Tf2O: Reduction of Amides to Amines by NaBH4 under Mild Conditions. *Synlett* **2010**, *2010* (12), 1829–1832.
(71) Bissel, P.; Castagnoli, N. Studies on the Cytochrome P450 Catalyzed Oxidation of 13C Labeled 1-Cyclopropyl-4-Phenyl-1,2,3,6-Tetrahydropyridine by 13C NMR. *Bioorg. Med. Chem.* **2005**, *13* (8), 2975–2980.
(72) Guengerich, F. P. Common and Uncommon Cytochrome P450 Reactions Related to Metabolism and Chemical Toxicity. *Chem. Res. Toxicol.* **2001**, *14* (6), 611–650.

(73) Nguyen, K. T.; Virus, C.; Günnewich, N.; Hannemann, F.; Bernhardt, R. Changing the Regioselectivity of a P450 from C15 to C11 Hydroxylation of Progesterone. *ChemBioChem* **2012**, *13* (8), 1161–1166.
(74) Okazaki, Renji, T., Norihiro. *Tetrahedron Lett.* **1984**, *25* (41), 4677.
(75) Kessar, S. V.; Singh, P.; Singh, K. N.; Singh, S. K. Facile α-Deprotonation–Electrophilic Substitution of Quinuclidine and DABCO. *Chem. Commun.* **1999**, No. 19, 1927–1928.
(76) Clayden, J.; Yasin, S. A. Pathways for Decomposition of THF by Organolithiums: The Role of HMPA. *New J. Chem.* **2002**, *26* (2), 191–192.
(77) Collum, D. B. Is N,N,N',N'-Tetramethylethylenediamine a Good Ligand for Lithium? *Acc. Chem. Res.* **1992**, *25* (10), 448–454.
(78) Stanetty, P.; Mihovilovic, M. D. Half-Lives of Organolithium Reagents in Common Ethereal Solvents. *J. Org. Chem.* **1997**, *62* (5), 1514–1515.
(79) Gessner, V. H.; Däschlein, C.; Strohmann, C. Structure Formation Principles and Reactivity of Organolithium Compounds. *Chem. – Eur. J.* **2009**, *15* (14), 3320–3334.
(80) Stey, T.; Stalke, D. Lead Structures in Lithium Organic Chemistry. In *PATAI'S Chemistry of Functional Groups*; American Cancer Society, 2009.
(81) Nichols, M. A.; Williard, P. G. Solid-State Structures of n-Butyllithium-TMEDA, -THF, and -DME Complexes. *J. Am. Chem. Soc.* **1993**, *115* (4), 1568–1572.
(82) Reich, H. J. Role of Organolithium Aggregates and Mixed Aggregates in Organolithium Mechanisms. *Chem. Rev.* **2013**, *113* (9), 7130–7178.
(83) García-Valverde, M.; Pedrosa, R.; Vicente, M. A Novel and Efficient Oxidation of 1,2-Amino Alcohols to Dialkylamides. *Synlett* **2002**, *2002* (12), 2092–2094.
(84) Lam, P. H.; Kerkovius, J. K.; Reisman, S. E. A Pyridine Dearomatization Approach for the Gram Scale Synthesis of (±)-Sparteine. *Org. Lett.* **2023**, *25* (46), 8230–8233.
(85) Still, W. C.; Kahn, M.; Mitra, A. Rapid Chromatographic Technique for Preparative Separations with Moderate Resolution. *J. Org. Chem.* **1978**, *43* (14), 2923–2925.
(86) Galasso, V.; Asaro, F.; Berti, F.; Pergolese, B.; Kovač, B.; Pichierri, F. On the Molecular and Electronic Structure of Matrine-Type Alkaloids. *Chem. Phys.* **2006**, *330* (3), 457–468.
(87) Ueno, A.; Morinaga, K.; Fukushima, S.; Iitaka, Y.; Koiso, Y.; Okuda, S. Studies on Lupin Alkaloids. VI. Isolation and Structure of (+)-Isomatrine. *Chem. Pharm. Bull. (Tokyo)* **1975**, *23* (11), 2560–2566.
(88) Ibragimov, B. T.; Talipov, S. A.; Tischenko, G. N.; Kushmuradov, Y. K.; Aripov, T. F. Molecular and Crystal-Structure of Matrine. *Kristallografiva* **1978**, *23*, 1189–1195.
(89) Ling, J. Y.; Zhang, G. Y.; Cui, Z. J.; Zhang, C. K. Supercritical Fluid Extraction of Quinolizidine Alkaloids from Sophora Flavescens Ait. and Purification by High-Speed Counter-Current Chromatography. *J. Chromatogr. A* **2007**, *1145* (1), 123–127.
(90) Bai, G.-Y.; Wang, D.-Q.; Ye, C.-H.; Liu, M.-L. 1H and13C Chemical Shift Assignments and Stereochemistry of Matrine and Oxymatrine. *Appl. Magn. Reson.* **2002**, *23* (2), 113–121.
(91) Watkin, S. V.; Camp, N. P.; Brown, R. C. D. Total Synthesis of the Tetracyclic Lupin Alkaloid (+)-Allomatrine. *Org. Lett.* **2013**, *15* (17), 4596–4599.

(92) Ibragimov, B. T.; Tishchenko, G. N.; Kushmuradov, Yu. K.; Aripov, T. F.; Sadykov, A. S. X-Ray Structural Investigation of Allomatrine and Its N-Oxide. *Chem. Nat. Compd.* **1979**, *15* (3), 368–369.
(93) Ibragimov, B. T.; Tishchenko, G. N.; Kushmuradov, Yu. K.; Aripov, T. F.; Sadykov, A. S. Molecular and Crystal Structure of Sophoridine. *Chem. Nat. Compd.* **1979**, *15* (3), 308–314.
(94) Qiao, L.; Huang, L.; Gao, C.; Zhao, Y.; Yang, X.; Zhang, L. NMR Studies of the Matrine Alkaloids. *J Peking Univ Health Sci* **1994**, *26*, 485–486.
(95) Ibragimov, B. T.; Tishchenko, G. N.; Talipov, S. A.; Kushmuradov, Y. K.; Aripov, T. F. Structure of Isosophoridine. *Khimiia Prir. Soedin.* **1981**, 460–465.
(96) Ibragimov, B. T.; Talipov, S. A.; Tishchenko, G. N.; Kushmuradov, Y. K.; Aripov, T. F. Molecular and Crystal Structure of Isosophoridine. *Khimiia Prir. Soedin.* **1979**, 586–588.
(97) Lyu, X. Stereoselective Total Synthesis of Lupin Alkaloids. phd, University of Southampton, 2018.
(98) *APEX2, Version 2 User Manual, M86-E01078, Bruker Analytical X-Ray Systems, Madison, WI, 2006.*
(99) *Sheldrick, G.M. SADABS (Version 2008/1): Program for Absorption Correction for Data from Area Detector Frames, University of Göttingen, 2008.*
(100) *Sheldrick, G. Acta Crystallogr., Sect. A: Found. Crystallogr. 2008, 64, 112.*
(101) *Sheldrick, G. M. Acta Crystallogr., Sect. C: Struct. Chem. 2015, C71, 3.*
(102) *Müller, P. Crystallogr. Rev. 2009, 15, 57.*
(103) Parsons, S.; Flack, H. D.; Wagner, T. Use of Intensity Quotients and Differences in Absolute Structure Refinement. *Acta Crystallogr. Sect. B Struct. Sci. Cryst. Eng. Mater.* **2013**, *69* (3), 249–259.
(104) Van Der Sluis, P.; Spek, A. L. BYPASS: An Effective Method for the Refinement of Crystal Structures Containing Disordered Solvent Regions. *Acta Crystallogr. Sect. A* **1990**, *46* (3), 194–201.
(105) Macrae, C. F.; Sovago, I.; Cottrell, S. J.; Galek, P. T. A.; McCabe, P.; Pidcock, E.; Platings, M.; Shields, G. P.; Stevens, J. S.; Towler, M.; Wood, P. A. Mercury 4.0: From Visualization to Analysis, Design and Prediction. *J. Appl. Crystallogr.* **2020**, *53* (1), 226–235.
(106) Frisch, M. J.; Trucks, G. W.; Schlegel, H. B.; Scuseria, G. E.; Robb, M. A.; Cheeseman, J. R.; Scalmani, G.; Barone, V.; Petersson, G. A.; Nakatsuji, H.; Li, X.; Caricato, M.; Marenich, A. V.; Bloino, J.; Janesko, B. G.; Gomperts, R.; Mennucci, B.; Hratchian, H. P.; Ortiz, J. V.; Izmaylov, A. F.; Sonnenberg, J. L.; Williams-Young, D.; Ding, F.; Lipparini, F.; Egidi, F.; Goings, J.; Peng, B.; Petrone, A.; Henderson, T.; Ranasinghe, D.; Zakrzewski, V. G.; Gao, J.; Rega, N.; Zheng, G.; Liang, W.; Hada, M.; Ehara, M.; Toyota, K.; Fukuda, R.; Hasegawa, J.; Ishida, M.; Nakajima, T.; Honda, Y.; Kitao, O.; Nakai, H.; Vreven, T.; Throssell, K.; Montgomery, Jr, J. A.; Peralta, J. E.; Ogliaro, F.; Bearpark, M. J.; Heyd, J. J.; Brothers, E. N.; Kudin, K. N.; Staroverov, V. N.; Keith, T. A.; Kobayashi, R.; Normand, J.; Raghavachari, K.; Rendell, A. P.; Burant, J. C.; Iyengar, S. S.; Tomasi, J.; Cossi, M.; Millam, J. M.; Klene, M.; Adamo, C.; Cammi, R.; Ochterski, J. W.; Martin, R. L.; Morokuma, K.; Farkas, O.; Foresman, J. B.; Fox, D. J. Gaussian 16 Rev. A.03, 2016.

(107) Pracht, P.; Bohle, F.; Grimme, S. Automated Exploration of the Low-Energy Chemical Space with Fast Quantum Chemical Methods. *Phys. Chem. Chem. Phys.* **2020**, *22* (14), 7169–7192.
(108) Chai, J.-D.; Head-Gordon, M. Long-Range Corrected Hybrid Density Functionals with Damped Atom–Atom Dispersion Corrections. *Phys. Chem. Chem. Phys.* **2008**, *10* (44), 6615–6620.
(109) Weigend, F.; Ahlrichs, R. Balanced Basis Sets of Split Valence, Triple Zeta Valence and Quadruple Zeta Valence Quality for H to Rn: Design and Assessment of Accuracy. *Phys. Chem. Chem. Phys.* **2005**, *7* (18), 3297–3305.
(110) Weigend, F. Accurate Coulomb-Fitting Basis Sets for H to Rn. *Phys. Chem. Chem. Phys.* **2006**, *8* (9), 1057–1065.
(111) Marenich, A. V.; Cramer, C. J.; Truhlar, D. G. Universal Solvation Model Based on Solute Electron Density and on a Continuum Model of the Solvent Defined by the Bulk Dielectric Constant and Atomic Surface Tensions. *J. Phys. Chem. B* **2009**, *113* (18), 6378–6396.
(112) Luchini, G.; Alegre-Requena, J. V.; Funes-Ardoiz, I.; Paton, R. S. GoodVibes: Automated Thermochemistry for Heterogeneous Computational Chemistry Data. F1000Research April 24, 2020. https://f1000research.com/articles/9-291 (accessed 2023-03-16).
(113) The PyMOL Molecular Graphics System.
(114) Dennington, R.; Keith, T. A.; Millam, J. M. GaussView, 2016.

Chapter 2

Convergent Fragment Couplings in the Construction of Complex Molecules

2.1 INTRODUCTION

The concept of convergency has long been known as powerful strategy to achieve scalable and efficient syntheses of complex molecules. In the ideal convergent approaches, the target molecule is disconnected in fragments of equal size and complexity that can be independently prepared and coupled late in the synthesis.[1] Carrying out multiple autonomous sequences reduces issues with cross-reactivity, increases material throughput and allows for more flexibility in the synthesis of fragments.[2] Hence, the application of this synthetic approach has been discussed in various reviews.[2–6] Despite excellent discussions[2,7–9] it has proven challenging to agree on an universal and practical approach that defines and evaluates complexity *objectively* through the lens of a chemist. Pioneered by Bertz, Randic and others,[10–12] topology-based methods to assess the architectural, or *intrinsic* complexity of molecules based on graph theory, have been developed. These methods are mathematically accurate and practical tools are available;[13] however, they

often do not account for complexity as it is perceived by a chemist – *the synthetic accessibility*. A topology-based complexity metric does not decipher the interplay between structure and reactivity. For example, it detects increased complexity in terms of an increased number of atoms, but not in terms of functional group complexity – an element that is obvious for the experienced organic chemist. Recent work by Eastgate[7] describes *current complexity* as a time-depended metric for synthetic accessibility, which unifies *intrinsic* (defined by graph theory, architectural) and *extrinsic* (perceived) complexity. Extrinsic complexity takes the advancement of new synthetic tools into account and therefore changes with time. For example, the synthesis of strychnine took Woodward 30 steps in 1954[14] whereas a broader toolbox of reactions enabled MacMillan to complete the same target in only 12 steps in 2011.[15] Arguably, the intrinsic complexity of strychnine remained the same over the years but the extrinsic complexity (synthetic accessibility) changed with the state of the art.

Figure 2.1: (A) Bar graphs represent the target complexity (light blue; white line if exceeded by intermediates) and intermediate complexity (dark blue). Values denote the percentage of target complexity. (B) Intermediates are shown in pink for fragments, teal if at least one coupling step occurred, and blue after at least one cyclization step.

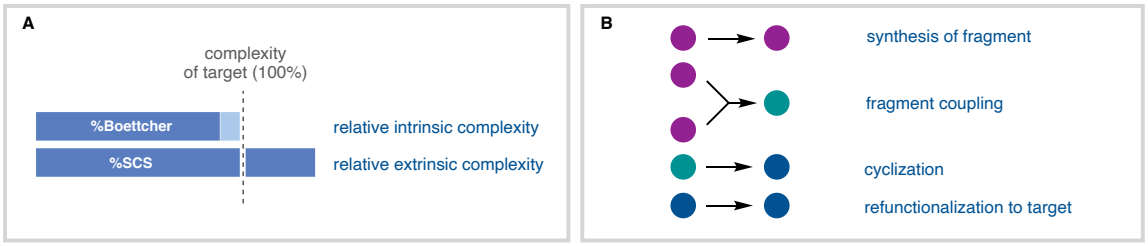

In this review, we aim to analyze the complexity patterns in recent convergent syntheses and evaluate their convergency. We discuss the limitations of the current state of art that prevent the achievement of what might be considered the ideal convergent synthesis. We include metrics for the intrinsic and synthetic complexity of key compounds. For this purpose, we determine the intrinsic complexity by an information theory-based method established by Böttcher[16] which is sensitive to stereochemistry, heteroatoms and symmetry. As estimate for the synthetic complexity we will use Coley's SCScore[17] which uses a neural network trained on the Reaxys data base to correlate a target molecule's complexity with the estimated number of steps required to reach it. It needs to be said that many other indices are available, and that complexity varies dependent on how it is defined in each method. We found that the selected approaches best capture the complexity through the eyes of an organic chemist and fit the purpose of this review best. In the following discussion, intrinsic (Böttcher) and extrinsic (SCScore) complexities of intermediates are reported relative to the corresponding target molecule. Accordingly, the bar graphs below each substrate depict the relative complexity of intermediates (dark blue) compared to the target (light blue or white line; see Figure 2.1A). For each synthesis, a schematic overview summarizing the overall strategy and the number of steps connecting the key intermediates is also provided (Figure 2.1B). We will determine both scores for each relevant intermediate and analyze the syntheses with the following criteria:

1. *How does the complexity of each fragment for the key coupling step differ intrinsically, extrinsically, and overall?* Ideal convergency would produce fragments of equal size and complexity.
2. *How does the combined complexity of fragments compare to the complexity of the*

target? Ideally the fragments complexity would exactly add up to the target's complexity. Under- or overshooting the targets complexity indicates inefficiencies in the synthesis.

3. *What is the ratio of complexity completed before and after the fragment coupling step?* An ideal convergent approach would feature a fragment coupling that directly yields the target, and hence there would be no change in complexity after the coupling.

2.2 SYNTHESIS OF VIRIDIN

(–)-Viridin (**1**) is a furanosteroid structurally related to wortmannin, a well-known, potent phosphatidylinositol 3-kinase (PI3K) inhibitor.[18–20] While therapeutic use of wortmannin has been limited by toxicity arising from high-affinity irreversible covalent bonding to PI3Ks, viridin presents as a promising candidate for PI3K inhibition-based chemotherapy.[21]

Figure 2.2: Schematic route to viridin. Number in circles represent the intermediate, numbers above the arrow indicate the step count.

Based on the regions of wortmannin where structural modifications lead to noticeable changes in potency,[22,23] the C and D rings of viridin are attractive areas for diversification. In the first synthesis of **1**, reported by Sorenson and coworkers in 2004,[24] early-stage C/D

ring formation was the foundation for a linear sequence used to construct the natural product. The Guerrero group envisioned a convergent strategy guided by the goal of late-stage installation of C/D-ring fragment derivatives would facilitate investigation of structure-activity relationships (SAR) by increasing the ability to simultaneously prepare differently substituted fragments.

Retrosynthetically, cleaving the pentacyclic natural product through the B ring reveals ideal fragments **2** and **3** (Figure 2.3A). After coupling of the two achiral precursors an enantioselective Heck cyclization could set the stereogenic quaternary center at C10, which in turn could govern the stereoselectivity of late-stage redox adjustments required on the A ring.

Figure 2.3: (A) Retrosynthetic analysis of (–)-viridin (**1**). Preparation of (B) fragment **6** and (C) fragment **10**.

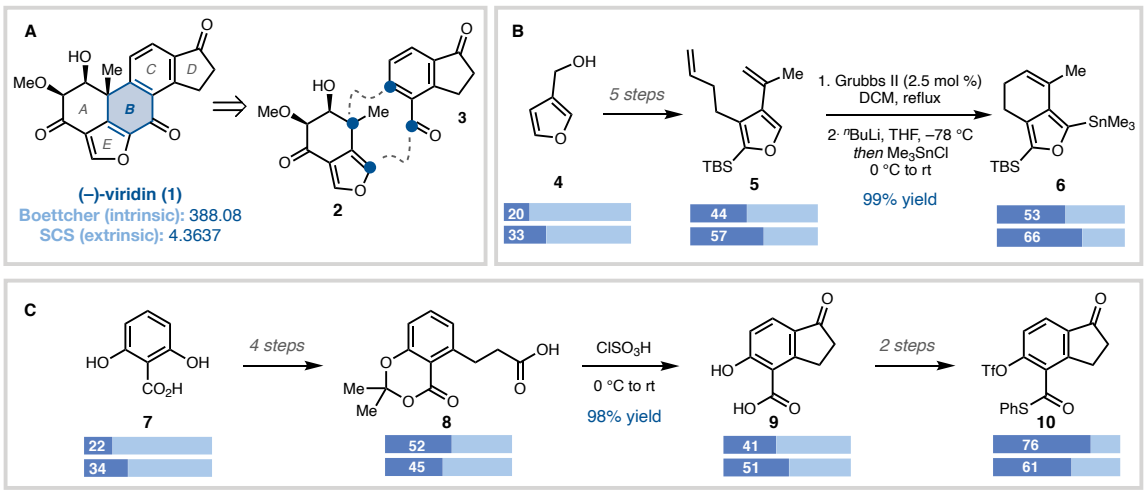

In the forward direction, each achiral fragment was prepared in seven linear steps from commercial material. Bicyclic **6** arose via ring-closing metathesis reaction of

bisalkene **5** using Grubbs's second-generation catalyst (Figure 2.3B). An intramolecular Friedel–Crafts acylation of dihydrocinnamic acid **7** was used to forge the indanone fragment (**10**, Figure 2.3C). The fragments were subjected to Liebeskind conditions; in the presence of a Pd(0) catalyst and copper source, thioester **10** underwent selective oxidative addition and coupling to furanyl stannane **6** to furnish ketone **16** in 83% yield (Figure 2.4A). Next, the key all-carbon quaternary stereocenter was established via enantioselective Heck reaction. Intramolecular coupling of aryl triflate and trisubstituted alkene occurred using a ^{t}Bu-PHOX-ligated Pd(0) complex. Ligand and base selection proved critical to increasing conversion and minimizing alkene isomerization, producing cyclized **12** in 75% yield and >99% ee.

Figure 2.4: (A) Convergent annulation sequence. (B) Completion of **1**.

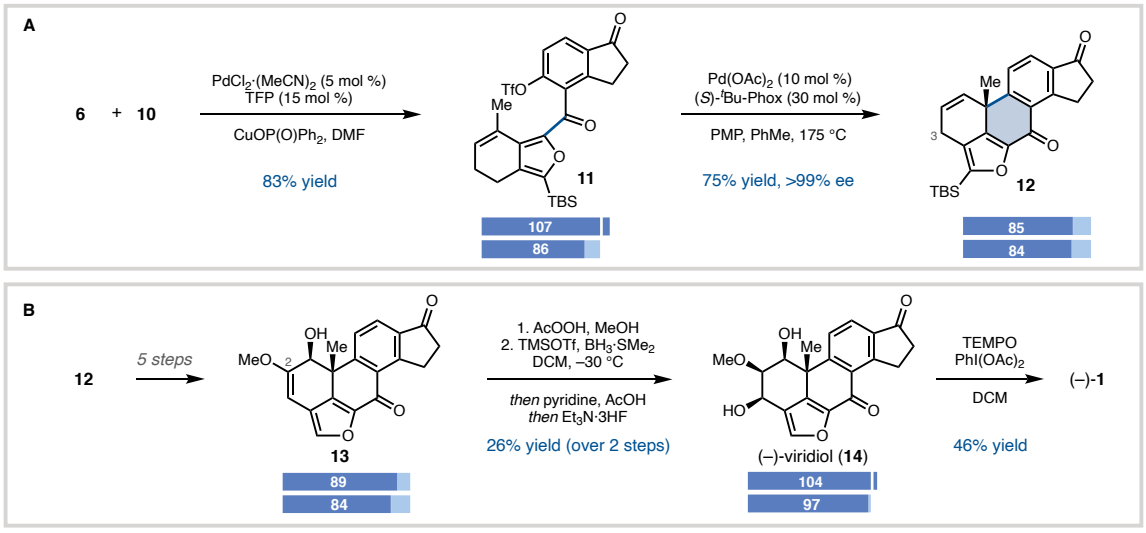

With the pentacycle thus constructed, the remaining complexity was introduced via manipulation of C-ring oxidation (Figure 2.2G). From intermediate **12**, subsequent steps

served to address: (1) regioselectivity versus the D-ring ketone and (2) diastereoselectivity, guided by the quaternary methyl group blocking one face of the flat carbon framework. Having failed to oxidize C3 directly from alkene **12**, the authors found an alternative route through protected pentacycle **13**. First, regio- and stereoselective reduction to alcohol **14** proceeded using a one-pot transient protection strategy. Then, transformation to (–)-viridiol (**15**) was accomplished by epoxidation in the presence of methanol to generate an intermediate hydroxy ketal which was diastereoselectively demethoxylated. In this case, oxidation occurred with 1:2 dr favoring the undesired diastereomer at C3; however, either diastereomer could be selectively oxidized to (–)-viridin (**1**) in 46–48% yield.

Multiple lessons can be learned from Guerrero's synthesis: While each fragment is of similar size and extrinsic complexity (i.e., synthesizability), indanone **10** possesses greater intrinsic (*i.e.*, structural) complexity (76% for **10** vs 53% for **6**). As the intrinsic complexity scales with number and diversity of atoms present, both the triflate and thioester functionalities increase the intrinsic score. When comparing the coupling partners with hypothetical, simplified fragments in which these functional groups are replaced by hydrogen, it becomes obvious that the intrinsic complexity shows a sharp decrease, while the trend for the extrinsic complexity is more ambiguous (Figure 2.5). The SCScore correlates complexity with a step-count estimate given by a machine learning model and aims to mimic an organic chemists perception of complexity. Therefore, the smaller impact and the slightly lower extrinsic complexity of indanone **10** compared to stannane **6** (61% vs 66%) can be explained by the recognition of 'commonly synthesized' functional groups, lowering their complexity contribution (Figure 2.2A/B). Both groups and the stannane in **6** are required to perform the coupling and cyclization steps and the product of this

annulation sequence (i.e., **12**) is substantially less complex than the sum of the requisite fragments (intrinsic: 129% vs 85% and extrinsic: 127% vs 84%); here, building 'excessive' intrinsic complexity into the fragments (in the form of reactive functional groups) was required to enable the desired annulation tactics (Figure 2.2F).

Figure 2.5: (A) Complexity difference (Δ) between **6** and simplified fragments **16**, **17** and **18**. Negative signs denote a complexity loss compared to **6**, while positive signs indicate an complexity gain. (B) Complexity difference (Δ) between **10** with simplified fragments **19** and **20**.

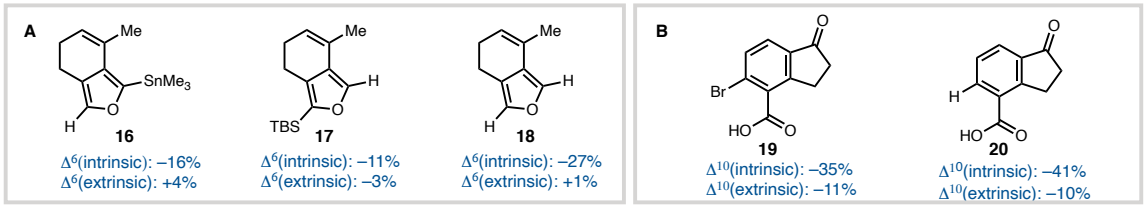

It can be concluded that the extrinsic score better matches the chemical intuition (the synthesizability both fragments is roughly the same), while the intrinsic score is a better read out for metrics like atom economy of reactions.

Following annulation, an 8-step sequence of redox steps is required to access viridin. (Figure 2.2G). The scores remain largely consistent over this sequence reflecting the need for lateral tactics and unanticipated troubleshooting to install the desired functionality. It's possible that use of a more fully functionalized A-ring in the Pd-catalyzed coupling/cyclization reactions (reflected in a higher level of fragment complexity; e.g., **2**), could have avoided the challenges encountered in oxidizing C3 of intermediate **12**.

2.3 SYNTHESIS OF RUBRIFLORDILACTONE A

Rubriflordilactone A (**20**), a bisnortriterpenoid, was isolated in 2006 from the medicinally relevant *Schisandra rubriflora*.[25] The *Schisandraceae* family, commonly found in China, includes many species that exhibit pharmaceutical properties such as antihepatitis, antitumor, and anti-HIV-1 activity.[26,27] Despite this, syntheses of this class of natural products are rare, with the total synthesis of schindilactone A by Yang in 2011 being the first report of a *Schisandraceae* triterpenoid.[28]

Figure 2.6: Schematic route to rubriflordilactone A.

Li and coworkers sought a convergent approach to Rubriflordilactone A **20** by first removing the butanolide fragment from the heptacyclic framework, followed by disconnetion through the central aryl ring, leading to the hypothetical fragments **21**, **22** and **23** (Figure 2.7).[29] The authors proposed using vinyl iodide **29** and vinylsilane **38** as coupling partners in a Pd-catalyzed cross coupling reaction, followed by a 6π-electrocyclization/aromatization to complete the central D ring (Figure 2.8A/B). Furane **29** was expected to be coupled late-stage to install the butanolide.

Figure 2.7:. Key disconnections of the central aryl D-ring and the idealized fragments **21**, **22** and **23** for Li's total synthesis of rubriflordilactone A. (**20**).

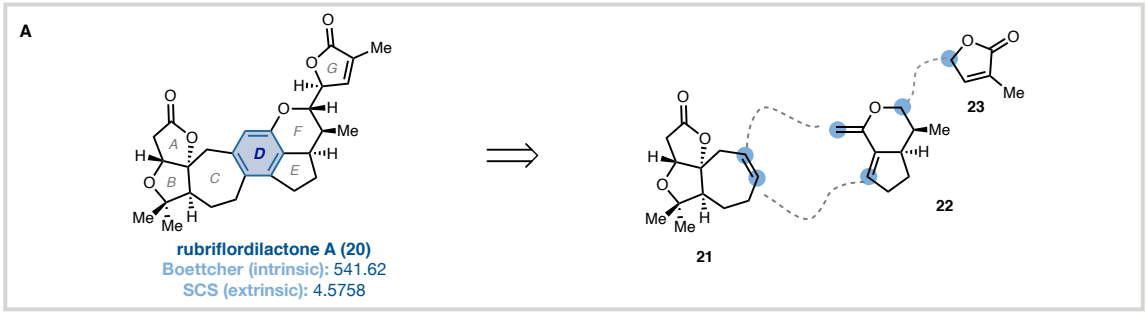

Fragment **29** was prepared from 2-iodo-2-cyclopentenone (Figure 2.4B). Corey-Bakshi-Shibata reduction, followed by Sonogashira coupling gave alkyne **27** in high yield and enantiomeric excess. A Johnson-Claisen rearrangement gave methyl ester **28** which could subsequently be demethylated with LiOH. Eventually, desired *E*-vinyl iodide coupling partner **29** was accessed in 52% yield and a total of 5 steps after undergoing a stereospecific iodo-lactonization.

Vinylsilane **35** was synthesized in 15 steps from oxazolidinone **31** and inspired by a route developed by Yang and co-workers in their synthesis of schindilactone A. The route was rendered asymmetric via Cu-catalyzed Diels-Alder reaction which produced enantioenriched ester **32** in 80% and 76% *ee*. After replacement of the oxazolidinone with a methyl group Yang's sequence was employed to access lactone **33**. A one carbon ring expansion to access the 7-membered ring was achieved via cyclopropanation to yield **34**, followed by Ag-mediated ring opening to give bromo alkene **35.** Bromo enone **35** could be resolved to 99% *ee* via recrystallization and elaborated to vinyl triflate **36** in 3 steps. An intramolecular Dieckman condensation upon treatment with LiHMDS gave a hemiaminal, which could deoxygenated with BF_3•OEt_2 and triethyl silane to yield lactone **37**. Pd-

catalyzed stannylation eventually gave the stannane coupling partner **38**.

Figure 2.8: Preparation of (A) fragment **29** and (B) fragment **38**.

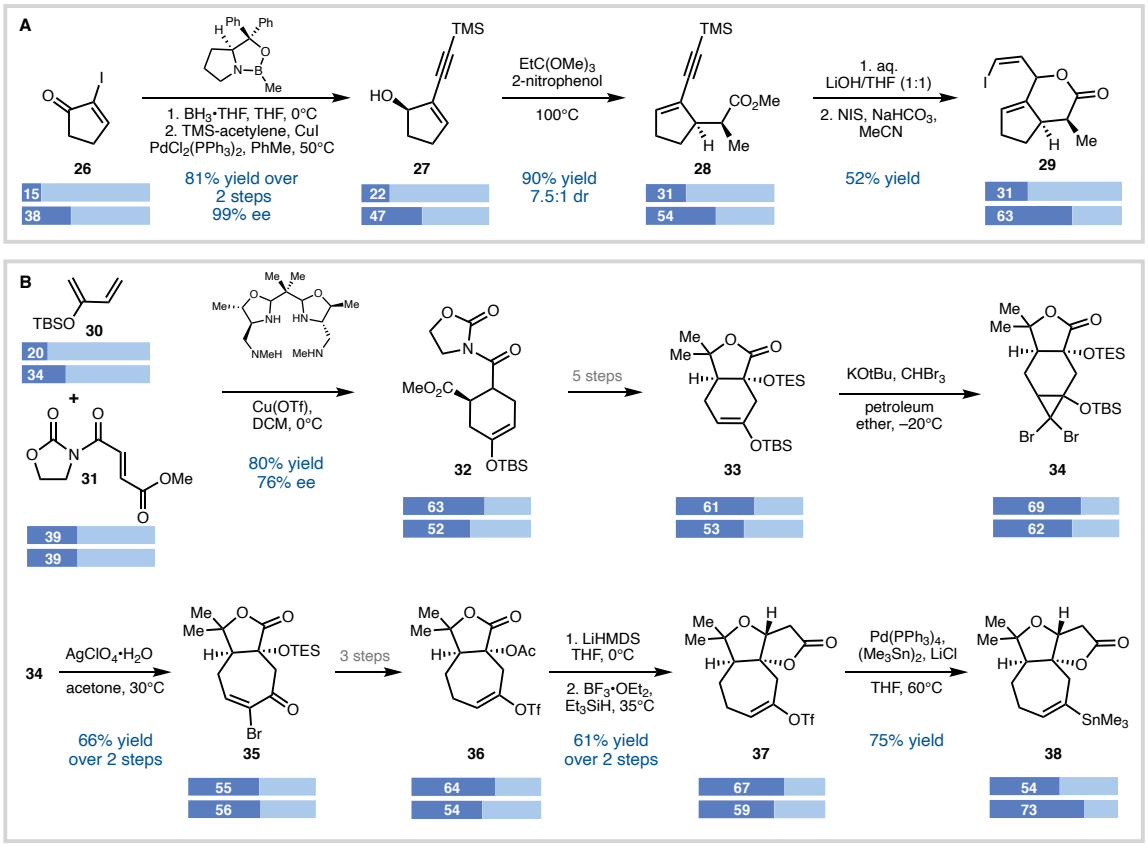

A mild Stille-Migita reaction using $Pd(PPh_3)_4$ and CuTC was employed to effectively couple vinyl iodide **29** and vinylsilane **35** in 96% yield with selectivity for the *E*-olefin. Triene **36** was heated to 145 °C under an atmosphere of air, resulting in a one-pot 6π-electrocyclization and aromatization to afford **37** in 73% yield. The olefin geometry was essential for the success of the electrocyclization of the highly substituted enol ester-containing triene. Regioselective reduction of the six-membered lactone was achieved using sterically demanding $LiAlH(O\text{-}t\text{Bu})_3$ to furnish a mixture of the lactol and ring-

opened aldehyde form.

The internal strain of the 6/5/6 system and the leaving group ability of the phenoxy group led to ring opening in attempts to directly couple the siloxy furan. Instead, the lactol/aldehyde mixture was treated with DAST to access fluoroacetal **38** which underwent a Mukaiyama aldol reaction to complete the synthesis. While other furans were not reactive enough to participate, treatment of a mixture of stannane **38** and $BF_3 \cdot OEt_2$ with fluoride **42** resulted in diastereoselective addition to give butenolide **20** in 66% yield and completed the first and asymmetric synthesis of rubriflordilactone A.

Figure 2.9: Convergent fragment coupling and completion of **20.**

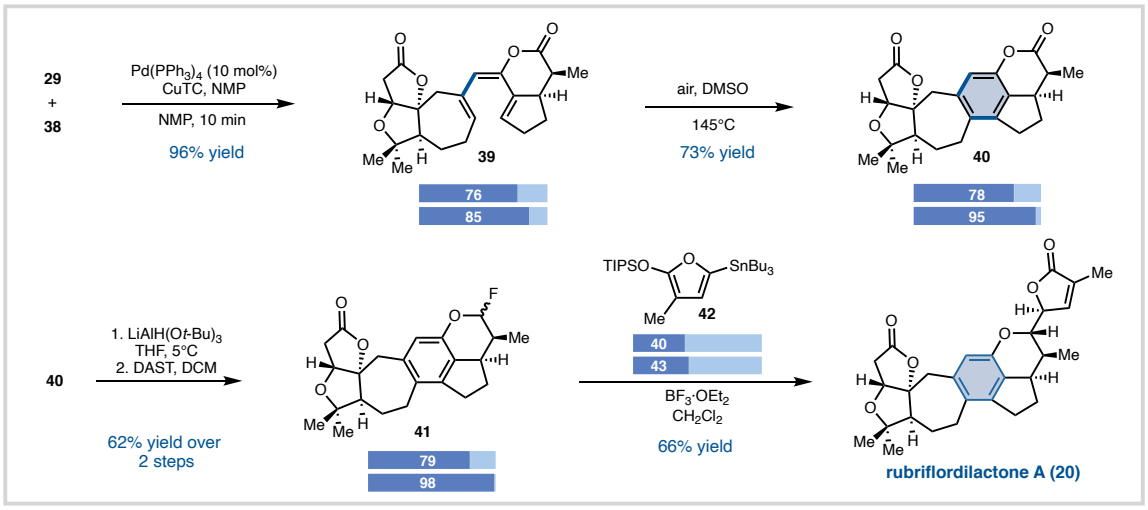

Li's strategy employs a fragment coupling approach of a higher degree, i.e., the convergency in the key fragment coupling step is strategically reduced and a second fragment coupling step (the installation of the butanolide) is required to complete the synthesis. This approach has multiple consequences: First, as expected the convergency of

the key fragment coupling is lowered as reflected in the step count and complexity scores for both fragments. Synthesis of stannane **38** requires 14 steps (54% intrinsic complexity) while vinyl iodide fragment **29**, lacking the butanolide motif is accessed in only 5 steps (31% intrinsic complexity). After a coupling and annulation sequence the complexity reaches 78%, slightly lower than the sum of its fragments. Intrinsic and extrinsic complexity remain mostly constant over the two-step sequence which installs the fluoride handle for the coupling. The requirement for an activated (stannyl) butanolide coupling partner results in high complexity scores of 40% (intrinsic) and 43% (extrinsic) of the fragment and, indicating inefficiencies due to the functional group requirements of the coupling reaction, as discussed before.

Second, if feasible late-stage installation of a fragment can ease potential reactivity or stability concerns by installing reactive motifs late in the synthesis and can enable SAR studies by modifying the fragment. To remain convergent, this approach requires a suitable disconnection which does not require extensive refunctionalization before and after the second coupling step and coupling conditions which are tolerant of highly functionalized fragments. The attached butanolide motif in rubriflordilactone A and the chosen Mukayama aldol conditions accomplish both, and lead to a short endgame sequence that has potential for the facile synthesis of other butanolide derivatives.

2.4 SYNTHESIS OF BISLACTONE LIMONOID ALKALOIDS

As methods emerge for exchanging (hetero)atoms embedded within a carbocyclic skeleton, their potential impact on synthetic design is clear.[30] Examples of single-atom editing utilized in the context of a convergent annulation approach to natural product

synthesis are rare but promising.[31] The unified synthesis of bislactone limonoid alkaloids by Newhouse and coworkers in 2019 is illustrative.[32]

Figure 2.10: Schematic route to bislactone limonoid alkaloids.

While limonoids of type **43** have demonstrated modest activity against protein tyrosine phosphatase 1B[33] — a target for treatment of diabetes and cancer, among others[34] — questions of structural characterization have most recently motivated efforts toward the chemical synthesis of these natural products. In particular, a series of related bislactone limonoids vary only in the stereochemical arrangement of oxidation at C3, an observation incongruent with the proposed biosynthetic pathway. The structure of (+)-granatumine A (**56**, R^1 = OMe, R^2 = H) has been confirmed by X-ray crystallography; the proposed opposite configuration at C3 of the xylogranatins remained uncertain.

With the synthesis of closely related xylogranatopyridines as guiding precedent,[35] the authors pursued a fragment coupling approach to **56**, envisioning convergent annulation of the central pyridine (Figure 2.11A). Initial studies[36] revealed successful pyridine formation from a C1 ketone; however, subsequent heterobenzylic oxidation proved challenging and necessitated pre-installation of C3 oxidation. The keyed 1,3-diketone (see ideal fragment **45**) could thus be advanced via an intermediate pyran (**44**), expected to serve as a temporary protecting group to guide selective reaction at C3 before conversion to the desired pyridine. Given the dearth of stereochemical control elements in the completed

pentacyclic core, stereocenters on both enantioenriched fragments would be established prior to annulation.

Figure 2.11: (A) Retrosynthetic analysis of bislactone limonoid alkaloids of type **43**. Preparation of fragments (B) **46** and (C) **45**.

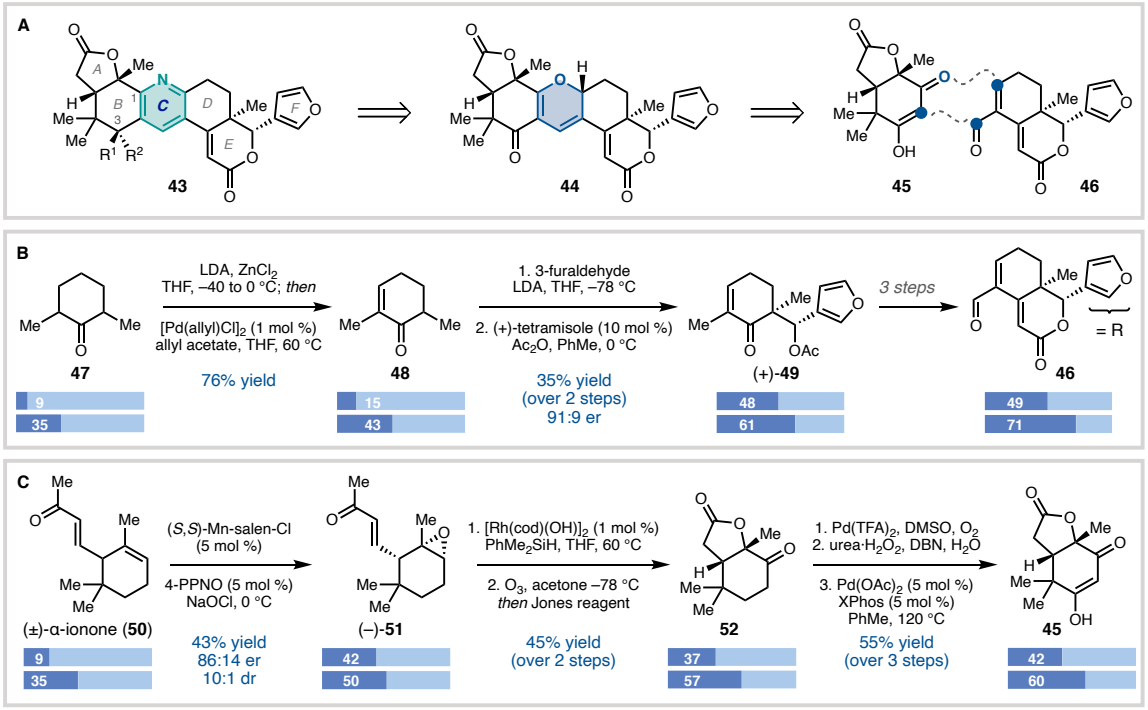

The route to the eastern fragment (**46**) was inspired by a previous route to (+)-azearalide (Figure 2.10B). Pd-catalyzed dehydrogenation, previously developed by the authors,[37] provided enone **48** from ketone **47**. Diastereoselective aldol and acylative chiral resolution then afforded furan (+)-**49** in 91:9 er, which could be advanced in three steps to aldehyde **46**. Toward western fragment **45**, direct kinetic resolution of racemic α-ionone afforded epoxide (–)-**51** in 43% yield and 86:14 er in a single step (Figure 2.11C). Hydrosilylation and ozonolysis were followed by oxidation under acidic conditions to give

rise to **52**; lactonization presumably occurs via epoxide opening and intramolecular carbocation trapping by the pendant intermediate acid. A final three-step sequence was used to access the complete fragment (**45**), requiring development of a Pd-catalyzed epoxide opening reaction to reveal the requisite 1,3-diketone moiety.

Following preparation of **43** and **45**, both fragments were joined via Knoevenagel condensation in the presence of ethylenediammonium diacetate to generate presumed intermediate **53**. Subsequent tandem thermal oxa-6π electrocyclization afforded a single product, 2H-pyran **54** (Figure 2.12A). In this key step, complete torquoselectivity was observed, and experimental and computational investigation revealed a thermodynamic preference for the desired regioisomer. Having effectively discriminated between the C1 and C3 ketones, selective Luche reduction was performed.

Figure 2.12: (A) Convergent annulation sequence and (B) completion of the synthesis of **56, 57**, and **58**.

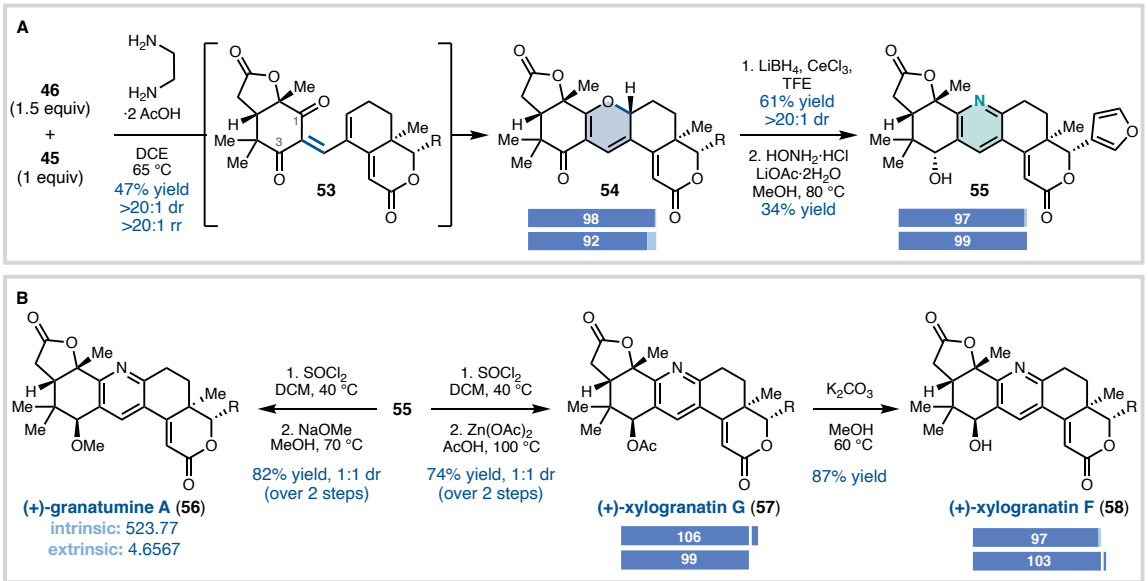

Subsequent treatment with hydroxylamine effected pyran/pyridine transmutation to arrive at **55**, presumably proceeding through a pyridine *N*-oxide that undergoes loss of water. From **55**, a short chlorination/methanolysis sequence afforded (+)-**56** as a separable 1:1 mixture of diastereomers (Figure 2.11B). Alternatively, displacement with acetate and deprotection gave (+)-xylogranatin G (**57**) and F (**58**), respectively, the X-ray crystal structure of these limonoids being used to revise the originally proposed.

Newhouse' synthesis highlights how increased fragment complexity – if compatible with the coupling conditions – can avoid end game challenges and exemplifies the strategic use of skeletal reorganization as an important component of synthetic design. After failing to realize their previous late-stage benzylic oxidation strategy, it became eminent that C3 oxidation must be installed prior to the coupling. The Knoevenagel condensation/oxa-6π electrocyclization sequence, proved not only compatible with the C3-oxidized fragment but also proceeded with great regio- and stereoselectivity for the desired compound. The intrinsic complexity increases slightly after cyclization (98%) compared to the sum of the fragments (91%), indicating an efficient transfer of complexity through the coupling. In contrast to the previously discussed syntheses, both fragments score similarly in complexity and step count and do not require "extra" protecting or functional groups to enable the coupling; "complexity loss" later in the synthesis upon interconversion/removal of these groups is therefore avoided. Interestingly, the intrinsic complexity for 2H-pyran **54** and pyridine **55** are almost identical (98% vs 97%), but the extrinsic complexity slightly increases from 92% to 99%, with the 2-H pyran being easier to synthesize. While the difference is small, it could hint that the model recognizes that 2H-pyran **54** provides an easier synthetic entry and potentially justifies the authors strategic decision to target the

oxacycle first. Interestingly, although intermediate **55** is distinct from natural product **58** only in the configuration at C3, **55** is ranked as slightly easier to synthesize than its epimer (i.e., **55** is 4% less extrinsically complex than **58**). Derived from a machine learning model, interpretation of these numbers should be done with caution, especially for small differences; however it is interesting to speculate if the model picked up on the undesired selectivity for the C3 ketone reduction, which requires inversion of the stereocenter to access its epimer **58.**

2.5 SYNTHESIS OF HAPERFORIN G

Haperforin G (**59**) is an limonoid tetranortriterpenoid natural product isolated from Harrisonia perforata.[38] Its sub-micromolar inhibition of human 11β-hydroxysteroid dehydrogenase type 1 (11β-HSD1) makes it a desirable target against illnesses such as Alzheimer's disease, vascular inflammation, cardiovascular disease, and glaucoma, however its low isolation efficiency (27 mg/kg) make biological studies impractical.[39,40]

Figure 2.13: Schematic route to haperforin G.

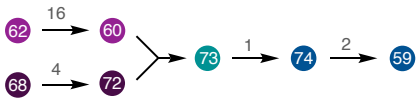

Yang and coworkers envisioned that a convergent approach could enable an efficient synthetic route suitable to help supply haperforin G for biological studies. Retrosynthetically, they dissect the novel limonoid 6/5/6 tricyclic carbon skeleton through the six-membered C ring (Figure 2.14), yielding theoretical fragments **60** and **61**. In a

forward sense, initial joining of enone **60** with alkyl iodide **72** fragment via visible-light photoredox-catalyzed radical coupling and subsequent, intramolecular aldol reaction would close the C ring and yield haperforin G after elimination of the resulting alcohol.

Figure 2.14: Retrosynthetic analysis of haperforin G **59**.

The synthesis of the enone fragment proceeded via Zakarian's enantioselective alkylation protocol (Figure 2.15A),.[41] In the presence of a chiral tetramine, which could be recycled, the desired product **62** was formed in 77% yield and 91% *ee*, establishing the C3 stereogenic center. After advancing this intermediate through an 8 steps sequence, chiral enyne **65** underwent Co-mediated Pauson-Khand reaction to give silyl enone **66** in 86% yield and setting the bridgehead all-carbon quaternary center at C10. After deprotection and regio- and diastereoselective epoxidation, **67** could be advanced in 4 steps to give enone coupling partner **60** in a total of 16 steps.

In contrast, preparation of iodolactone fragment **72** was accomplished in only 4 steps (Figure 2.15B). Enantioselective vinylation of 3-furaldehyde **68** via Nugents (+)-MIB-mediated protocol[42] gave allylic alcohol **70** in 93% yield with 99% *ee*. NIS-mediated ketalization with *tert*-butyl vinyl ether set the stage for a Pd-catalyzed iodide atom transfer cyclization (IATC) which gave the desired lactone **72** after Jones oxidation.

Figure 2.15: Preparation of fragments (A) **60** and (B) **72.**

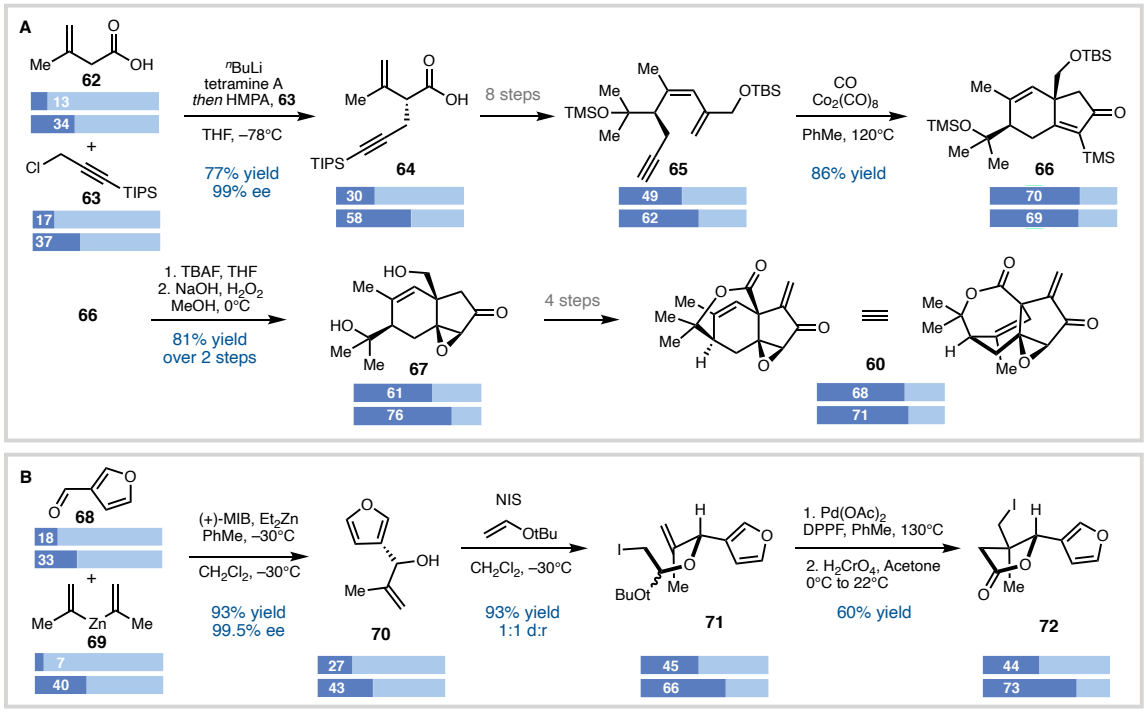

In the fragment coupling step, the key bond formation was accomplished via photoredox-catalyzed Giese addition of **72** into enone **60** and gave product **73** diastereoselectively in 64% yield (Figure 2.16). Annulation of the C ring was completed by treatment with *t*BuOK, and aldol product **72** could be obtained as a single diastereomer. Advancement of the resulting alcohol to haperforin G was concluded after a short elimination sequence employing $SOCl_2$/py and DBU.

Yang's haperforin G synthesis highlights how strategic derivation from ideal convergency (i.e. non-equal sized fragments) can benefit the overall convergency of a route (i.e. having less post-coupling modification steps). Comparing the two fragments in size and step count reveals a drastic difference (16 steps for **60** vs. 4 steps for **72**). While this difference is also reflected in the complexity scores, it is less pronounced. The intrinsic

complexity of the enone fragment is 60% (extrinsic: 90%), and 46% (extrinsic: 86%) for the iodide coupling partner, respectively.

Figure 2.16: Completion of the synthesis of **59.**

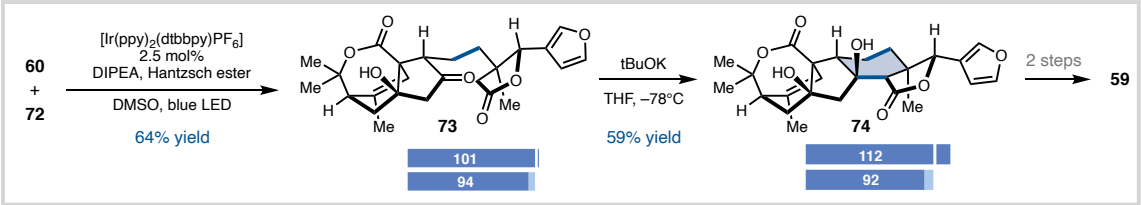

While unequal fragments generally decrease the convergency, retrosynthetic analysis of haperforin G reveals, that disconnection through the D ring is preferable over dissection of the C ring as it avoids formation of the bridgehead all-carbon quaternary center during the fragment coupling step. The cyclohexene in the D ring also enables "full utilization" of the enone motif; First, it acts as Giese acceptor to couple the fragments, the remaining carbonyl group then facilitates the aldol cyclization step after resulting in an alcohol, which is eventually eliminated to give the desired alkene. In contrast to previously discussed examples in which "extra" functional groups were required to facilitate couplings, this approach leverages the instrinsic functionality of the target, and its efficiency is also reflected in the conservation of intrinsic complexity during the fragment coupling step. The sum of intrinsic complexity is 106%, very close to the ideal 100% to only slightly increases after annulation (112%). As both fragments closely map on the natural product (i.e. no adjustments required, no large protecting groups), lateral complexity changes are avoided and a short endgame can be achieved. Despite the endgame efficiency, unequal step counts decimate certain benefits of a convergent strategy, such as increased material throughput.

Interestingly, the small difference in intrinsic and extrinsic complexity scores does not correlate to the difference in step count. This is partially explained by the linear, sequential build-up of bridged tricyle **60** from a simple five carbon precursor, while lactone **72** benefits from "buying" complexity in form of the 3-furaldehyde fragment. Overall, intrinsic complexity gains per step are larger for the lactone fragment than the enone, which experiences mostly lateral complexity changes (i.e. deprotection, functional group interconversions) after the Pauson-Khand reaction. This potentially indicates inefficiencies in the synthesis. Notably, the extrinsic complexity constantly increases in accordance with the increasing perceived complexity or synthesizability of the bridged tetracycle.

The second half of this review is dedicated to natural products containing bridging ring systems as they can be generally considered more complex and expected to require more post-coupling modifications than similar sized fused compounds.

2.6 SYNTHESIS OF WELWITINDOLINONES

The welwitindolinone natural products possess a bridging ring system and have long been the target of chemical synthesis due to their wide range of biological activities — insecticidal, antimycotic, and anticancer,[43,44] for example — and intriguing structural features.[45–72]

Figure 2.17: Schematic route to *N*-methylwelwitindolinone D.

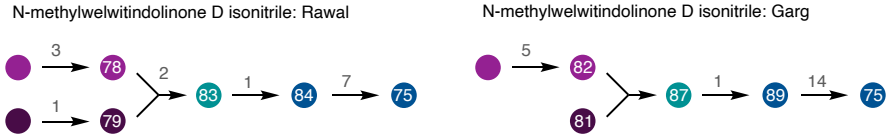

The first successful synthetic strategy to welwitindolinones **75**, **76** and **77** was independently published by the groups of Rawal[73] and Garg[66] in 2011 and established the central bicyclo[4.3.1]decane core common to all but one welwitindolinone via convergent joining of functionalized indole and cyclohexyl building blocks (Figure 2.18A/B). In each of these syntheses, assembly of the bicyclo[4.3.1]decane ring system establishes a common intermediate (e.g., **80**) that serves as a strategic branching point to access several members of the natural product family.[71,74] Analysis of the two routes to *N*-methylwelwitindolinone C and D reveals general challenges that arise in the design and implementation of convergent annulation.

Figure 2.18: (A) Selected welwitindolinone natural products and (B) retrosynthetic analysis.

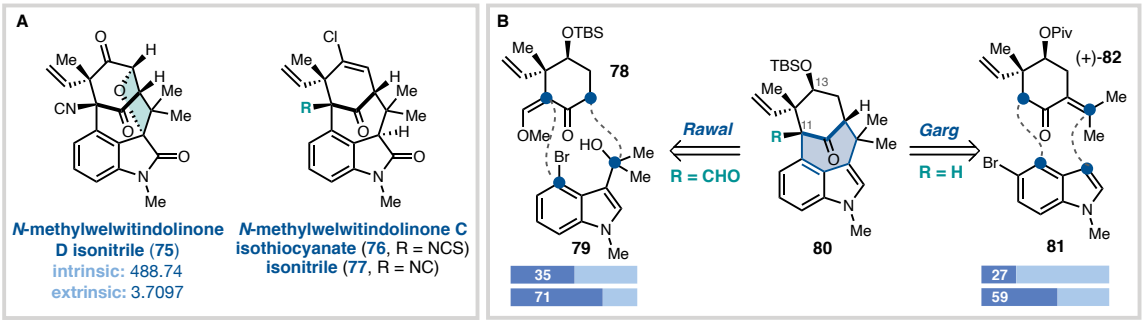

In the Rawal synthesis, an aldehyde (i.e., **80**, R = CHO) was selected as the key intermediate (Figure 2.18B). This substrate could be oxidized at C13 to give an alkenyl chloride moiety and the functional group appended to C11 was expected to aid late-stage transformation to the eponymous isonitrile of natural products **75** and **77** and/or the isothiocyanate of related **76**. Sequential α-functionalization reactions of cyclohexanone

fragment **78** using partner indole **79** were envisioned to stitch together the bridging bicyclic system.

To initiate the annulation sequence (Figure 2.19A), Friedel–Crafts-type alkylation proceeded via silyl enol ether formation from fragment **78** followed by Lewis acid-promoted reaction with electron-rich indole **79** to afford **83** in 78% yield. Completion of the bicyclo[4.3.1]decane scaffold was achieved using a Pd-catalyzed intramolecular enolate arylation installed a quaternary center vicinal to C11 (i.e., C12 of **84**).

Figure 2.19: (A) Convergent annulation, (B) synthesis of the *N*-methylwelwitindolinones by Rawal.

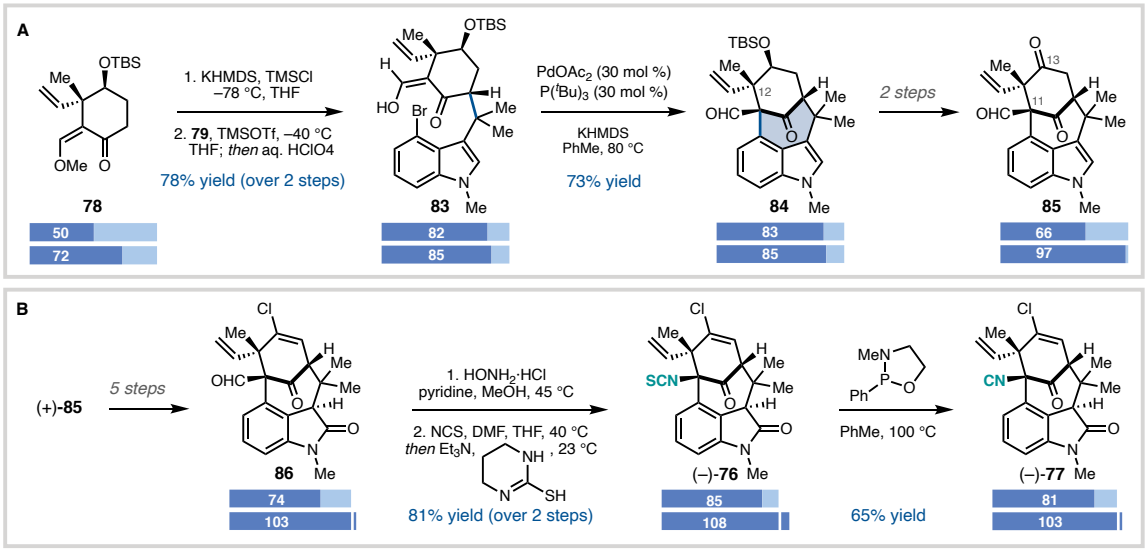

A series of steps was required to reveal ketone **85**, then to introduce the remaining features. First, the alkenyl chloride was established in a five-step sequence, which required the reduction and reoxidation of the aldehyde C13 to prevent an undesired Cope rearrangement pathway (Figure 2.19B). Treatment of aldehyde **86** with hydroxyl amine generates the oxime. The subsequent step treating with the sulfur reagent is then required

for the oxime-to-isothiocyanate rearrangement, furnishing (–)-*N*-methylwelwitinolinone C isothiocyanate **76,** and correcting the previously reported structural assignment; desulfurization then gave (–)-*N*-methylwelwitinolinone C isonitrile **77**. Alternatively, divergent intermediate **85** was selectively α-brominated (Figure 2.21B). Subsequent indole oxidation occurred with concomitant spirocyclic ether closure, and the aldehyde of product **89** was advanced to *N*-methylwelwitinolinone D isonitrile **75** via the developed 3-step sequence.

Figure 2.20: (A) Convergent annulation, (B) synthesis of the *N*-methylwelwitindolinones by Garg.

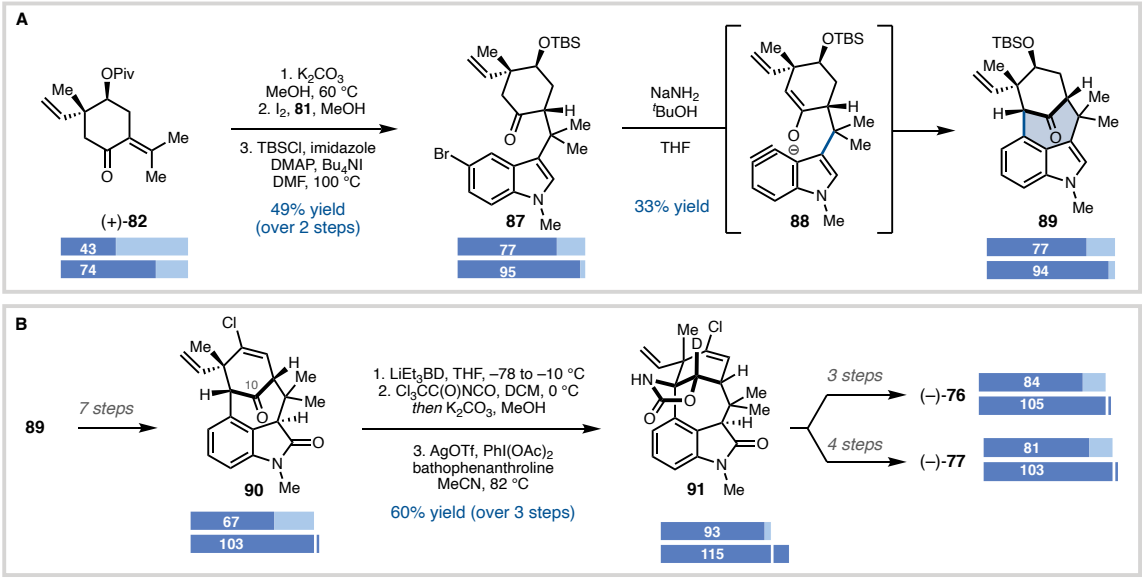

Garg and coworkers implemented a conceptually related approach to welwitindolinone synthesis that relied on transannular indolyne cyclization to access the bicyclic framework of key intermediate **89** (Figure 2.18). Conjugate addition of commercially available indole fragment **81** into enone partner **82**, prepared in five steps

from (*S*)-carvone, was catalyzed by I_2, then protection yielded coupled product **87**. Subsequent treatment of bromoindole **87** with a 3:1 $NaNH_2$/^{t}BuOH complex base mixture served to generate presumed electrophilic indolyne intermediate **88** which underwent intramolecular enolate trapping to give cyclized **89** in 33% yield. With the bicyclo[4.3.1]decane core completed, alkenyl chloride **90** was prepared from protected alcohol **89** in seven steps via formation of the vinyl stannane (Figure 2.20).

Figure 2.21: (A) Rawal's synthesis of N-methylwelwitindolinone D. (B) Garg's synthesis of N-methylwelwitindolinone D.

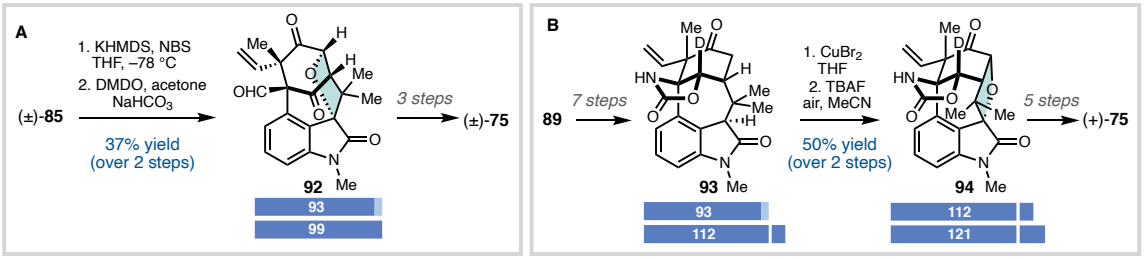

Finally, functionalization of C11 was pursued via activation of the bridgehead C–H bond. Intramolecular nitrene insertion proved to be a viable route; reduction and carbamoylation preceded Ag-catalyzed formation of functionalized **93** in 60% yield over the three steps. With the introduction of an additional ring, both the structural and the synthetic complexity of the intermediate oxazolidinone were significantly increased; 'hard-to-synthesize' **91** required deuterium incorporation to prevent competitive reaction at C10 and promote regioselective C–N bond formation. A series of refunctionalization reactions were then used to access natural products **76** or **77** in three or four additional steps, respectively. Alternatively, intermediate **89** could be advanced through the same C–H

functionalization sequence (Figure 2.21). From the resulting pentacycle, spiroetherification was possible via α-bromination. Oxidation in the presence of base and air was then followed by spontaneous halide displacement to forge **93**, and natural product **75** was furnished after five steps of functional group manipulations.[75]

Application of convergent annulation to welwitindolinone synthesis highlights a common strategic dilemma. Strategic disconnections allow to leverage the intrinsic reactivity of each fragment (i.e. α-functionalization of the cyclohexanone, conjugate addition of the indole) for the fragment coupling and minimize the requirement for additional functional groups. In both syntheses there is little change of the intrinsic complexity after annulation compared to the sum of both fragments (83% vs 85% for Rawal and 70% vs 77% for Garg) highlighting the efficiency of the approach. The fragments score overall low on intrinsic complexity and are commercial or rapidly accessible from known compounds. This strategically reduces the risk as the fragment coupling key step can be tested early in the synthesis and reconsidered if necessary.

While the common welwitindolinone core can be accessed rapidly, the relatively low intrinsic complexities foreshadow that excessive post-coupling modifications are necessary to complete the syntheses. The highly decorated framework, prone to side reactivity and exhibiting increased steric congestion, complicates functionalization (i.e., via undesired Cope rearrangement or challenging bridgehead functionalization). In both syntheses, multistep endgames might have been avoided by introduction of the alkenyl chloride and indole oxidation prior to bridging ring formation. However, the ability to access to N-methylwelwitindolinone D could justify delay of such transformations, as one of them becomes obsolete and the other enables concise intramolecular ether formation,

respectively. Strategically minimizing the complexity of individual fragments may be inefficient but can allow divergent access to related natural products.

We should note that the extrinsic complexities calculated for the here discussed welwitindolinones are relatively high and seem to be consistently higher than their intrinsic counterparts. Originating from a machine learning model this trend cannot necessarily be rationalized intuitively; 1,3 diketone **84** scores 85% in "synthesizability", while related cyclohexanone **89** scores 94% and only differs by the absence of the bridgehead aldehyde. However, this could indicate the recognition of more common motifs i.e. a 1,3 dicarbonyls, which are found frequently in literature. As the model was trained on the Reaxys data base, such substructures are found in higher frequency and the training data likely includes structures from the welwitindolinone's families (including the substituent on C11), possibly leading to overestimation of the synthesizability of related compounds.

2.7 SYNTHESIS OF BATRACHOTOXIN

(–)-Batrachotoxin (**95**), a steroidal alkaloid first isolated from the skins of *Phyllobates* poison-dart frogs in Colombia[76], is one of the most toxic materials known to mankind (LD_{50} = 2 μg/kg) due to its ability to alter the function of voltage-gated sodium channels (Na_V).[77] As full antagonist of Na_V, it leads to a hyperpolarized shift in the voltage dependence and inhibits inactivation of the channel.[78–80] Structure-activity studies of **95** could help guide the design of small molecule modulators of Na_V, however the world-wide supply in 2009 was less than 170 mg and many syntheses were too lengthy to readily supply (–)-Batrachotoxin and derivatives (> 45 linear steps).[81]

Figure 2.22: Schematic route to Batrachotoxin.

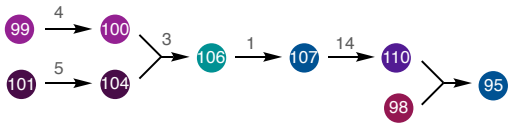

In 2016, Du Bois and coworkers reported a concise total synthesis of (–)-batrachotoxin. Their strategy applied a convergent assembly of the steroid-like core by disconnecting the central C ring into two fragments (Figure 2.23A). This topological simplification allowed the authors to identify alkenyl bromide **104** and methylenecyclopentenone **100**, which were envisioned to be coupled through an 1,2 addition and subsequent radical cascade. Enone **100** was synthesized in 5 steps from known chiral building block **99**, which can be obtained in high optical purity through lipase-mediated kinetic resolution of the corresponding unprotected secondary alcohol (Figure 2.23B). Fragment **104** was accessed in 5 linear steps from (*S*)-(+)-Hajos-Parrish ketone following a modified route developed by Parsons and coworkers (Figure 2.23C).[82]

The fragment coupling was initiated by Li-Br exchange of vinyl bromide **104** with *t*-BuLi and sequential addition of enone **100** to afford the 1,2-addition product in 65% yield as a single diastereomer (Figure 2.24). Initial attempts using *n*-BuLi furnished the desired product in low yield (<30%) due to competing α-deprotonation of **100**. *In situ* generation of LiBr enabled reproducible access to the coupling product on multi-gram scale. Alkyne desilylation and treatment of the resulting alcohol with alkynylsilyl chloride **105** furnished silylether **106** in 46% yield over three steps. The radical cyclization was initiated with *n*-

Bu_3SnH and Et_3B at 150 °C resulting in exclusive but unexpected formation of allylstannane **107** in 75% yield. The reaction is believed to proceed by initial *6-endo*-trig ring closure followed by 1,4-H atom transfer of an intermediate vinyl radical, which completed the tetracyclic steroid core of the natural product.

Figure 2.23: Du Bois' total synthesis of (–)-batrachotoxin (**95**). (A) Retrosynthetic analysis of **95**. Preparation of fragments (B) **100** and (C) **104**.

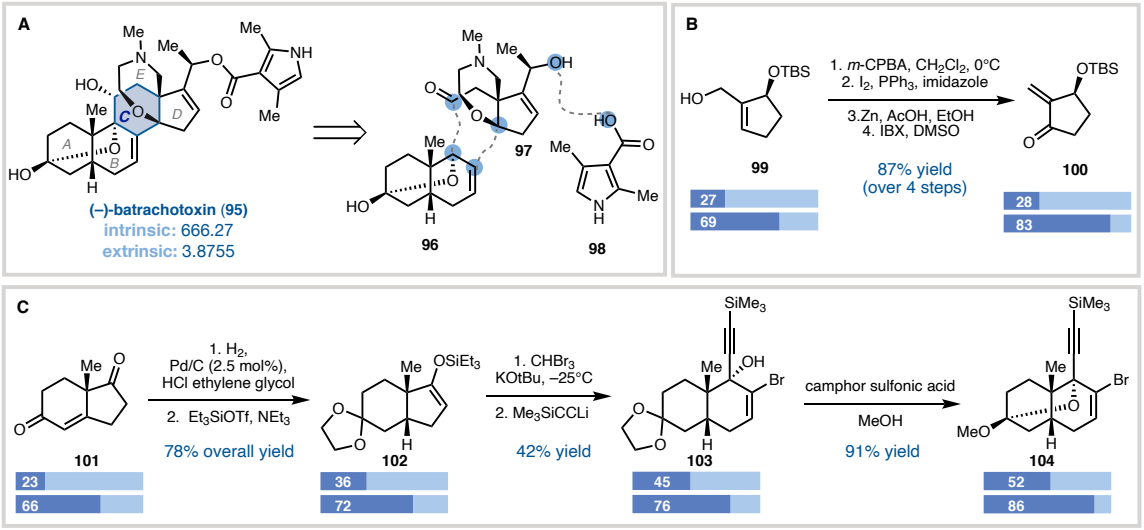

From there, a three-step sequence of bridging silyl ether excision, vinylsilane cleavage, and reductive amination gave chloroacetamide **108**. Base-mediated ring closure (NaOEt, 92% yield) installed the homo-morpholinamide ring E. Protodestannylation and alkene cleavage were unsuccessful, but an unprecedented oxidation of the stannane with $CuCl_2$ and O_2 gave an aldehyde, which could be converted in the desired ketone in 4 steps. Protecting group interconversions, installation of the methyl ketone and global reduction gave (–)-batrachotoxin A **110** and (–)-batrachotoxin **95** after esterification. The synthesis of (–)-batrachotoxin was completed in 0.25 % overall yield and 24 steps from (*S*)-(+)-

Hajos-Parrish ketone.

Du Bois' synthesis reiterates two lessons: First, step counts alone can be misleading if used to track (intrinsic) complexity. Second, bridged systems often require adjustments to the "ideal" fragments to facilitate the coupling and therefore require more steps after the coupling. While both fragments are accessed in the same number of steps, and their extrinsic complexities are comparable (83% vs 86%), their size and intrinsic complexities differ (28% vs 52%) drastically.

Figure 2.24: Completion of the synthesis of **95**.

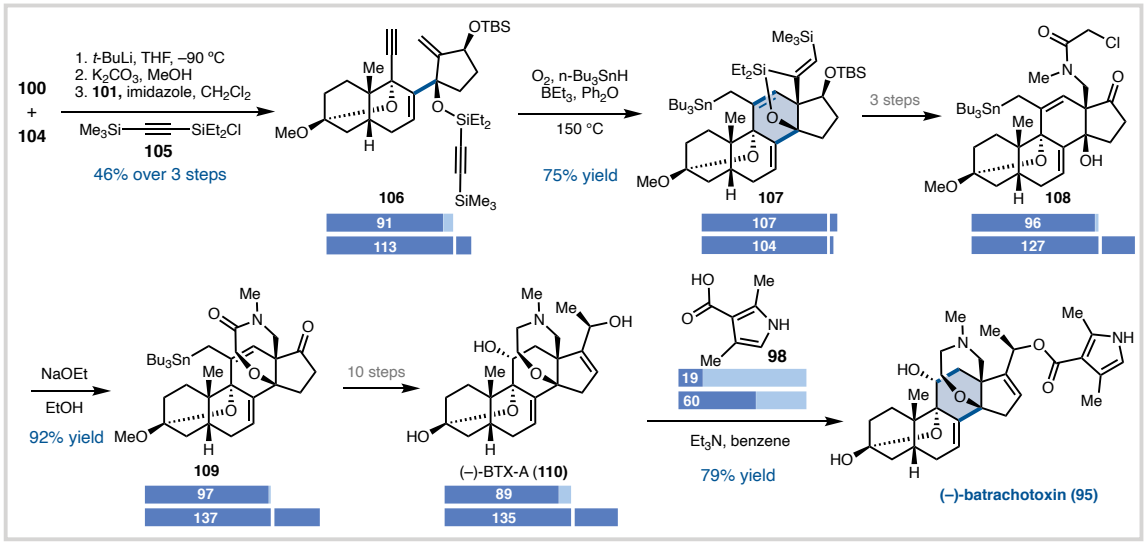

As the chosen extrinsic complexity metric is determined by a model's prediction of the step count, it is not surprising that both scores (and step counts) are similar, however the large difference in intrinsic complexity hints at a common dilemma: step counts are highly dependent on the availability of complex starting materials. As the western fragment maps onto (*S*)-(+)-Hajos-Parrish ketone, the functionalized, bridged tricyle **104** can be

accessed in only 5 steps.

Surprisingly, the route to "simple" cyclopentanone fragment **100** is of similar length and proceeds with similar changes in extrinsic complexity. This is in contrast with the almost threefold difference between the intrinsic and extrinsic score of the enone fragment, which foreshadows that the simple fragment is likely to require substantial synthetic effort. Indeed, while the entire carbon skeleton is present in the starting martial, extensive refunctionalization is required; however, this does not result in a gain of intrinsic complexity (27% in the starting material to 28% in the fragment). As discussed in the synthesis of haperforin G, equal step counts increase the synthetic utility, however maximum convergence requires balancing demands of required steps and desired fragment complexity. Multiple considerations could have factored in the selection of enone **96** as coupling partner: First, it was recognized that a higher degree of convergency (i.e., late stage coupling of pyrrole **98**) enables access to batrachotoxin A as well as batrachotoxin and prevents potential incompatibility during the installation of the homo-morpholinamide. Second, realization of the conceptual fragment coupling shown in Fig, 7A is improbable, and simplification of the fragments is most likely required. Strategic disconnection of bridging rings (if present) can simplify the fragment synthesis and coupling step. Comparison of the fused and bridged natural products discussed in this review indicates, that bridged compounds typically require more post-coupling modification steps; in Du Bois' approach installation of the homo-morpholinamide ring and additional adjustments require 14 steps to complete the carbocyclic framework. Despite an incomplete carbon skeleton, intrinsic and extrinsic complexities remain consistently high during the endgame. For example, removal of the extra methylene group of the stannane, a relic of the radical

cyclization, required multiple steps but constitutes in an overall complexity loss (less atoms). Despite these challenges, the strategy nearly cut in half the previously shortest step count and enabled the milligram-scale preparation of (–)-**95**, its non-natural enantiomer (+)-**95**, and multiple analogues. Facilitated by their synthesis, electrophysiological characterization against Na_V subtypes established the non-natural toxin enantiomer as a reversible antagonist of channel function, while mutagenesis experiments suggest a shared binding state for the enantiomers in the inner pore cavity of Na_V.

2.8 SYNTHESIS OF PERSEANOL

Retrosynthetic disconnection into two complex fragments can be challenging for natural products featuring highly caged skeletons. In these cases, one or more carbocyclic rings or other skeletal bonds must first be disconnected to enable convergent annulation of a central ring. Alternatively, the cyclization step can be used to establish more than one ring to rapidly build complexity in the key sequence. A prime example of a synthesis that addresses the challenges of a caged synthetic target while achieving convergency is the Reisman synthesis of the isoryanodane diterpene perseanol.[83]

Figure 2.25: Schematic route to Perseanol.

(+)-Perseanol (**111**), isolated in 1996 from tropical shrub *Persea indica*,[84] bears a central 5/6/5 carbocycle that is further decorated with nine stereogenic centers, including six free hydroxyl groups; a seven-membered bridging lactol and bridging E ring complete the skeleton. Two approaches to isoryanodane diterpenes have been reported,[85] including a 16-step convergent synthesis of **111** from the Reisman group in 2019.

Figure 2.26: Retrosynthetic analysis of (+)-perseanol (**111**).

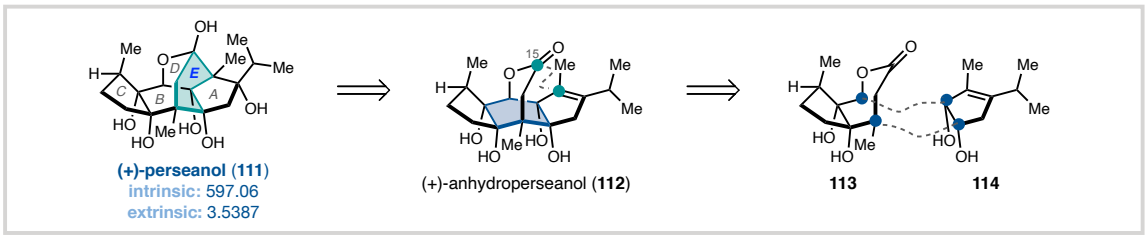

To render the highly caged pentacyclic skeleton of perseanol amenable to a convergent synthetic approach, Reisman and coworkers envisioned **111** arising from a simplified precursor, anhydroperseanol (**112**, Figure 2.26). Inspired by a similar, successful approach to the related natural product, (+)-ryanodol,[86] reductive cyclization was anticipated to form the E ring at a late stage. In turn, the B ring central to tetracycle **112** could be established via convergent annulation of hypothetical fragments **113** and **114**. In practice, the authors found a less-complex, monocyclic C-ring fragment (**118**) to be suitable for coupling to similarly-complex A-ring fragment **121**. A complexity-generating cascade reaction was envisioned to generate the bridging 7-membered lactone, both B and D rings could be simultaneously set.

To deploy this strategy, the two requisite fragments were each prepared in six steps.

Enantiopure enal **118** was derived from (*R*)-(+)-pulegone (**115**, Figure 2.27A); following ring contraction, stereoselective α-oxidation then epoxide rearrangement set in place the B/C ring fusion diol prior to annulation. Subsequent benzylidene formation and a reduction/oxidation sequence furnished fully elaborated fragment **118**, which could be accessed on gram-scale.

Figure 2.27: Preparation of fragments (A) **118** and (B) **121**.

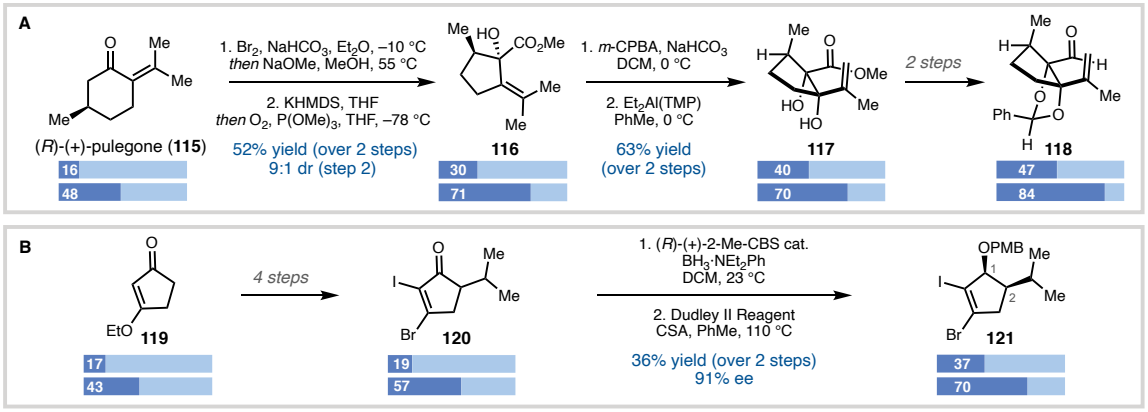

For bifunctional precursor **121**, the presence of the alkenyl halide moiety required for the chosen coupling/cyclization reactions necessitated installation of the vicinal diol at the A/B ring fusion *after* attachment of fragment **118** (Figure 2.27B). In addition, the methyl group found in the A-ring of the natural product was strategically omitted from the fragment to facilitate enantioenrichment of **121** via kinetic resolution. Alkylation and iodination of vinylogous ester **119**, was followed by regioselective installation of the alkenyl bromide after reveal of the diketone moiety; differentiation of the carbonyls proceeded via bromination of the enol tautomer distal to the isopropyl group upon treatment with oxalyl chloride in DMF. Finally, kinetic resolution via Corey-Bakshi-

Shibata reduction – strategically placed late in the synthesis to avoid racemization – and protection gave the desired enantioenriched C-ring fragment. To effect the fragment coupling step, selective lithiation of vicinal dihalide **121** was followed by 1,2-addition into aldehyde **118** to give alcohol **122** with 3.2:1 dr. Completion of the two-step annulation sequence via a carbopalladation/carbonylation cascade simultaneously established two rings and the all-carbon quaternary center of the tetracyclic core of perseanol (Figure 2.28A).

Figure 2.28: (A) Convergent annulation sequence and (B) completion of the synthesis.

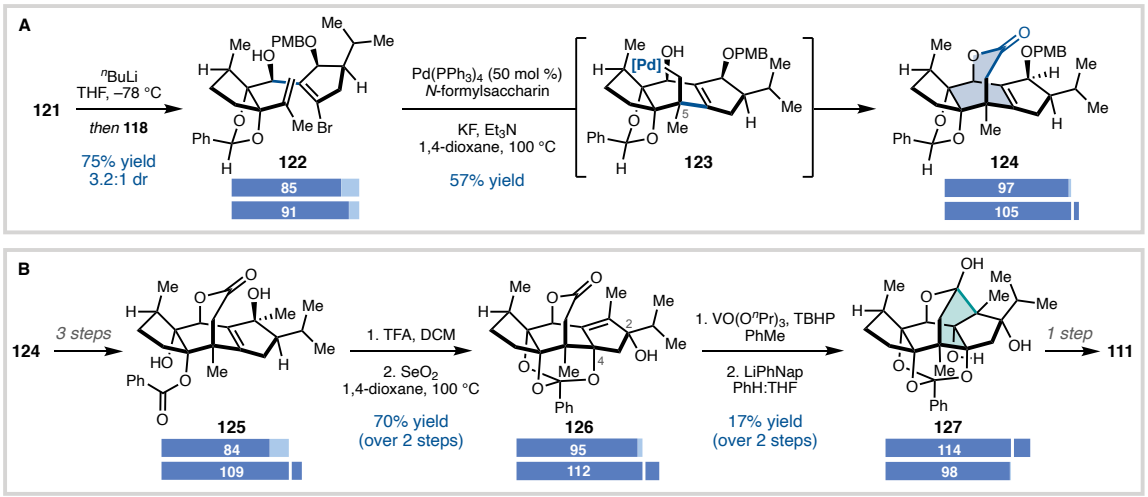

Reisman and coworkers hypothesized that following oxidative addition of alkenyl bromide **122**, regioselective 6-*exo*-trig cyclization would furnish alkyl–Pd intermediate **123**. Unable to undergo β-hydride elimination, **123** could instead engage CO in migratory insertion. Intramolecular trapping with the pendant alcohol would then afford the C–O bond of lactone **124**. Indeed, extensive optimization revealed that $Pd(PPh_3)_4$ in the presence

of triethylamine gave rise to annulated product **124** in 57% yield upon treatment of **122** with *N*-formylsaccharin and KF, which presumably serves to generate CO at a controlled rate, minimizing catalyst deactivation by CO. The endgame of the synthesis proceeded via refunctionalization of **124** (Figure 2.28B). Unexpected assistance of the benzylidene acetal protecting group on C4 alcohol installation, as well as stereospecific allylic oxidation at C2, served to increase the efficiency of late-stage functional group manipulations. Final epoxidation introduced the remaining hydroxyl group after reductive closure of the E ring, furnishing (+)-perseanol.

The carbopalladation-carbonylation annulation sequence employed in Reisman's approach highlights the power of cascade reactions for the convergent synthesis bridged natural products. The intrinsic complexity of the fragments is conserved through the initial coupling of the fragments via 1,2 addition. The fragments are thoughtfully designed to enable the subsequent annulation of the two rings of the bridging ring system of perseanol: Initial 6-*exo*-trig cyclization completes the central B ring, and subsequent carbonylation of the alkyl-Palladium intermediate forges the bridging D ring. The closure of the central lactone is highly efficient, adding a 1-C fragment and forming 2 C-C bonds while obtaining control over the quaternary center at C5. As expected, this leads to a jump in the complexity scores; The intrinsic complexity increases by 12%, while the extrinsic complexity does by 14%. In contrast to the previously discussed synthesis of Batrachotoxin, the formed bridging ring does not need to be refunctionalized and is set up to for facile formation of the E ring. While the endgame sequence must still address methylation and redox adjustments of the A ring, it can be kept relatively concise. While the complexity score remains mainly constant or decreases after the removal of large protecting groups (for the

intrinsic complexity), the intrinsic complexity increases by 19% during the final epoxidation/annulation sequence to close the E ring highlighting the strategic benefit of the endgame. While highly caged structures bring synthetic challenges, high functional group density can also be an opportunity for complexity-generating cascades reactions.

2.9 CONCLUDING REMARKS

In conclusion, convergent fragment couplings provide a powerful strategy for the synthesis of a variety of complex molecules by streamlining synthetic routes. Complexity metrics can help quantifying otherwise subjective observations; together with expert knowledge, they can also be used to reveal hidden lessons and guide the design of new routes. While there is no single 'ideal' complexity index, that can measure the (synthetically relevant) complexity perfectly, establishing quantifiable metrics becomes more important as synthetic organic chemistry continues to incorporate *in silico* methods in their toolbox. Advances in determining synthetic accessibilities could help bridge the gap between an experienced chemist's assessment and the 'naïve' approach current retrosynthetic algorithms often fall into. In this review, we aimed to discuss relevant syntheses of the last 10 years with the help of current complexity metrics and highlight the power of the convergent approach. The various lessons that can be learned for the approach of structurally divers targets are inspiration and guidance to drive the exploration of new, powerful strategies that can continue to innovate natural product synthesis.

2.10 NOTES AND REFERENCES

(1) Hendrickson, J. B. Systematic Synthesis Design. 6. Yield Analysis and Convergency. *J. Am. Chem. Soc.* **1977**, *99* (16), 5439–5450.
(2) Hsu, I. T.; Tomanik, M.; Herzon, S. B. Metric-Based Analysis of Convergence in Complex Molecule Synthesis. *Acc. Chem. Res.* **2021**, *54* (4), 903–916.
(3) Gao, Y.; Ma, D. In Pursuit of Synthetic Efficiency: Convergent Approaches. *Acc. Chem. Res.* **2021**, *54* (3), 569–582.
(4) Urabe, D.; Asaba, T.; Inoue, M. Convergent Strategies in Total Syntheses of Complex Terpenoids. *Chem. Rev.* **2015**, *115* (17), 9207–9231.
(5) Hill, N.; Paruch, K.; Švenda, J. Late-Stage Annulative Convergency in Natural Product Synthesis. *Tetrahedron* **2016**, *72* (24), 3345–3368.
(6) Tomanik, M.; Hsu, I. T.; Herzon, S. B. Fragment Coupling Reactions in Total Synthesis That Form Carbon–Carbon Bonds via Carbanionic or Free Radical Intermediates. *Angew. Chem. Int. Ed.* **2021**, *60* (3), 1116–1150.
(7) Li, J.; Eastgate, M. D. Current Complexity: A Tool for Assessing the Complexity of Organic Molecules. *Org. Biomol. Chem.* **2015**, *13* (26), 7164–7176.
(8) Bertz, S. H. Complexity of Synthetic Routes: Linear, Convergent and Reflexive Syntheses. *New J. Chem.* **2003**, *27* (5), 870–879.
(9) Bertz, S. H. Convergence, Molecular Complexity, and Synthetic Analysis. *J. Am. Chem. Soc.* **1982**, *104* (21), 5801–5803.
(10) Bertz, S. H. The First General Index of Molecular Complexity. *J. Am. Chem. Soc.* **1981**, *103* (12), 3599–3601.
(11) Hosoya, H. Topological Index. A Newly Proposed Quantity Characterizing the Topological Nature of Structural Isomers of Saturated Hydrocarbons. *Bull. Chem. Soc. Jpn.* **1971**, *44* (9), 2332–2339.
(12) Randic, M. Characterization of Molecular Branching. *J. Am. Chem. Soc.* **1975**, *97* (23), 6609–6615.
(13) Paton, R.; Lunchini, G.; Sowndarya Santhanalakkshmi Vejaykummar, S. Patonlab/Molcomplex.
(14) Woodward, R. B.; Cava, M. P.; Ollis, W. D.; Hunger, A.; Daeniker, H. U.; Schenker, K. THE TOTAL SYNTHESIS OF STRYCHNINE. *J. Am. Chem. Soc.* **1954**, *76* (18), 4749–4751.
(15) Jones, S. B.; Simmons, B.; Mastracchio, A.; MacMillan, D. W. C. Collective Synthesis of Natural Products by Means of Organocascade Catalysis. *Nature* **2011**, *475* (7355), 183–188.
(16) Böttcher, T. An Additive Definition of Molecular Complexity. *J. Chem. Inf. Model.* **2016**, *56* (3), 462–470.
(17) Coley, C. W.; Rogers, L.; Green, W. H.; Jensen, K. F. SCScore: Synthetic Complexity Learned from a Reaction Corpus. *J. Chem. Inf. Model.* **2018**, *58* (2), 252–261.
(18) Powis, G.; Bonjouklian, R.; Berggren, M. M.; Gallegos, A.; Abraham, R.; Ashendel, C.; Zalkow, L.; Matter, W. F.; Dodge, J.; Grindey, G. Wortmannin, a Potent and Selective Inhibitor of Phosphatidylinositol-3-Kinase. *Cancer Res.* **1994**, *54* (9), 2419–2423.

(19) Yano, H.; Nakanishi, S.; Kimura, K.; Hanai, N.; Saitoh, Y.; Fukui, Y.; Nonomura, Y.; Matsuda, Y. Inhibition of Histamine Secretion by Wortmannin through the Blockade of Phosphatidylinositol 3-Kinase in RBL-2H3 Cells. *J. Biol. Chem.* **1993**, *268* (34), 25846–25856.
(20) Arcaro, A.; Wymann, M. P. Wortmannin Is a Potent Phosphatidylinositol 3-Kinase Inhibitor: The Role of Phosphatidylinositol 3,4,5-Trisphosphate in Neutrophil Responses. *Biochem. J.* **1993**, *296* (Pt 2), 297–301.
(21) Wipf, P.; Halter, R. J. Chemistry and Biology of Wortmannin. *Org. Biomol. Chem.* **2005**, *3* (11), 2053–2061.
(22) Creemer, L. C.; Kirst, H. A.; Vlahos, C. J.; Schultz, R. M. Synthesis and in Vitro Evaluation of New Wortmannin Esters: Potent Inhibitors of Phosphatidylinositol 3-Kinase. *J. Med. Chem.* **1996**, *39* (25), 5021–5024.
(23) Norman, B. H.; Shih, C.; Toth, J. E.; Ray, J. E.; Dodge, J. A.; Johnson, D. W.; Rutherford, P. G.; Schultz, R. M.; Worzalla, J. F.; Vlahos, C. J. Studies on the Mechanism of Phosphatidylinositol 3-Kinase Inhibition by Wortmannin and Related Analogs. *J. Med. Chem.* **1996**, *39* (5), 1106–1111.
(24) Anderson, E. A.; Alexanian, E. J.; Sorensen, E. J. Synthesis of the Furanosteroidal Antibiotic Viridin. *Angew. Chem. Int. Ed Engl.* **2004**, *43* (15), 1998–2001.
(25) *Rubriflordilactones A and B, Two Novel Bisnortriterpenoids from Schisandra rubriflora and Their Biological Activities | Organic Letters*.
(26) Xia, Y.-G.; Yang, B.-Y.; Kuang, H.-X. Schisandraceae Triterpenoids: A Review. *Phytochem. Rev.* **2015**, *14* (2), 155–187.
(27) Xiao, W.-L.; Li, R.-T.; Huang, S.-X.; Pu, J.-X.; Sun, H.-D. Triterpenoids from the Schisandraceae Family. *Nat. Prod. Rep.* **2008**, *25* (5), 871–891.
(28) Xiao, Q.; Ren, W.-W.; Chen, Z.-X.; Sun, T.-W.; Li, Y.; Ye, Q.-D.; Gong, J.-X.; Meng, F.-K.; You, L.; Liu, Y.-F.; Zhao, M.-Z.; Xu, L.-M.; Shan, Z.-H.; Shi, Y.; Tang, Y.-F.; Chen, J.-H.; Yang, Z. Diastereoselective Total Synthesis of (±)-Schindilactone A. *Angew. Chem. Int. Ed.* **2011**, *50* (32), 7373–7377.
(29) Li, J.; Yang, P.; Yao, M.; Deng, J.; Li, A. Total Synthesis of Rubriflordilactone A. *J. Am. Chem. Soc.* **2014**, *136* (47), 16477–16480.
(30) Jurczyk, J.; Woo, J.; Kim, S. F.; Dherange, B. D.; Sarpong, R.; Levin, M. D. Single-Atom Logic for Heterocycle Editing. *Nat. Synth.* **2022**, *1* (5), 352–364.
(31) Hui, C.; Wang, Z.; Wang, S.; Xu, C. Molecular Editing in Natural Product Synthesis. *Org. Chem. Front.* **2022**, *9* (5), 1451–1457.
(32) Schuppe, A. W.; Zhao, Y.; Liu, Y.; Newhouse, T. R. Total Synthesis of (+)-Granatumine A and Related Bislactone Limonoid Alkaloids via a Pyran to Pyridine Interconversion. *J. Am. Chem. Soc.* **2019**, *141* (23), 9191–9196.
(33) Zhou, Z.-F.; Liu, H.-L.; Zhang, W.; Kurtán, T.; Mándi, A.; Bényei, A.; Li, J.; Taglialatela-Scafati, O.; Guo, Y.-W. Bioactive Rearranged Limonoids from the Chinese Mangrove *Xylocarpus Granatum* Koenig. *Tetrahedron* **2014**, *70* (37), 6444–6449.
(34) Zhang, S.; Zhang, Z.-Y. PTP1B as a Drug Target: Recent Developments in PTP1B Inhibitor Discovery. *Drug Discov. Today* **2007**, *12* (9–10), 373–381.

(35) Schuppe, A. W.; Huang, D.; Chen, Y.; Newhouse, T. R. Total Synthesis of (−)-Xylogranatopyridine B via a Palladium-Catalyzed Oxidative Stannylation of Enones. *J. Am. Chem. Soc.* **2018**, *140* (6), 2062–2066.
(36) Schuppe, A. W.; Liu, Y.; Gonzalez-Hurtado, E.; Zhao, Y.; Jiang, X.; Ibarraran, S.; Huang, D.; Wang, X.; Lee, J.; Loria, J. P.; Dixit, V. D.; Li, X.; Newhouse, T. R. Unified Total Synthesis of the Limonoid Alkaloids: Strategies for the de Novo Synthesis of Highly Substituted Pyridine Scaffolds. *Chem* **2022**, *8* (10), 2856–2887.
(37) Chen, Y.; Huang, D.; Zhao, Y.; Newhouse, T. R. Allyl-Palladium-Catalyzed Ketone Dehydrogenation Enables Telescoping with Enone α,β-Vicinal Difunctionalization. *Angew. Chem. Int. Ed.* **2017**, *56* (28), 8258–8262.
(38) Khuong-Huu, Q.; Chiaroni, A.; Riche, C.; Nguyen-Ngoc, H.; Nguyen-Viet, K.; Khuong-Huu, F. New Rearranged Limonoids from Harrisonia Perforata. III. *J. Nat. Prod.* **2001**, *64* (5), 634–637.
(39) Yan, X.-H.; Yi, P.; Cao, P.; Yang, S.-Y.; Fang, X.; Zhang, Y.; Bin Wu; Leng, Y.; Di, Y.-T.; Lv, Y.; Hao, X.-J. 16-nor Limonoids from Harrisonia Perforata as Promising Selective 11β-HSD1 Inhibitors. *Sci. Rep.* **2016**, *6* (1), 36927.
(40) *Medicinal Chemistry of Inhibitors of 11β-Hydroxysteroid Dehydrogenase Type 1 (11β-HSD1) | Journal of Medicinal Chemistry*.
(41) Stivala, C. E.; Zakarian, A. Highly Enantioselective Direct Alkylation of Arylacetic Acids with Chiral Lithium Amides as Traceless Auxiliaries. *J. Am. Chem. Soc.* **2011**, *133* (31), 11936–11939.
(42) Nugent, W. A. MIB: An Advantageous Alternative to DAIB for the Addition of Organozinc Reagents to Aldehydes. *Chem. Commun.* **1999**, No. 15, 1369–1370.
(43) Zhang, X.; Smith, C. D. Microtubule Effects of Welwistatin, a Cyanobacterial Indolinone That Circumvents Multiple Drug Resistance. *Mol. Pharmacol.* **1996**, *49* (2), 288.
(44) Smith, C. D.; Zilfou, J. T.; Stratmann, K.; Patterson, G. M.; Moore, R. E. Welwitindolinone Analogues That Reverse P-Glycoprotein-Mediated Multiple Drug Resistance. *Mol. Pharmacol.* **1995**, *47* (2), 241.
(45) Konopelski, J. P.; Deng, H.; Schiemann, K.; Keane, J. M.; Olmstead, M. M. Stereoselective Conjugate Addition Directed by an Enantiomerically Pure Ketal. Preparation of the Cyclohexanone Fragment of N-Methylwelwitindolinone C Isothiocyanate. *Synlett* **2000**, *1998*, 1105–1107.
(46) Wood, J. L.; Holubec, A. A.; Stoltz, B. M.; Weiss, M. M.; Dixon, J. A.; Doan, B. D.; Shamji, M. F.; Chen, J. M.; Heffron, T. P. Application of Reactive Enols in Synthesis: A Versatile, Efficient, and Stereoselective Construction of the Welwitindolinone Carbon Skeleton. *J. Am. Chem. Soc.* **1999**, *121* (26), 6326–6327.
(47) Deng, H.; Konopelski, J. P. Aryllead(IV) Reagents in Synthesis: Formation of the C11 Quaternary Center of N-Methylwelwitindolinone C Isothiocyanate. *Org. Lett.* **2001**, *3* (19), 3001–3004.
(48) Kaoudi, T.; Quiclet-Sire, B.; Seguin, S.; Zard, S. Z. An Expedient Construction of Seven-Membered Rings Adjoining Aromatic Systems. *Angew. Chem.* **2000**, *112* (4), 747–749.

(49) Jung, M. E.; Slowinski, F. Rhodium-Catalyzed Decomposition of Indole-Substituted α-Diazo-β-Keto Esters: Three Different Reactions Based on Indole Oxidation State. *Tetrahedron Lett.* **2001**, *42* (39), 6835–6838.
(50) López-Alvarado, P.; García-Granda, S.; Álvarez-Rúa, C.; Avendaño, C. Controlled Generation of Three Contiguous Stereocentres in the Michael Addition of 1-Pyrrolidinocyclohexene to (E)-(1-Methyl-2-Oxoindolin-3-Ylidene)Acetophenone. *Eur. J. Org. Chem.* **2002**, *2002* (10), 1702–1707.
(51) Ready, J. M.; Reisman, S. E.; Hirata, M.; Weiss, M. M.; Ovaska, T. V.; Wood, J. L. A Mild and Efficient Synthesis of Oxindoles: Progress Toward the Synthesis of Welwitindolinone A Isonitrile.
(52) MacKay, J. A.; Bishop, R. L.; Rawal, V. H. Rapid Synthesis of the N-Methylwelwitindolinone Skeleton. *Org. Lett.* **2005**, *7* (16), 3421–3424.
(53) Greshock, T. J.; Funk, R. L. An Approach to the Total Synthesis of Welwistatin. *Org. Lett.* **2006**, *8* (12), 2643–2645.
(54) Lauchli, R.; Shea, K. J. A Synthesis of the Welwistatin Core. *Org. Lett.* **2006**, *8* (23), 5287–5289.
(55) Xia, J.; Brown, L. E.; Konopelski, J. P. Welwistatin Support Studies: Expansion and Limitation of Aryllead(IV) Coupling Reactions. *J. Org. Chem.* **2007**, *72* (18), 6885–6890.
(56) Richter, J. M.; Ishihara, Y.; Masuda, T.; Whitefield, B. W.; Llamas, T.; Pohjakallio, A.; Baran, P. S. Enantiospecific Total Synthesis of the Hapalindoles, Fischerindoles, and Welwitindolinones via a Redox Economic Approach. *J. Am. Chem. Soc.* **2008**, *130* (52), 17938–17954.
(57) Boissel, V.; S. Simpkins, N.; Bhalay, G.; J. Blake, A.; Lewis, W. Bridgehead Enolates and Bridgehead Alkenes in a Welwistatin Model Series. *Chem. Commun.* **2009**, *0* (11), 1398–1400.
(58) Tian, X.; Huters, A. D.; Douglas, C. J.; Garg, N. K. Concise Synthesis of the Bicyclic Scaffold of N-Methylwelwitindolinone C Isothiocyanate via an Indolyne Cyclization. *Org. Lett.* **2009**, *11* (11), 2349–2351.
(59) Trost, B. M.; McDougall, P. J. Access to a Welwitindolinone Core Using Sequential Cycloadditions. *Org. Lett.* **2009**, *11* (16), 3782–3785.
(60) Brailsford, J. A.; Lauchli, R.; Shea, K. J. Synthesis of the Bicyclic Welwitindolinone Core via an Alkylation/Cyclization Cascade Reaction. *Org. Lett.* **2009**, *11* (22), 5330–5333.
(61) Freeman, D. B.; Holubec, A. A.; Weiss, M. W.; Dixon, J. A.; Kakefuda, A.; Ohtsuka, M.; Inoue, M.; Vaswani, R. G.; Ohki, H.; Doan, B. D.; Reisman, S. E.; Stoltz, B. M.; Day, J. J.; Tao, R. N.; Dieterich, N. A.; Wood, J. L. Welwitindolinone C Synthetic Studies. Construction of the Welwitindolinone Carbon Skeleton via a Transannular Nitrone Cycloaddition. *Tetrahedron* **2010**, *66* (33), 6647–6655.
(62) Heidebrecht, R. W. Jr.; Gulledge, B.; Martin, S. F. Approaches to N-Methylwelwitindolinone C Isothiocyanate: Facile Synthesis of the Tetracyclic Core. *Org. Lett.* **2010**, *12* (11), 2492–2495.
(63) Ruiz, M.; López-Alvarado, P.; Carlos Menéndez, J. Concise and Very Efficient Synthesis of the N -Methylwelwistatin Tetracyclic Core Based on an Anionic Domino Process. *Org. Biomol. Chem.* **2010**, *8* (20), 4521–4523.

(64) Baran, P. S.; Richter, J. M. Enantioselective Total Syntheses of Welwitindolinone A and Fischerindoles I and G. *J. Am. Chem. Soc.* **2005**, *127* (44), 15394–15396.
(65) Reisman, S. E.; Ready, J. M.; Hasuoka, A.; Smith, C. J.; Wood, J. L. Total Synthesis of (±)-Welwitindolinone A Isonitrile. *J. Am. Chem. Soc.* **2006**, *128* (5), 1448–1449.
(66) Huters, A. D.; Quasdorf, K. W.; Styduhar, E. D.; Garg, N. K. Total Synthesis of (−)-N-Methylwelwitindolinone C Isothiocyanate. *J. Am. Chem. Soc.* **2011**, *133* (40), 15797–15799.
(67) Huters, A. D.; Styduhar, E. D.; Garg, N. K. Total Syntheses of the Elusive Welwitindolinones with Bicyclo[4.3.1] Cores. *Angew. Chem. Int. Ed.* **2012**, *51* (16), 3758–3765.
(68) Fu, T.; McElroy, W. T.; Shamszad, M.; Martin, S. F. Formal Syntheses of Naturally Occurring Welwitindolinones. *Org. Lett.* **2012**, *14* (15), 3834–3837.
(69) Cleary, L.; Pitzen, J.; Brailsford, J. A.; Shea, K. J. Progress toward the Total Synthesis of N-Methylwelwitindolinone B Isothiocyanate. *Org. Lett.* **2014**, *16* (17), 4460–4463.
(70) Fu, T.; McElroy, W. T.; Shamszad, M.; Heidebrecht, R. W.; Gulledge, B.; Martin, S. F. Studies toward Welwitindolinones: Formal Syntheses of *N*-Methylwelwitindolinone C Isothiocyanate and Related Natural Products. *Tetrahedron* **2013**, *69* (27), 5588–5603.
(71) Reyes, J. R.; Xu, J.; Kobayashi, K.; Bhat, V.; Rawal, V. H. Total Synthesis of (−)-N-Methylwelwitindolinone B Isothiocyanate. *Angew. Chem. Int. Ed.* **2017**, *56* (33), 9962–9966.
(72) Ruiz-Serrano, M.; López-Alvarado, P.; Menéndez, J. C. A New Method for the Introduction of an Acylsulfonamide Moiety Applied to a 3-Substituted Functionalized Indole Framework -Related to the Welwitindolinone Alkaloids. *Synlett* **2023**, *34*, 1920–1924.
(73) Bhat, V.; Allan, K. M.; Rawal, V. H. Total Synthesis of N-Methylwelwitindolinone D Isonitrile. *J. Am. Chem. Soc.* **2011**, *133* (15), 5798–5801.
(74) Allan, K. M.; Kobayashi, K.; Rawal, V. H. A Unified Route to the Welwitindolinone Alkaloids: Total Syntheses of (−)-N-Methylwelwitindolinone C Isothiocyanate, (−)-N-Methylwelwitindolinone C Isonitrile, and (−)-3-Hydroxy-N-Methylwelwitindolinone C Isothiocyanate. *J. Am. Chem. Soc.* **2012**, *134* (3), 1392–1395.
(75) Styduhar, E. D.; Huters, A. D.; Weires, N. A.; Garg, N. K. Enantiospecific Total Synthesis of N-Methylwelwitindolinone D Isonitrile. *Angew. Chem.* **2013**, *125* (47), 12648–12651.
(76) Märki, F.; Witkop, B. The Venom of the Colombian Arrow Poison frogPhyllobates Bicolor. *Experientia* **1963**, *19* (7), 329–338.
(77) Tokuyama, T.; Daly, J.; Witkop, B.; Karle, I. L.; Karle, J. The Structure of Batrachotoxinin A, a Novel Steroidal Alkaloid from the Columbian Arrow Poison Frog, Phyllobates Aurotaenia. *J. Am. Chem. Soc.* **1968**, *90* (7), 1917–1918.
(78) Catterall, W. A. Activation of the Action Potential Na+ Ionophore by Neurotoxins. An Allosteric Model. *J. Biol. Chem.* **1977**, *252* (23), 8669–8676.
(79) Wang, S.-Y.; Wang, G. K. Voltage-Gated Sodium Channels as Primary Targets of Diverse Lipid-Soluble Neurotoxins. *Cell. Signal.* **2003**, *15* (2), 151–159.

(80) Khodorov, B. I. Batrachotoxin as a Tool to Study Voltage-Sensitive Sodium Channels of Excitable Membranes. *Prog. Biophys. Mol. Biol.* **1985**, *45* (2), 57–148.
(81) Martin Garraffo, H.; F. Spande, T. Discovery of Batrachotoxin: The Launch of the Frog Alkaloid Program at NIH. *HETEROCYCLES* **2009**, *79* (1), 195.
(82) Lacrouts, P.; Parsons, P. J.; Penkett, C. S.; Raza, A. R. A Palladium-Assisted Ring Annulation for the Synthesis of the Batrachotoxin Ring System. *Synlett* **2005**, *2005*, 2767–2768.
(83) Han, A.; Tao, Y.; Reisman, S. E. A 16-Step Synthesis of the Isoryanodane Diterpene (+)-Perseanol. *Nature* **2019**, *573* (7775), 563–567.
(84) González-Coloma, A.; Terrero, D.; Perales, A.; Escoubas, P.; Fraga, B. M. Insect Antifeedant Ryanodane Diterpenes from Persea Indica. *J. Agric. Food Chem.* **1996**, *44* (1), 296–300.
(85) Koshimizu, M.; Nagatomo, M.; Inoue, M. Construction of a Pentacyclic Ring System of Isoryanodane Diterpenoids by SmI2-Mediated Transannular Cyclization. *Tetrahedron* **2018**, *74* (26), 3384–3390.
(86) Chuang, K. V.; Xu, C.; Reisman, S. E. A 15-Step Synthesis of (+)-Ryanodol. *Science* **2016**, *353* (6302), 912–915.

[This chapter is temporarily embargoed.]

Appendix 1

Spectra Relevant to Chapter 1:

A Pyridine Dearomatization Approach to the Matrine-Type Lupin Alkaloids

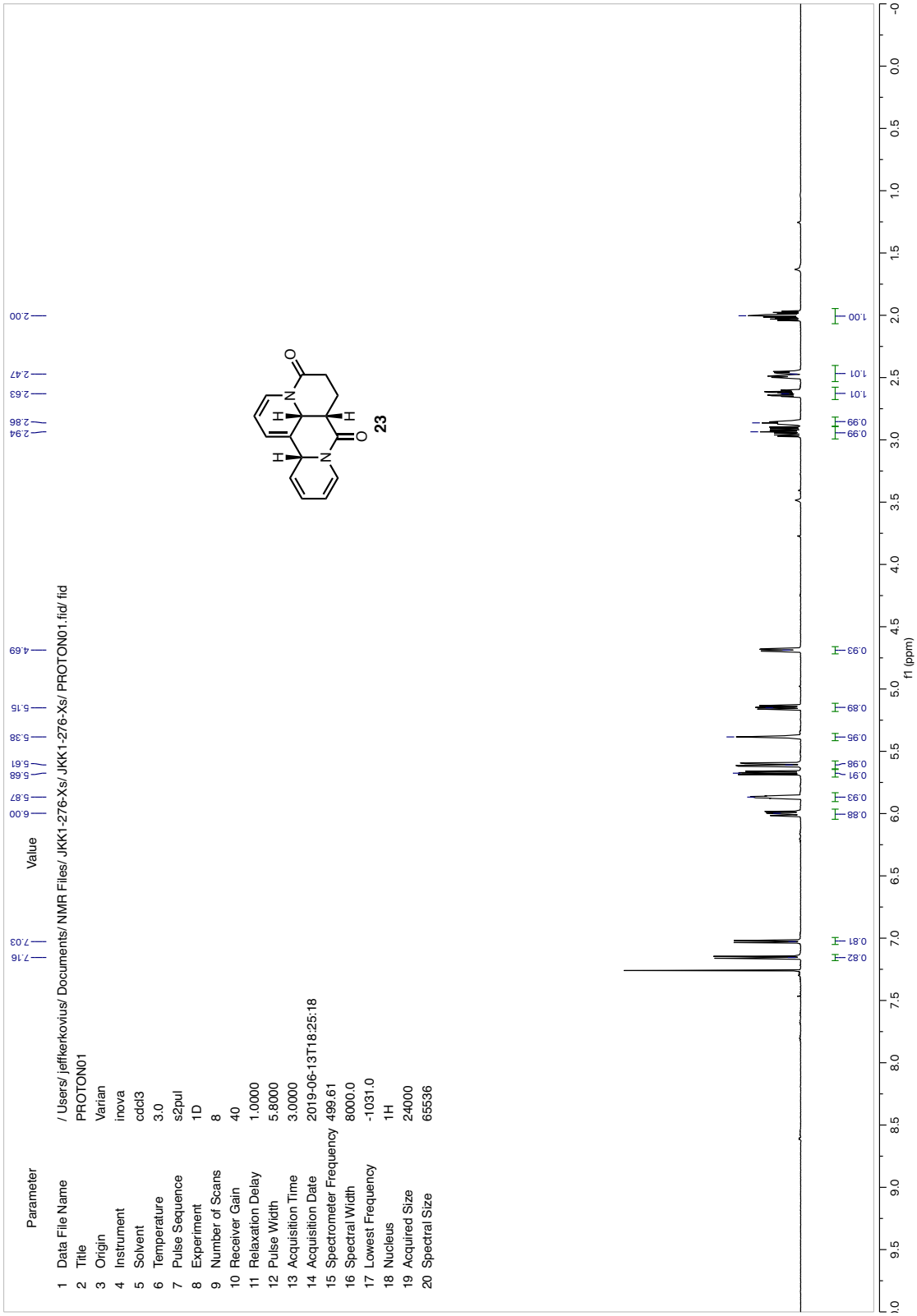
Parameter
Value
1 Data File Name / Users/ jeffkerkovius/ Documents/ NMR Files/ JKK1-276-Xs/ JKK1-276-Xs/ PROTON01.fid/ fid
2 Title PROTON01
3 Origin Varian
4 Instrument inova
5 Solvent cdcl3
6 Temperature 3.0
7 Pulse Sequence s2pul
8 Experiment 1D
9 Number of Scans 8
10 Receiver Gain 40
11 Relaxation Delay 1.0000
12 Pulse Width 5.8000
13 Acquisition Time 3.0000
14 Acquisition Date 2019-06-13T18:25:18
15 Spectrometer Frequency 499.61
16 Spectral Width 8000.0
17 Lowest Frequency -1031.0
18 Nucleus 1H
19 Acquired Size 24000
20 Spectral Size 65536
7.16
7.03
6.00
5.87
5.68
5.61
5.38
5.15
4.69
2.94
2.86
2.63
2.47
2.00
0.82
0.81
0.88
0.93
0.91
0.98
0.95
0.89
0.93
0.99
0.99
1.01
1.01
1.00
23
f1 (ppm)

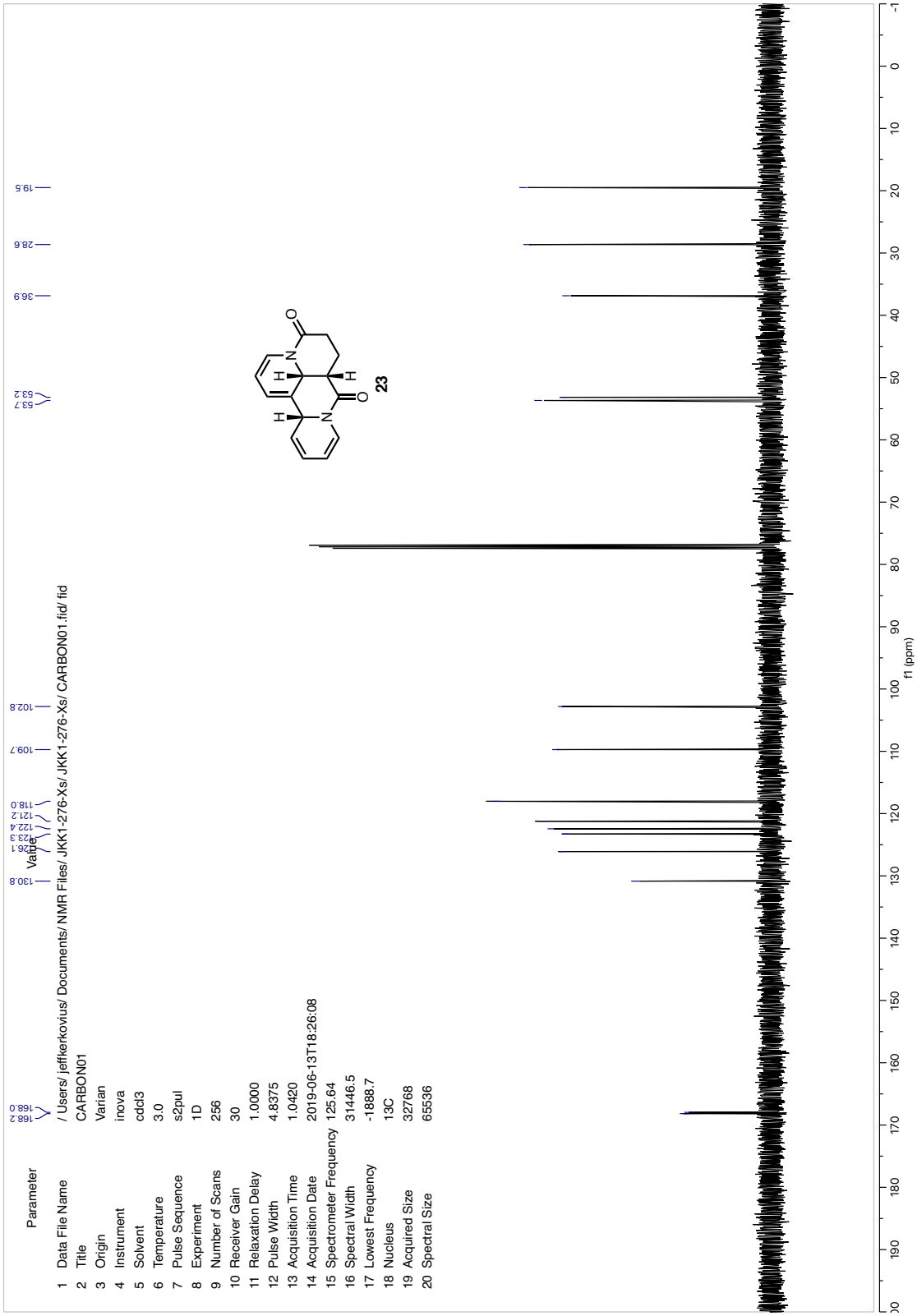
Parameter
1 Data File Name / Users/ jeffkerkovius/ Documents/ NMR Files/ JKK1-276-Xs/ JKK1-276-Xs/ CARBON01.fid/ fid
2 Title CARBON01
3 Origin Varian
4 Instrument inova
5 Solvent cdcl3
6 Temperature 3.0
7 Pulse Sequence s2pul
8 Experiment 1D
9 Number of Scans 256
10 Receiver Gain 30
11 Relaxation Delay 1.0000
12 Pulse Width 4.8375
13 Acquisition Time 1.0420
14 Acquisition Date 2019-06-13T18:26:08
15 Spectrometer Frequency 125.64
16 Spectral Width 31446.5
17 Lowest Frequency -1888.7
18 Nucleus 13C
19 Acquired Size 32768
20 Spectral Size 65536
Value
168.2
168.0
130.8
126.1
123.3
122.4
121.2
118.0
109.7
102.8
53.7
53.2
36.9
28.6
19.5
23
f1 (ppm)

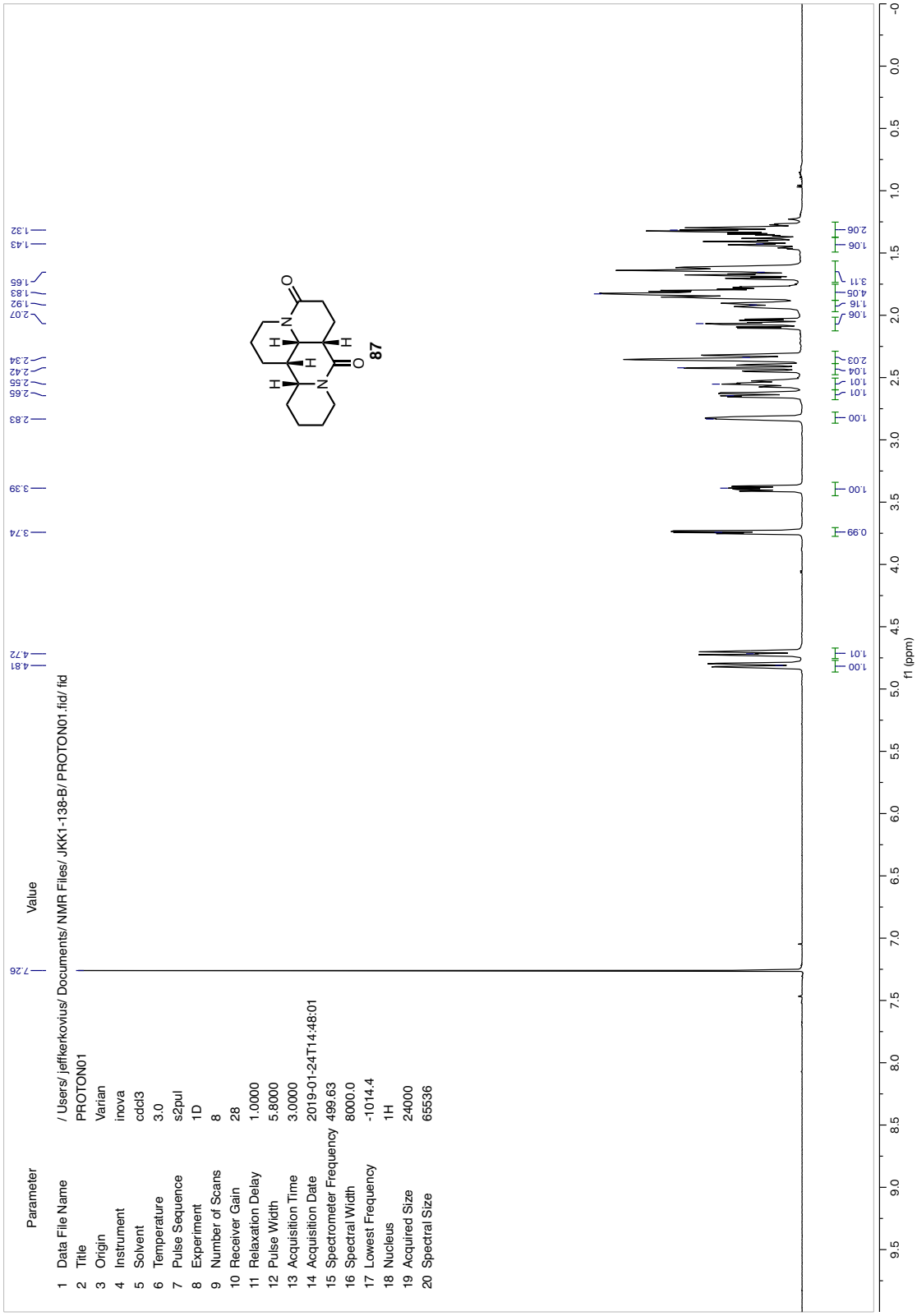
Parameter Value
1 Data File Name / Users/ jeffkerkovius/ Documents/ NMR Files/ JKK1-138-B/ PROTON01.fid/ fid
2 Title PROTON01
3 Origin Varian
4 Instrument inova
5 Solvent cdcl3
6 Temperature 3.0
7 Pulse Sequence s2pul
8 Experiment 1D
9 Number of Scans 8
10 Receiver Gain 28
11 Relaxation Delay 1.0000
12 Pulse Width 5.8000
13 Acquisition Time 3.0000
14 Acquisition Date 2019-01-24T14:48:01
15 Spectrometer Frequency 499.63
16 Spectral Width 8000.0
17 Lowest Frequency -1014.4
18 Nucleus 1H
19 Acquired Size 24000
20 Spectral Size 65536
87
f1 (ppm)

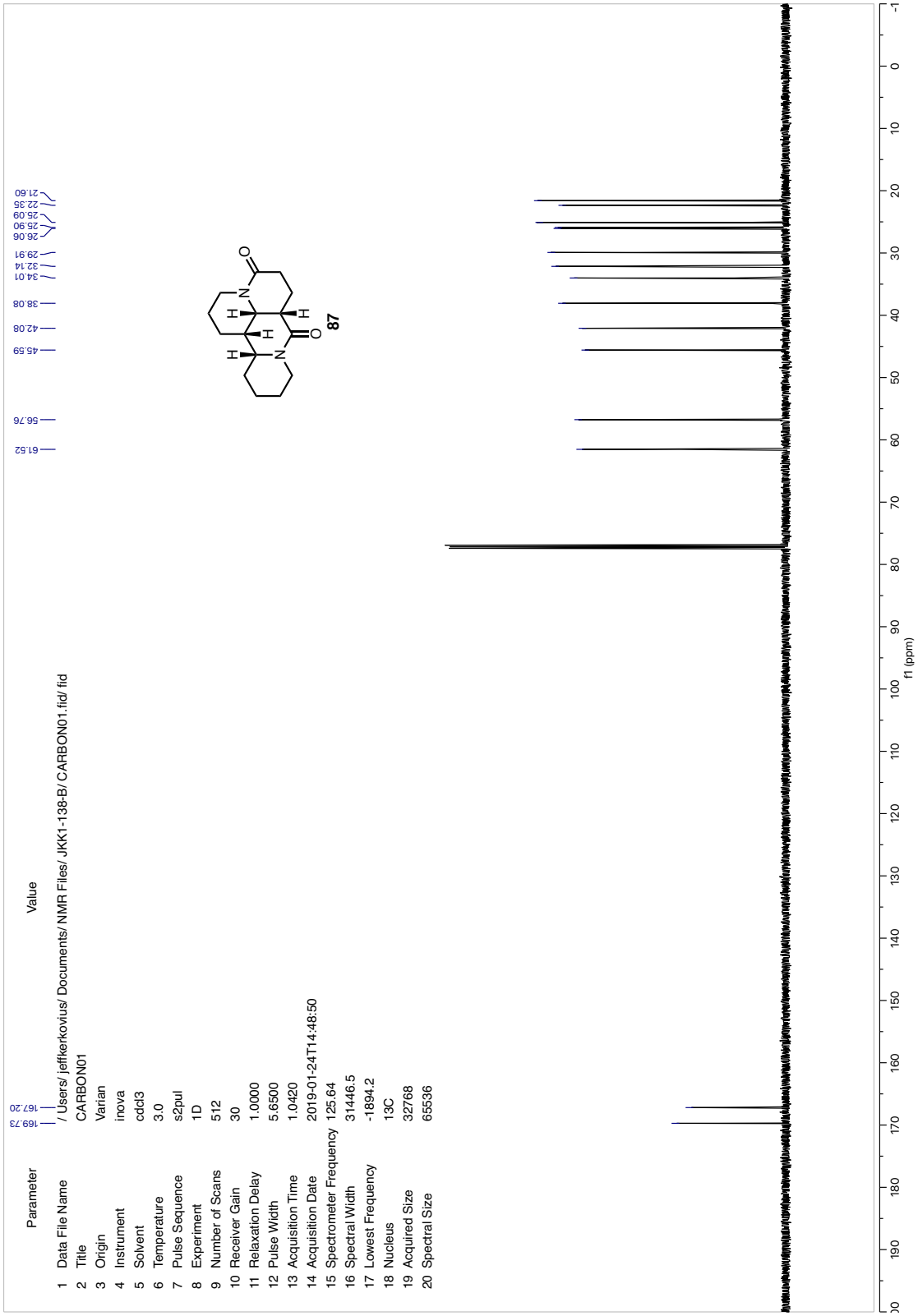
Parameter Value
1 Data File Name / Users/ jeffkerkovius/ Documents/ NMR Files/ JKK1-138-B/ CARBON01.fid/ fid
2 Title CARBON01
3 Origin Varian
4 Instrument inova
5 Solvent cdcl3
6 Temperature 3.0
7 Pulse Sequence s2pul
8 Experiment 1D
9 Number of Scans 512
10 Receiver Gain 30
11 Relaxation Delay 1.0000
12 Pulse Width 5.6500
13 Acquisition Time 1.0420
14 Acquisition Date 2019-01-24T14:48:50
15 Spectrometer Frequency 125.64
16 Spectral Width 31446.5
17 Lowest Frequency -1894.2
18 Nucleus 13C
19 Acquired Size 32768
20 Spectral Size 65536
169.73
167.20
61.52
56.76
45.59
42.08
38.08
34.01
32.14
29.91
26.06
25.90
25.09
22.35
21.60
87
f1 (ppm)

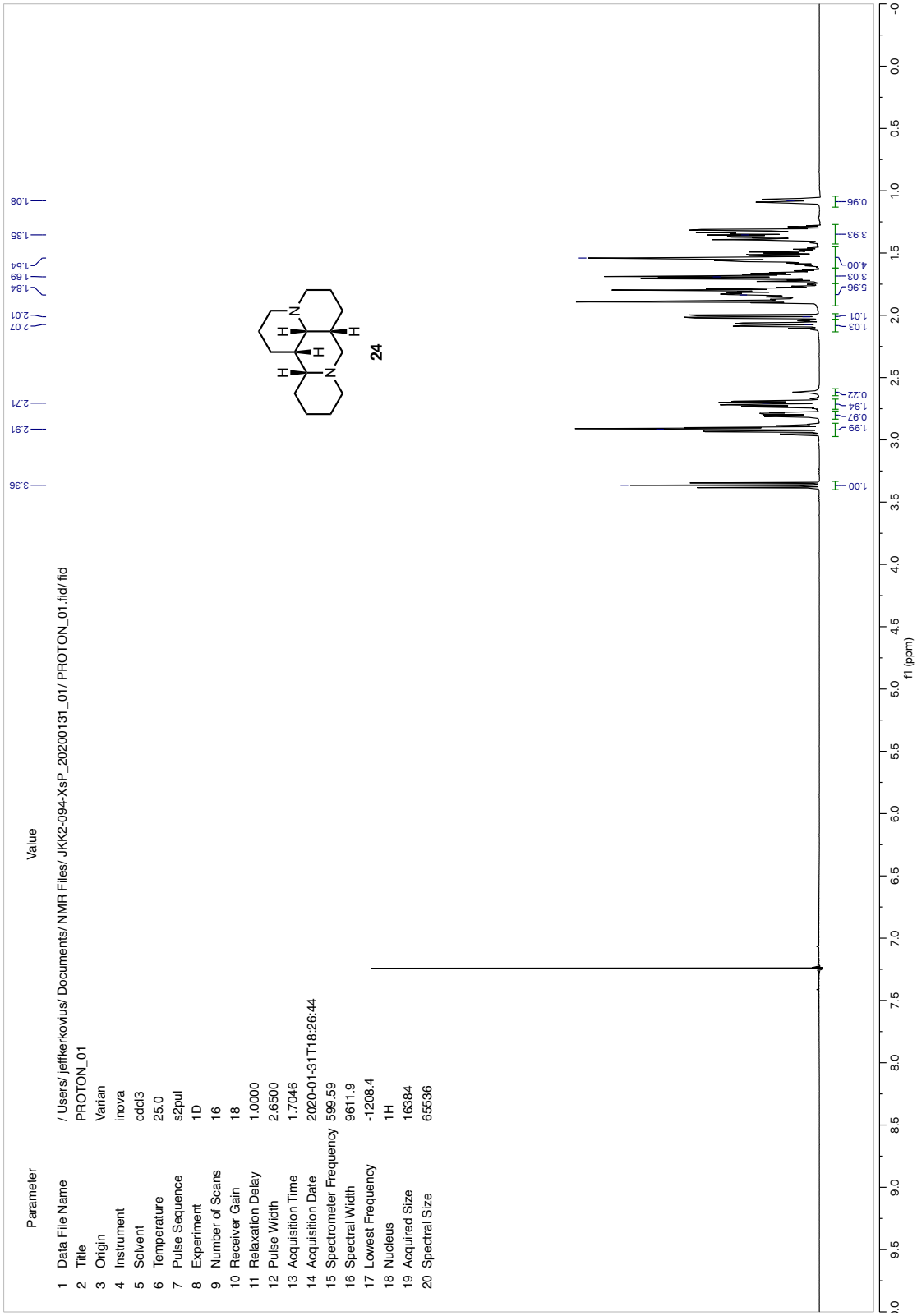
Parameter
Value
1 Data File Name / Users/ jeffkerkovius/ Documents/ NMR Files/ JKK2-094-XsP_20200131_01/ PROTON_01.fid/ fid
2 Title PROTON_01
3 Origin Varian
4 Instrument inova
5 Solvent cdcl3
6 Temperature 25.0
7 Pulse Sequence s2pul
8 Experiment 1D
9 Number of Scans 16
10 Receiver Gain 18
11 Relaxation Delay 1.0000
12 Pulse Width 2.6500
13 Acquisition Time 1.7046
14 Acquisition Date 2020-01-31T18:26:44
15 Spectrometer Frequency 599.59
16 Spectral Width 9611.9
17 Lowest Frequency -1208.4
18 Nucleus 1H
19 Acquired Size 16384
20 Spectral Size 65536
24
f1 (ppm)

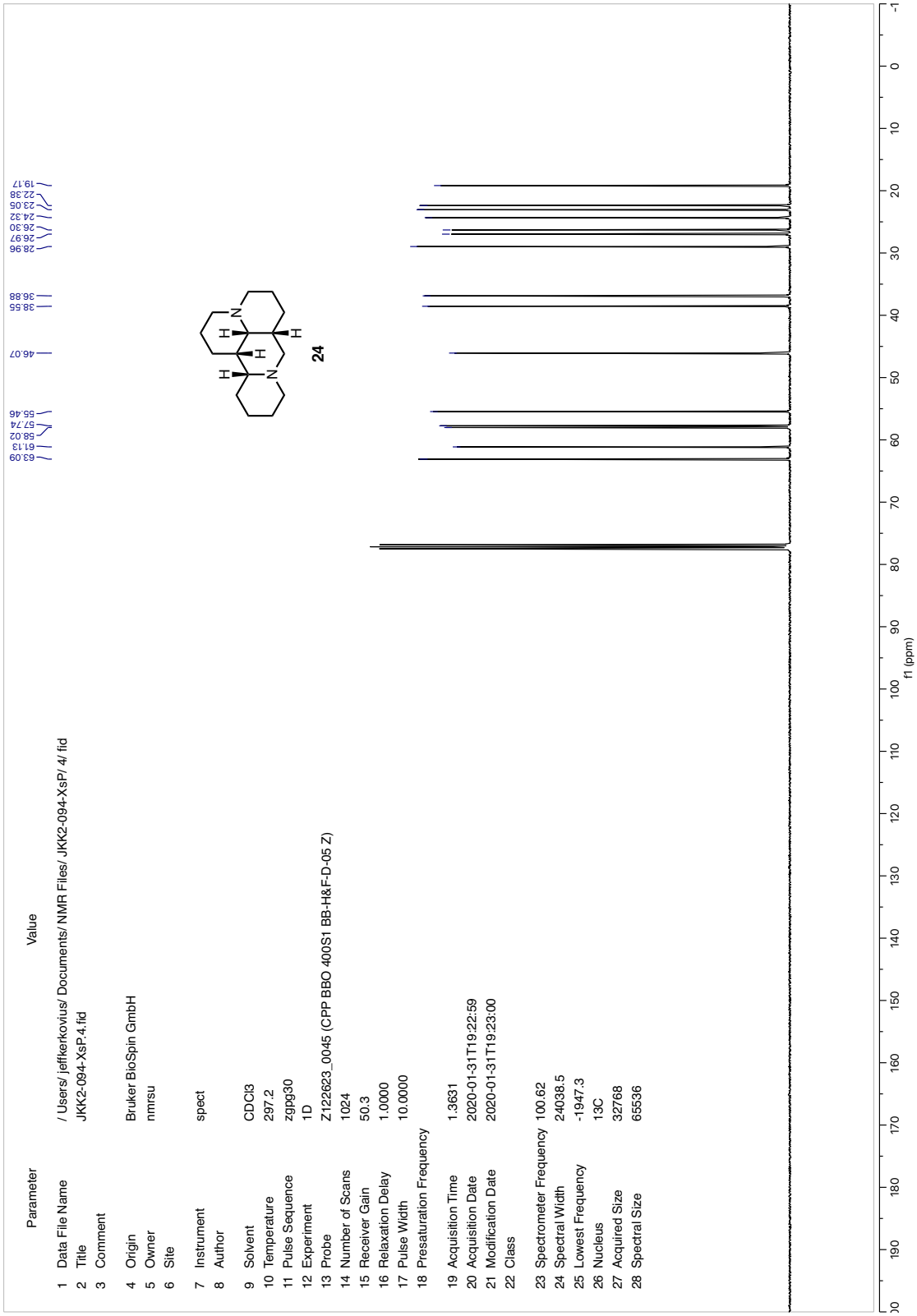
Parameter
Value
1 Data File Name / Users/ jeffkerkovius/ Documents/ NMR Files/ JKK2-094-XsP/ 4/ fid
2 Title JKK2-094-XsP.4.fid
3 Comment
4 Origin Bruker BioSpin GmbH
5 Owner nmrsu
6 Site
7 Instrument spect
8 Author
9 Solvent CDCl3
10 Temperature 297.2
11 Pulse Sequence zgpg30
12 Experiment 1D
13 Probe Z122623_0045 (CPP BBO 400S1 BB-H&F-D-05 Z)
14 Number of Scans 1024
15 Receiver Gain 50.3
16 Relaxation Delay 1.0000
17 Pulse Width 10.0000
18 Presaturation Frequency
19 Acquisition Time 1.3631
20 Acquisition Date 2020-01-31T19:22:59
21 Modification Date 2020-01-31T19:23:00
22 Class
23 Spectrometer Frequency 100.62
24 Spectral Width 24038.5
25 Lowest Frequency -1947.3
26 Nucleus 13C
27 Acquired Size 32768
28 Spectral Size 65536
63.09
61.13
58.02
57.74
55.46
46.07
38.55
36.88
28.96
26.97
26.30
24.32
23.05
22.38
19.17
24
f1 (ppm)

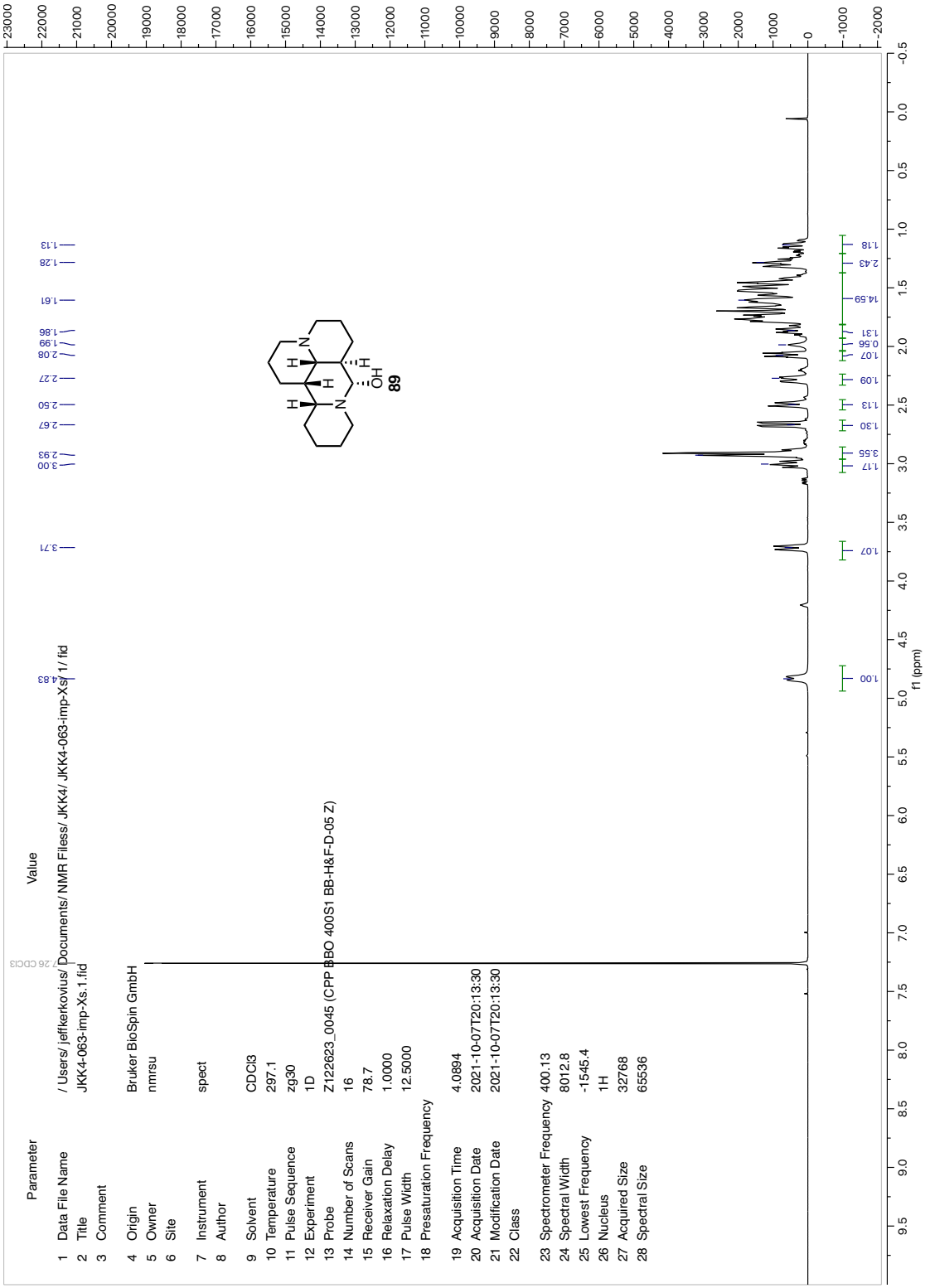
Parameter
Value
1 Data File Name / Users/ jeffkerkovius/ Documents/ NMR Files/ JKK4/ JKK4-063-imp-Xs/ 1/ fid
2 Title JKK4-063-imp-Xs.1.fid
3 Comment
4 Origin Bruker BioSpin GmbH
5 Owner nmrsu
6 Site
7 Instrument spect
8 Author
9 Solvent CDCl3
10 Temperature 297.1
11 Pulse Sequence zg30
12 Experiment 1D
13 Probe Z122623_0045 (CPP BBO 400S1 BB-H&F-D-05 Z)
14 Number of Scans 16
15 Receiver Gain 78.7
16 Relaxation Delay 1.0000
17 Pulse Width 12.5000
18 Presaturation Frequency
19 Acquisition Time 4.0894
20 Acquisition Date 2021-10-07T20:13:30
21 Modification Date 2021-10-07T20:13:30
22 Class
23 Spectrometer Frequency 400.13
24 Spectral Width 8012.8
25 Lowest Frequency -1545.4
26 Nucleus 1H
27 Acquired Size 32768
28 Spectral Size 65536
89
f1 (ppm)

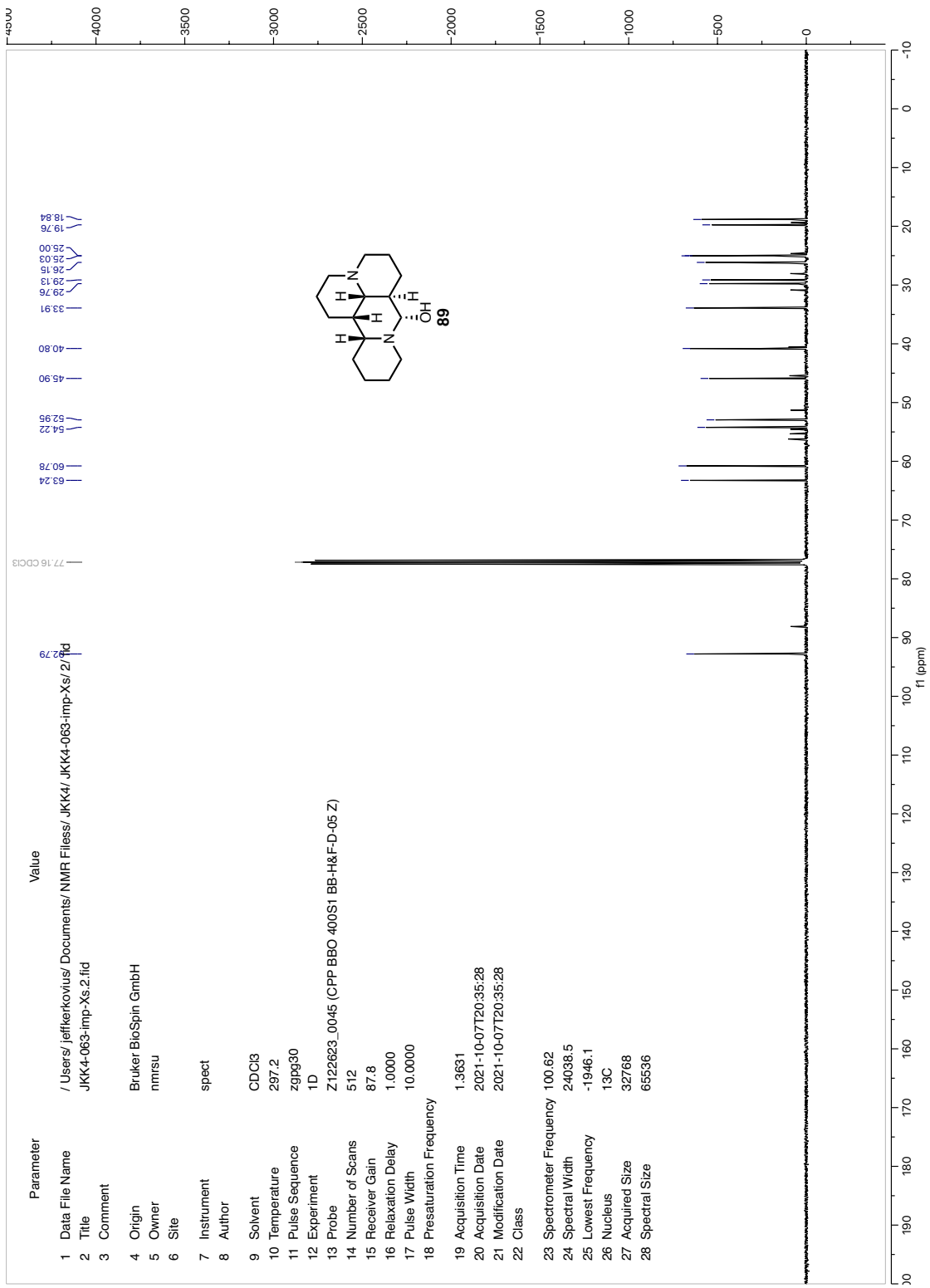
Parameter
Value
1 Data File Name / Users/ jeffkerkovius/ Documents/ NMR Files/ JKK4/ JKK4-063-imp-Xs/ 2/fid
2 Title JKK4-063-imp-Xs.2.fid
3 Comment
4 Origin Bruker BioSpin GmbH
5 Owner nmrsu
6 Site
7 Instrument spect
8 Author
9 Solvent CDCl3
10 Temperature 297.2
11 Pulse Sequence zgpg30
12 Experiment 1D
13 Probe Z122623_0045 (CPP BBO 400S1 BB-H&F-D-05 Z)
14 Number of Scans 512
15 Receiver Gain 87.8
16 Relaxation Delay 1.0000
17 Pulse Width 10.0000
18 Presaturation Frequency
19 Acquisition Time 1.3631
20 Acquisition Date 2021-10-07T20:35:28
21 Modification Date 2021-10-07T20:35:28
22 Class
23 Spectrometer Frequency 100.62
24 Spectral Width 24038.5
25 Lowest Frequency -1946.1
26 Nucleus 13C
27 Acquired Size 32768
28 Spectral Size 65536
77.16 CDCl3
82.79
63.24
60.78
54.22
52.95
45.90
40.80
33.91
29.76
29.13
26.15
25.03
25.00
19.76
18.84
89
f1 (ppm)

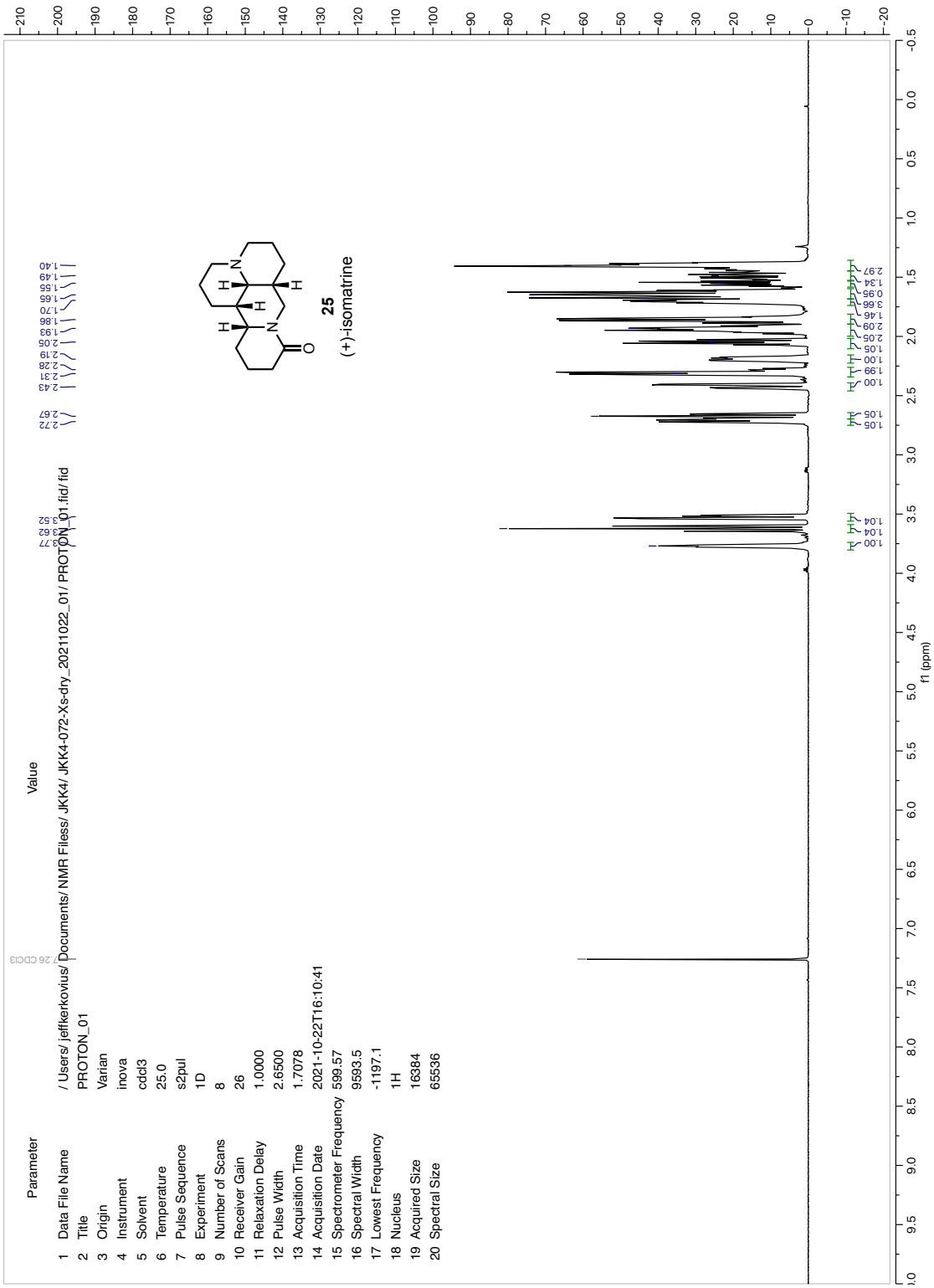
Parameter
Value
1 Data File Name / Users/ jeffkerkovius/ Documents/ NMR Files/ JKK4/ JKK4-072-Xs-dry_20211022_01/ PROTON_01.fid/ fid
2 Title PROTON_01
3 Origin Varian
4 Instrument inova
5 Solvent cdcl3
6 Temperature 25.0
7 Pulse Sequence s2pul
8 Experiment 1D
9 Number of Scans 8
10 Receiver Gain 26
11 Relaxation Delay 1.0000
12 Pulse Width 2.6500
13 Acquisition Time 1.7078
14 Acquisition Date 2021-10-22T16:10:41
15 Spectrometer Frequency 599.57
16 Spectral Width 9593.5
17 Lowest Frequency -1197.1
18 Nucleus 1H
19 Acquired Size 16384
20 Spectral Size 65536
7.26 CDCl3
3.77
3.62
3.52
2.72
2.67
2.43
2.31
2.28
2.19
2.06
1.93
1.86
1.70
1.66
1.55
1.49
1.40
1.00
1.04
1.04
1.05
1.05
1.00
1.00
1.99
1.05
2.09
1.46
3.66
0.95
1.34
2.97
25
(+)-isomatrine
f1 (ppm)

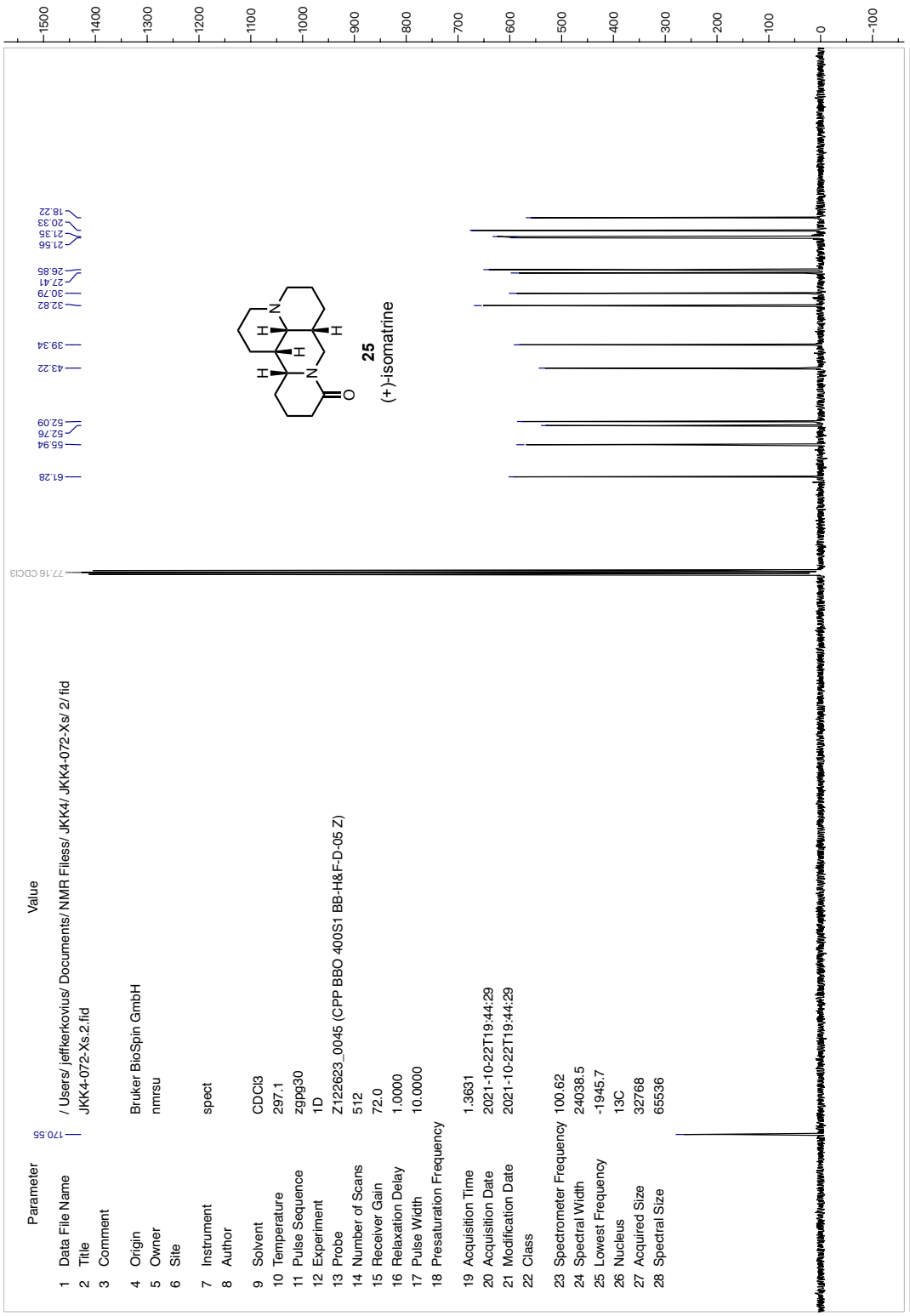
Parameter
Value
1 Data File Name / Users/ jeffkerkovius/ Documents/ NMR Files/ JKK4/ JKK4-072-Xs/ 2/ fid
2 Title JKK4-072-Xs.2.fid
3 Comment
4 Origin Bruker BioSpin GmbH
5 Owner nmrsu
6 Site
7 Instrument spect
8 Author
9 Solvent CDCl3
10 Temperature 297.1
11 Pulse Sequence zgpg30
12 Experiment 1D
13 Probe Z122623_0045 (CPP BBO 400S1 BB-H&F-D-05 Z)
14 Number of Scans 512
15 Receiver Gain 72.0
16 Relaxation Delay 1.0000
17 Pulse Width 10.0000
18 Presaturation Frequency
19 Acquisition Time 1.3631
20 Acquisition Date 2021-10-22T19:44:29
21 Modification Date 2021-10-22T19:44:29
22 Class
23 Spectrometer Frequency 100.62
24 Spectral Width 24038.5
25 Lowest Frequency -1945.7
26 Nucleus 13C
27 Acquired Size 32768
28 Spectral Size 65536
170.55
77.16 CDCl3
61.28
55.94
52.76
52.09
43.22
39.34
32.82
30.79
27.41
26.85
21.56
21.35
20.33
18.22
25
(+)-isomatrine
f1 (ppm)

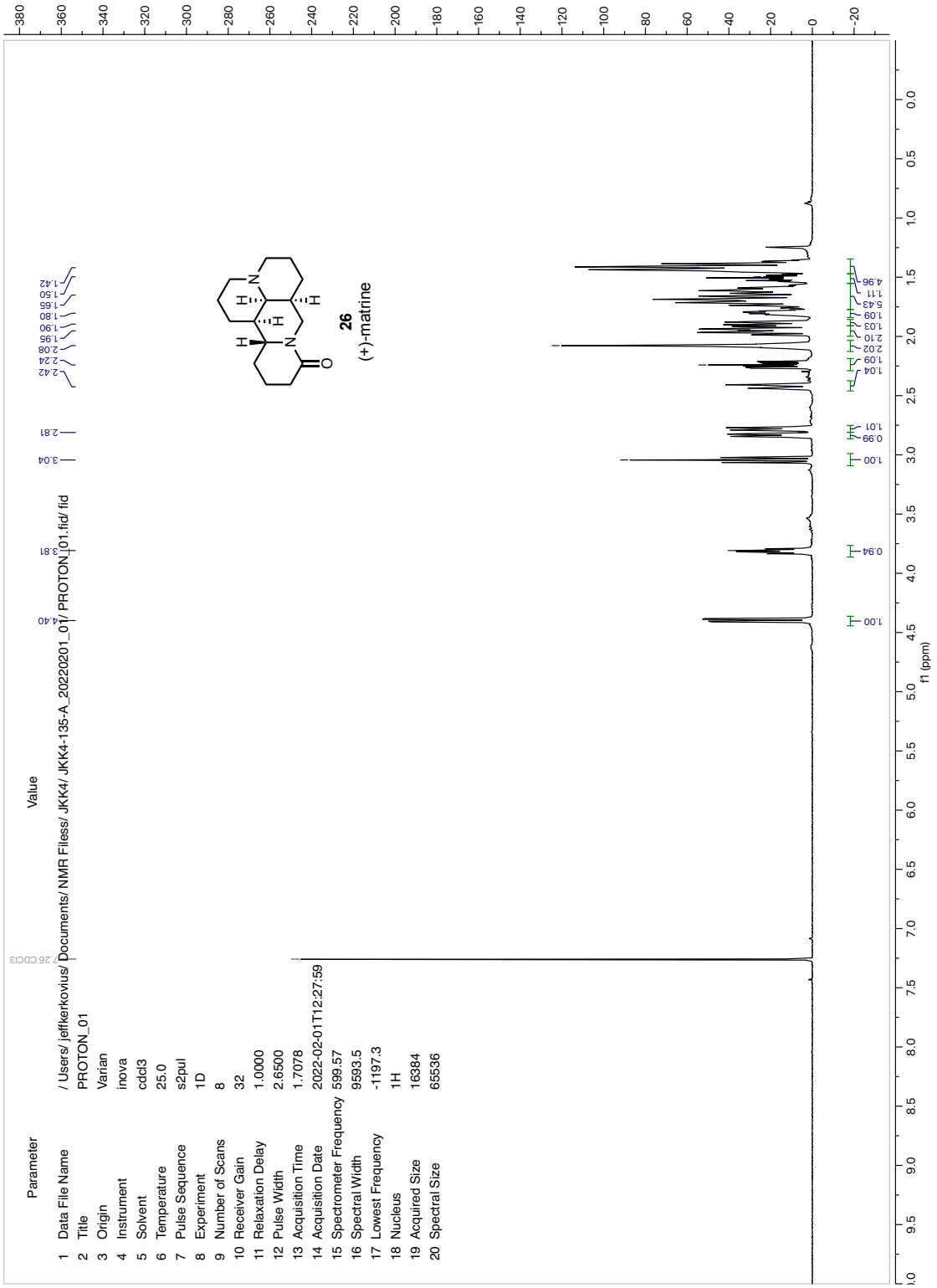
Parameter
Value
1 Data File Name / Users/ jeffkerkovius/ Documents/ NMR Files/ JKK4/ JKK4-135-A_20220201_01/ PROTON_01.fid/ fid
2 Title PROTON_01
3 Origin Varian
4 Instrument inova
5 Solvent cdcl3
6 Temperature 25.0
7 Pulse Sequence s2pul
8 Experiment 1D
9 Number of Scans 8
10 Receiver Gain 32
11 Relaxation Delay 1.0000
12 Pulse Width 2.6500
13 Acquisition Time 1.7078
14 Acquisition Date 2022-02-01T12:27:59
15 Spectrometer Frequency 599.57
16 Spectral Width 9593.5
17 Lowest Frequency -1197.3
18 Nucleus 1H
19 Acquired Size 16384
20 Spectral Size 65536
7.26 CDCl3
4.40
3.81
3.04
2.81
2.42
2.24
2.08
1.95
1.90
1.80
1.65
1.50
1.42
1.00
0.94
1.00
1.04
1.09
2.02
2.10
1.03
1.09
5.43
1.11
4.96
1.00
0.99
1.01
26
(+)-matrine
f1 (ppm)

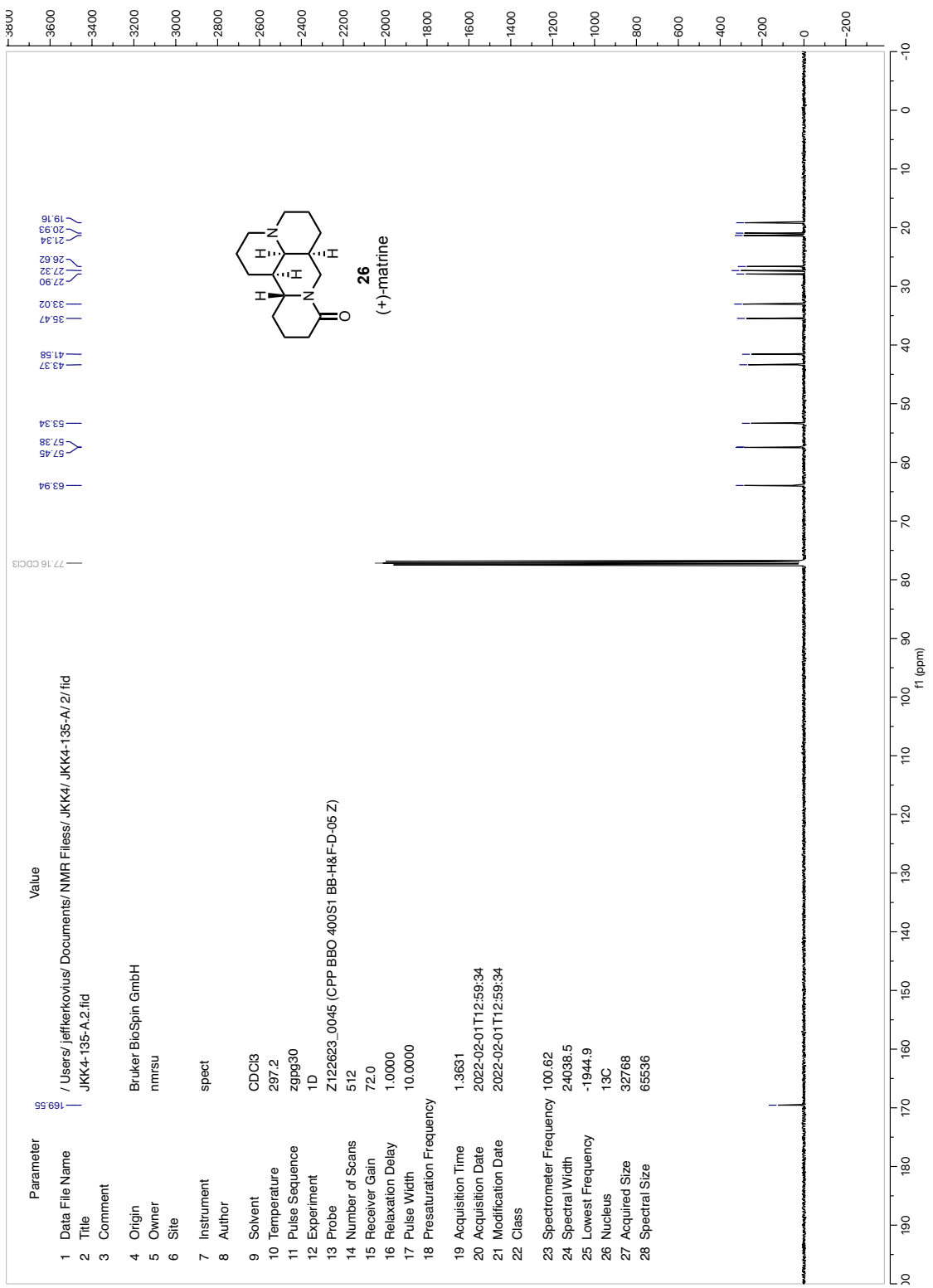
Parameter
Value
1 Data File Name / Users/ jeffkerkovius/ Documents/ NMR Files/ JKK4/ JKK4-135-A/ 2/ fid
2 Title JKK4-135-A.2.fid
3 Comment
4 Origin Bruker BioSpin GmbH
5 Owner nmrsu
6 Site
7 Instrument spect
8 Author
9 Solvent CDCl3
10 Temperature 297.2
11 Pulse Sequence zgpg30
12 Experiment 1D
13 Probe Z122623_0045 (CPP BBO 400S1 BB-H&F-D-05 Z)
14 Number of Scans 512
15 Receiver Gain 72.0
16 Relaxation Delay 1.0000
17 Pulse Width 10.0000
18 Presaturation Frequency
19 Acquisition Time 1.3631
20 Acquisition Date 2022-02-01T12:59:34
21 Modification Date 2022-02-01T12:59:34
22 Class
23 Spectrometer Frequency 100.62
24 Spectral Width 24038.5
25 Lowest Frequency -1944.9
26 Nucleus 13C
27 Acquired Size 32768
28 Spectral Size 65536
169.55
77.16 CDCl3
63.94
57.45
57.38
53.34
43.37
41.58
35.47
33.02
27.90
27.32
26.62
21.34
20.93
19.16
26
(+)-matrine
f1 (ppm)

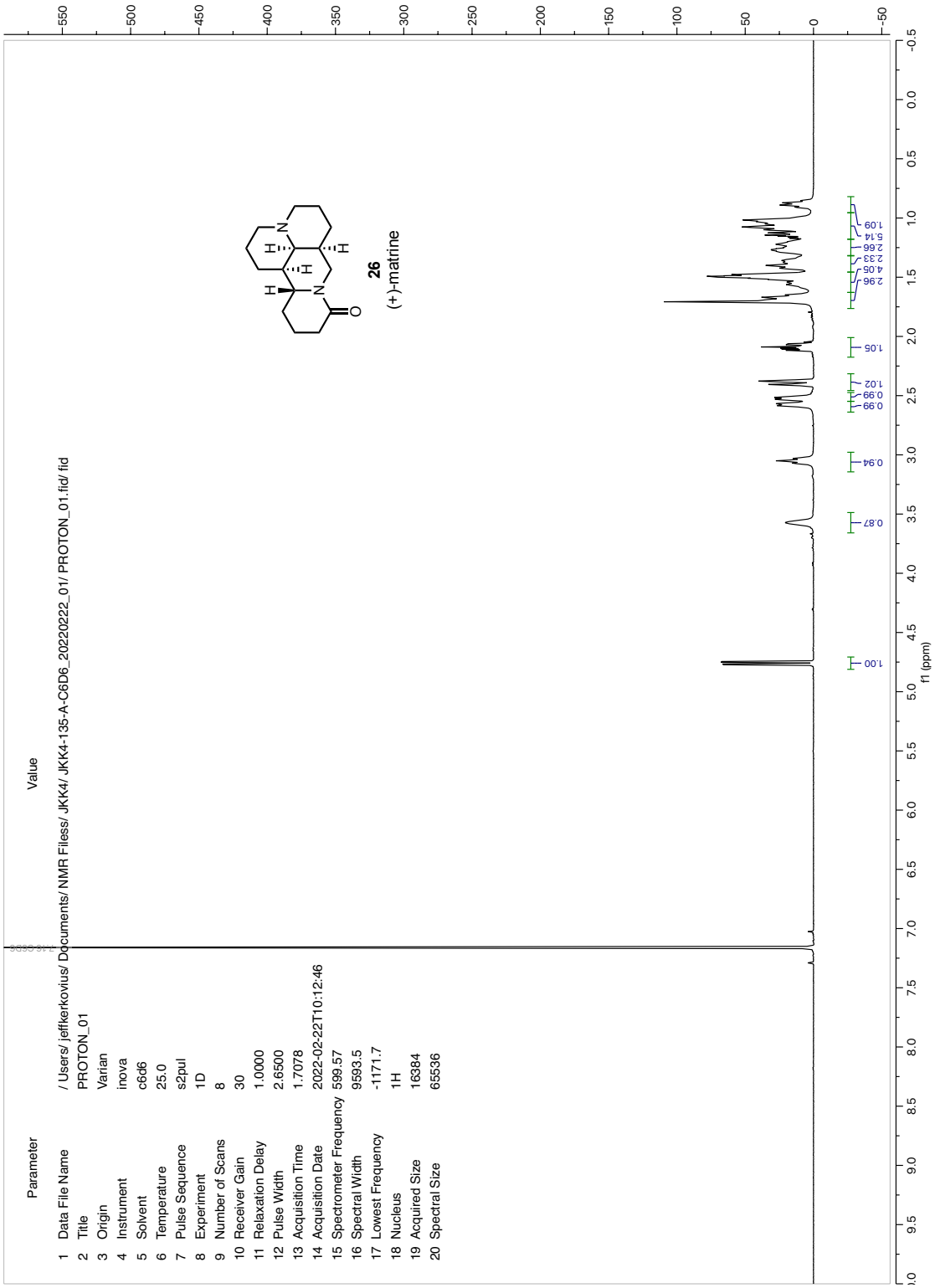
Parameter
Value
1 Data File Name / Users/ jeffkerkovius/ Documents/ NMR Files/ JKK4/ JKK4-135-A-C6D6_20220222_01/ PROTON_01.fid/ fid
2 Title PROTON_01
3 Origin Varian
4 Instrument inova
5 Solvent c6d6
6 Temperature 25.0
7 Pulse Sequence s2pul
8 Experiment 1D
9 Number of Scans 8
10 Receiver Gain 30
11 Relaxation Delay 1.0000
12 Pulse Width 2.6500
13 Acquisition Time 1.7078
14 Acquisition Date 2022-02-22T10:12:46
15 Spectrometer Frequency 599.57
16 Spectral Width 9593.5
17 Lowest Frequency -1171.7
18 Nucleus 1H
19 Acquired Size 16384
20 Spectral Size 65536
26
(+)-matrine
1.00
0.87
0.94
0.99
1.02
1.05
2.96
4.05
2.33
2.66
5.14
1.09
f1 (ppm)

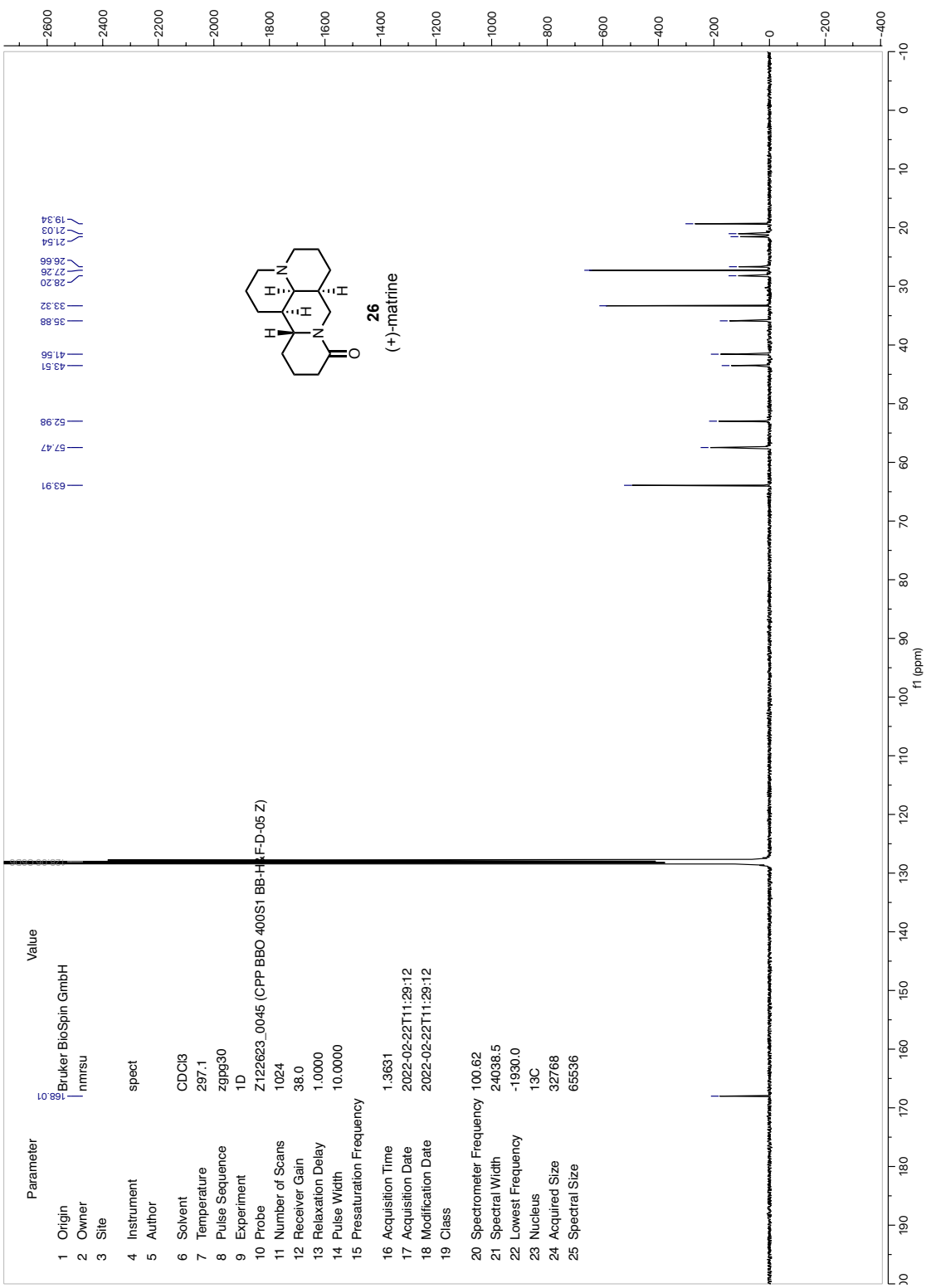
Parameter Value
1 Origin Bruker BioSpin GmbH
2 Owner nmrsu
3 Site
4 Instrument spect
5 Author
6 Solvent CDCl3
7 Temperature 297.1
8 Pulse Sequence zgpg30
9 Experiment 1D
10 Probe Z122623_0045 (CPP BBO 400S1 BB-H&F-D-05 Z)
11 Number of Scans 1024
12 Receiver Gain 38.0
13 Relaxation Delay 1.0000
14 Pulse Width 10.0000
15 Presaturation Frequency
16 Acquisition Time 1.3631
17 Acquisition Date 2022-02-22T11:29:12
18 Modification Date 2022-02-22T11:29:12
19 Class
20 Spectrometer Frequency 100.62
21 Spectral Width 24038.5
22 Lowest Frequency -1930.0
23 Nucleus 13C
24 Acquired Size 32768
25 Spectral Size 65536
168.01
63.91
57.47
52.98
43.51
41.56
35.88
33.32
28.20
27.26
26.66
21.54
21.03
19.34
26
(+)-matrine
f1 (ppm)

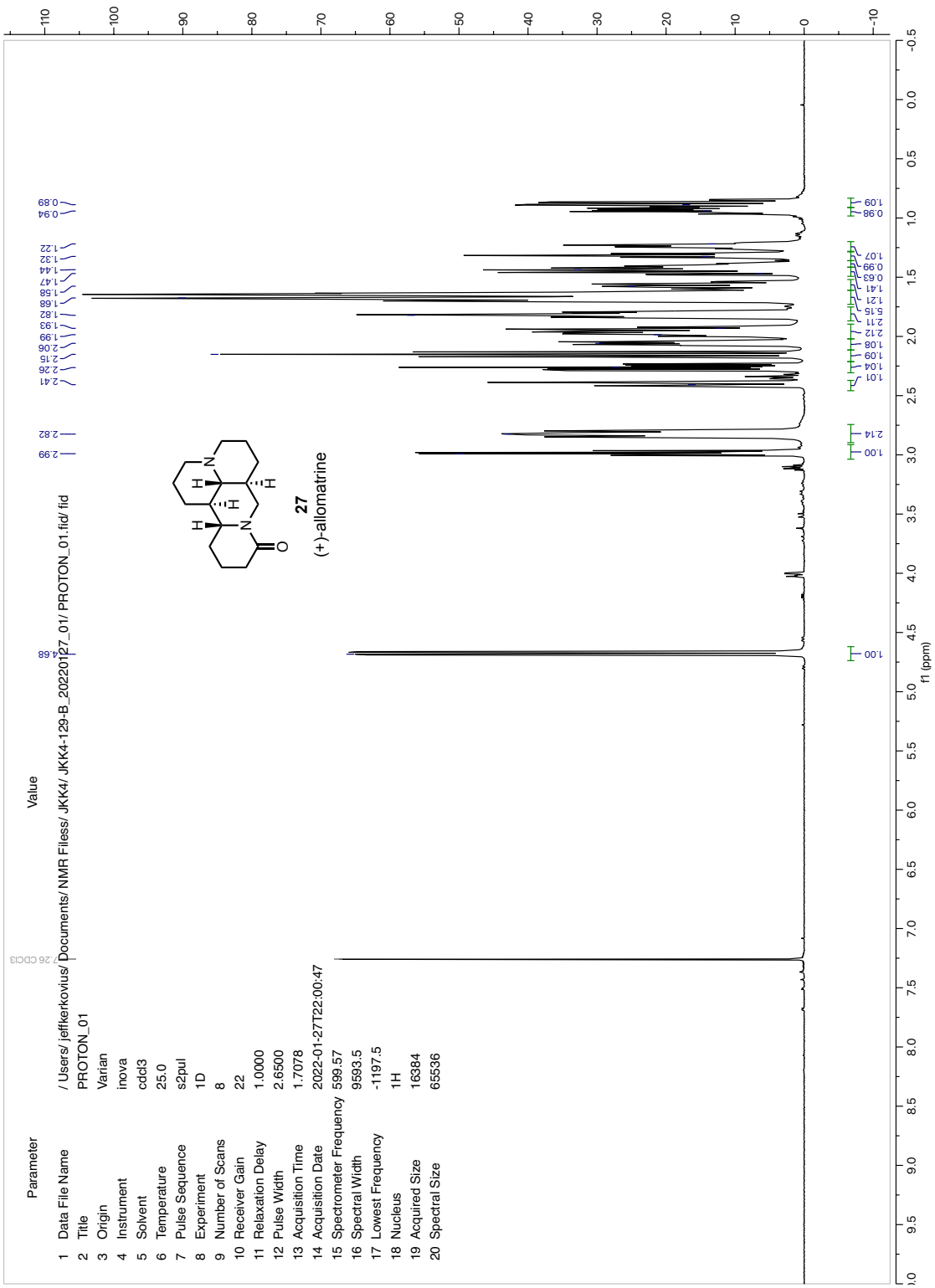
Parameter
Value
1 Data File Name / Users/ jeffkerkovius/ Documents/ NMR Files/ JKK4/ JKK4-129-B_20220127_01/ PROTON_01.fid/ fid
2 Title PROTON_01
3 Origin Varian
4 Instrument inova
5 Solvent cdcl3
6 Temperature 25.0
7 Pulse Sequence s2pul
8 Experiment 1D
9 Number of Scans 8
10 Receiver Gain 22
11 Relaxation Delay 1.0000
12 Pulse Width 2.6500
13 Acquisition Time 1.7078
14 Acquisition Date 2022-01-27T22:00:47
15 Spectrometer Frequency 599.57
16 Spectral Width 9593.5
17 Lowest Frequency -1197.5
18 Nucleus 1H
19 Acquired Size 16384
20 Spectral Size 65536
27
(+)-allomatrine
f1 (ppm)

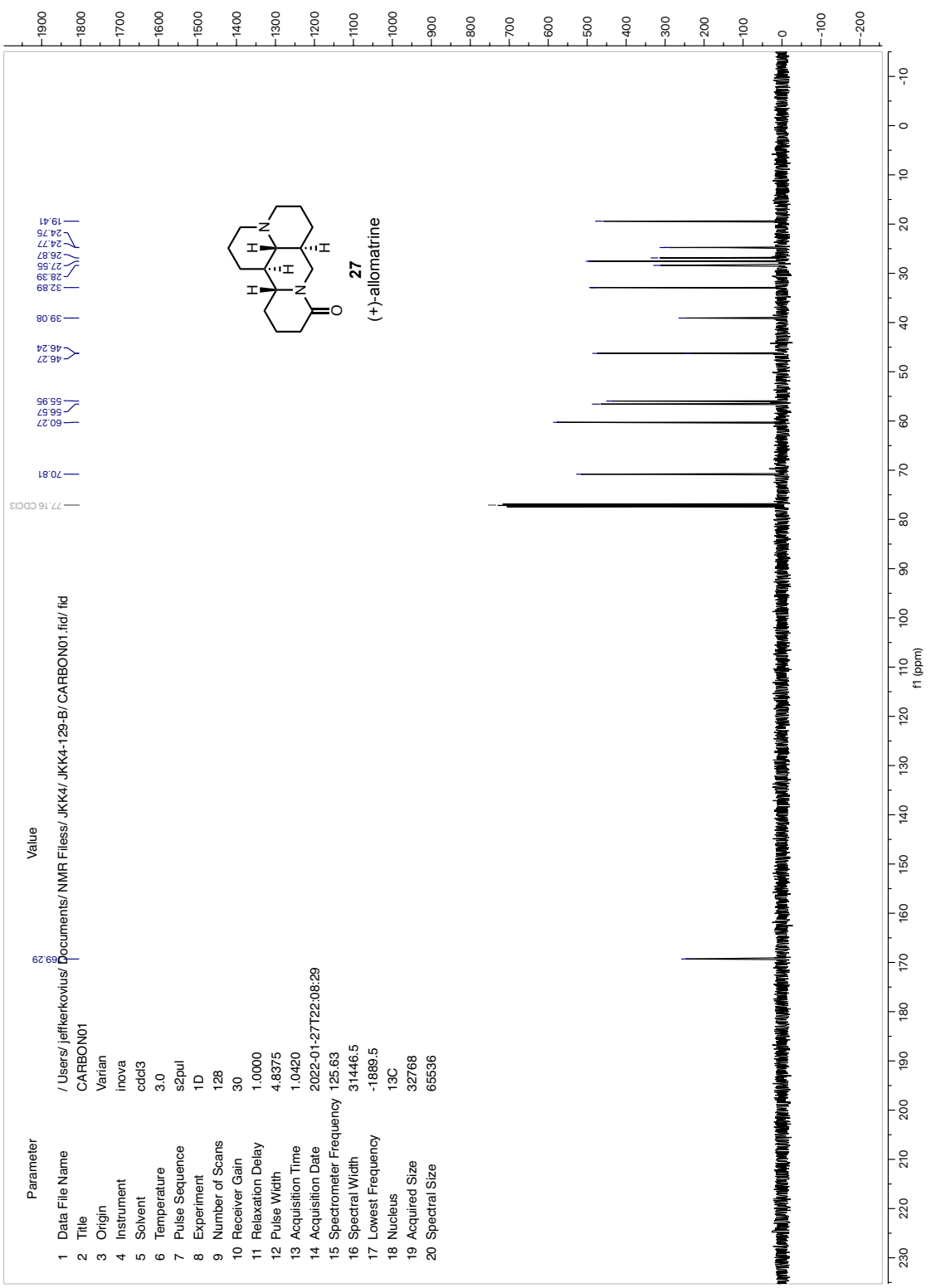
Parameter Value
1 Data File Name / Users/ jeffkerkovius/ Documents/ NMR Files/ JKK4/ JKK4-129-B/ CARBON01.fid/ fid
2 Title CARBON01
3 Origin Varian
4 Instrument inova
5 Solvent cdcl3
6 Temperature 3.0
7 Pulse Sequence s2pul
8 Experiment 1D
9 Number of Scans 128
10 Receiver Gain 30
11 Relaxation Delay 1.0000
12 Pulse Width 4.8375
13 Acquisition Time 1.0420
14 Acquisition Date 2022-01-27T22:08:29
15 Spectrometer Frequency 125.63
16 Spectral Width 31446.5
17 Lowest Frequency -1889.5
18 Nucleus 13C
19 Acquired Size 32768
20 Spectral Size 65536
169.29
77.16 CDCl3
70.81
60.27
56.57
55.96
46.27
46.24
39.08
32.89
28.39
27.55
26.87
24.77
24.75
19.41
27
(+)-allomatrine
f1 (ppm)

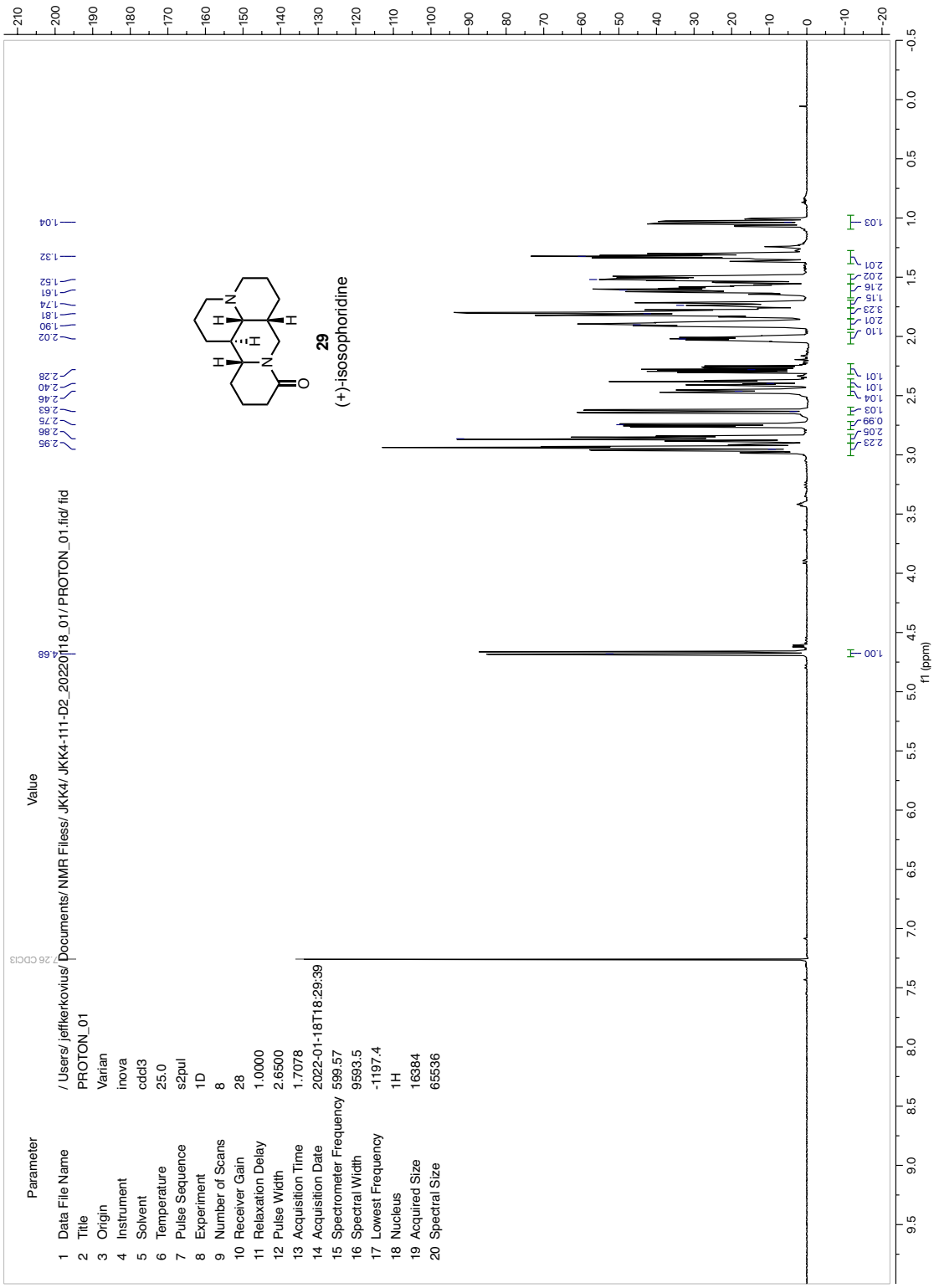
Parameter
Value
1 Data File Name / Users/ jeffkerkovius/ Documents/ NMR Files/ JKK4/ JKK4-111-D2_20220118_01/ PROTON_01.fid/ fid
2 Title PROTON_01
3 Origin Varian
4 Instrument inova
5 Solvent cdcl3
6 Temperature 25.0
7 Pulse Sequence s2pul
8 Experiment 1D
9 Number of Scans 8
10 Receiver Gain 28
11 Relaxation Delay 1.0000
12 Pulse Width 2.6500
13 Acquisition Time 1.7078
14 Acquisition Date 2022-01-18T18:29:39
15 Spectrometer Frequency 599.57
16 Spectral Width 9593.5
17 Lowest Frequency -1197.4
18 Nucleus 1H
19 Acquired Size 16384
20 Spectral Size 65536
7.26 CDCl3
4.68
2.95
2.86
2.75
2.63
2.46
2.40
2.28
2.02
1.90
1.81
1.74
1.61
1.52
1.32
1.04
2.23
0.99
2.06
1.03
1.04
1.01
1.01
1.00
1.10
2.01
3.23
1.15
2.16
2.02
2.01
1.03
29
(+)-isosophoridine
f1 (ppm)

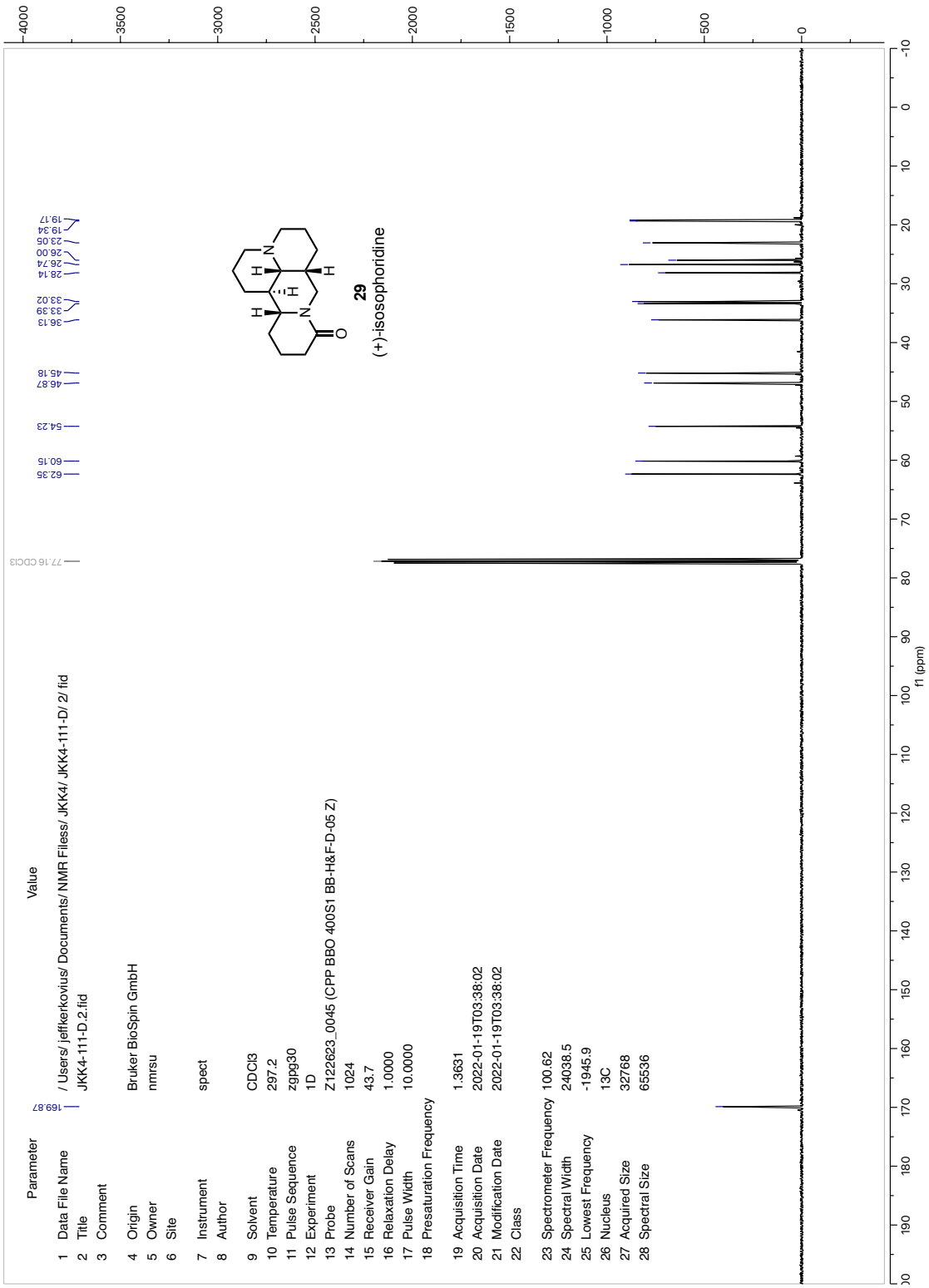
Parameter
Value
1 Data File Name / Users/ jeffkerkovius/ Documents/ NMR Files/ JKK4/ JKK4-111-D/ 2/ fid
2 Title JKK4-111-D.2.fid
3 Comment
4 Origin Bruker BioSpin GmbH
5 Owner nmrsu
6 Site
7 Instrument spect
8 Author
9 Solvent CDCl3
10 Temperature 297.2
11 Pulse Sequence zgpg30
12 Experiment 1D
13 Probe Z122623_0045 (CPP BBO 400S1 BB-H&F-D-05 Z)
14 Number of Scans 1024
15 Receiver Gain 43.7
16 Relaxation Delay 1.0000
17 Pulse Width 10.0000
18 Presaturation Frequency
19 Acquisition Time 1.3631
20 Acquisition Date 2022-01-19T03:38:02
21 Modification Date 2022-01-19T03:38:02
22 Class
23 Spectrometer Frequency 100.62
24 Spectral Width 24038.5
25 Lowest Frequency -1945.9
26 Nucleus 13C
27 Acquired Size 32768
28 Spectral Size 65536
169.87
77.16 CDCl3
62.35
60.15
54.23
46.87
45.18
36.13
33.39
33.02
28.14
26.74
26.00
23.05
19.34
19.17
29
(+)-isosophoridine
f1 (ppm)

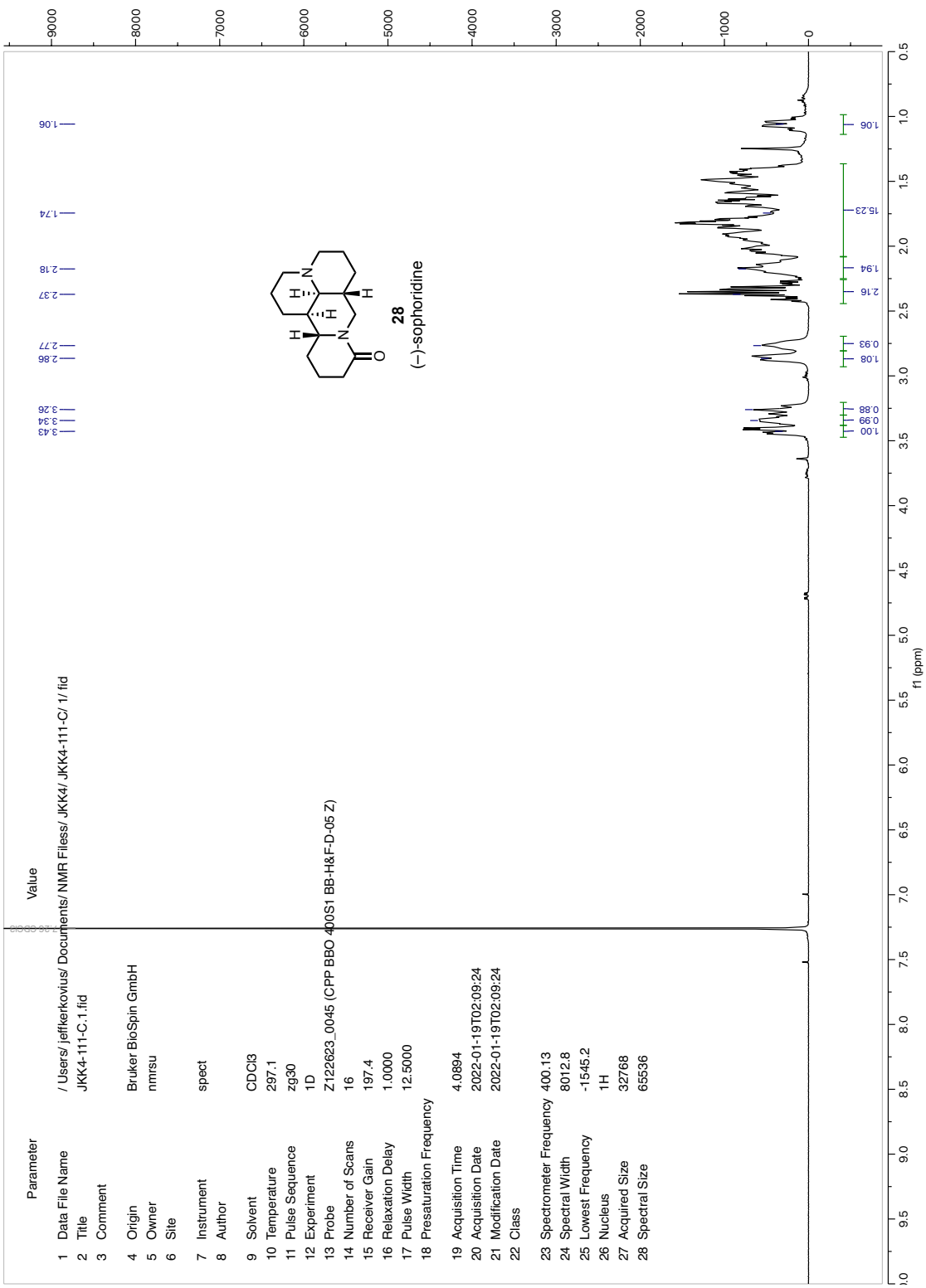
Parameter
Value
1 Data File Name / Users/ jeffkerkovius/ Documents/ NMR Files/ JKK4/ JKK4-111-C/ 1/ fid
2 Title JKK4-111-C.1.fid
3 Comment
4 Origin Bruker BioSpin GmbH
5 Owner nmrsu
6 Site
7 Instrument spect
8 Author
9 Solvent CDCl3
10 Temperature 297.1
11 Pulse Sequence zg30
12 Experiment 1D
13 Probe Z122623_0045 (CPP BBO 400S1 BB-H&F-D-05 Z)
14 Number of Scans 16
15 Receiver Gain 197.4
16 Relaxation Delay 1.0000
17 Pulse Width 12.5000
18 Presaturation Frequency
19 Acquisition Time 4.0894
20 Acquisition Date 2022-01-19T02:09:24
21 Modification Date 2022-01-19T02:09:24
22 Class
23 Spectrometer Frequency 400.13
24 Spectral Width 8012.8
25 Lowest Frequency -1545.2
26 Nucleus 1H
27 Acquired Size 32768
28 Spectral Size 65536
28
(–)-sophoridine
f1 (ppm)

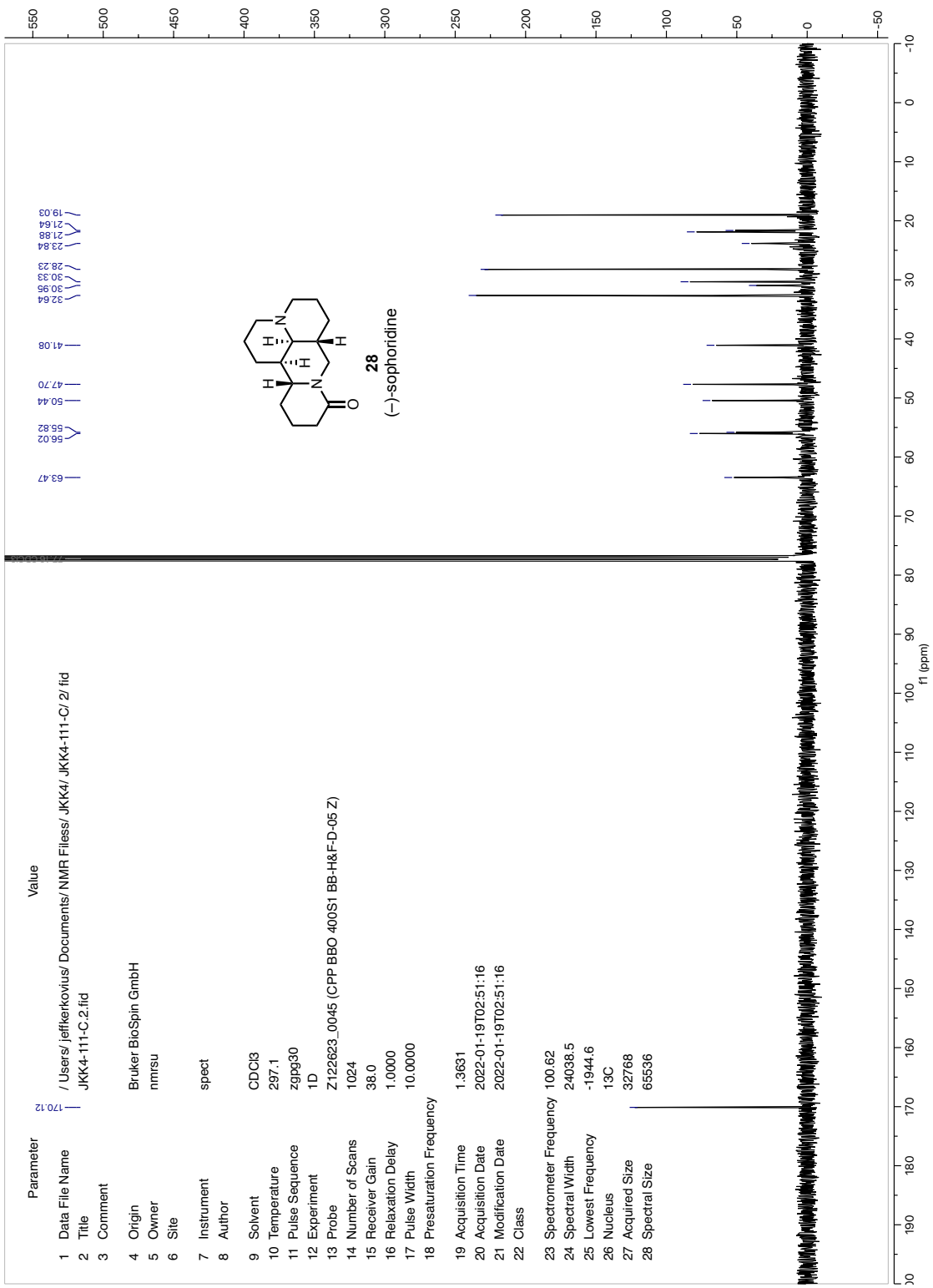
Parameter
Value
1 Data File Name / Users/ jeffkerkovius/ Documents/ NMR Files/ JKK4/ JKK4-111-C/ 2/ fid
2 Title JKK4-111-C.2.fid
3 Comment
4 Origin Bruker BioSpin GmbH
5 Owner nmrsu
6 Site
7 Instrument spect
8 Author
9 Solvent CDCl3
10 Temperature 297.1
11 Pulse Sequence zgpg30
12 Experiment 1D
13 Probe Z122623_0045 (CPP BBO 400S1 BB-H&F-D-05 Z)
14 Number of Scans 1024
15 Receiver Gain 38.0
16 Relaxation Delay 1.0000
17 Pulse Width 10.0000
18 Presaturation Frequency
19 Acquisition Time 1.3631
20 Acquisition Date 2022-01-19T02:51:16
21 Modification Date 2022-01-19T02:51:16
22 Class
23 Spectrometer Frequency 100.62
24 Spectral Width 24038.5
25 Lowest Frequency -1944.6
26 Nucleus 13C
27 Acquired Size 32768
28 Spectral Size 65536
170.12
63.47
56.02
55.82
50.44
47.70
41.08
32.64
30.95
30.33
28.23
23.84
21.88
21.64
19.03
28
(−)-sophoridine
f1 (ppm)

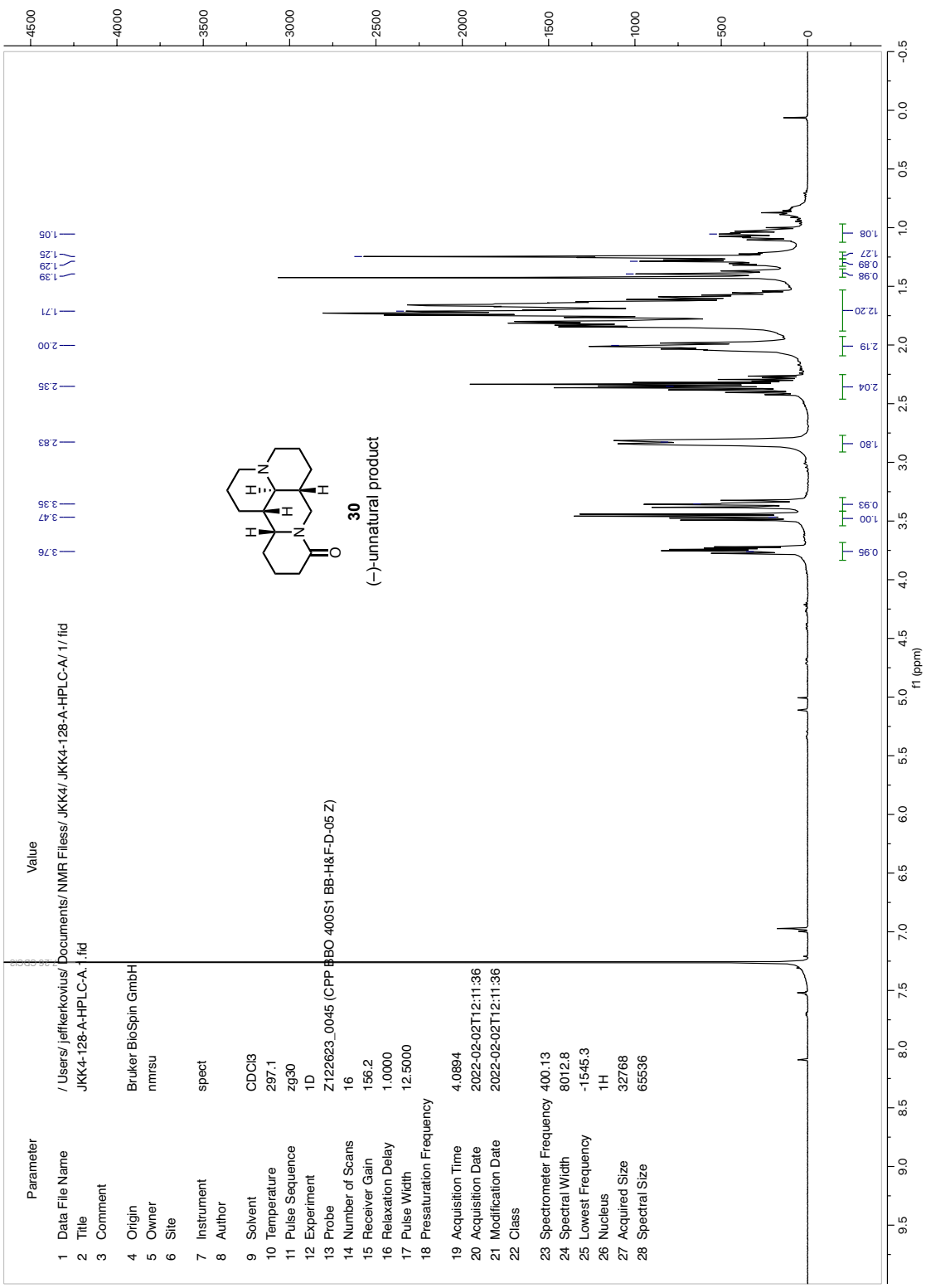
Parameter
Value
1 Data File Name / Users/ jeffkerkovius/ Documents/ NMR Files/ JKK4/ JKK4-128-A-HPLC-A/ 1/ fid
2 Title JKK4-128-A-HPLC-A, 1, fid
3 Comment
4 Origin Bruker BioSpin GmbH
5 Owner nmrsu
6 Site
7 Instrument spect
8 Author
9 Solvent CDCl3
10 Temperature 297.1
11 Pulse Sequence zg30
12 Experiment 1D
13 Probe Z122623_0045 (CPP BBO 400S1 BB-H&F-D-05 Z)
14 Number of Scans 16
15 Receiver Gain 156.2
16 Relaxation Delay 1.0000
17 Pulse Width 12.5000
18 Presaturation Frequency
19 Acquisition Time 4.0894
20 Acquisition Date 2022-02-02T12:11:36
21 Modification Date 2022-02-02T12:11:36
22 Class
23 Spectrometer Frequency 400.13
24 Spectral Width 8012.8
25 Lowest Frequency -1545.3
26 Nucleus 1H
27 Acquired Size 32768
28 Spectral Size 65536
30
(–)-unnatural product
f1 (ppm)

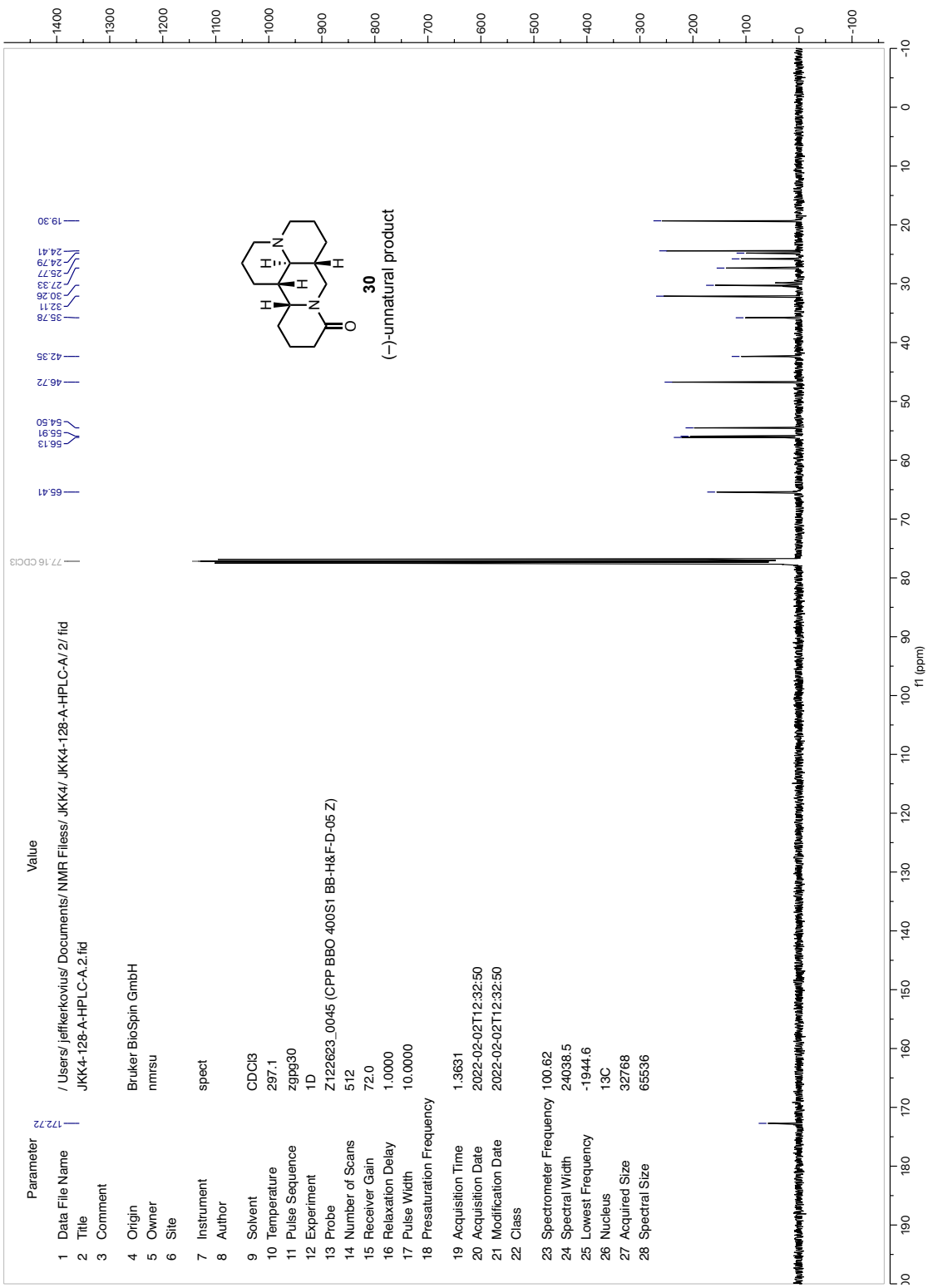
Parameter
Value
1 Data File Name / Users/ jeffkerkovius/ Documents/ NMR Files/ JKK4/ JKK4-128-A-HPLC-A/ 2/ fid
2 Title JKK4-128-A-HPLC-A.2.fid
3 Comment
4 Origin Bruker BioSpin GmbH
5 Owner nmrsu
6 Site
7 Instrument spect
8 Author
9 Solvent CDCl3
10 Temperature 297.1
11 Pulse Sequence zgpg30
12 Experiment 1D
13 Probe Z122623_0045 (CPP BBO 400S1 BB-H&F-D-05 Z)
14 Number of Scans 512
15 Receiver Gain 72.0
16 Relaxation Delay 1.0000
17 Pulse Width 10.0000
18 Presaturation Frequency
19 Acquisition Time 1.3631
20 Acquisition Date 2022-02-02T12:32:50
21 Modification Date 2022-02-02T12:32:50
22 Class
23 Spectrometer Frequency 100.62
24 Spectral Width 24038.5
25 Lowest Frequency -1944.6
26 Nucleus 13C
27 Acquired Size 32768
28 Spectral Size 65536
172.72
77.16 CDCl3
65.41
56.13
55.91
54.50
46.72
42.35
35.78
32.11
30.26
27.33
25.77
24.79
24.41
19.30
30
(−)-unnatural product
f1 (ppm)

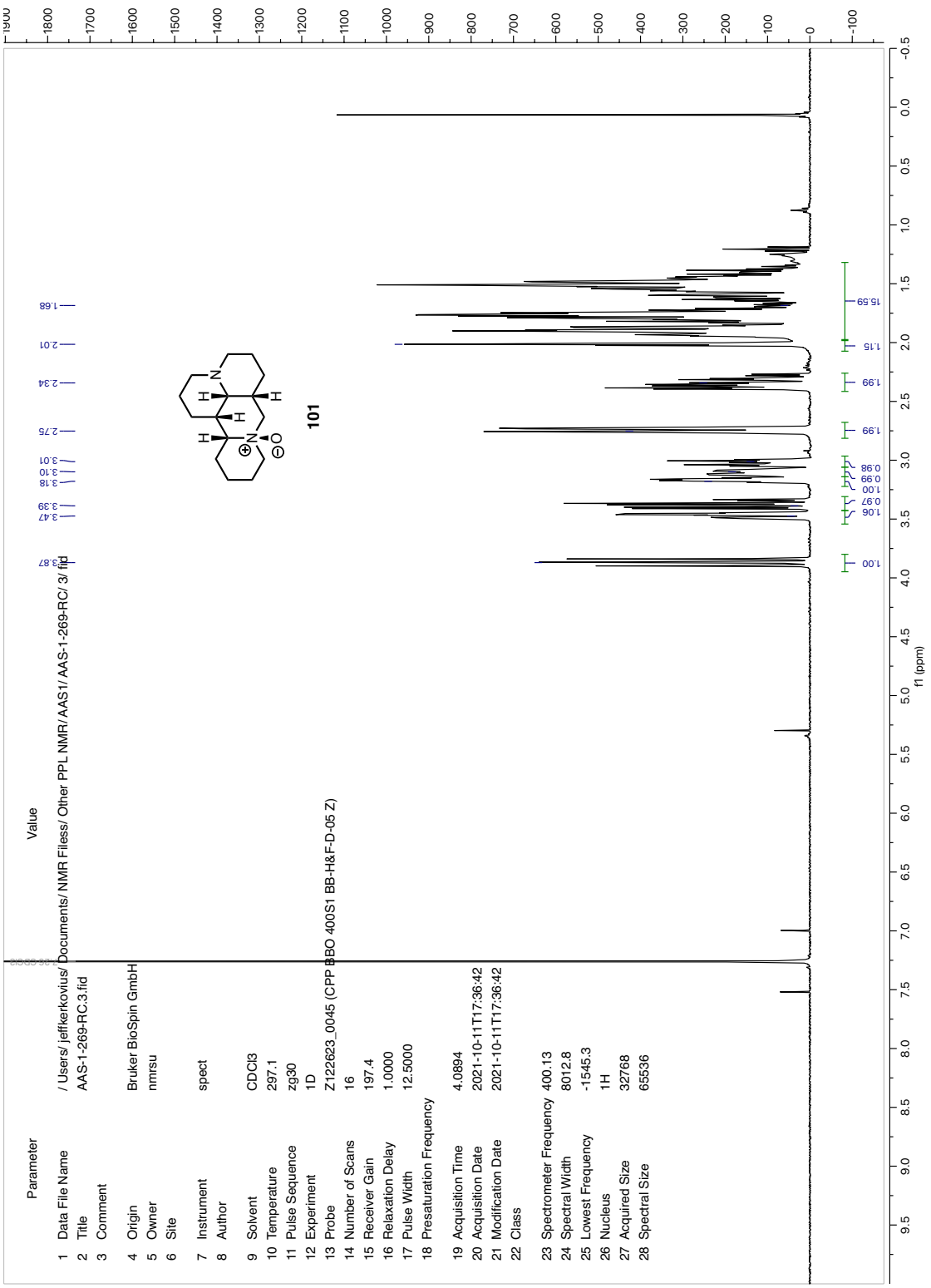
Parameter
Value
1 Data File Name / Users/ jeffkerkovius/ Documents/ NMR Files/ Other PPL NMR/ AAS1/ AAS-1-269-RC/ 3/ fid
2 Title AAS-1-269-RC.3.fid
3 Comment
4 Origin Bruker BioSpin GmbH
5 Owner nmrsu
6 Site
7 Instrument spect
8 Author
9 Solvent CDCl3
10 Temperature 297.1
11 Pulse Sequence zg30
12 Experiment 1D
13 Probe Z122623_0045 (CPP BBO 400S1 BB-H&F-D-05 Z)
14 Number of Scans 16
15 Receiver Gain 197.4
16 Relaxation Delay 1.0000
17 Pulse Width 12.5000
18 Presaturation Frequency
19 Acquisition Time 4.0894
20 Acquisition Date 2021-10-11T17:36:42
21 Modification Date 2021-10-11T17:36:42
22 Class
23 Spectrometer Frequency 400.13
24 Spectral Width 8012.8
25 Lowest Frequency -1545.3
26 Nucleus 1H
27 Acquired Size 32768
28 Spectral Size 65536
101
1.68
2.01
2.34
2.75
3.01
3.10
3.18
3.39
3.47
3.87
15.59
1.15
1.99
1.99
0.98
0.99
1.00
0.97
1.06
1.00
f1 (ppm)

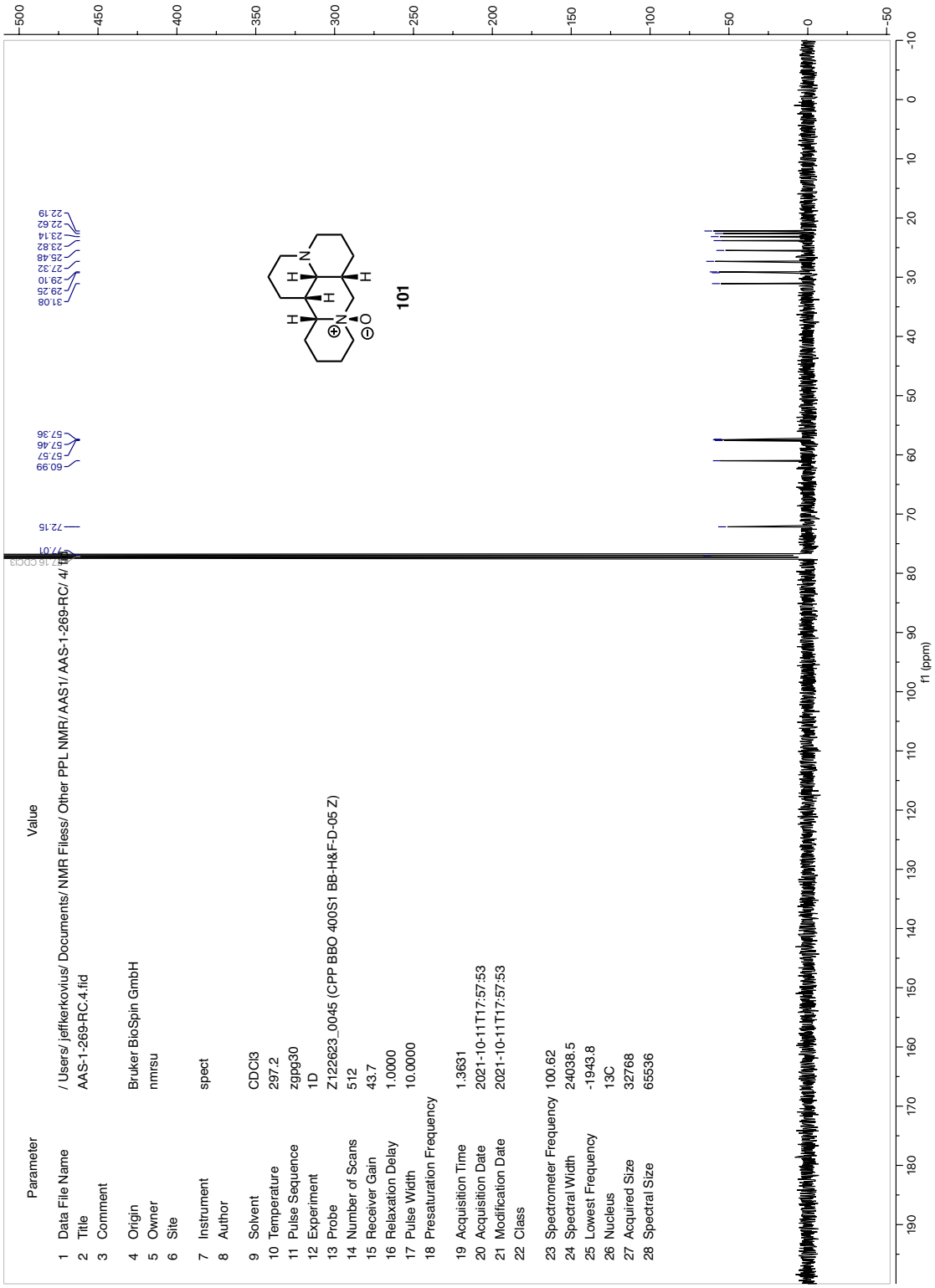
Parameter
Value
1 Data File Name / Users/ jeffkerkovius/ Documents/ NMR Files/ Other PPL NMR/ AAS1/ AAS-1-269-RC/ 4/
2 Title AAS-1-269-RC.4.fid
3 Comment
4 Origin Bruker BioSpin GmbH
5 Owner nmrsu
6 Site
7 Instrument spect
8 Author
9 Solvent CDCl3
10 Temperature 297.2
11 Pulse Sequence zgpg30
12 Experiment 1D
13 Probe Z122623_0045 (CPP BBO 400S1 BB-H&F-D-05 Z)
14 Number of Scans 512
15 Receiver Gain 43.7
16 Relaxation Delay 1.0000
17 Pulse Width 10.0000
18 Presaturation Frequency
19 Acquisition Time 1.3631
20 Acquisition Date 2021-10-11T17:57:53
21 Modification Date 2021-10-11T17:57:53
22 Class
23 Spectrometer Frequency 100.62
24 Spectral Width 24038.5
25 Lowest Frequency -1943.8
26 Nucleus 13C
27 Acquired Size 32768
28 Spectral Size 65536
77.01
72.15
60.99
57.57
57.46
57.36
31.08
29.25
29.10
27.32
25.48
23.82
23.14
22.62
22.19
101
f1 (ppm)

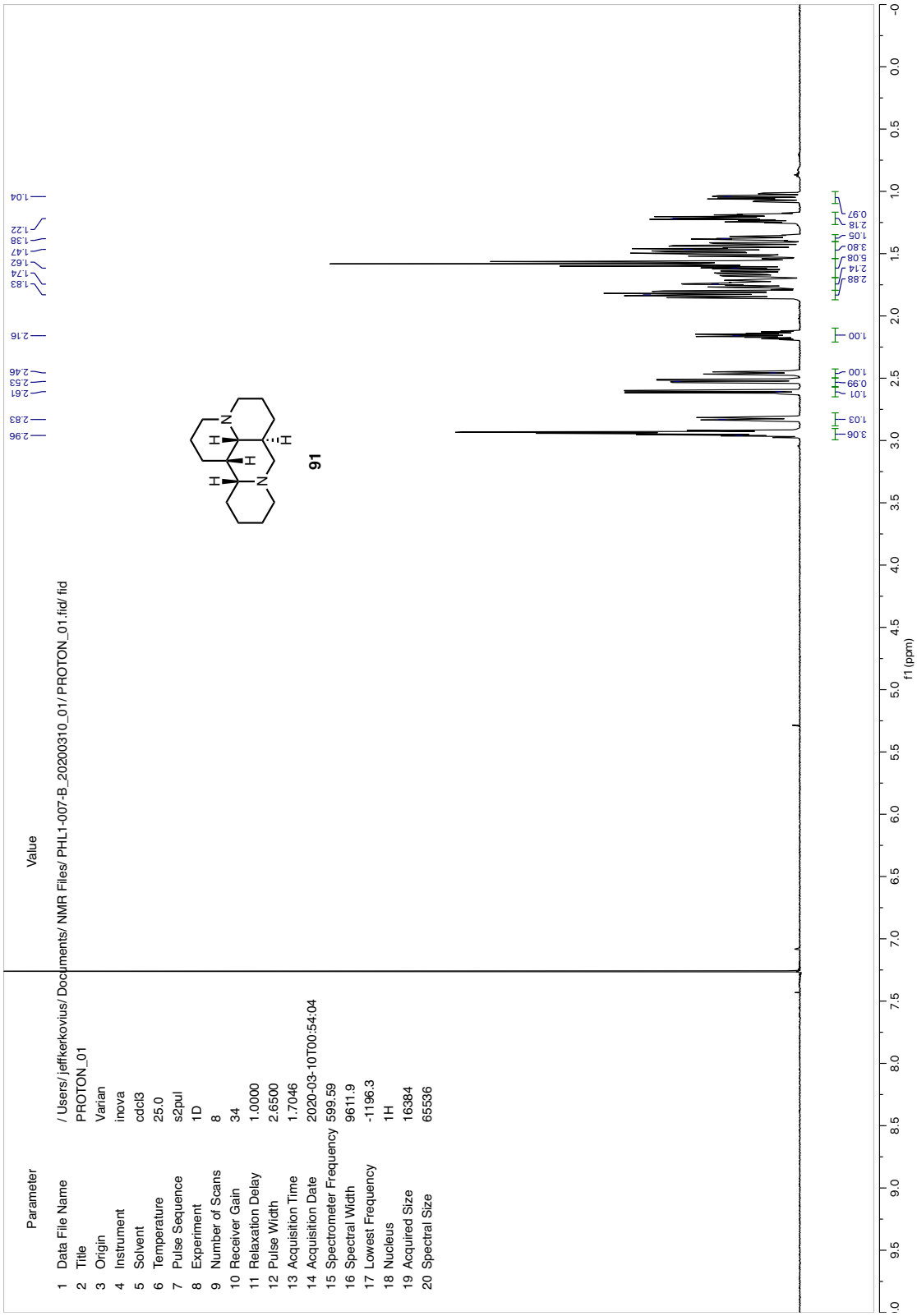
Parameter
Value
1 Data File Name / Users/ jeffkerkovius/ Documents/ NMR Files/ PHL1-007-B_20200310_01/ PROTON_01.fid/ fid
2 Title PROTON_01
3 Origin Varian
4 Instrument inova
5 Solvent cdcl3
6 Temperature 25.0
7 Pulse Sequence s2pul
8 Experiment 1D
9 Number of Scans 8
10 Receiver Gain 34
11 Relaxation Delay 1.0000
12 Pulse Width 2.6500
13 Acquisition Time 1.7046
14 Acquisition Date 2020-03-10T00:54:04
15 Spectrometer Frequency 599.59
16 Spectral Width 9611.9
17 Lowest Frequency -1196.3
18 Nucleus 1H
19 Acquired Size 16384
20 Spectral Size 65536
91
f1 (ppm)

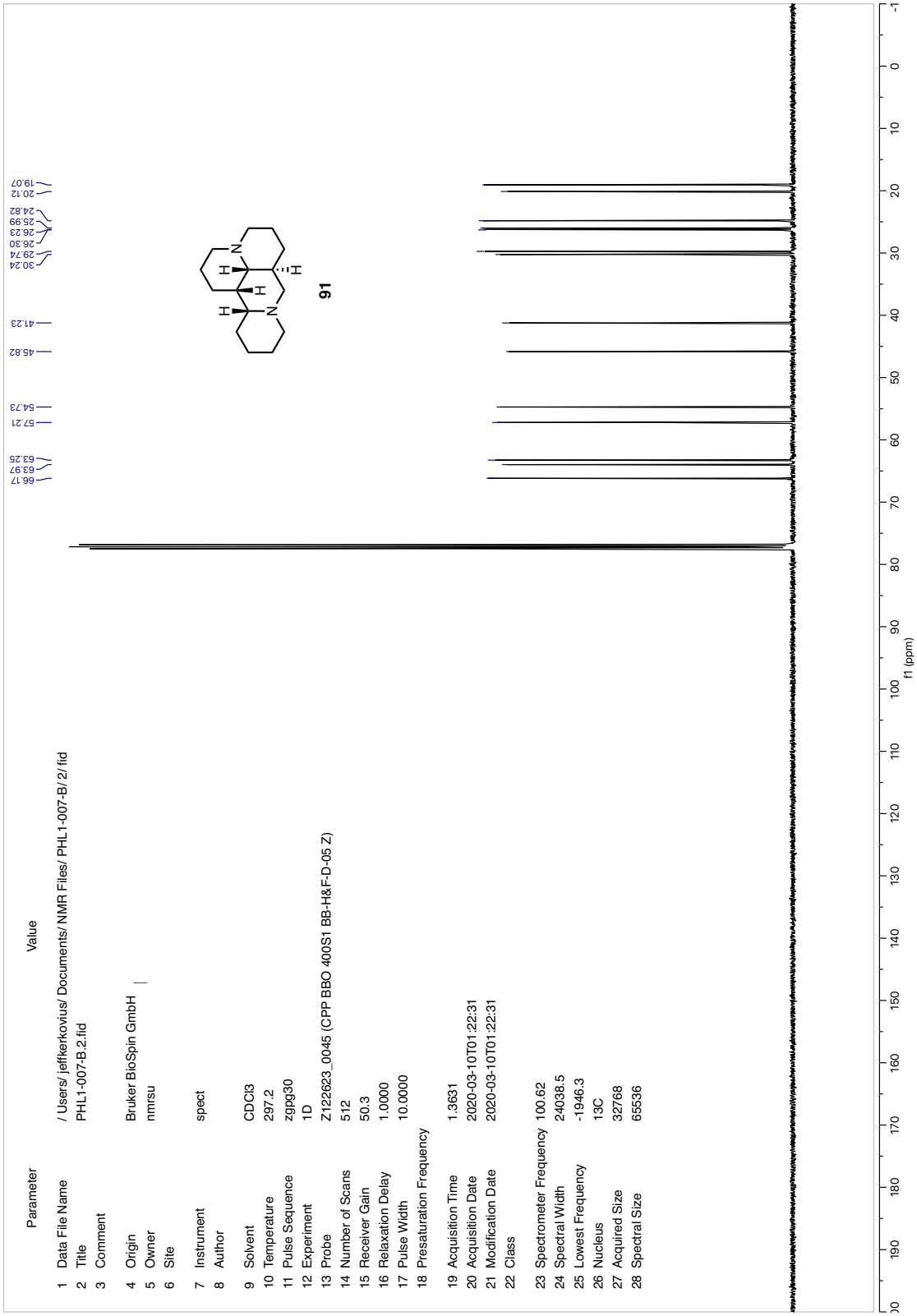
Parameter
Value
1 Data File Name / Users/ jeffkerkovius/ Documents/ NMR Files/ PHL1-007-B/ 2/ fid
2 Title PHL1-007-B.2.fid
3 Comment
4 Origin Bruker BioSpin GmbH
5 Owner nmrsu
6 Site
7 Instrument spect
8 Author
9 Solvent CDCl3
10 Temperature 297.2
11 Pulse Sequence zgpg30
12 Experiment 1D
13 Probe Z122623_0045 (CPP BBO 400S1 BB-H&F-D-05 Z)
14 Number of Scans 512
15 Receiver Gain 50.3
16 Relaxation Delay 1.0000
17 Pulse Width 10.0000
18 Presaturation Frequency
19 Acquisition Time 1.3631
20 Acquisition Date 2020-03-10T01:22:31
21 Modification Date 2020-03-10T01:22:31
22 Class
23 Spectrometer Frequency 100.62
24 Spectral Width 24038.5
25 Lowest Frequency -1946.3
26 Nucleus 13C
27 Acquired Size 32768
28 Spectral Size 65536
19.07
20.12
24.82
25.99
26.23
26.30
29.74
30.24
41.23
45.82
54.73
57.21
63.25
63.97
66.17
91
f1 (ppm)

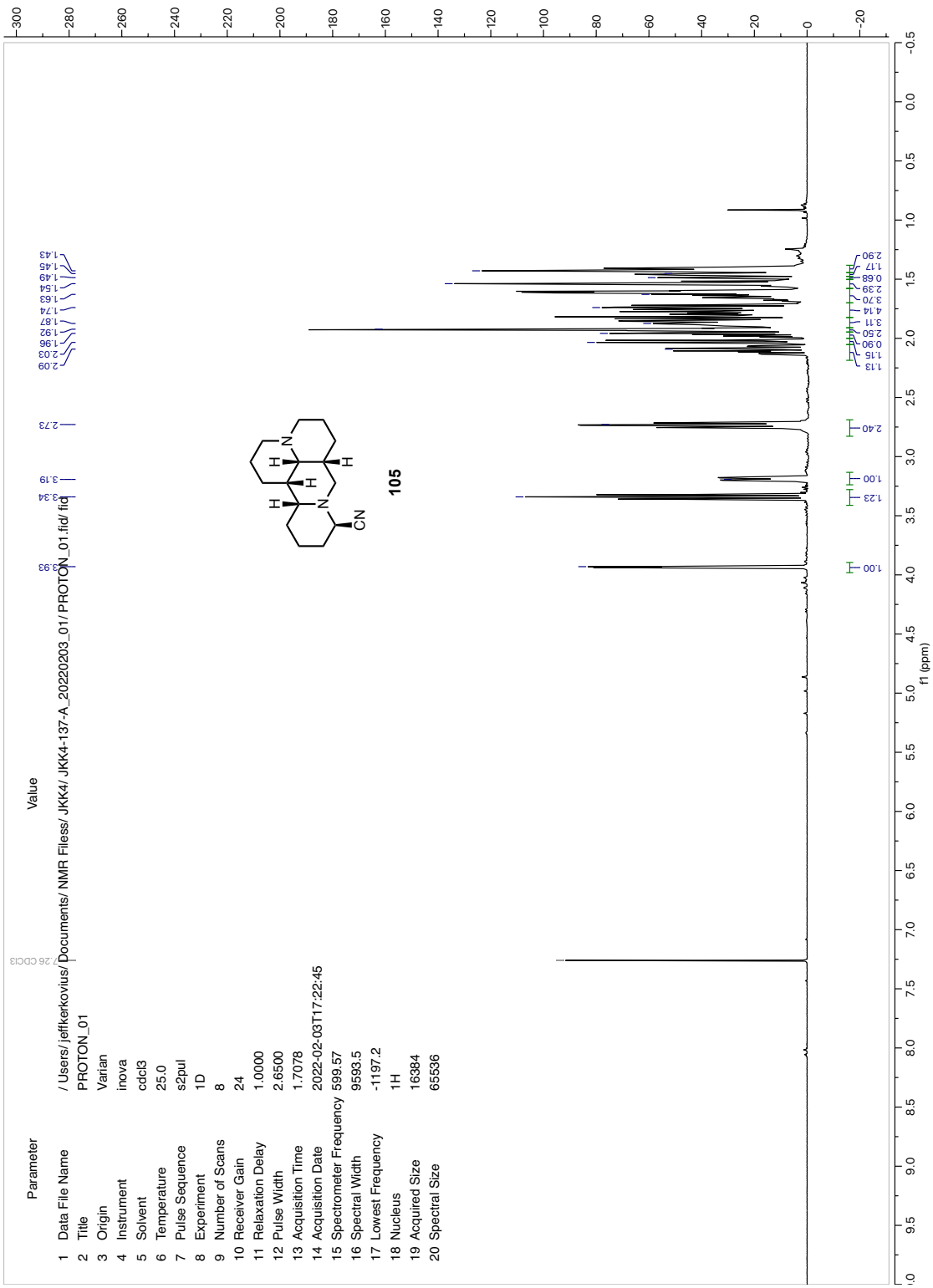
Parameter
Value
1 Data File Name / Users/ jeffkerkovius/ Documents/ NMR Files/ JKK4/ JKK4-137-A_20220203_01/ PROTON_01.fid/ fid
2 Title PROTON_01
3 Origin Varian
4 Instrument inova
5 Solvent cdcl3
6 Temperature 25.0
7 Pulse Sequence s2pul
8 Experiment 1D
9 Number of Scans 8
10 Receiver Gain 24
11 Relaxation Delay 1.0000
12 Pulse Width 2.6500
13 Acquisition Time 1.7078
14 Acquisition Date 2022-02-03T17:22:45
15 Spectrometer Frequency 599.57
16 Spectral Width 9593.5
17 Lowest Frequency -1197.2
18 Nucleus 1H
19 Acquired Size 16384
20 Spectral Size 65536
105
f1 (ppm)

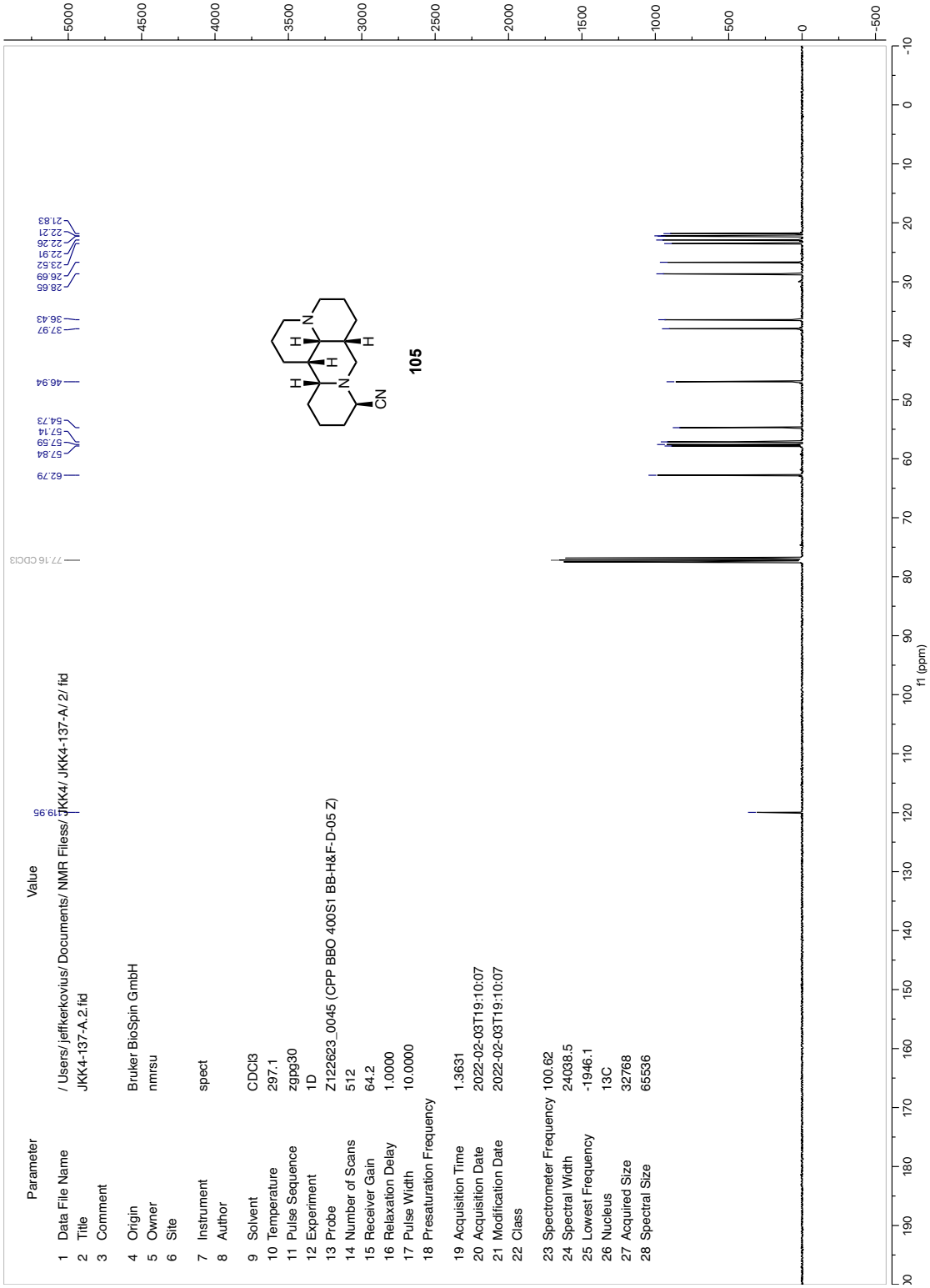
Parameter
Value
1 Data File Name / Users/ jeffkerkovius/ Documents/ NMR Files/ JKK4/ JKK4-137-A/ 2/ fid
2 Title JKK4-137-A.2.fid
3 Comment
4 Origin Bruker BioSpin GmbH
5 Owner nmrsu
6 Site
7 Instrument spect
8 Author
9 Solvent CDCl3
10 Temperature 297.1
11 Pulse Sequence zgpg30
12 Experiment 1D
13 Probe Z122623_0045 (CPP BBO 400S1 BB-H&F-D-05 Z)
14 Number of Scans 512
15 Receiver Gain 64.2
16 Relaxation Delay 1.0000
17 Pulse Width 10.0000
18 Presaturation Frequency
19 Acquisition Time 1.3631
20 Acquisition Date 2022-02-03T19:10:07
21 Modification Date 2022-02-03T19:10:07
22 Class
23 Spectrometer Frequency 100.62
24 Spectral Width 24038.5
25 Lowest Frequency -1946.1
26 Nucleus 13C
27 Acquired Size 32768
28 Spectral Size 65536
119.95
77.16 CDCl3
62.79
57.84
57.59
57.14
54.73
46.94
37.97
36.43
28.65
26.69
23.52
22.91
22.26
22.21
21.83
105
f1 (ppm)

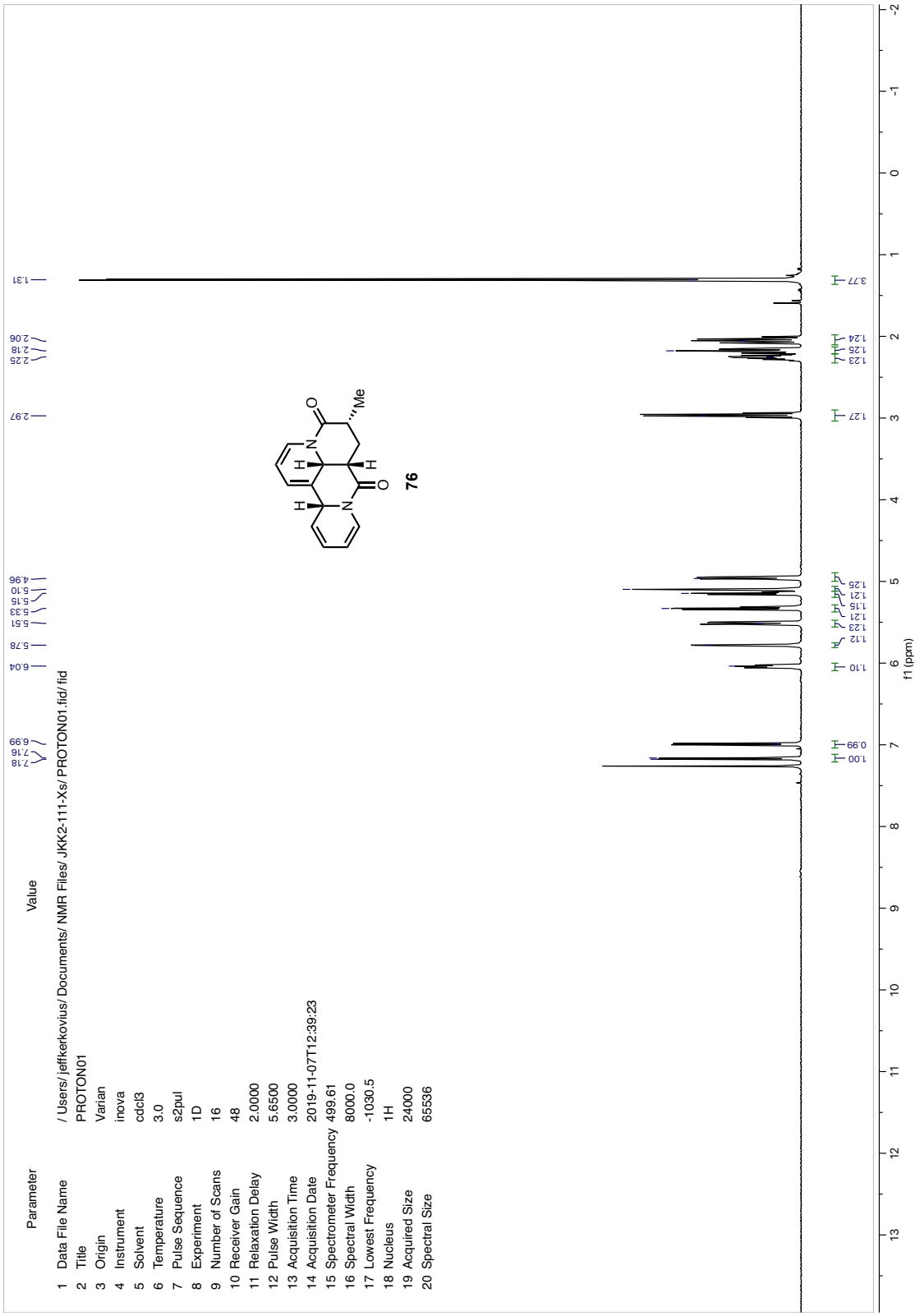
Parameter Value
1 Data File Name / Users/ jeffkerkovius/ Documents/ NMR Files/ JKK2-111-Xs/ PROTON01.fid/ fid
2 Title PROTON01
3 Origin Varian
4 Instrument inova
5 Solvent cdcl3
6 Temperature 3.0
7 Pulse Sequence s2pul
8 Experiment 1D
9 Number of Scans 16
10 Receiver Gain 48
11 Relaxation Delay 2.0000
12 Pulse Width 5.6500
13 Acquisition Time 3.0000
14 Acquisition Date 2019-11-07T12:39:23
15 Spectrometer Frequency 499.61
16 Spectral Width 8000.0
17 Lowest Frequency -1030.5
18 Nucleus 1H
19 Acquired Size 24000
20 Spectral Size 65536
7.18
7.16
6.99
6.04
5.78
5.51
5.33
5.15
5.10
4.96
2.97
2.25
2.18
2.06
1.31
0.99
1.00
1.10
1.12
1.23
1.21
1.21
1.15
1.21
1.25
1.27
1.23
1.25
1.24
3.77
Me
76
f1 (ppm)

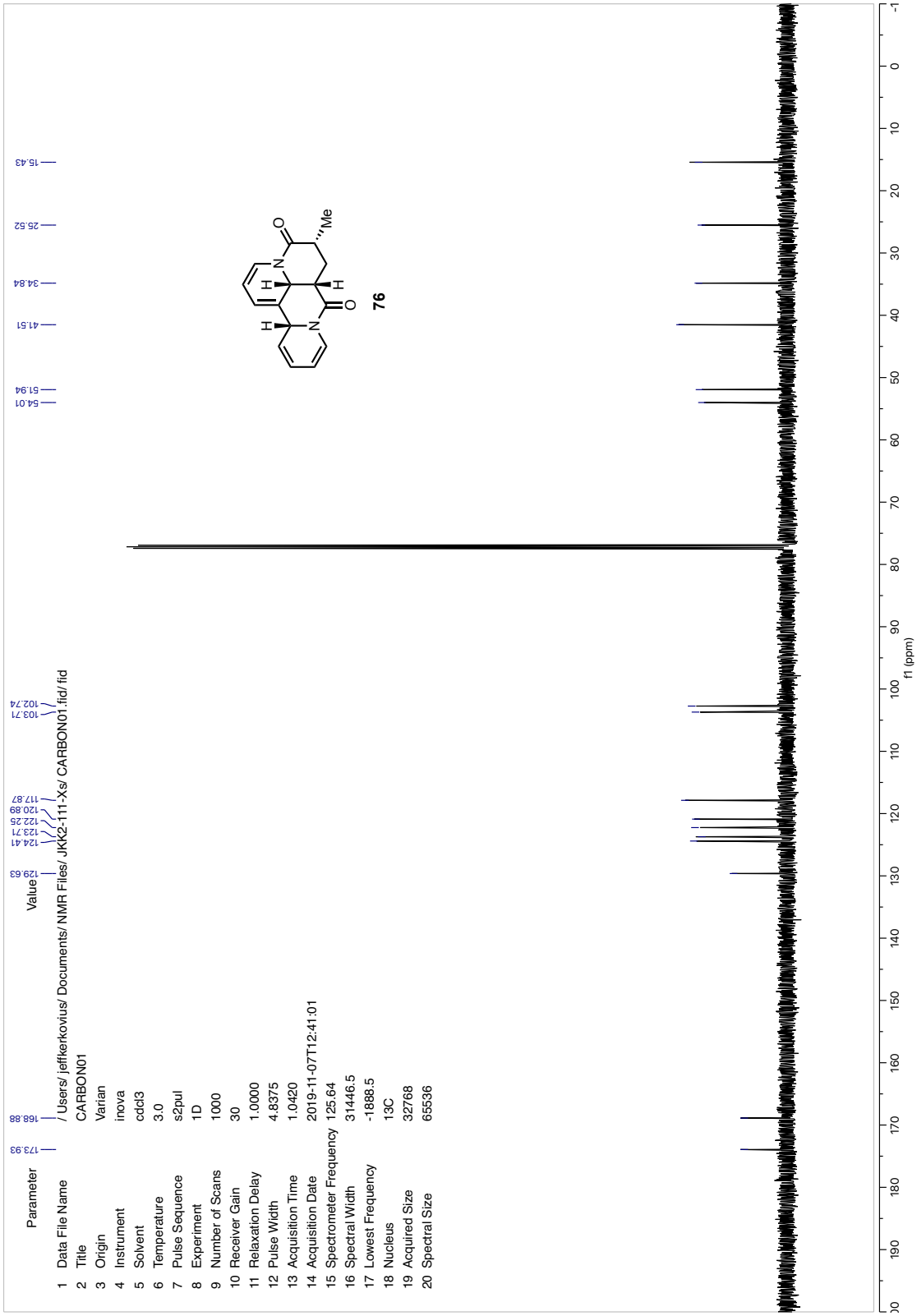
Parameter Value
1 Data File Name / Users/ jeffkerkovius/ Documents/ NMR Files/ JKK2-111-Xs/ CARBON01.fid/ fid
2 Title CARBON01
3 Origin Varian
4 Instrument inova
5 Solvent cdcl3
6 Temperature 3.0
7 Pulse Sequence s2pul
8 Experiment 1D
9 Number of Scans 1000
10 Receiver Gain 30
11 Relaxation Delay 1.0000
12 Pulse Width 4.8375
13 Acquisition Time 1.0420
14 Acquisition Date 2019-11-07T12:41:01
15 Spectrometer Frequency 125.64
16 Spectral Width 31446.5
17 Lowest Frequency -1888.5
18 Nucleus 13C
19 Acquired Size 32768
20 Spectral Size 65536
173.93
168.88
129.63
124.41
123.71
122.25
120.89
117.87
103.71
102.74
54.01
51.94
41.51
34.84
25.52
15.43
Me
76
f1 (ppm)

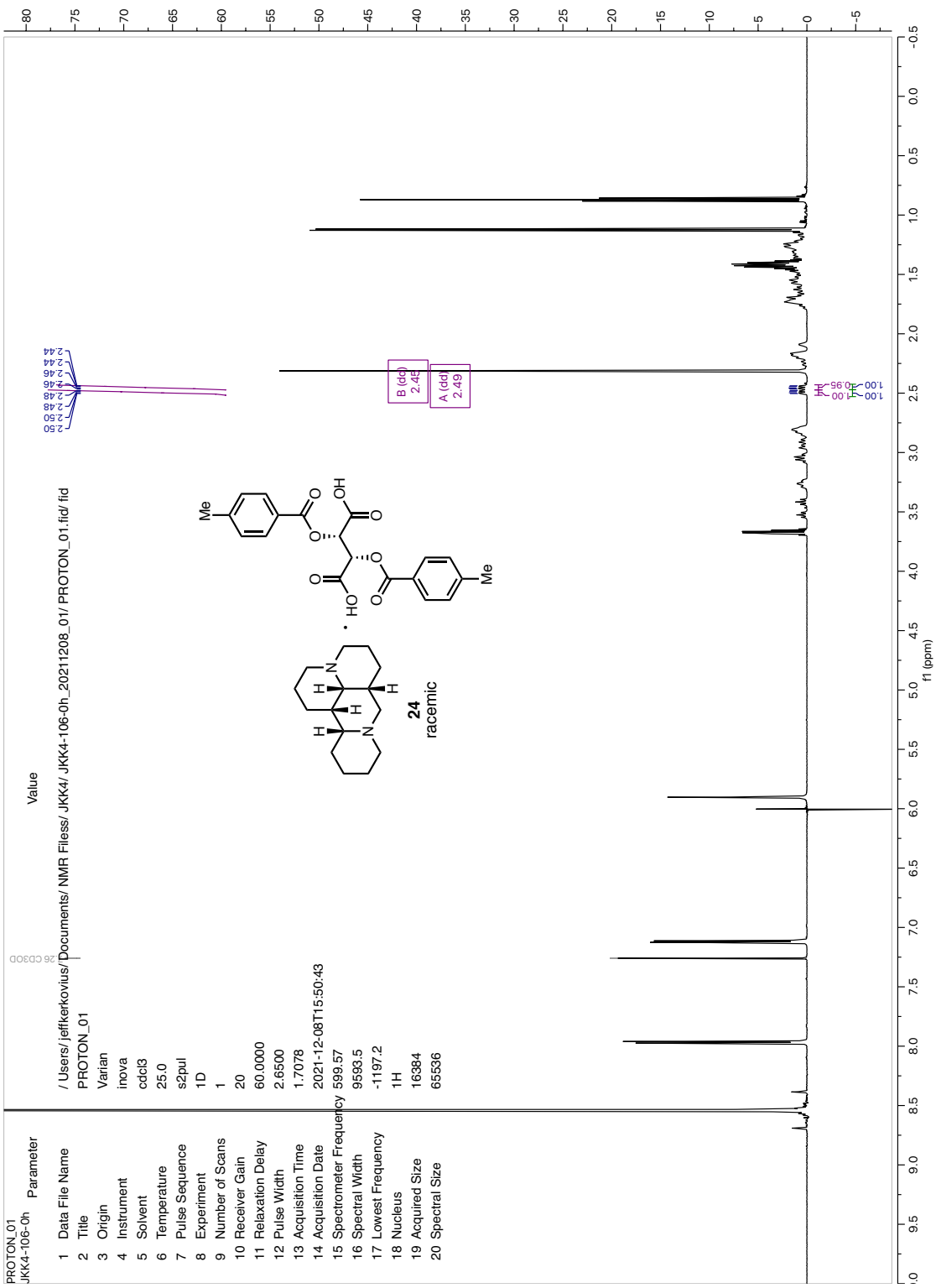
PROTON_01
JKK4-106-0h
Parameter Value
1 Data File Name / Users/ jeffkerkovius/ Documents/ NMR Files/ JKK4/ JKK4-106-0h_20211208_01/ PROTON_01.fid/ fid
2 Title PROTON_01
3 Origin Varian
4 Instrument inova
5 Solvent cdcl3
6 Temperature 25.0
7 Pulse Sequence s2pul
8 Experiment 1D
9 Number of Scans 1
10 Receiver Gain 20
11 Relaxation Delay 60.0000
12 Pulse Width 2.6500
13 Acquisition Time 1.7078
14 Acquisition Date 2021-12-08T15:50:43
15 Spectrometer Frequency 599.57
16 Spectral Width 9593.5
17 Lowest Frequency -1197.2
18 Nucleus 1H
19 Acquired Size 16384
20 Spectral Size 65536
26 CD3OD
B (dd) 2.45
A (dd) 2.49
1.00
1.00
0.95
1H
24
racemic
f1 (ppm)

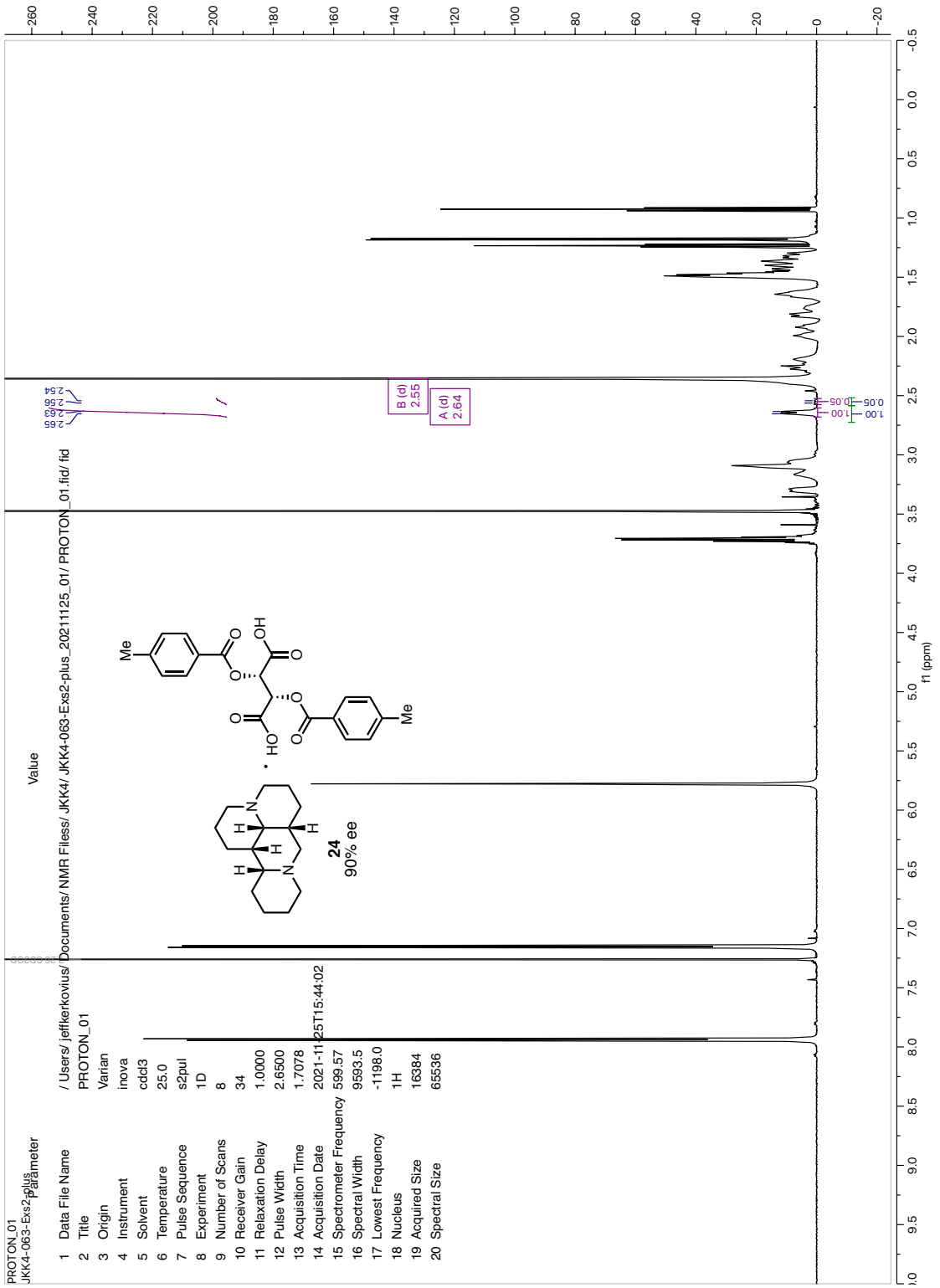
PROTON_01
JKK4-063-Exs2-plus
Parameter Value
1 Data File Name / Users/ jeffkerkovius/ Documents/ NMR Files/ JKK4/ JKK4-063-Exs2-plus_20211125_01/ PROTON_01.fid/ fid
2 Title PROTON_01
3 Origin Varian
4 Instrument inova
5 Solvent cdcl3
6 Temperature 25.0
7 Pulse Sequence s2pul
8 Experiment 1D
9 Number of Scans 8
10 Receiver Gain 34
11 Relaxation Delay 1.0000
12 Pulse Width 2.6500
13 Acquisition Time 1.7078
14 Acquisition Date 2021-11-25T15:44:02
15 Spectrometer Frequency 599.57
16 Spectral Width 9593.5
17 Lowest Frequency -1198.0
18 Nucleus 1H
19 Acquired Size 16384
20 Spectral Size 65536
24
90% ee
B (d) 2.55
A (d) 2.64
2.65
2.63
2.56
2.54
1.00
0.05
f1 (ppm)

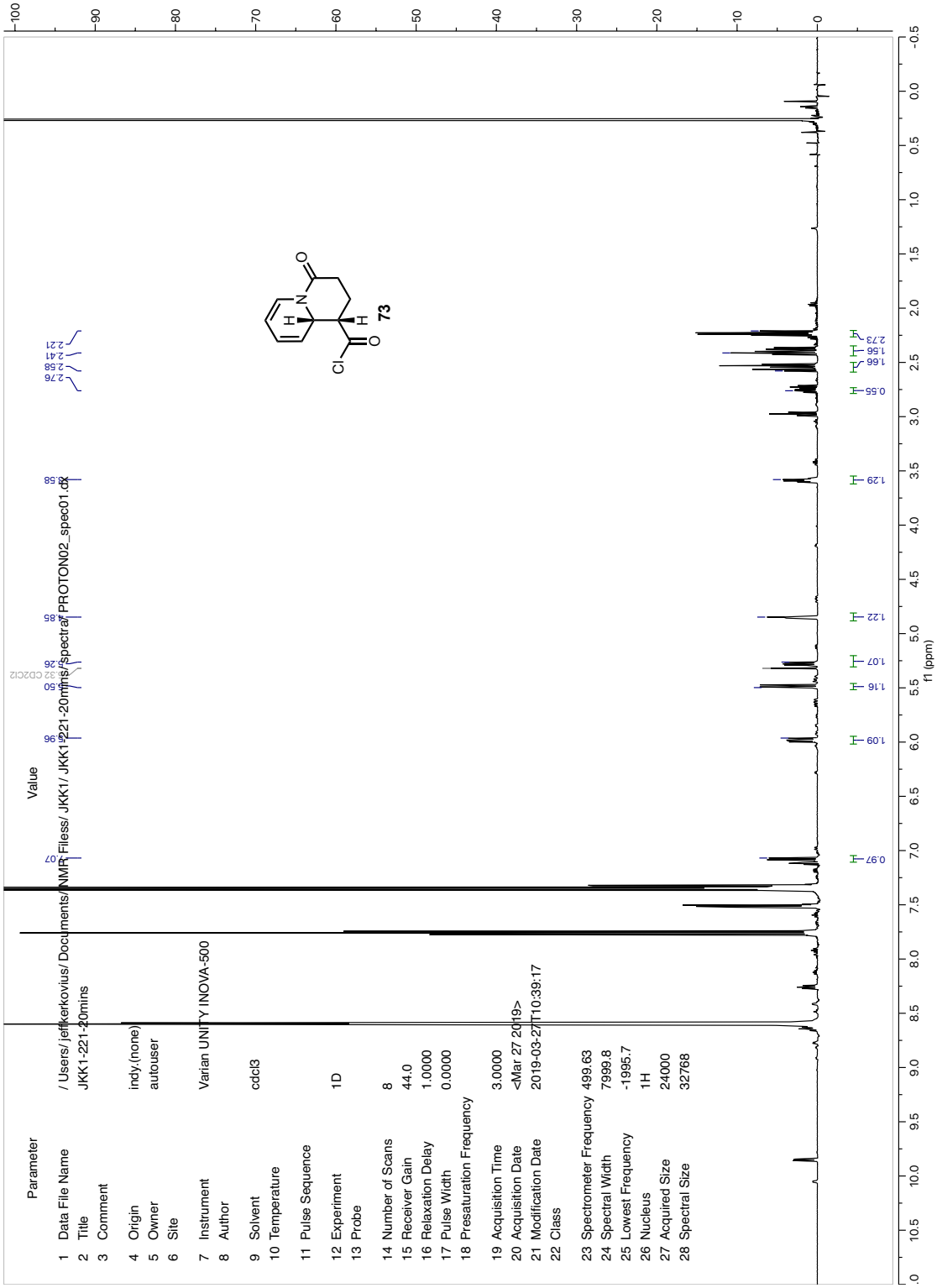
Parameter
Value
1 Data File Name / Users/ jeffkerkovius/ Documents/ NMR Files/ JKK1/ JKK1-221-20mins/ spectra/ PROTON02_spec01.dx
2 Title JKK1-221-20mins
3 Comment
4 Origin indy.(none)
5 Owner autouser
6 Site
7 Instrument Varian UNITY INOVA-500
8 Author
9 Solvent cdcl3
10 Temperature
11 Pulse Sequence
12 Experiment 1D
13 Probe
14 Number of Scans 8
15 Receiver Gain 44.0
16 Relaxation Delay 1.0000
17 Pulse Width 0.0000
18 Presaturation Frequency
19 Acquisition Time 3.0000
20 Acquisition Date <Mar 27 2019>
21 Modification Date 2019-03-27T10:39:17
22 Class
23 Spectrometer Frequency 499.63
24 Spectral Width 7999.8
25 Lowest Frequency -1995.7
26 Nucleus 1H
27 Acquired Size 24000
28 Spectral Size 32768
73
f1 (ppm)

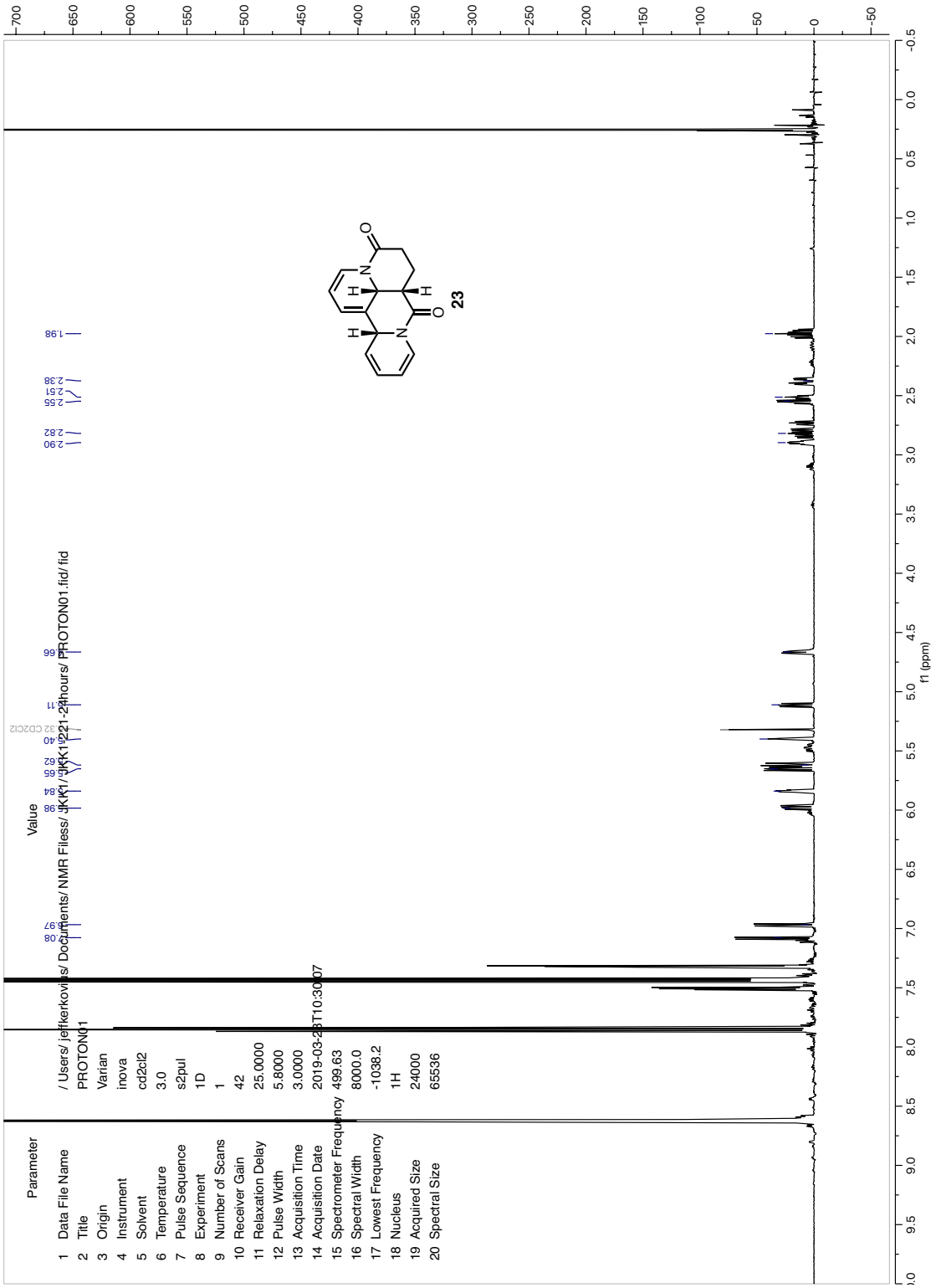
Parameter
Value
1 Data File Name / Users/ jeffkerkovius/ Documents/ NMR Files/ JKK1/ JKK1-221-24hours/ PROTON01.fid/ fid
2 Title PROTON01
3 Origin Varian
4 Instrument inova
5 Solvent cd2cl2
6 Temperature 3.0
7 Pulse Sequence s2pul
8 Experiment 1D
9 Number of Scans 1
10 Receiver Gain 42
11 Relaxation Delay 25.0000
12 Pulse Width 5.8000
13 Acquisition Time 3.0000
14 Acquisition Date 2019-03-28T10:30:07
15 Spectrometer Frequency 499.63
16 Spectral Width 8000.0
17 Lowest Frequency -1038.2
18 Nucleus 1H
19 Acquired Size 24000
20 Spectral Size 65536
1.98
2.38
2.51
2.55
2.82
2.90
11
66
40
62
65
84
98
97
08
CD2Cl2
23
f1 (ppm)

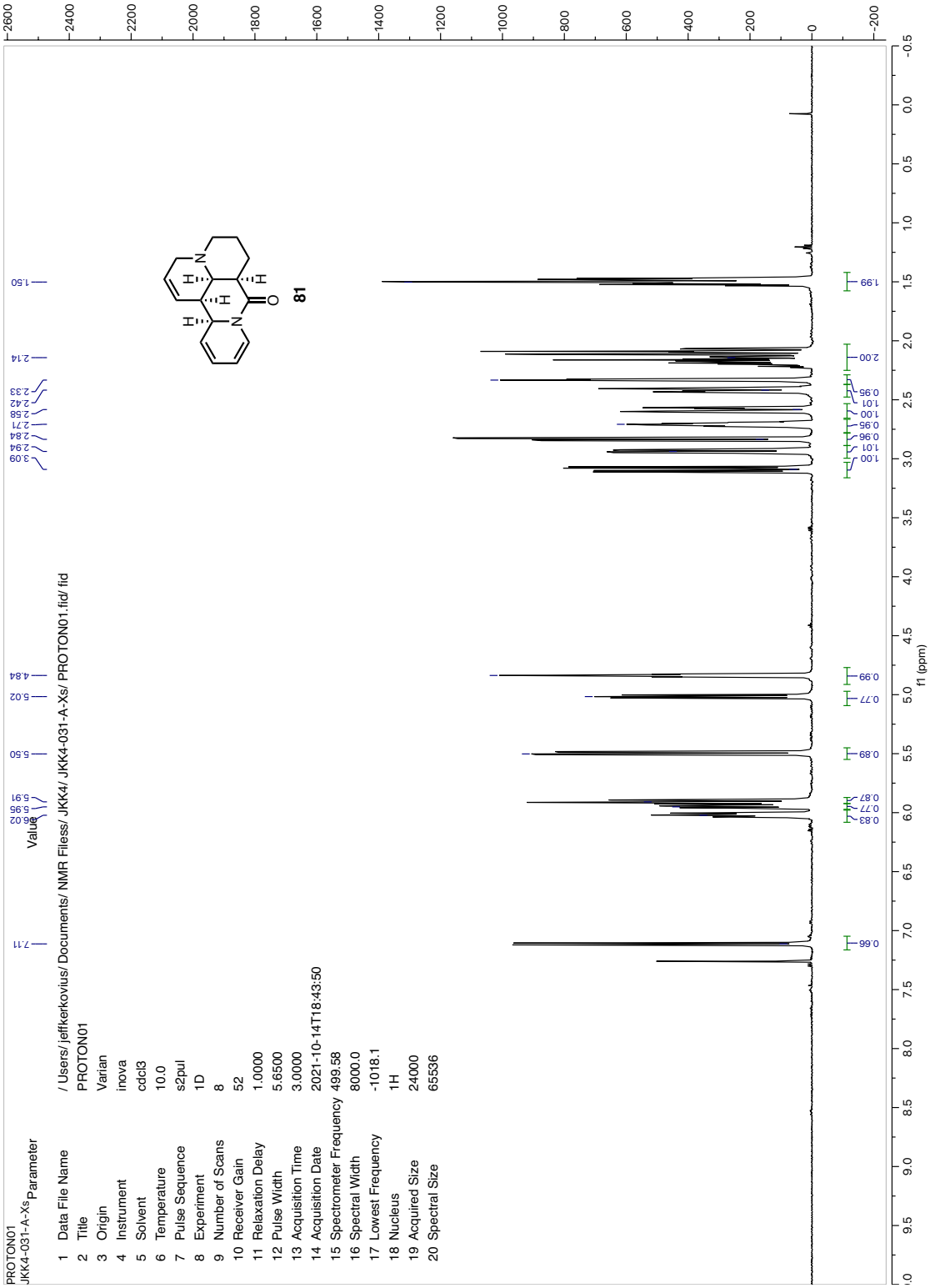
PROTON01
JKK4-031-A-Xs
Parameter Value
1 Data File Name / Users/ jeffkerkovius/ Documents/ NMR Files/ JKK4/ JKK4-031-A-Xs/ PROTON01.fid/ fid
2 Title PROTON01
3 Origin Varian
4 Instrument inova
5 Solvent cdcl3
6 Temperature 10.0
7 Pulse Sequence s2pul
8 Experiment 1D
9 Number of Scans 8
10 Receiver Gain 52
11 Relaxation Delay 1.0000
12 Pulse Width 5.6500
13 Acquisition Time 3.0000
14 Acquisition Date 2021-10-14T18:43:50
15 Spectrometer Frequency 499.58
16 Spectral Width 8000.0
17 Lowest Frequency -1018.1
18 Nucleus 1H
19 Acquired Size 24000
20 Spectral Size 65536
81
f1 (ppm)

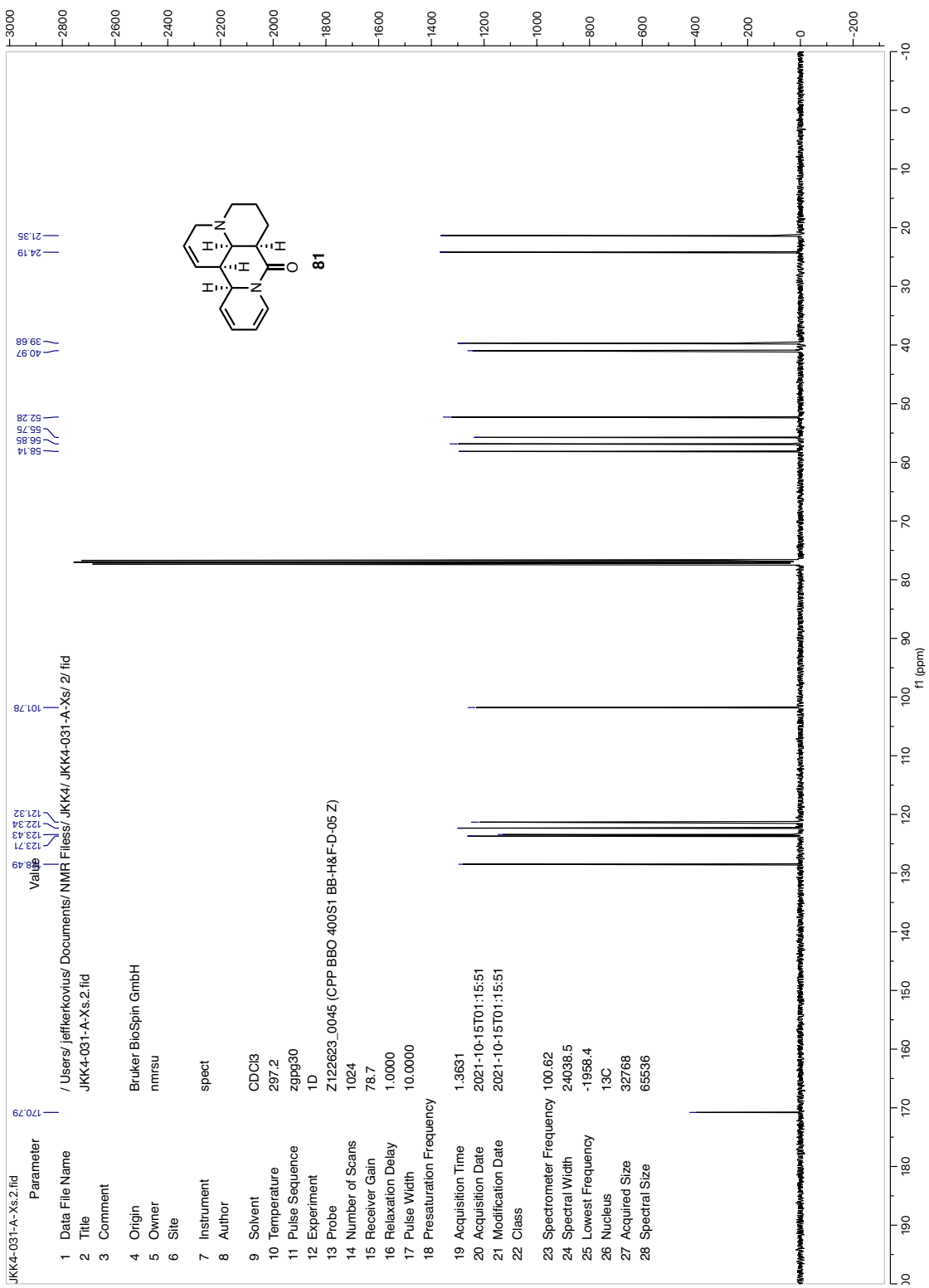
JKK4-031-A-Xs.2.fid
Parameter Value
1 Data File Name / Users/ jeffkerkovius/ Documents/ NMR Files/ JKK4/ JKK4-031-A-Xs/ 2/ fid
2 Title JKK4-031-A-Xs.2.fid
3 Comment
4 Origin Bruker BioSpin GmbH
5 Owner nmrsu
6 Site
7 Instrument spect
8 Author
9 Solvent CDCl3
10 Temperature 297.2
11 Pulse Sequence zgpg30
12 Experiment 1D
13 Probe Z122623_0045 (CPP BBO 400S1 BB-H&F-D-05 Z)
14 Number of Scans 1024
15 Receiver Gain 78.7
16 Relaxation Delay 1.0000
17 Pulse Width 10.0000
18 Presaturation Frequency
19 Acquisition Time 1.3631
20 Acquisition Date 2021-10-15T01:15:51
21 Modification Date 2021-10-15T01:15:51
22 Class
23 Spectrometer Frequency 100.62
24 Spectral Width 24038.5
25 Lowest Frequency -1958.4
26 Nucleus 13C
27 Acquired Size 32768
28 Spectral Size 65536
170.79
138.49
123.71
123.43
122.34
121.32
101.78
58.14
56.85
56.75
52.28
40.97
39.68
24.19
21.35
81
f1 (ppm)

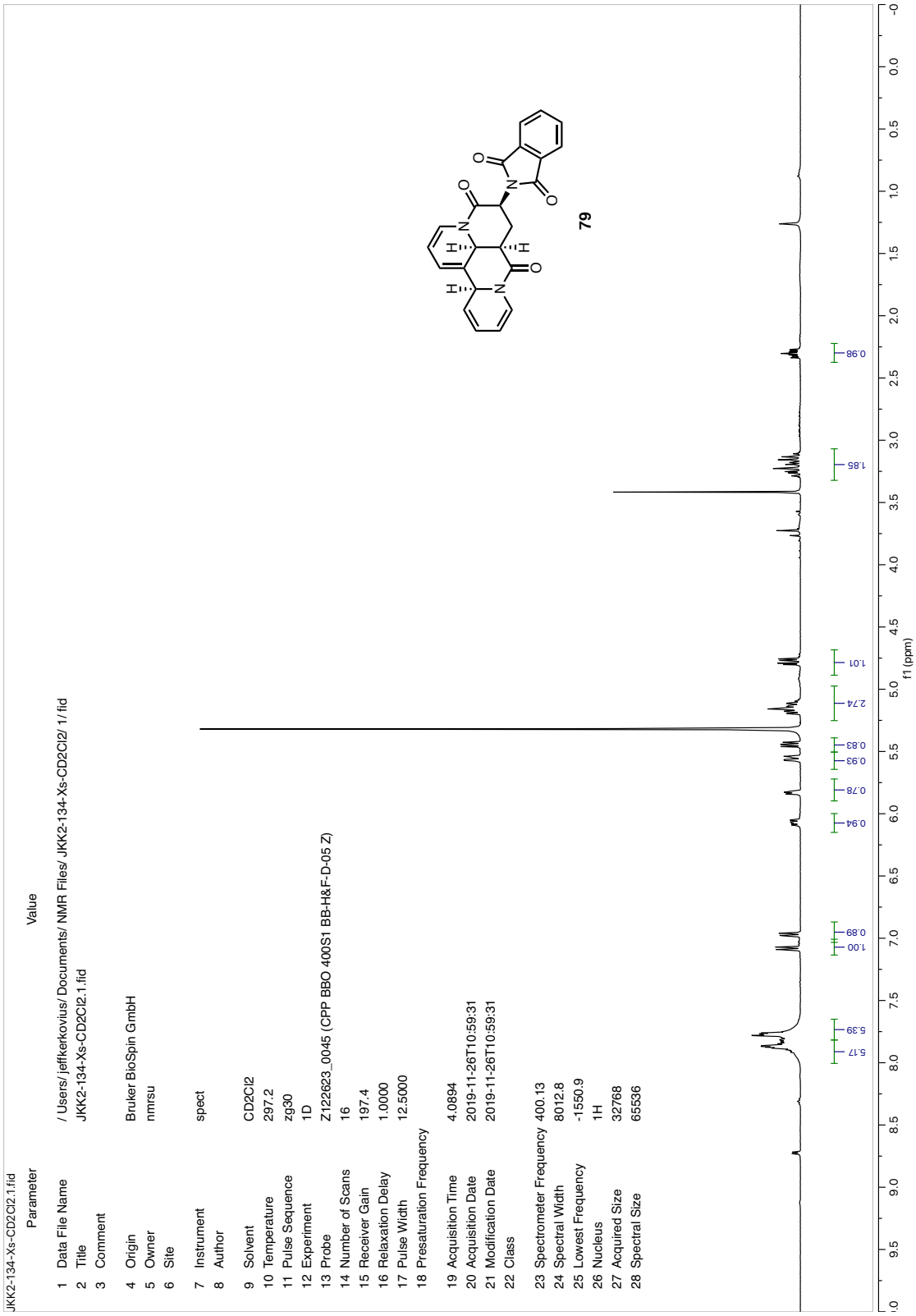
JKK2-134-Xs-CD2Cl2.1.fid
Parameter
Value
1 Data File Name / Users/ jeffkerkovius/ Documents/ NMR Files/ JKK2-134-Xs-CD2Cl2/ 1/ fid
2 Title JKK2-134-Xs-CD2Cl2.1.fid
3 Comment
4 Origin Bruker BioSpin GmbH
5 Owner nmrsu
6 Site
7 Instrument spect
8 Author
9 Solvent CD2Cl2
10 Temperature 297.2
11 Pulse Sequence zg30
12 Experiment 1D
13 Probe Z122623_0045 (CPP BBO 400S1 BB-H&F-D-05 Z)
14 Number of Scans 16
15 Receiver Gain 197.4
16 Relaxation Delay 1.0000
17 Pulse Width 12.5000
18 Presaturation Frequency
19 Acquisition Time 4.0894
20 Acquisition Date 2019-11-26T10:59:31
21 Modification Date 2019-11-26T10:59:31
22 Class
23 Spectrometer Frequency 400.13
24 Spectral Width 8012.8
25 Lowest Frequency -1550.9
26 Nucleus 1H
27 Acquired Size 32768
28 Spectral Size 65536
79
5.39
5.17
1.00
0.89
0.94
0.78
0.93
0.83
2.74
1.01
1.85
0.98
f1 (ppm)

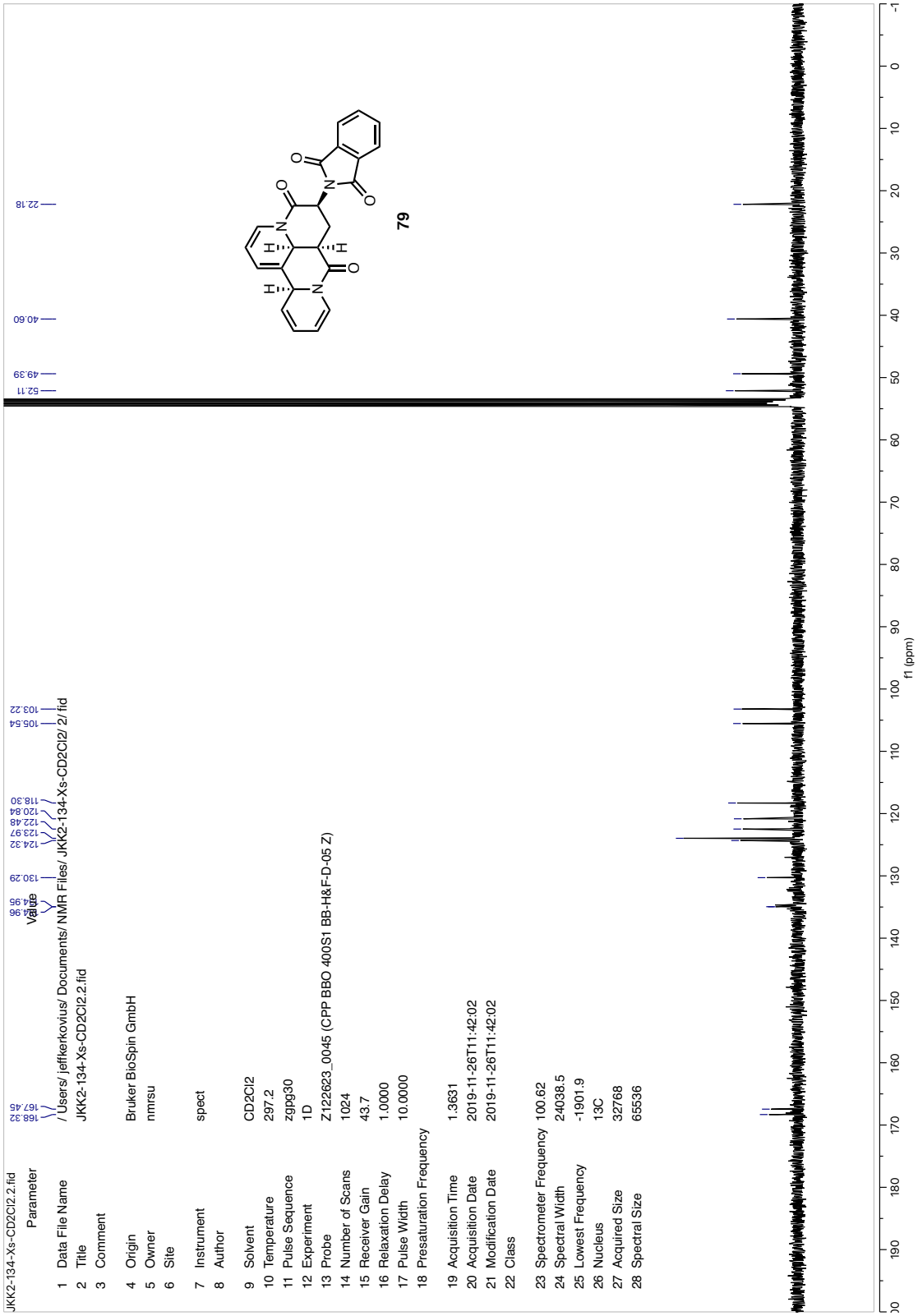
JKK2-134-Xs-CD2Cl2.2.fid
Parameter
Value
1 Data File Name / Users/ jeffkerkovius/ Documents/ NMR Files/ JKK2-134-Xs-CD2Cl2/ 2/ fid
2 Title JKK2-134-Xs-CD2Cl2.2.fid
3 Comment
4 Origin Bruker BioSpin GmbH
5 Owner nmrsu
6 Site
7 Instrument spect
8 Author
9 Solvent CD2Cl2
10 Temperature 297.2
11 Pulse Sequence zgpg30
12 Experiment 1D
13 Probe Z122623_0045 (CPP BBO 400S1 BB-H&F-D-05 Z)
14 Number of Scans 1024
15 Receiver Gain 43.7
16 Relaxation Delay 1.0000
17 Pulse Width 10.0000
18 Presaturation Frequency
19 Acquisition Time 1.3631
20 Acquisition Date 2019-11-26T11:42:02
21 Modification Date 2019-11-26T11:42:02
22 Class
23 Spectrometer Frequency 100.62
24 Spectral Width 24038.5
25 Lowest Frequency -1901.9
26 Nucleus 13C
27 Acquired Size 32768
28 Spectral Size 65536
168.32
167.45
105.54
103.22
130.29
124.32
123.97
122.48
120.84
118.30
52.11
49.39
40.60
22.18
79
f1 (ppm)

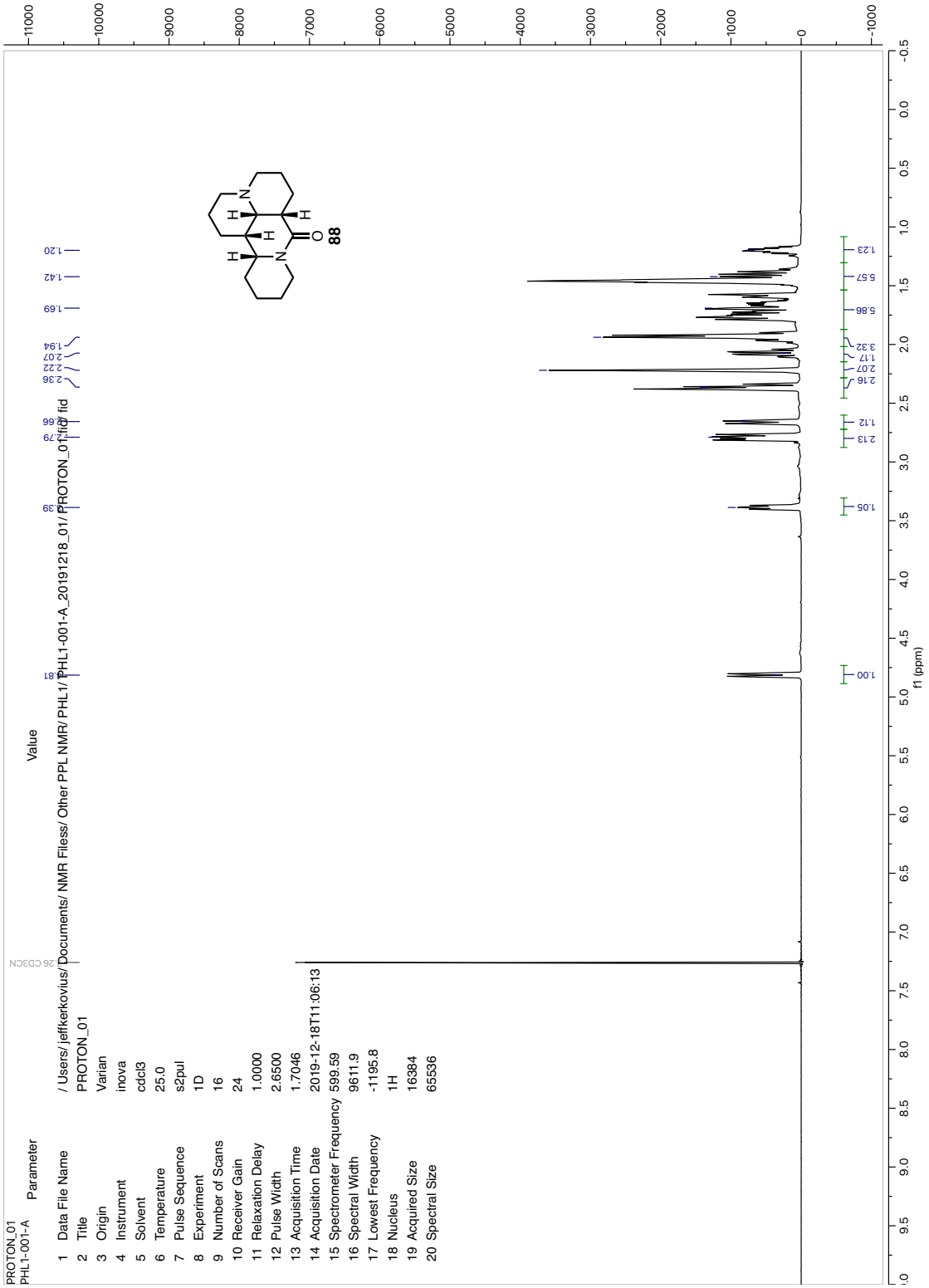
PROTON_01
PHL1-001-A
Parameter Value
1 Data File Name / Users/ jeffkerkovius/ Documents/ NMR Files/ Other PPL NMR/ PHL1/ PHL1-001-A_20191218_01/ PROTON_01.fid/ fid
2 Title PROTON_01
3 Origin Varian
4 Instrument inova
5 Solvent cdcl3
6 Temperature 25.0
7 Pulse Sequence s2pul
8 Experiment 1D
9 Number of Scans 16
10 Receiver Gain 24
11 Relaxation Delay 1.0000
12 Pulse Width 2.6500
13 Acquisition Time 1.7046
14 Acquisition Date 2019-12-18T11:06:13
15 Spectrometer Frequency 599.59
16 Spectral Width 9611.9
17 Lowest Frequency -1195.8
18 Nucleus 1H
19 Acquired Size 16384
20 Spectral Size 65536
88
f1 (ppm)

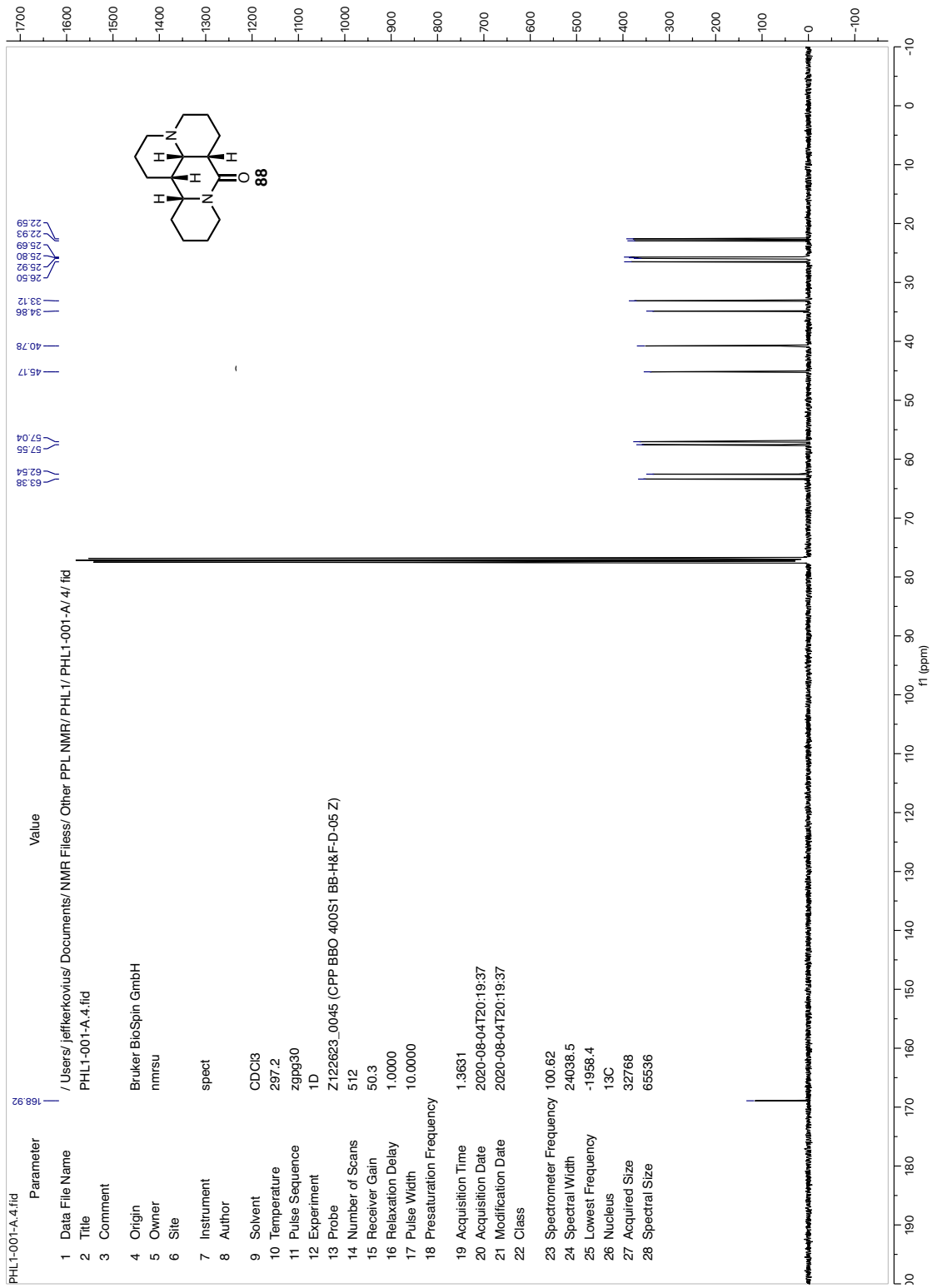
PHL1-001-A.4.fid
Parameter
Value
1 Data File Name / Users/ jeffkerkovius/ Documents/ NMR Files/ Other PPL NMR/ PHL1/ PHL1-001-A/ 4/ fid
2 Title PHL1-001-A.4.fid
3 Comment
4 Origin Bruker BioSpin GmbH
5 Owner nmrsu
6 Site
7 Instrument spect
8 Author
9 Solvent CDCl3
10 Temperature 297.2
11 Pulse Sequence zgpg30
12 Experiment 1D
13 Probe Z122623_0045 (CPP BBO 400S1 BB-H&F-D-05 Z)
14 Number of Scans 512
15 Receiver Gain 50.3
16 Relaxation Delay 1.0000
17 Pulse Width 10.0000
18 Presaturation Frequency
19 Acquisition Time 1.3631
20 Acquisition Date 2020-08-04T20:19:37
21 Modification Date 2020-08-04T20:19:37
22 Class
23 Spectrometer Frequency 100.62
24 Spectral Width 24038.5
25 Lowest Frequency -1958.4
26 Nucleus 13C
27 Acquired Size 32768
28 Spectral Size 65536
168.92
63.38
62.54
57.55
57.04
45.17
40.78
34.86
33.12
26.50
25.92
25.80
25.69
22.93
22.59
88
f1 (ppm)

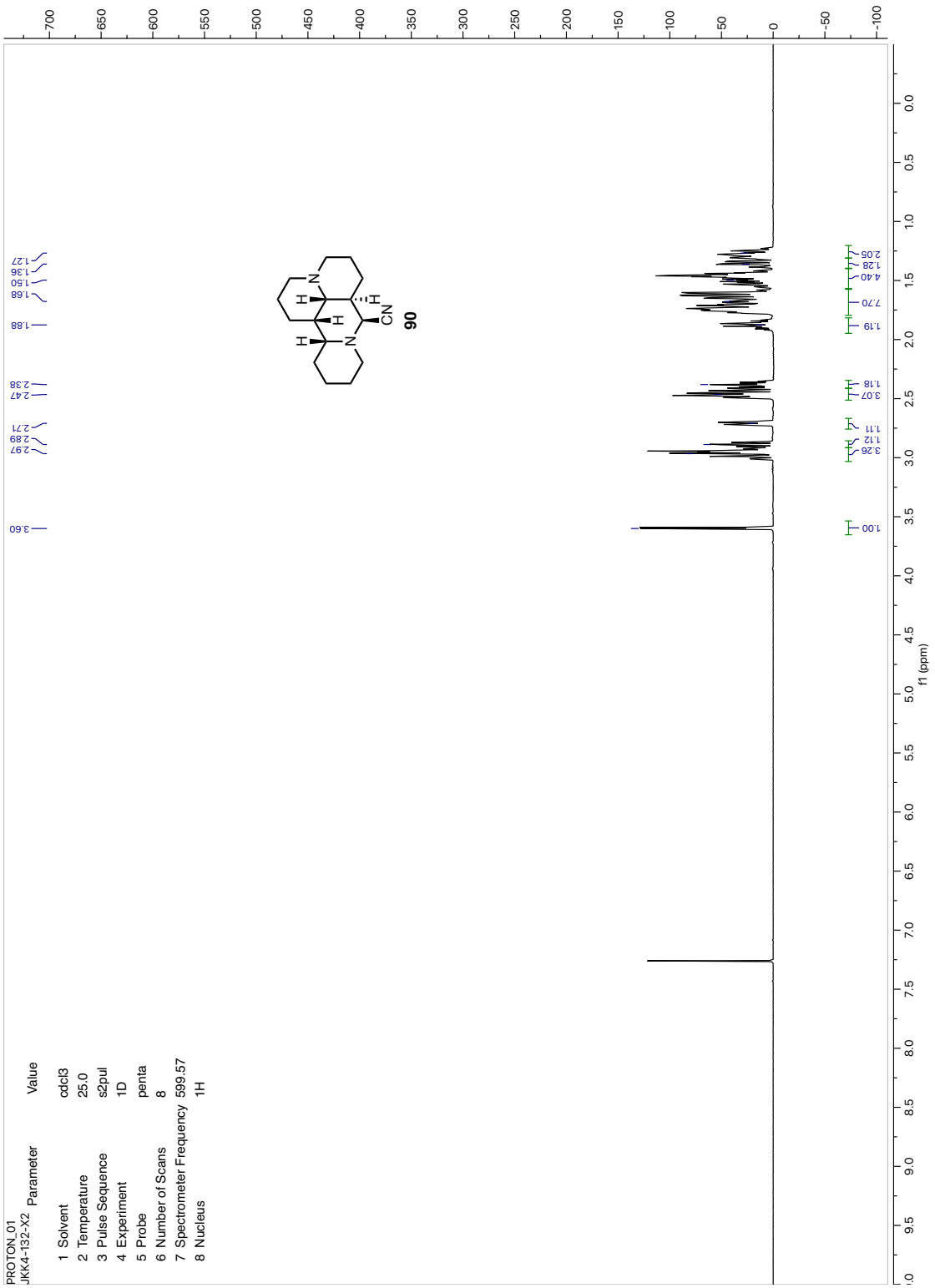
PROTON_01
JKK4-132-X2
Parameter Value
1 Solvent cdcl3
2 Temperature 25.0
3 Pulse Sequence s2pul
4 Experiment 1D
5 Probe penta
6 Number of Scans 8
7 Spectrometer Frequency 599.57
8 Nucleus 1H
90
f1 (ppm)

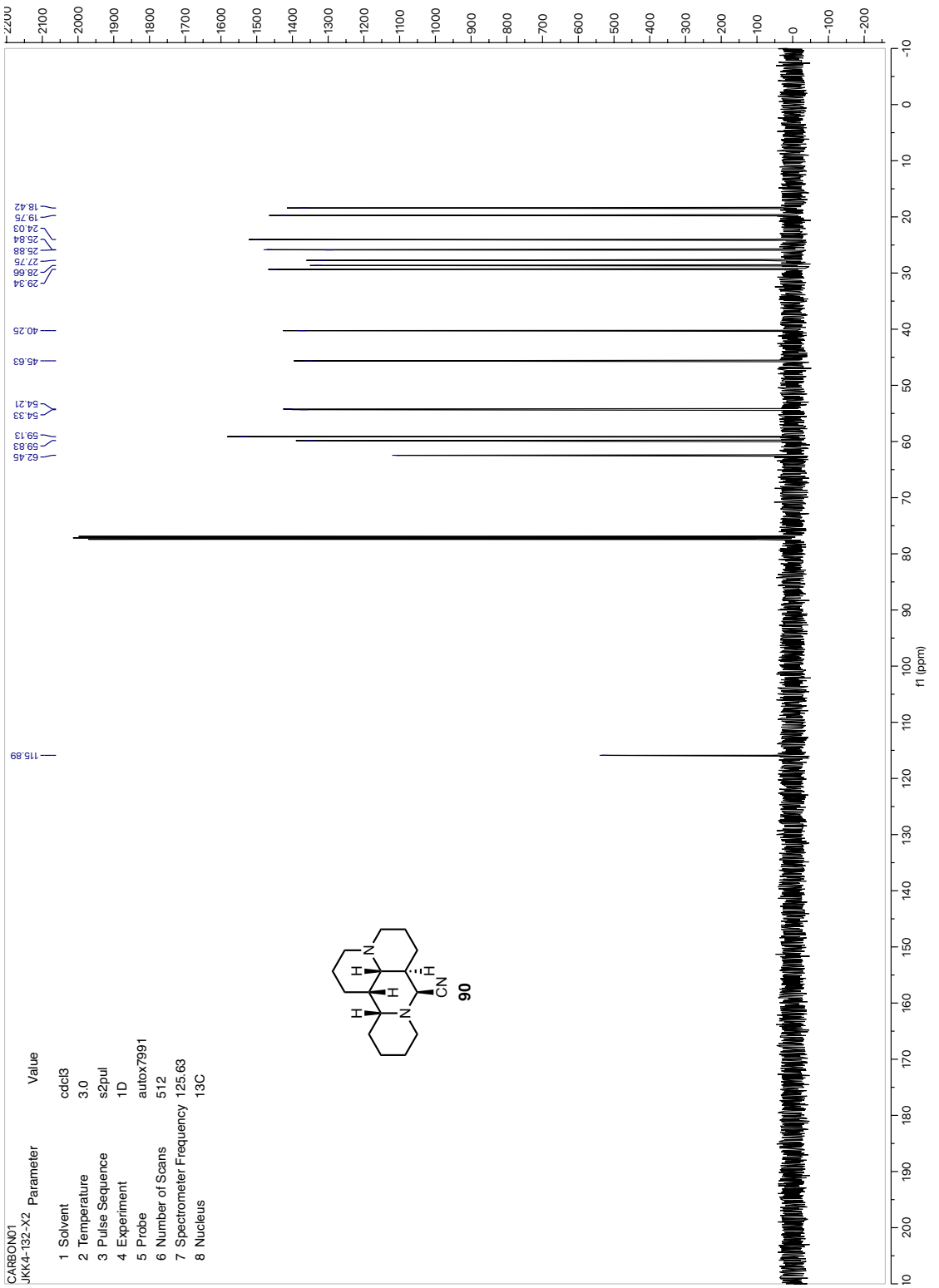
CARBON01
JKK4-132-X2
Parameter Value
1 Solvent cdcl3
2 Temperature 3.0
3 Pulse Sequence s2pul
4 Experiment 1D
5 Probe autox7991
6 Number of Scans 512
7 Spectrometer Frequency 125.63
8 Nucleus 13C
18.42
19.75
24.03
25.84
25.88
27.75
28.66
29.34
40.25
45.63
54.21
54.33
59.13
59.83
62.45
115.89
90
f1 (ppm)

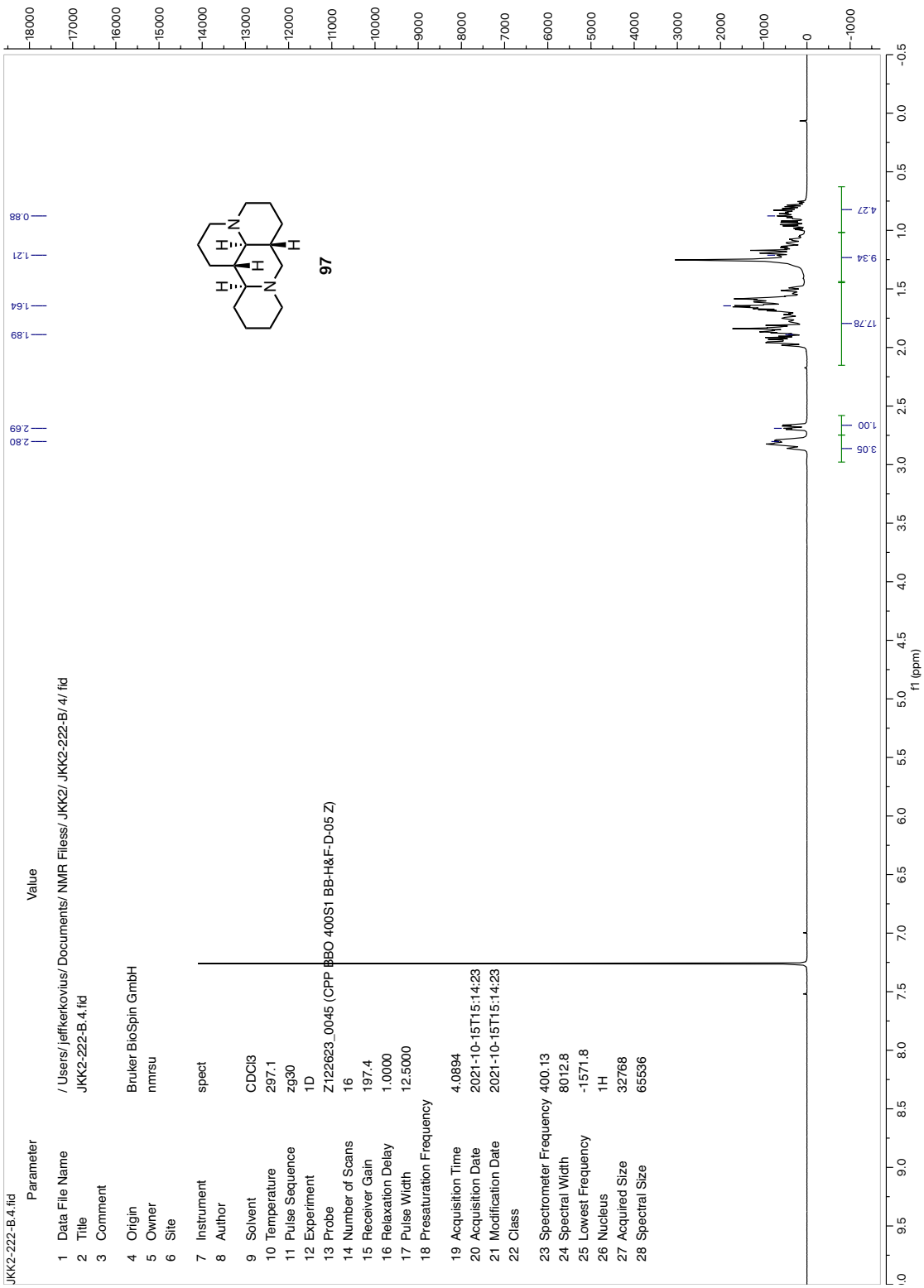
JKK2-222-B.4.fid
Parameter
Value
1 Data File Name / Users/ jeffkerkovius/ Documents/ NMR Files/ JKK2/ JKK2-222-B/ 4/ fid
2 Title JKK2-222-B.4.fid
3 Comment
4 Origin Bruker BioSpin GmbH
5 Owner nmrsu
6 Site
7 Instrument spect
8 Author
9 Solvent CDCl3
10 Temperature 297.1
11 Pulse Sequence zg30
12 Experiment 1D
13 Probe Z122623_0045 (CPP BBO 400S1 BB-H&F-D-05 Z)
14 Number of Scans 16
15 Receiver Gain 197.4
16 Relaxation Delay 1.0000
17 Pulse Width 12.5000
18 Presaturation Frequency
19 Acquisition Time 4.0894
20 Acquisition Date 2021-10-15T15:14:23
21 Modification Date 2021-10-15T15:14:23
22 Class
23 Spectrometer Frequency 400.13
24 Spectral Width 8012.8
25 Lowest Frequency -1571.8
26 Nucleus 1H
27 Acquired Size 32768
28 Spectral Size 65536
97
0.88
1.21
1.64
1.89
2.69
2.80
4.27
9.34
17.78
1.00
3.05
f1 (ppm)

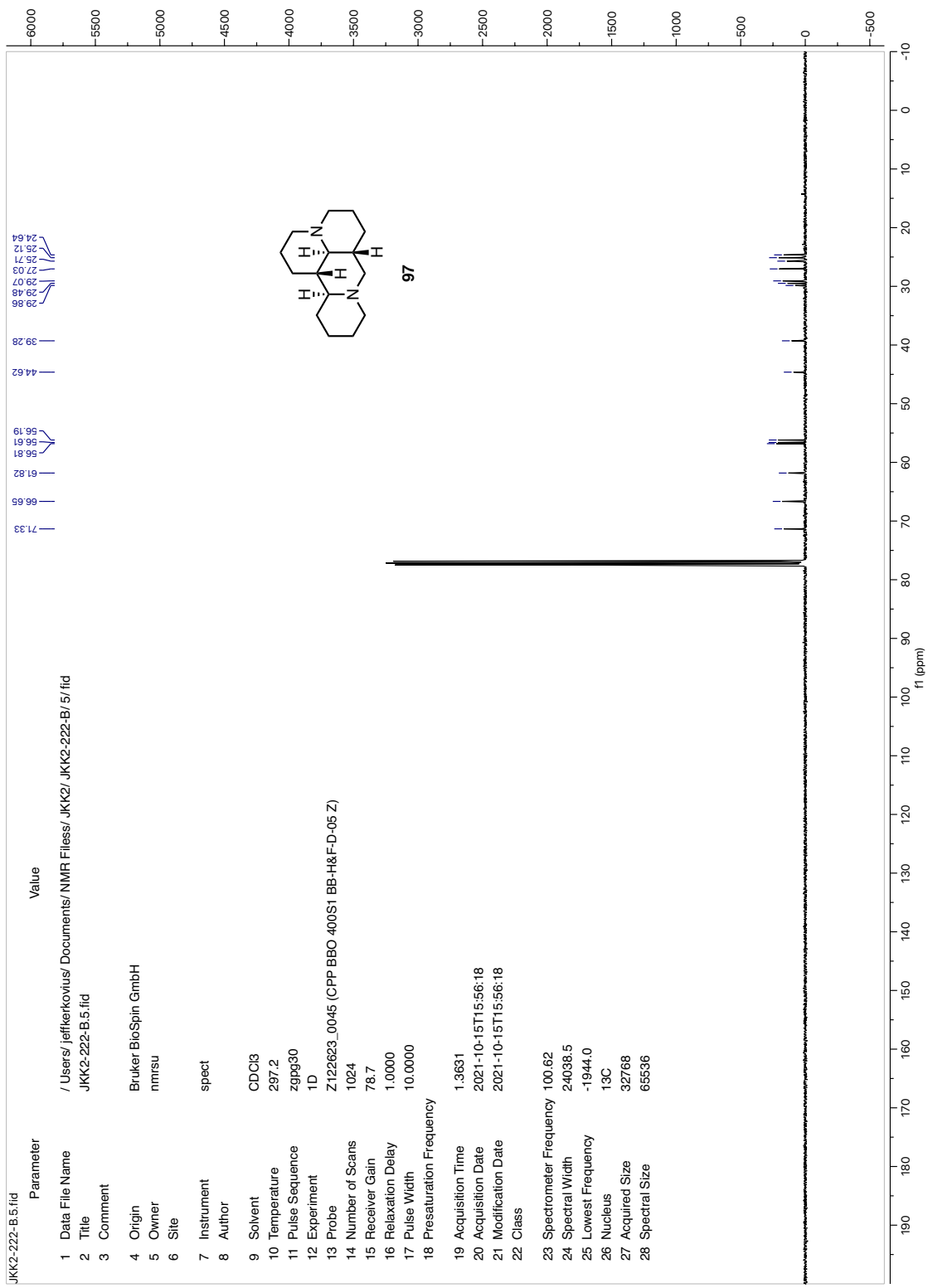
JKK2-222-B.5.fid
Parameter
Value
1 Data File Name / Users/ jeffkerkovius/ Documents/ NMR Files/ JKK2/ JKK2-222-B/ 5/ fid
2 Title JKK2-222-B.5.fid
3 Comment
4 Origin Bruker BioSpin GmbH
5 Owner nmrsu
6 Site
7 Instrument spect
8 Author
9 Solvent CDCl3
10 Temperature 297.2
11 Pulse Sequence zgpg30
12 Experiment 1D
13 Probe Z122623_0045 (CPP BBO 400S1 BB-H&F-D-05 Z)
14 Number of Scans 1024
15 Receiver Gain 78.7
16 Relaxation Delay 1.0000
17 Pulse Width 10.0000
18 Presaturation Frequency
19 Acquisition Time 1.3631
20 Acquisition Date 2021-10-15T15:56:18
21 Modification Date 2021-10-15T15:56:18
22 Class
23 Spectrometer Frequency 100.62
24 Spectral Width 24038.5
25 Lowest Frequency -1944.0
26 Nucleus 13C
27 Acquired Size 32768
28 Spectral Size 65536
71.33
66.65
61.82
56.81
56.61
56.19
44.62
39.28
29.86
29.48
29.07
27.03
25.71
25.12
24.64
97
f1 (ppm)

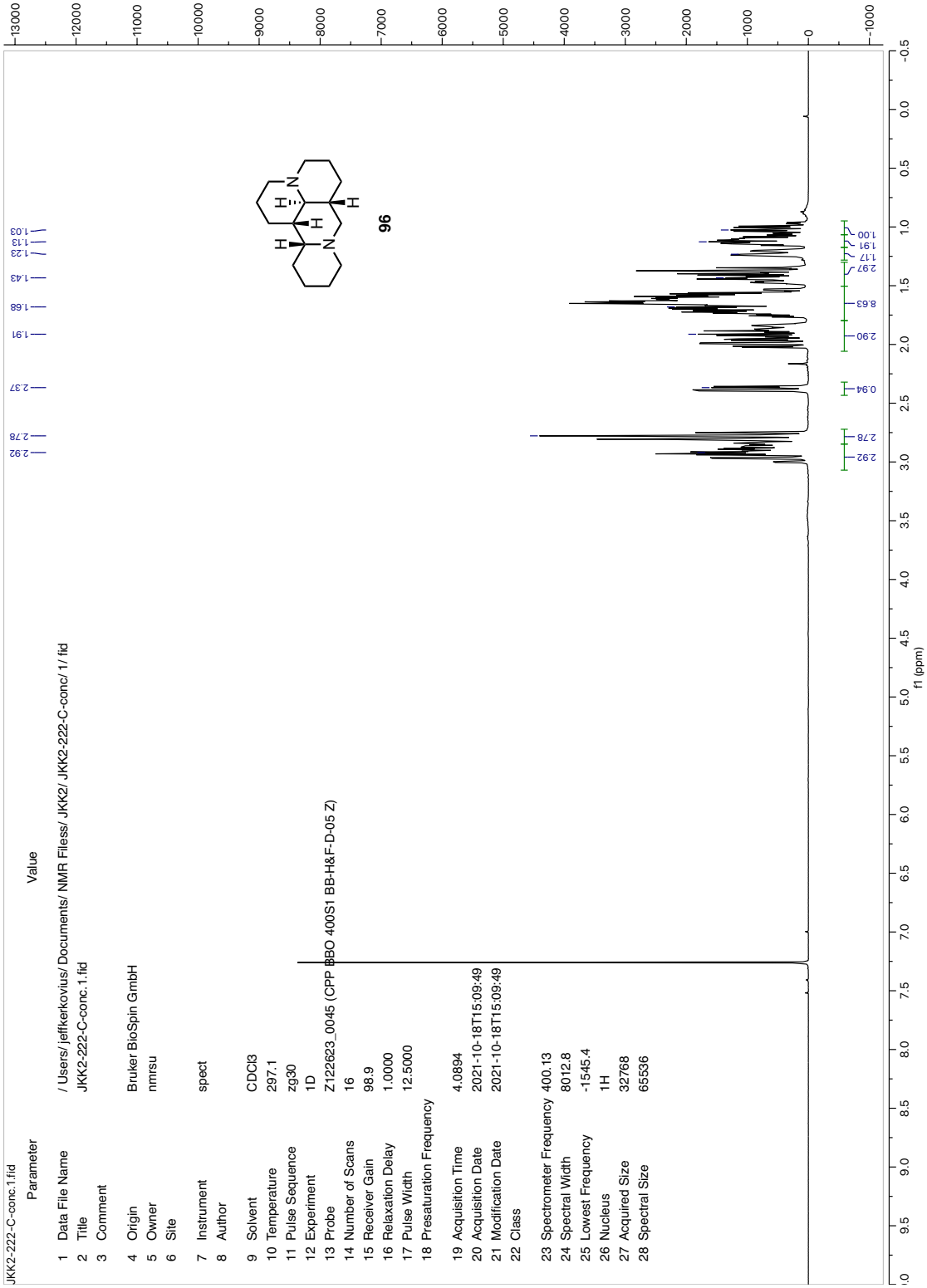
JKK2-222-C-conc.1.fid
Parameter
Value
1 Data File Name / Users/ jeffkerkovius/ Documents/ NMR Files/ JKK2/ JKK2-222-C-conc/ 1/ fid
2 Title JKK2-222-C-conc.1.fid
3 Comment
4 Origin Bruker BioSpin GmbH
5 Owner nmrsu
6 Site
7 Instrument spect
8 Author
9 Solvent CDCl3
10 Temperature 297.1
11 Pulse Sequence zg30
12 Experiment 1D
13 Probe Z122623_0045 (CPP BBO 400S1 BB-H&F-D-05 Z)
14 Number of Scans 16
15 Receiver Gain 98.9
16 Relaxation Delay 1.0000
17 Pulse Width 12.5000
18 Presaturation Frequency
19 Acquisition Time 4.0894
20 Acquisition Date 2021-10-18T15:09:49
21 Modification Date 2021-10-18T15:09:49
22 Class
23 Spectrometer Frequency 400.13
24 Spectral Width 8012.8
25 Lowest Frequency -1545.4
26 Nucleus 1H
27 Acquired Size 32768
28 Spectral Size 65536
96
f1 (ppm)

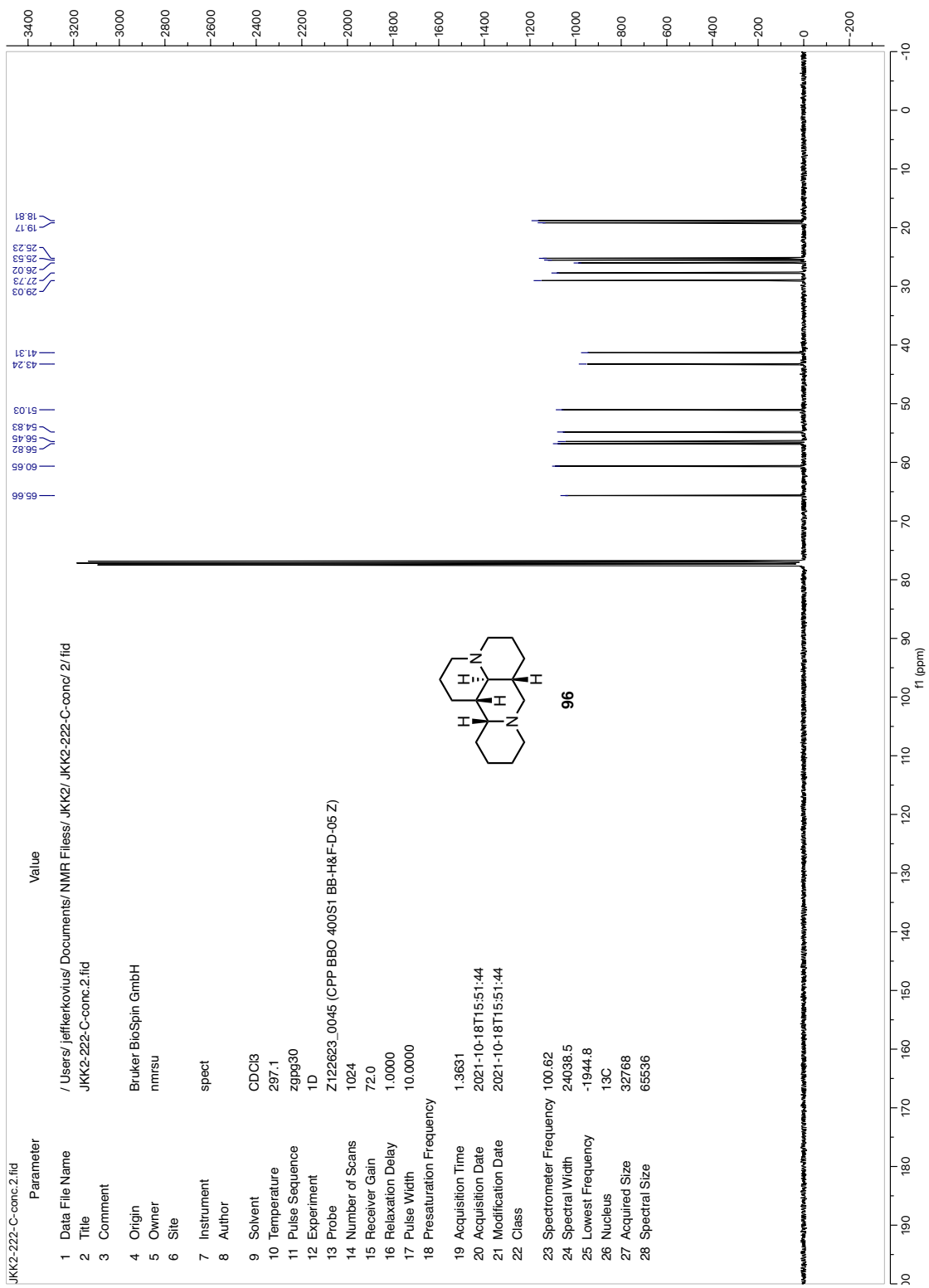
JKK2-222-C-conc.2.fid
Parameter
Value
1 Data File Name / Users/ jeffkerkovius/ Documents/ NMR Files/ JKK2/ JKK2-222-C-conc/ 2/ fid
2 Title JKK2-222-C-conc.2.fid
3 Comment
4 Origin Bruker BioSpin GmbH
5 Owner nmrsu
6 Site
7 Instrument spect
8 Author
9 Solvent CDCl3
10 Temperature 297.1
11 Pulse Sequence zgpg30
12 Experiment 1D
13 Probe Z122623_0045 (CPP BBO 400S1 BB-H&F-D-05 Z)
14 Number of Scans 1024
15 Receiver Gain 72.0
16 Relaxation Delay 1.0000
17 Pulse Width 10.0000
18 Presaturation Frequency
19 Acquisition Time 1.3631
20 Acquisition Date 2021-10-18T15:51:44
21 Modification Date 2021-10-18T15:51:44
22 Class
23 Spectrometer Frequency 100.62
24 Spectral Width 24038.5
25 Lowest Frequency -1944.8
26 Nucleus 13C
27 Acquired Size 32768
28 Spectral Size 65536
65.66
60.65
56.82
56.45
54.83
51.03
43.24
41.31
29.03
27.73
26.02
25.53
25.23
19.17
18.81
96
f1 (ppm)

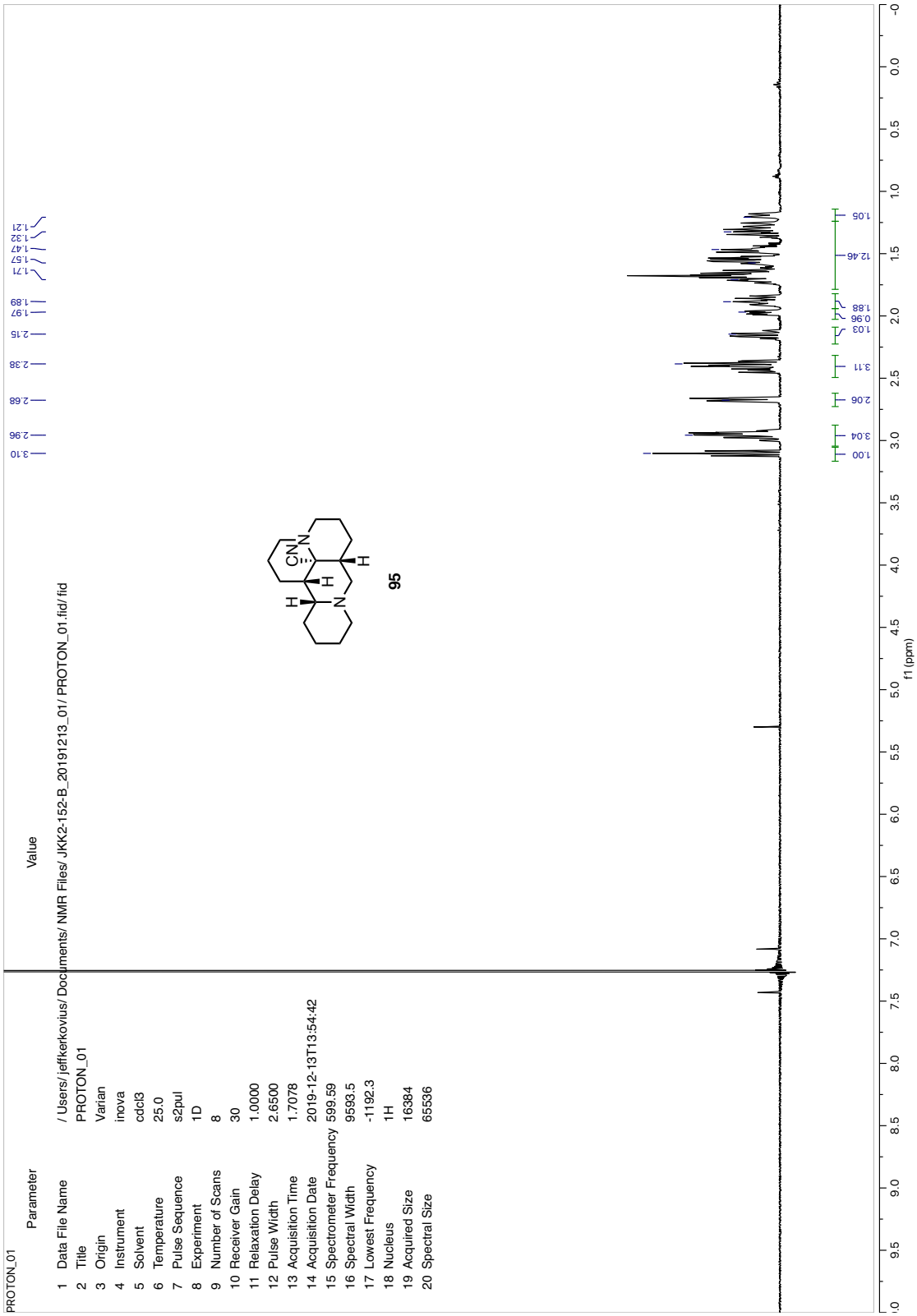
PROTON_01
Parameter
Value
1 Data File Name / Users/ jeffkerkovius/ Documents/ NMR Files/ JKK2-152-B_20191213_01/ PROTON_01.fid/ fid
2 Title PROTON_01
3 Origin Varian
4 Instrument inova
5 Solvent cdcl3
6 Temperature 25.0
7 Pulse Sequence s2pul
8 Experiment 1D
9 Number of Scans 8
10 Receiver Gain 30
11 Relaxation Delay 1.0000
12 Pulse Width 2.6500
13 Acquisition Time 1.7078
14 Acquisition Date 2019-12-13T13:54:42
15 Spectrometer Frequency 599.59
16 Spectral Width 9593.5
17 Lowest Frequency -1192.3
18 Nucleus 1H
19 Acquired Size 16384
20 Spectral Size 65536
3.10
2.96
2.68
2.38
2.15
1.97
1.89
1.71
1.57
1.47
1.32
1.21
1.00
3.04
2.06
3.11
1.03
0.96
1.88
12.46
1.05
f1 (ppm)

95

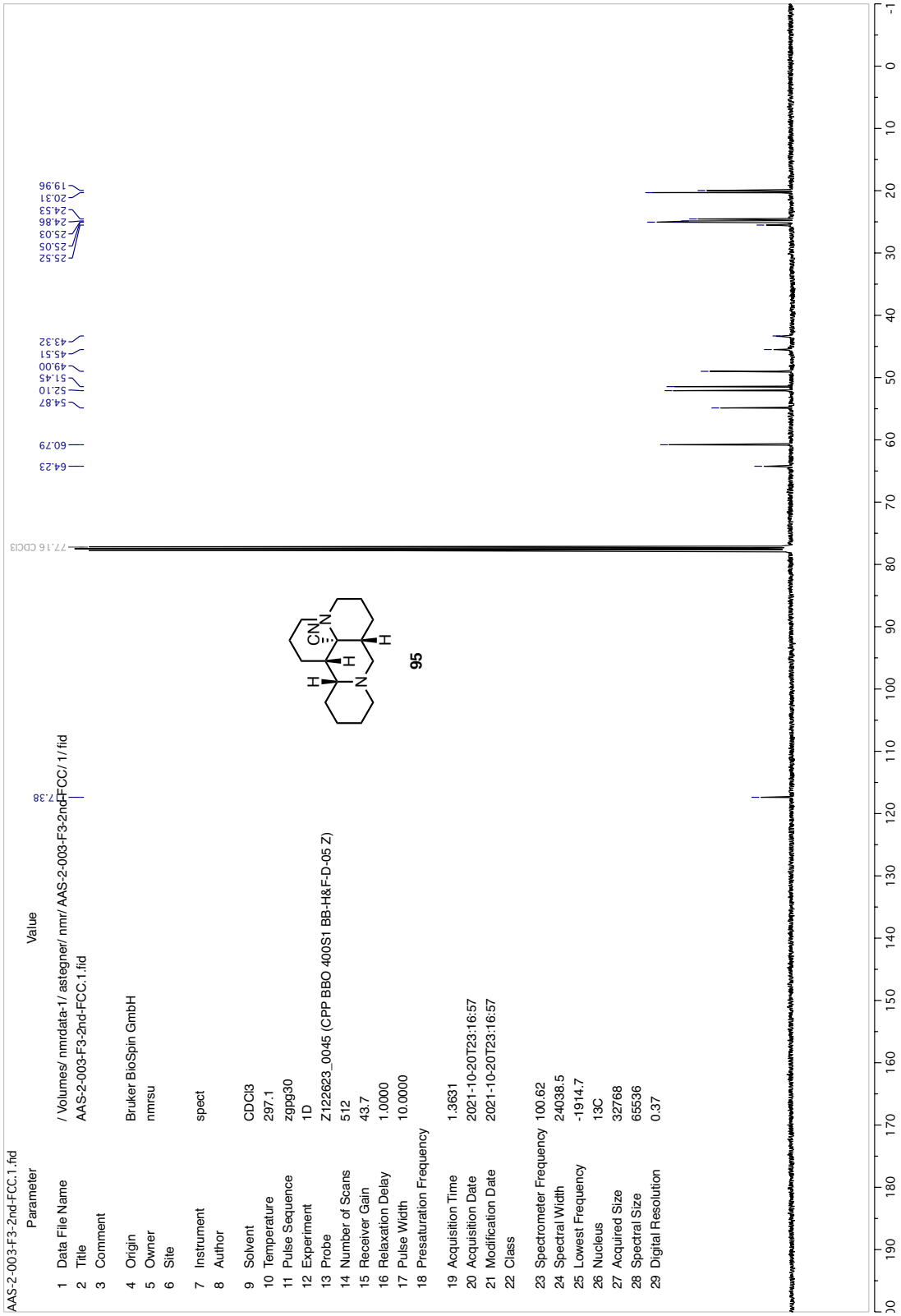
AAS-2-003-F3-2nd-FCC.1.fid
Parameter
Value
1 Data File Name / Volumes/ nmrdata-1/ astegner/ nmr/ AAS-2-003-F3-2nd-FCC/ 1/ fid
2 Title AAS-2-003-F3-2nd-FCC.1.fid
3 Comment
4 Origin Bruker BioSpin GmbH
5 Owner nmrsu
6 Site
7 Instrument spect
8 Author
9 Solvent CDCl3
10 Temperature 297.1
11 Pulse Sequence zgpg30
12 Experiment 1D
13 Probe Z122623_0045 (CPP BBO 400S1 BB-H&F-D-05 Z)
14 Number of Scans 512
15 Receiver Gain 43.7
16 Relaxation Delay 1.0000
17 Pulse Width 10.0000
18 Presaturation Frequency
19 Acquisition Time 1.3631
20 Acquisition Date 2021-10-20T23:16:57
21 Modification Date 2021-10-20T23:16:57
22 Class
23 Spectrometer Frequency 100.62
24 Spectral Width 24038.5
25 Lowest Frequency -1914.7
26 Nucleus 13C
27 Acquired Size 32768
28 Spectral Size 65536
29 Digital Resolution 0.37
77.16 CDCl3
64.23
60.79
54.87
52.10
51.45
49.00
45.51
43.32
25.52
25.05
25.03
24.86
24.53
20.31
19.96
95
f1 (ppm)

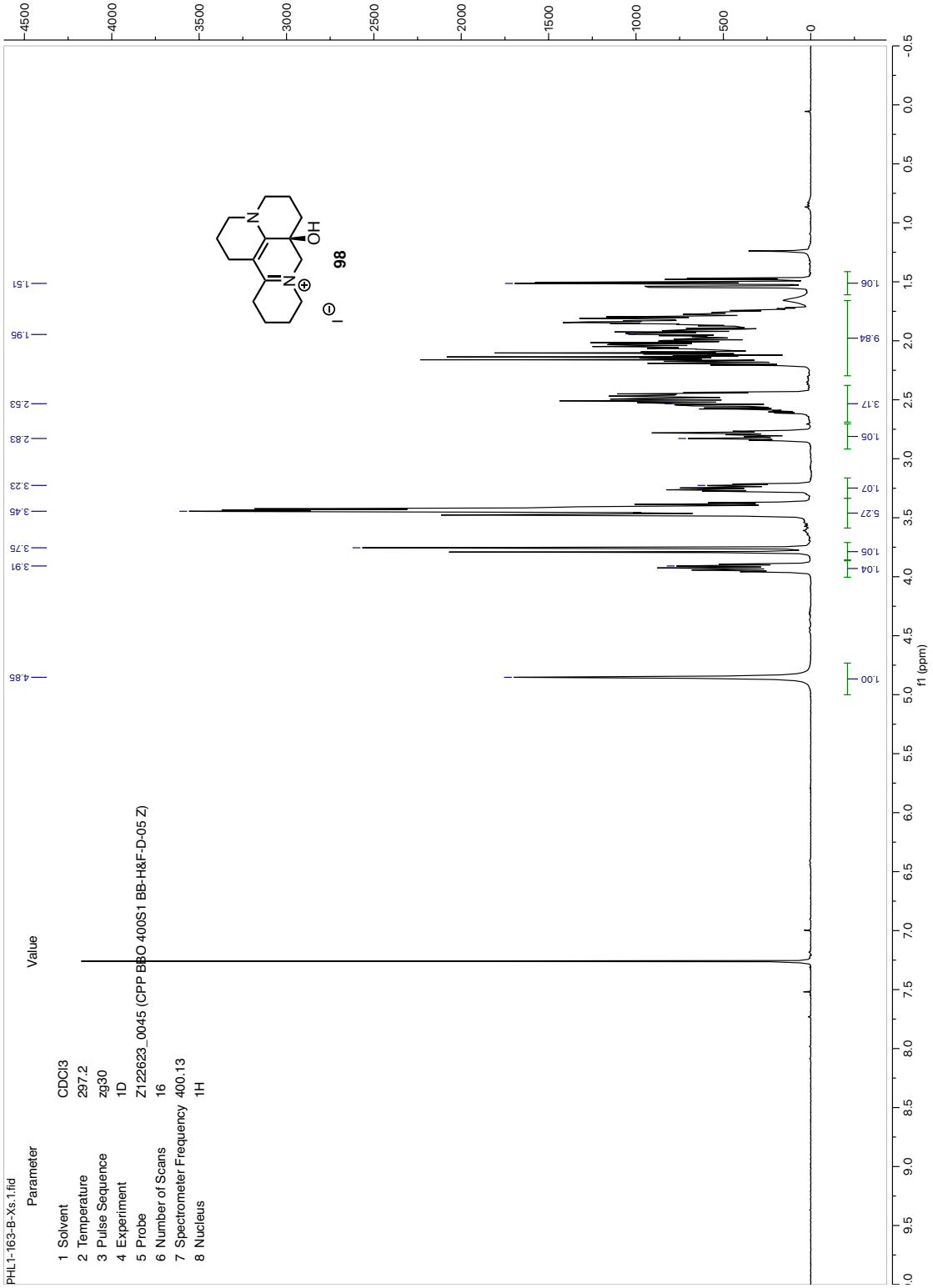
98
I
OH
PHL1-163-B-Xs.1.fid
Parameter Value
1 Solvent CDCl3
2 Temperature 297.2
3 Pulse Sequence zg30
4 Experiment 1D
5 Probe Z122623_0045 (CPP BBO 400S1 BB-H&F-D-05 Z)
6 Number of Scans 16
7 Spectrometer Frequency 400.13
8 Nucleus 1H
f1 (ppm)

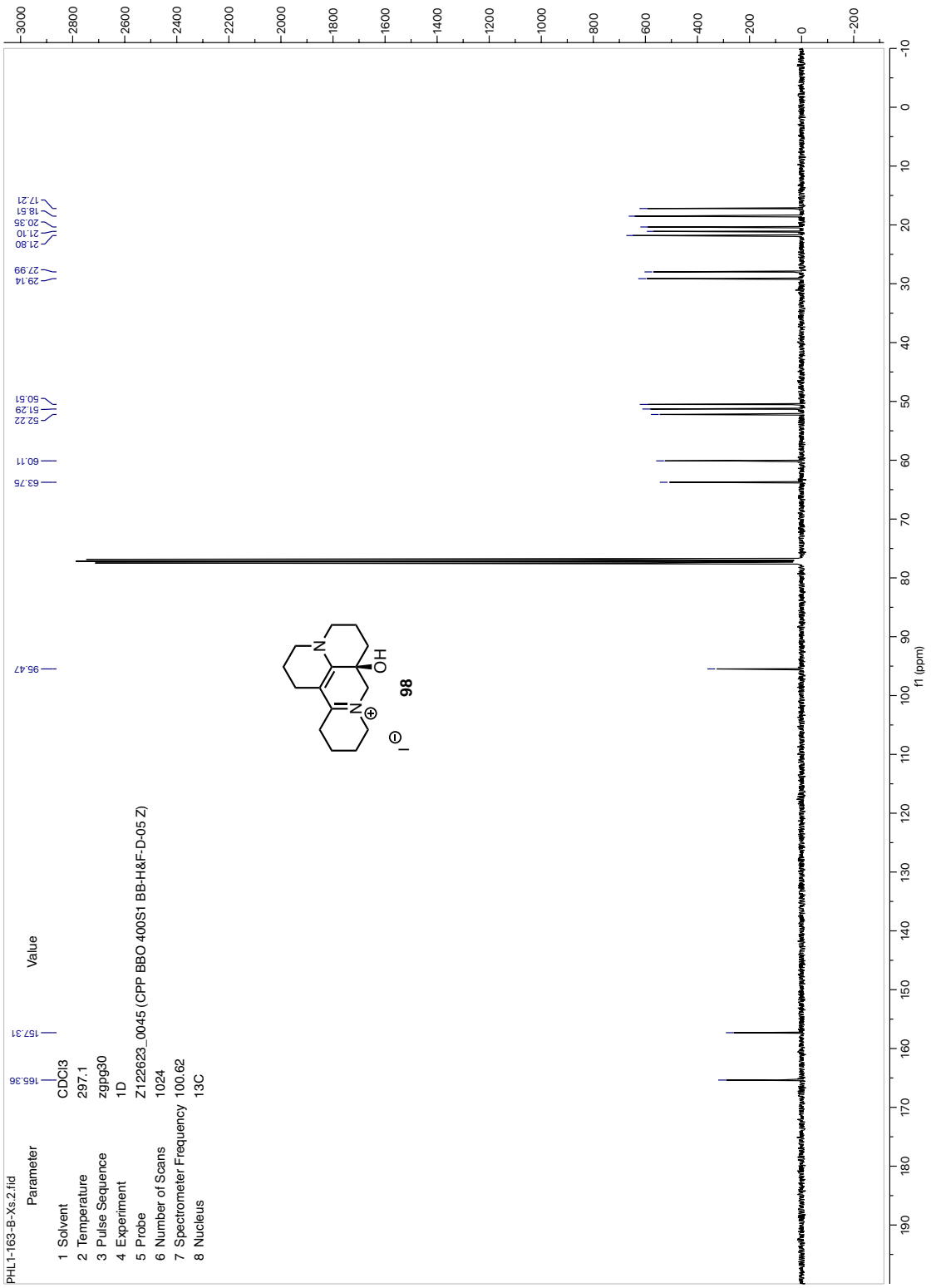
PHL1-163-B-Xs.2.fid
Parameter Value
1 Solvent CDCl3
2 Temperature 297.1
3 Pulse Sequence zgpg30
4 Experiment 1D
5 Probe Z122623_0045 (CPP BBO 400S1 BB-H&F-D-05 Z)
6 Number of Scans 1024
7 Spectrometer Frequency 100.62
8 Nucleus 13C
157.31
165.36
95.47
63.75
60.11
52.22
51.29
50.51
29.14
27.99
21.80
21.10
20.35
18.51
17.21
OH
98
I
f1 (ppm)

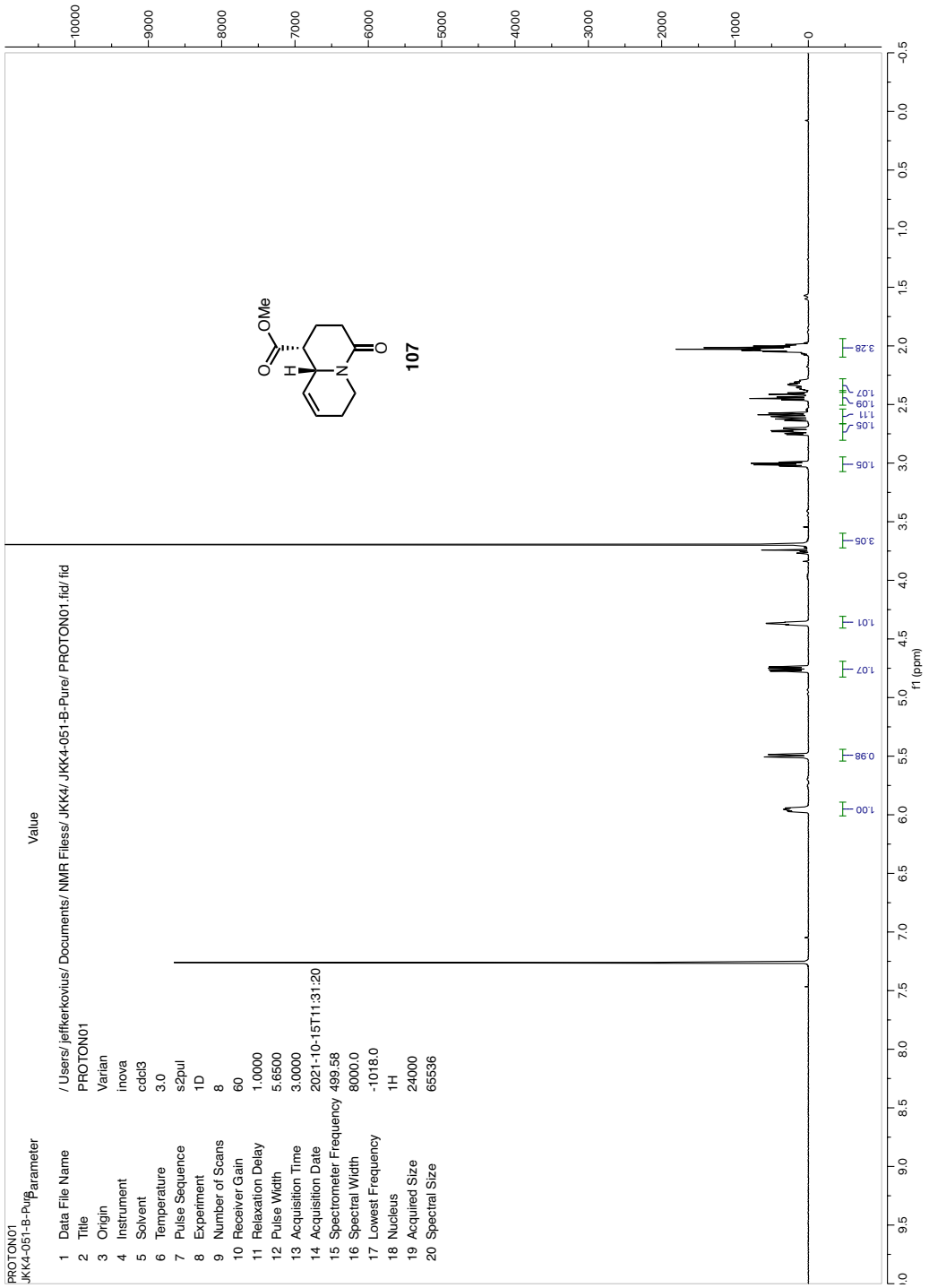
PROTON01
JKK4-051-B-Pure
Parameter
Value
1 Data File Name / Users/ jeffkerkovius/ Documents/ NMR Files/ JKK4/ JKK4-051-B-Pure/ PROTON01.fid/ fid
2 Title PROTON01
3 Origin Varian
4 Instrument inova
5 Solvent cdcl3
6 Temperature 3.0
7 Pulse Sequence s2pul
8 Experiment 1D
9 Number of Scans 8
10 Receiver Gain 60
11 Relaxation Delay 1.0000
12 Pulse Width 5.6500
13 Acquisition Time 3.0000
14 Acquisition Date 2021-10-15T11:31:20
15 Spectrometer Frequency 499.58
16 Spectral Width 8000.0
17 Lowest Frequency -1018.0
18 Nucleus 1H
19 Acquired Size 24000
20 Spectral Size 65536
OMe
O
H
N
O
107
3.28
1.07
1.09
1.11
1.05
1.05
3.05
1.01
1.07
0.98
1.00
f1 (ppm)

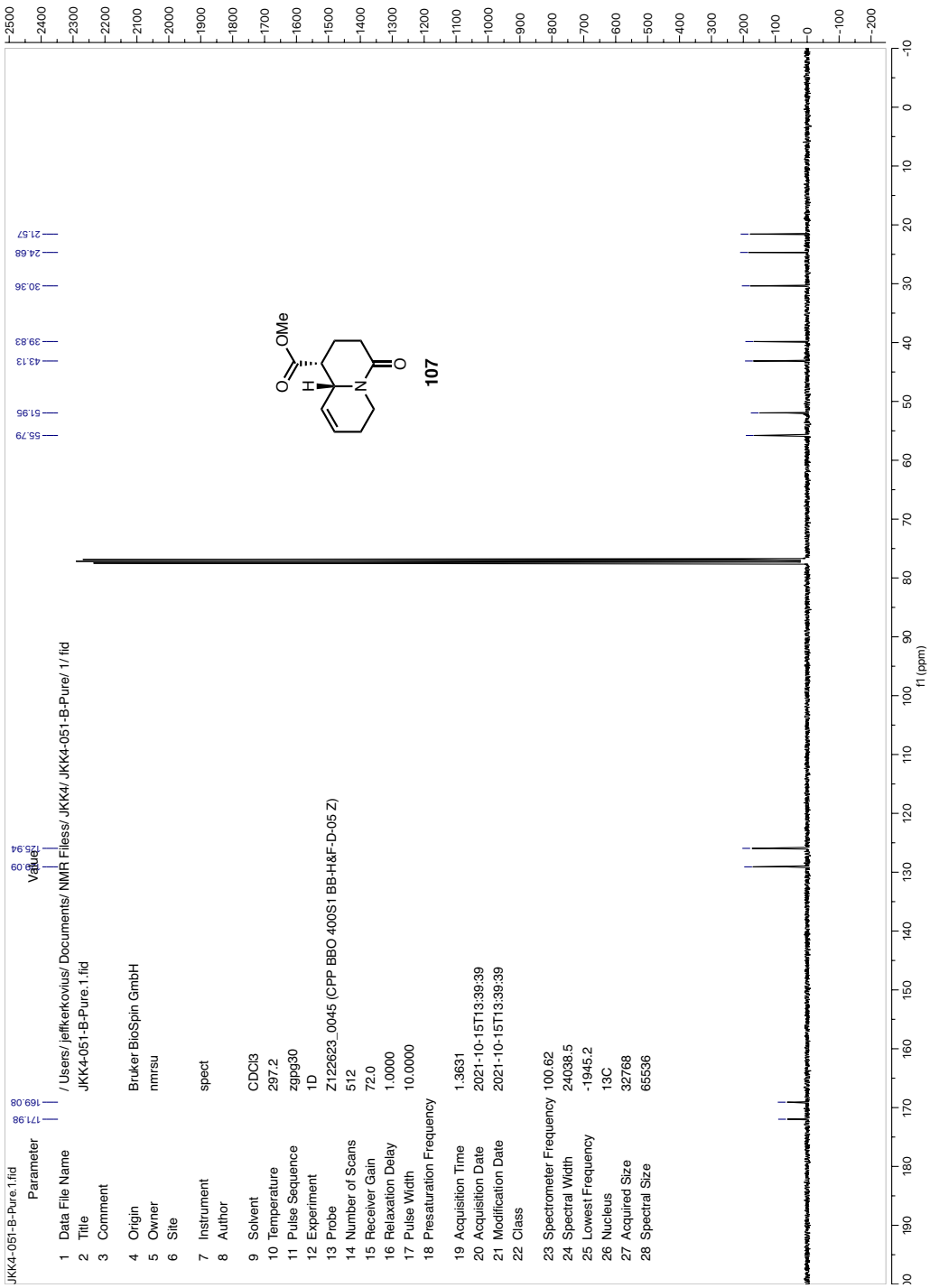
JKK4-051-B-Pure.1.fid
Parameter
Value
1 Data File Name / Users/ jeffkerkovius/ Documents/ NMR Files/ JKK4/ JKK4-051-B-Pure/ 1/ fid
2 Title JKK4-051-B-Pure.1.fid
3 Comment
4 Origin Bruker BioSpin GmbH
5 Owner nmrsu
6 Site
7 Instrument spect
8 Author
9 Solvent CDCl3
10 Temperature 297.2
11 Pulse Sequence zgpg30
12 Experiment 1D
13 Probe Z122623_0045 (CPP BBO 400S1 BB-H&F-D-05 Z)
14 Number of Scans 512
15 Receiver Gain 72.0
16 Relaxation Delay 1.0000
17 Pulse Width 10.0000
18 Presaturation Frequency
19 Acquisition Time 1.3631
20 Acquisition Date 2021-10-15T13:39:39
21 Modification Date 2021-10-15T13:39:39
22 Class
23 Spectrometer Frequency 100.62
24 Spectral Width 24038.5
25 Lowest Frequency -1945.2
26 Nucleus 13C
27 Acquired Size 32768
28 Spectral Size 65536
171.98
169.08
55.79
51.95
43.13
39.83
30.36
24.68
21.57
OMe
O
H
N
O
107
f1 (ppm)

[This chapter is temporarily embargoed.]

ABOUT THE AUTHOR

Andrea Anna Therese Stegner grew up on the southern edge of Munich, Germany, where weekend hikes in the Bavarian Alps and long hours at the stables fostered equal parts curiosity and perseverance. After graduating from Max-Planck-Gymnasium, Munich, she enrolled at Ludwig-Maximilians-Universität (LMU) Munich and received a B.Sc. in chemistry and biochemistry.

Andrea remained at LMU for her M.Sc., where she joined the laboratory of Prof. Dirk Trauner to develop an enantioselective route to a key intermediate and a Kornblum-oxidation protocol *en route* to the alkaloid sinoracutine. Subsequently, she was offered a research assistant position with Prof. Oliver Thorn-Seshold, in which she synthesized novel photo-switchable scaffolds for optical control of microtubule dynamics. Seeking broader perspective, she completed her master's thesis in the laboratory of Prof. Abigail Doyle at Princeton University, investigating photocatalytic hydroacylation of styrenes with carboxylic acids.

Andrea returned to the US to pursue her Ph.D. in organic chemistry at the California Institute of Technology under the guidance of Prof. Sarah Reisman. Her doctoral work combines complexity-generating annulations and transition metal-catalyzed cross-coupling reactions to access lupin-alkaloid and ent-kauranoid natural products.

Outside the laboratory, Andrea can usually be found in the saddle, on a mountain trail, or sharing a campsite (and snacks) friends, her dog Lance and sometimes her cats Smokey and Foggy.